Scientific Research Associates, inc.

50 Nye Road, P.O. Box 1058
Glastonbury, Connecticut 06033
(203) 659-0333 FAX (203) 633-0676

FINAL REPORT, VOLUME II

SRA Report R93-9083-F

Simulation of Preburner Sprays

Scientific Research Associates, Inc.

in conjunction with Subcontractor

Imperial College of Science & Technology

Prepared for NASA/George C. Marshall Space Flight Center
Marshall Space Flight Center, AL 35812

Under Contract NAS8-38872

May 1993

IMPERIAL COLLEGE OF SCIENCE, TECHNOLOGY AND MEDICINE
Mechanical Engineering Department
Thermofluids Section
Exhibition Road
London SW7 2BX

COAXIAL AIRBLAST ATOMIZERS

20 APRIL 1993

Contract NAS8-38872

PREPARED BY

Y. Hardalupas and J.H. Whitelaw

PREPARED FOR :

NASA / George C. Marshall Space Flight Centre
Marshall Space Flight Centre, Alabama 35812

TABLE OF CONTENTS

COAXIAL AIRBLAST ATOMIZERS

Y. Hardalupas and J.H. Whitelaw
Imperial College of Science, Technology and Medicine
Mechanical Engineering Department
London SW7 2BX, United Kingdom.

1. PURPOSE OF THE STUDY

The atomization of liquid oxygen by a high velocity coaxial hydrogen stream is required in the preburner of the main engine of the space shuttle (SSME). The combustion stability of rocket engines has been shown to depend on the geometry of the coaxial injectors and on the gaseous and liquid injection velocity (Wanhainen et al, 1966). The combustion efficiency of rocket engines is affected by the size characteristics and the spray width (Priem and Heidman 1959), since both parameters affect the evaporation of the oxidizer and its mixing with the fuel.

It is important to be able to control and predict the size characteristics of the sprays produced by coaxial injectors for the performance of rocket engines and they have been studied, for example, by Weiss and Worsham (1959), Burick (1972), Falk (1975) and Ferrenberg et al (1985). The characteristics of sprays produced by airblast atomizers have been reviewed by Ferrenberg et al (1985) and Lefebvre (1989) and results summarised by empirical correlations between the mean diameters and the parameters affecting atomization such as the velocity, density, viscosity and surface tension of the gas and the liquid and the geometry of the nozzle. It is common the above parameters to be expressed as non-dimensional numbers, e.g. exit Weber number, Reynolds numbers of the gas and the liquid jet, and gas-to-liquid ratios of velocities, mass flowrates and the momentum fluxes. Most of these sprays were characterized by their spray angle and mean droplet size averaged over the spray rather than local values, which makes it difficult to evaluate the effect of each parameters. So these correlations are unable to reproduce spray characteristics over a wide range of conditions and, most important, for the conditions of the preburners of the SSME.

Early work on sprays produced by coaxial airblast injectors was performed by droplet capture and imaging techniques (Weiss and Worsham, 1959) and hot wax freezing (Burick, 1972; Falk, 1975), but accuracy was limited. Optical non-intrusive techniques have allowed more accurate and detailed size measurements. Laser diffraction provides the droplet mean diameter averaged over the line of sight of the laser beam and has shown that the Sauter mean diameter increases with the radial distance from the axis of the spray (Caré and Ledoux 1991),

but can be misleading without deconvolution to provide local size information (Cossali and Hardalupas, 1992) and they do not provide the droplet velocity. The combined visibility and intensity based interferometric technique measures the local size and velocity of sprays (Ferrenberg et al, 1985), but with limited accuracy particularly for the smaller droplets in the dilute regions of the sprays and larger inaccuracy over all droplet sizes due to attenuation of the incident laser beams and the scattered light (Kliafas et al, 1990) in the dense regions of the sprays.

The phase Doppler anemometer provides local spray characteristics with high spatial resolution and better accuracy than previous non-intrusive techniques and has been used successfully to characterize sprays produced by coaxial injectors in the present study (Hardalupas et al, 1992; Hardalupas and Whitelaw, 1993) and also by, for example, Eroglu and Chigier (1991), Sankar et al (1991) & (1992) and Zaller and Klem (1991). Eroglu and Chigier (1991) examined nozzles with initial conditions different from those of the SSME (exit Weber numbers up to 200 and liquid jet Reynolds numbers up to 4500) and found that the radial distribution of the Sauter mean diameter had two maxima, at the centre and towards the spray boundary, in contrast to Caré and Ledoux (1991). Sankar et al (1991) and Zaller and Klem (1991) examined sprays produced from nozzles with initial conditions close to the values of rocket engines and found maximum mean diameters close to the centre, but the range of the spray conditions was limited and the effect of the recess of the liquid tube upstream of the exit of the gaseous jet on spray size characteristics was not clear. Also, the development of the sprays with distance from the nozzle was not examined and no effort was made to correlate spray characteristics with the initial conditions of the gas and the liquid at the exit of the nozzle.

The main spray characteristics of importance to combustion applications, as suggested, for example, by Faeth (1983) and (1987) and Law (1982), are the mean droplet size, which influences the evaporation rate and the droplet response to the gaseous flow field, and the rate of spread, which influences the mixing between fuel and oxidiser. These two characteristics of sprays from coaxial airblast nozzles will be examined during the present study to establish how they are affected by the gas and liquid flow conditions and the geometry of the nozzle.

The mean diameter of the sprays produced by airblast atomizers, as suggested by most of the empirical correlations summarised by Lefebvre (1989), is inversely proportional to the exit Weber number and the gas-to-liquid mass flowrate ratio. The exit Weber number is defined :

$$We_{exit} = \frac{\rho_g (U_g - U_l)^2 D_l}{\sigma} \qquad (1a)$$

where ρ_g is the gas density, $U_g - U_l$ is the relative velocity between the gaseous and the liquid jets at the exit, D_l is the diameter of the liquid jet exit and σ is the surface tension. The gas-to-liquid mass flowrate ratio is :

$$MFR = \frac{\rho_g U_g (D_{gas}^2 - D_{le}^2)}{\rho_l U_l D_l^2} \qquad (1b)$$

where D_{le} is the external diameter of the liquid tube and D_{gas} is the gaseous jet diameter. All these correlations predict mean diameters, which, in some of the sprays of the present study, are erroneous by more than one order of magnitude, either larger or lower than the measured values. Also our measurements show that , in some cases, the mean diameter increased with the increase of the exit Weber number, in contrast to suggestions of the existing correlations. The following text will explain that the local Weber number of the droplets, quantified by the local slip velocity, $u_g - u_l$, between the gas and droplets with diameter d :

$$We_{loc} = \frac{\rho_g (u_g - u_l)^2 d}{\sigma} \qquad (1c)$$

rather than the exit Weber number is important for secondary atomization and is likely to determine the droplet size of the sprays. Two additional scaling parameters which are likely to affect the atomization process will be considered, the gas-to-liquid momentum and velocity ratio, which are:

$$MR = \frac{\rho_g U_g^2 (D_{gas}^2 - D_{le}^2)}{\rho_l U_l^2 D_l^2} \qquad (1d)$$

$$VR = \frac{U_g}{U_l} \qquad (1e)$$

The rate of spread of sprays from coaxial airblast atomizers has been shown to affect the rocket engine combustion efficiency (Nurick, 1971) and has been examined either by intrusive probe collection methods (e.g. Nurick and Clapp, 1969; Burick, 1972) or by photographic methods reviewed by Lefebvre (1989), which only qualitatively show the spread of the spray. The present study will measure the rate of spread by non-intrusive methods and will provide local measurements with distance from the nozzle exit.

Another parameter affecting atomization and rate of spread is the presence of swirl in the gaseous stream, but its influence has not been examined for geometries of coaxial atomizers of the present study. The swirl number, S, defined as the ratio of the axial flux of the angular

momentum to the axial flux of axial momentum (Beér and Chigier, 1972), will be used to quantify the swirl intensity in the gaseous stream and is :

$$S = \frac{\int_{R_0}^{R_{gas}} U\ W\ r^2\ dr}{R_{gas} \int_{R_0}^{R_{gas}} U^2\ r\ dr} \qquad (2)$$

where R_{gas} is the radius of the gaseous jet, R_0 is the outside radius of the liquid tube, U and W are the local mean axial and tangential velocity at the exit of gaseous jet respectively and r is the local radius.

The purposes of this study are to :

(i) Measure the droplet size and rate of spread of the sprays produced by single coaxial airblast nozzles with axial gaseous stream by examining the local droplet size, velocity and flux characteristics for a wide range of gas and liquid flowrates and correlate the results with the conditions at the nozzle exit.

(ii) Examine the effect of the geometry of single coaxial airblast atomizers on spray characteristics by varying the gas and liquid tube diameter, the liquid tube recess and the shape of the exit of the gaseous jet from straight to converging.

(iii) Quantify the effect of swirl in the gaseous stream on the spray characteristics produced by single coaxial airblast nozzles.

(iv) Quantify the effect of reatomisation by impingement of the spray on a flat disc positioned around 200 mm from the nozzle exit. This explores the possibility of spray impingement on the turbopump dome during the startup process of the preburner of the SSME. Wang (1991) suggested that combustion can occur in the first and second stage blades of the gas turbine or on the turbopump dome, causing cracks on housings, sheetmetal, nozzles and blade shunks, which may suggest that the liquid oxidiser reaches the turbopump dome probably due to delayed ignition.

(v) Study the interaction between multiple sprays without and with swirl in their gaseous stream by comparing the spray characteristics of single nozzles and three identical nozzles with their axis at a small distance from each other. This part simulates the sprays in the preburner of the SSME, where there are around 260 elements on the faceplate of the combustion chamber. This effect has never been studied before and its importance was emphasised by Ferrenberg et al (1985).

(vi) Design an experimental facility to study the characteristics of sprays at high pressure conditions and at supercritical pressure and temperature for the gas but supercritical pressure and subcritical temperature for the liquid. This will allow the simulation of the conditions of the preburner of the SSME and examination of the effect of the gaseous fuel density and the

supercritical conditions on the characteristics of the atmospheric pressure sprays examined during the current project.

This report describes the experimental arrangement and the instrumentation, presents the results and relevant scaling parameters, discusses their implications for the operation of the preburner of the SSME, and summarises the main findings.

2. EXPERIMENTAL ARRANGEMENT AND INSTRUMENTATION

2.1 Single coaxial airblast atomizers

The airblast atomizer of figure 1 was constructed and operated at atmospheric pressure with air replacing the hydrogen and water the liquid oxygen of the Space Shuttle Main Engine (SSME). A central tube provided the liquid to the nozzle and consisted initially of a 10 mm diameter tube which reduced to an external diameter of 2.95 mm with internal diameter D_l = 2.3 mm (0.090") and with length to diameter ratio 22; a second internal tube with external diameter 1.47 mm and internal diameter D_l = 1.1 mm with length to diameter ratio 45 was also used. The exit of the liquid tube could be adjusted, to be in the plane of the exit of the gaseous jet or recessed. Although the effect of the liquid tube diameter was examined, most of the experiments were performed for the diameter of the exit of the liquid tube of 2.3 mm (0.090"), because this is similar to that of the liquid oxygen tubes in the SSME.

The gas flowrate was supplied to the nozzle by four gas inlets with their axes normal to that of the nozzle (figure 1). Flow straighteners were used to remove residual swirling motion and ensure axisymmetric flow. The gaseous flow was accelerated by a conical shape contraction before the exit of the nozzle to reduce possible flow asymmetries. Nozzles with straight and converging exits, as shown in figure 2a, could be attached at the exit of the gaseous jet with diameter of 8.95, 14.95 and 22.95 mm resulting in annular widths of 3, 6 and 10 mm and 3.74, 6.74 and 10.74 mm when liquid jet tubes with external diameters of 2.95 mm and 1.47 mm were used respectively. The length of the straight part of the nozzle was 18, 28 and 38 mm for 8.95, 14.95 and 22.95 mm gaseous jet diameters respectively. A converging nozzle of 8.95 mm exit diameter, 28° half angle and 23.5 mm length was used to examine the effect of the shape of the exit of the gaseous jet on atomization, while keeping the exit diameter constant.

A wide range of flow conditions were examined for sprays without swirling gas and their parameters are summarised in tables 1a and b for internal liquid tube diameter of 2.3 and 1.1 mm respectively and cover a range of Weber numbers at the exit of the nozzle from 200 to 3500, of gas-to-liquid momentum ratio from 2 to 250, velocity ratio from 10 to 85, mass flowrate ratio from 0.2 to 4, liquid jet Reynolds number from 10000 to 55000 and gaseous jet Reynolds number from 90000 to 190000. The Reynolds number of the gaseous jet was based

on the velocity averaged over the area of the annulus at the exit, U_g, and the exit diameter of the gaseous jet, D_{gas}. Also the other parameters were based on the gas and liquid velocities averaged over the area of the annulus and the area of the liquid jet respectively.

Swirl is another parameter affecting atomization. During the examination of the effect of swirl, the liquid tube had external diameter of 2.95 mm and internal diameter of 2.3 mm and the exits of the liquid and the gaseous jet were on the same plane. Two methods were used to generate swirling gaseous stream in the annulus. The first method used four tangential inlets, additional to the four axial inlets as shown in figure 1, to introduce gaseous flow in the annulus and generate maximum swirl number, S, at the exit of the nozzle with 10 mm annular width of the gaseous jet of around 0.35, according to equation (2). The swirl number decreased with the reduction of the nozzle annular width because of the increase of the friction on the wall of the annulus. The conditions of the examined sprays generated by swirling gaseous stream nozzles using the above method are shown in table 2. The second method used triple start helical swirlers to generate higher swirl numbers than the former method at the exit of the nozzle even for small annular widths. The swirlers consisted by three helical grooves, cut with 6.35 mm pitch, with their starts shifted by 120°, axial width of each groove 1.6 mm, wall thickness of 0.6 mm resulting in helix angles of 5°, 7.5° and 13° for the 10, 6 and 3 mm annulus respectively. The rest of the dimensions and the position of the swirlers in the gaseous jet with 3, 6 and 10 mm annulus are shown in figure 2b. The flow conditions at the exit of the nozzles with helical swirlers and the angle of the velocity vector at the exit of the swirler blades relative to the axis of symmetry of the spray are given in table 3. The swirl number could not be estimated according to equation (2), because the recirculation zone at the exit of the nozzle affects the pressure distribution and the measurements of U and W there do not represent the actual flow at the exit of the swirler. So the swirl number for the high swirl nozzles was evaluated according to the inclination of the velocity vector relative to the axis of symmetry at the exit of the swirler and its dimensions as suggested by Wall (1987) for guided vane cascade in an axial tube :

$$S' = \frac{2}{3}\left(\frac{1 - \left(\frac{D_{le}}{D_{gas}}\right)^3}{1 - \left(\frac{D_{le}}{D_{gas}}\right)^2}\right)\tan\alpha \qquad (2a)$$

where α is the angle of the vanes relative to the axis of symmetry at the exit of the swirler, D_{le} is the external diameter of the liquid tube and D_{gas} the diameter of the gaseous jet. The swirl number S' is given in table 3 and is larger than the critical value of 0.67 required for a recirculation zone to exist at the nozzle exit (Wall, 1987). However, comparison between the estimate by equation (2a) and the measured value by Joseph et al (1987) for a similar helical swirler shows overestimation by more than 100%. The helical swirler generated high swirl,

but the flow was not uniform at the exit of the nozzle because of the distinct jets emerging at the exit of each groove, while the tangential inlets generated low swirl but uniform.

The axial and swirling gas was supplied to the nozzle by a compressor and were metered separately by rotameters before passing to separate settling chambers. From each chamber four tubes supplied gas to the axial and tangential inlets of the experimental arrangement of figure 1. The liquid was pumped from a tank and the flowrate was adjusted by a valve in the return line of excess liquid to the tank and metered by a rotameter, which operated at a gauge pressure between 10 and 600 KPa. The atomizer was positioned in the vertical direction and the resulting spray exhausted vertically downwards towards a collection tank, which collected most of the liquid content of the spray. An exhaust system attached at the side of the collection tank removed the gas with the mist of the small droplets generated by the spray. Flow straighteners were positioned at the entrance of the collection tank to ensure that the spray remained undisturbed by the exhaust system. When swirl was generated by the helical swirlers, gas was supplied to the experimental facility only through the four axial inlets. The gas rotameters operated at a gauge pressure between 30 and 300 KPa and the flow rates were corrected to N.T.P. from calibration charts provided by the manufacturer. The gaseous and liquid flowrates supplied to the nozzle during the measurements were kept constant within 5%. The gas flow was occasionally seeded with TiO_2 powder, which was nominally micron-sized and small enough to trace the gaseous flow, when the velocity characteristics of the gas flow in the annulus at the exit of the nozzle and the development of the gaseous jet without the presence of a liquid jet in the flow were measured. The refractory powder was dispensed by two reverse cyclone feeders (Glass and Kennedy, 1977), which were connected at two of the axial inlets of the atomizer. The gas flowrate calculated by the integration of the axial velocity profiles of the gas flow measured at the exit of the nozzle were within 15% of that measured by the rotameters and this agreement was satisfactory after taking into account the uncertainties involved in the measurement and the integration procedure.

2.2 Single spray impingement on a flat disc

A flat horizontal disc of 50 mm diameter was positioned 215 mm downstream from the nozzle exit of figure 1 and the geometry and the reference coordinate system are shown in figure 3. The choice of a distance of 215 mm between the nozzle exit and the disc is justified by the approximate distance between the faceplate, where the injector elements are supported, and the turbopump dome in the combustion chamber of the preburners of the SSME. The coaxial injector was the same as that described above and the tests were limited to impingement of sprays produced by nozzles with axial gaseous stream. The gas and the liquid flowrate of the sprays were varied according to cases 2, 14 and 19 of table 1a.

2.3 Multiple coaxial airblast atomizers

The effect of the interaction between sprays produced by multiple identical nozzles was studied by modifying the experimental facility of figure 1 to include three identical nozzles with liquid tube external and internal diameter 2.95 and 2.3 mm respectively and annular width of the gaseous stream 3 mm positioned in a triangular arrangement with 18 mm distance between their axis of symmetry, as shown in figure 4. The gas and liquid flowrates were supplied and metered in the same way as for the single nozzle tests. Differences between the gaseous and liquid flowrates supplied to each of the nozzles were less than 5% during the tests. The tests included sprays produced by nozzles either with axial only gaseous flow or with swirling gaseous flow, generated by using the helical type swirlers described earlier in the text. The reference coordinate system used during the measurements is shown in figure 4.

2.4 Phase Doppler instrument

The velocity, diameter, flux and number density of the fuel droplets were measured by the phase-Doppler velocimeter (Hardalupas, 1989 & 1990), which comprised transmitting optics based on a rotating grating as beam splitter and frequency shifter and integrated receiving optics which collected the light scattered from the measuring volume in the forward direction at an off-axis scattering angle of 30° on the bisector plane of the two laser beams to ensure that refraction through the droplets dominated the scattered light. The collected light was focused to the centre of a 100 μm slit and passed through a mask with three evenly spaced rectangular apertures before reaching the three photodetectors. The beam intersection angle of the anemometer was adjusted to allow the measurement of droplet diameters up to 360 μm and the optical characteristics of the instrument are given in table 4.

The measured size distributions and the mean diameters at each point were based on 20000 measurements resulting in statistical uncertainties of less than 2% (Tate, 1982) and the sizing accuracy of the instrument was less than 2 μm for droplets larger than 20 μm. The uncertainty is larger for the smaller droplets due to the tolerance of the phase-measuring electronic circuit and the oscillations of the phase shift remaining on the calibration curve of the instrument (Hardalupas, 1989). Droplet velocities were obtained in 60 size classes, with a 6 μm range in each size class. The uncertainties were less than 1% and 4% for the mean and rms values respectively, based on the average sample size of at least 1000 in each class for the smaller sizes and around 2% and 6% for the larger droplets due to the smaller sample size. The reduced number of measurements in the larger droplet size bins is due to the low number density of large droplets in the spray.

The representative diameters of the sprays were estimated from the temporal size distribution (# / m^2 s), which is related to the flux of liquid droplets, rather than the spatial (# /

m^3), which is related to the number density of the droplets, as explained by Hardalupas and Taylor (1989) and Bachalo et al (1988). The reason for this choice is that the liquid flux is a conserved quantity and is used by current prediction models for the calculations of local droplet characteristics as explained in detail by Dodge et al (1987). The representative diameters used to characterise the sprays were the Arithmetic Mean Diameter (AMD), the Sauter Mean Diameter (SMD) and the Mass Median Diameter (MMD) defined as follows :

$$AMD = \frac{\sum_{i=1}^{N} n_i \, d_i}{\sum_{i=1}^{N} n_i} \tag{3}$$

$$SMD = \frac{\sum_{i=1}^{N} n_i \, d_i^3}{\sum_{i=1}^{N} n_i \, d_i^2} \tag{4}$$

$$MMD = d_{0.5} = \text{diameter carrying the 50\% of the cumulative mass flux} \tag{5}$$

where n_i is the number of measurements in the size bin "i" which corresponds to a droplet diameter d_i and N is the total number of bins. The overall statistical and measurement uncertainty of the mean diameters is expected to be around 5%.

The mean and rms of the fluctuations of the radial, V and v', and tangential, W and w', velocity components, as well as the time average cross correlation terms $\overline{uv}$ and $\overline{uw}$, were measured as a function of droplet diameter by rotating the plane of the laser beams by ±45° around the direction parallel to the axis of the flow. These two size-velocity correlation measurements combined with that in the direction of the axis of the system were used to estimate the radial and tangential velocity components according to the method described by Hardalupas and Liu (1992). The uncertainty of the mean and the rms of the fluctuations of the radial and tangential velocity components as a function of droplet size was 3% and 10% respectively, when the number of measurements in the considered size bins was around 1000. The corresponding uncertainty in the correlation coefficient $\overline{uv}/u' v'$ or $\overline{uw}/u' w'$ was around 20%. The number of individual droplet realisations at each point for each of the required three measurements was at least 30000, to provide statistical accuracy for the estimate of the radial and tangential velocity components.

The volume flux (m^3 of liquid / m^2 s) and concentration (m^3 of liquid / m^3) of the liquid droplets were measured according to the method of Hardalupas and Taylor (1989) and did not

involve droplets larger than 360 μm set by the size range of the instrument. Uncertainties in the measurement of flux and number density of the liquid droplets in sprays has been discussed by Dodge et al (1987), Bachalo et al (1988) and Hardalupas and Taylor (1989), although not in a conclusive way. During this study, the uncertainties were as follows. The size distributions indicated that the number of droplets larger than 300 μm was at least two orders of magnitude smaller than the maximum probability for most of the measurements, so the error to the flux and concentration measurement due to the contribution of droplet sizes larger than 360 μm was small. The rejection of measurements by the validation procedure of the instrument was larger in the dense region of the spray due to attenuation of the laser beams and occurrence of multiple droplets in the probe volume and resulted in systematic reduction of the flux measurements. Thus, the estimated values of the liquid flowrate after integration of the measured liquid flux radial profiles at axial distance around $z/D_{liquid} = 50$ from the nozzle was around 50% lower than the liquid flowrate measured by the rotameter, but the difference decreased with the increase of the axial distance from the nozzle. However, in some sprays farther away from the nozzle, the integration of the radial profiles of liquid flux resulted in estimated values of the liquid flowrate larger than that measured by the rotameters by as much as 30%. This observation is surprising, since the validation procedure of the instrument rejected around 20% of the attempted measurements at that location, but was also observed by Dodge et al (1987) who suggested that it was caused by the measurement of large droplets which were outside the probe volume of the instrument due to aberrations of the optics and misalignment. However, more information is needed to explain this effect and is currently under investigation. For this reason the radial profiles of flux are presented as relative values after normalisation by the local centreline value measured by the instrument and the relative flux is likely to be precise to within 15%. The rate of spread of the spray was evaluated using the measured flux half width at each axial station from the nozzle, namely the radial position where the liquid flux was half the value on the axis of the spray at each axial station, and the uncertainty of this measurement is expected to be around 15%, as for the relative flux. The concentration is expected to have similar errors as the liquid flux, although there is no way to check the error of this measurement since is not a conserved quantity.

3. RESULTS AND DISCUSSION

The sprays from single coaxial airblast nozzles with an external flow of gas are examined first and the effect of the nozzle geometry and swirl of the external gas flow then determined. The effects of impingement of the sprays and of interaction of sprays from three nozzles are quantified. The velocity characteristics of droplet sizes in the range of 6-12 μm, 48-54 μm and 102-108 μm, which are referred as 9, 50 and 105 μm in the rest of the text; the smallest droplets followed the mean and turbulent flow characteristics of the gaseous phase

faithfully, the 50 μm droplets corresponded to a value close to the most probable diameter in a large part of the spray and the 105 μm droplets indicated the motion of the droplets, which carry most of the liquid volume flux. The mean velocity and the rms of the fluctuations were normalised by the liquid velocity averaged over the area at the exit of the liquid tube, U_{liquid}, or the gas velocity averaged over the area of the annulus, U_{gas}, depending on the examined flow and will be explained in the text. The radial distances from the axis of the spray along the r and x directions, and the axial distance along the z direction from the exit of the nozzle were normalised by the diameter of the liquid jet exit, D_{liquid}, or the diameter of the gaseous jet, D_{gas}. The radial profiles of volume flux and concentration of the droplets were normalised by the local centreline value of the flux and concentration, G_m and C_m respectively, as measured by the instrument.

3.1 Sprays from single coaxial airblast nozzles with axial gaseous stream.

The characteristics of sprays with an axial gaseous stream have been presented by Hardalupas et al (1992) and Hardalupas and Whitelaw (1993) and both publications are attached as Appendix A. As a consequence a summary of the observations is presented in the following section and in tables 5a and b, which indicates the mean diameters at a distance of around 80 mm from the nozzle exit. The size characteristics should be compared close to the nozzle, since the rate of spread can affect the spatial distribution of the droplets and modify the mean diameters. The minimum distance from the nozzle exit was, however, limited by the ability of the phase Doppler instrument to measure in the dense spray and by the requirement of spherical droplets and an axial distance of 80 mm was chosen as a compromise. The change of the mean diameter along this distance from the nozzle was small and did not affect the conclusions.

a) The characteristics of the sprays

Figure 5 presents the characteristics of coaxial atomizer sprays for an annular width of the gaseous jet of 10 mm, exit Weber number of 208 and momentum ratio of 13.6 (case no. 1 of table 1a) at axial distances z/D_{liquid}=26, 52, 91 and 130 from the nozzle. The spatial variation of the characteristics of all the examined sprays are qualitatively similar to the case presented below.

The radial variation of the arithmetic, Sauter and the mass mean diameters of the spray show large values at the centre, where the liquid jet breaks up, and smaller towards the edge of the spray. The small droplets were generated by the high shear at the interface between the fast moving gas jet and the liquid jet at the initial stage of breakup or, later, by secondary breakup of the larger droplets, which remain close to the centre. This suggests that the finding of Caré

and Ledoux (1991) with a laser diffraction instrument, namely that the Sauter Mean Diameter (SMD) was a minimum at the centre, was erroneous and due to averaging of the spray droplet diameters over the line of sight of the diffraction instrument. Also, the observation of two maxima in the radial distribution of the SMD, one at the centre and one at the edge of the spray (Eroglu and Chigier, 1991) may be a characteristic of the near nozzle region at low exit Weber number condition, which does not correspond to the conditions of the sprays in the preburners of the SSME. One observation from our results is that the ratio of the Mass Median Diameter (MMD) to the Sauter Mean Diameter (SMD) was around 1.2 (tables 5a and b), and the size distributions of the sprays close to the nozzle follow the root-normal distribution for this ratio as suggested by Simmons (1977) and observed also by Ferrenberg et al (1985), Lefebvre (1989) and Faeth (1990). So, according to Simmons (1977), the SMD is sufficient to describe the size distribution and will be used in the rest of the text to quantify the quality of atomization.

Most of the volume flux of the liquid droplets remained close to the axis and the radial position where the spray flux became half of its centeline value, defined as the flux half width of the spray, increased from around $1.5D_{liquid}$ at $z/D_{liquid}=26$ to around $4D_{liquid}$ at $z/D_{liquid}=130$ and is an important parameter for the mixing of the liquid droplets with the surrounding gas.

The mean axial velocities of the 9, 50 and 105 μm droplets were low close to the axis and suggest delayed acceleration of the gas in the central part of the spray, while the droplet velocity was higher away from the axis where the gas velocity was also higher and accelerated the droplets. The rate of acceleration of the droplets in the central region was higher than at the edge, and the velocity minimum disappeared after $z/D_{liquid}=91$. The small droplets moved faster than the larger droplets up to the shear layer of the gas jet and decelerated faster than the larger droplets, as the gas jet expanded and the gas velocity decreased, due to their better response to the gaseous phase. The large droplets at the edge of the spray moved faster than the gas since they could not follow the gas phase motion and maintained their upstream velocity for a larger distance. The velocity difference between small and large droplets quantified the slip velocity between the gas phase and the large droplets and so the local Weber number was of the order of 1 for droplet diameters equal to the Sauter mean diameter and much smaller than the exit Weber number.

The rms fluctuations of the axial velocity of the smaller droplets indicate the turbulence characteristics of the gaseous phase and were lower at the centre, where most of the liquid existed and led to a reduction of the turbulence characteristics, and a maximum in the shear layer of the jet. The fluctuations of the axial velocity of the large droplets were lower than those of the gas phase close to the nozzle, but became similar farther downstream. This occurred, in contrast to their negligible response to the continuous phase turbulence, due to the deterministic motion of droplets reaching at the measuring point from different upstream

positions with a wide range of axial velocities, as suggested by the 'fan-spreading' effect (Hardalupas et al, 1989).

It should be noted that the spray characteristics produced by nozzles with a coaxial gaseous stream were symmetrical around their geometrical axis of symmetry, as indicated by the results in figure 5. Sankar et al (1992) observed large asymmetries possibly due to the geometry of their nozzle which had a smaller annular width than the 3 mm, which was the minimum of the present study.

b) The effect of gas and liquid flowrates

Figure 6 shows the effect of gas flowrate on atomization and the rate of spread of the sprays produced by nozzles with 3 and 6 mm annular width of the gaseous jet, while the liquid flowrate remained constant. It should be noted that increase of the gas flowrate caused an increase of all the parameters used to scale the sprays, namely the exit Weber number and the gas-to-liquid jet momentum, velocity and mass flowrate ratio as indicated in tables 1a and b. The increase of the gas flowrate improved atomization, since the Sauter mean diameter along the centerline was lower for the higher gas flowrate for both nozzles with different annular widths. The Sauter mean diameter increased along the centreline up to a certain distance from the nozzle, as the small droplets dispersed away from the spray axis faster than the larger droplets. When the large droplets also dispersed away from the centreline, the Sauter mean diameter decreased again and the radial distribution of droplet sizes in the spray became more uniform as for the 3 mm annulus nozzle and closer to the nozzle for the higher gas flowrate because the droplet sizes in the spray were smaller and could respond to the gas phase flow and disperse in a shorter distance.

The increase in the gas flowrate also decreased the rate of spread (figure 6b) from both nozzles, in contrast to opposite expectations due to the improved atomization by the increased gas flowrate, and this suggests that the higher momentum of the gas phase jet close to the nozzle for the higher gas flowrate limited the spread of the otherwise finer droplets and, although the atomization was improved, the mixing of the fuel with the oxidiser was reduced. Thus, a compromise is required between finer atomization and mixing with the increase of the gas flowrate.

The effects of liquid flowrate on atomization and rate of spread of the sprays produced by nozzles with 3, 6 and 10 mm annular width of the gaseous jet are shown in figure 7. It reduced atomization with all these nozzles, but had little effect on the exit Weber number, since the change in the relative velocity between the gas and the liquid jet was small, but resulted in lower gas-to-liquid momentum, mass flowrate and velocity ratios, suggesting that the decrease of the momentum or velocity ratio for constant exit Weber number would result in poorer atomization. Also it seems that the exit Weber number cannot scale the performance of

the atomizers. It is also clear that increase of the liquid flowrate caused the rate of spread to decrease, as expected due to the poorer atomization. Thus, an increase in liquid flowrate results in poorer atomization and decreased rate of spread.

c) The effect of nozzle geometry

i) Gaseous tube diameter

Experiments were carried out with gaseous tube diameters of 8.95, 14.95 and 22.95 mm, corresponding to annular widths of 3, 6 and 10 mm respectively, but it is impossible to maintain all the other parameters, e.g. the exit Weber number, the gas-to-liquid mass flowrate, momentum and velocity ratio and liquid tube diameter, constant at the same time. For example, increase of the gaseous tube diameter, maintaining constant liquid tube diameter and gas-to-liquid velocity ratio, resulted in increased annular width and gas-to-liquid mass flowrate and momentum ratios and the effect of this diameter could not be studied independently. In summary, the results have shown that reduction of the gaseous tube diameter, while the liquid tube diameter remains constant, reduced the gas flowrate required to atomize the same liquid flowrate with the same efficiency.

ii) Liquid tube diameter

Liquid tube diameters of 2.3 and 1.1 mm were used with a wide range of gas and liquid flowrates, determined in tables 1a and b. Decrease of the diameter of the liquid tube by around 50%, improved the atomization by around 25%, but decreased the rate of spread of the sprays by 20%, for sprays with similar gas-to-liquid velocity ratios. So there is a trade off between improved atomization and rate of spread.

iii) Converging gaseous jet exit

A converging exit of the gaseous jet, with a half angle of 28° improved atomization by around 20% and 10% for gas-to-liquid velocity ratios of 24 and 41 respectively and the rate of spread by 20% for gas-to-liquid exit velocity ratios up to around 45 relative to the straight exit nozzle. For gas-to-liquid velocity ratios higher than 45 atomization was not improved but the rate of spread of the sprays was reduced close to the nozzle.

iv) Liquid tube recess

This effect was examined for the straight and the converging gaseous jet nozzles with 3 mm annular width at the exit. For the straight exit nozzle, a recess of $2D_l$ of the liquid tube improved atomization by 15% and a recess of $3D_l$ reduced it again. However, the recess improved the rate of spread of the sprays by around 40%, which could justify the differences in the local sizing characteristics and could be responsible for the improvement on combustion

stability observed by Wanhainen et al (1966). The effect of a liquid tube recess with the converging exit nozzle was to reduce atomization by 10% and 15% for recesses $2D_l$ and $3D_l$.with greater reductions for gas-to-liquid velocity ratios higher than 40.

d) Atomization in coaxial airblast nozzles with axial gaseous stream.

The empirical correlations used to reproduce the mean diameter of sprays produced by coaxial injectors, for example those of Kim and Marshall (1971), Lorenzetto and Lefebvre, (1977), Burick (1972) and Falk (1975) have limitations and only the two first include parameters, which allow them to extrapolate to conditions of the preburner of the SSME. None of these correlations can predict the size characteristics, although Ferrenberg et al (1985) suggested the use of that of Kim and Marshall (1971), since no other was available. However, no effort has been made to develop a physically based model to predict the size characteristics of sprays from coaxial airblast atomizers and this section attempts to remedy this omission based on present results.

The atomization mechanism will be divided in two parts : primary atomization, which is related with the initial break up of the liquid jet and secondary atomization related with the breakup of the initially generated droplets and ligaments due to the shear of the gaseous stream. The primary atomization of a liquid jet in a high speed gaseous stream was examined theoretically by Taylor (1940) using an analogy between the liquid jet surface and a flat liquid surface and suggested that, provided that the velocity of the gaseous stream is sufficient to avoid gravity effects, the length of the liquid core, L_c, is independent of the velocity of the gaseous stream, U_g :

$$\frac{L_c}{D_l} = K \left(\frac{\rho_l}{\rho_g} \right)^{0.5} \qquad (6)$$

and depends only on the density ratio and the diameter of the liquid tube and has been confirmed (e.g. Chehroudi et al, 1985). For low gas velocities, Eroglu et al (1991) showed that a more complex correlation exists for the length of the liquid core. However, according to Taylor (1940), the most probable droplet size decreases as U_g^{-2} and the range of droplet sizes in the size distribution depends on a parameter $q=(\rho_l / \rho_g)\,(\sigma / \mu_l^2 U_g^2)$. The subscripts g and l refer to the gas and liquid properties respectively, ρ is the density, μ is the viscosity and σ the surface tension. When q is very large the range of droplet sizes can vary by a factor of 5. This analysis would predict, for example, for case 10 of table 1a that the droplet sizes produced by the nozzle would be smaller than 40 μm, limiting the chances of the occurrence of secondary breakup.

Our observations show that the length of the liquid core was always of the order of the a few liquid tube diameters, D_l, in agreement with Taylor (1940), and rather independent of the gas velocity. However, the measured droplet sizes were much larger than the estimated values, which suggests that the assumption that the liquid jet surface is flat is not correct. The variation of droplet size with the diameter of the liquid tube and the liquid flowrate, which is not considered possible by the above analysis, supports the above argument. A mechanism for the primary breakup of the liquid jet, Faragó and Chigier (1991), is that a large scale instability at the edge of the liquid core breaks up the liquid jet into large droplets or ligaments and more work is required to establish the size distribution of droplets produced by the primary breakup of a liquid jet in coaxial atomizers. The existence of large droplets at the end of the primary breakup makes secondary breakup of the droplets very important and is examined below.

The droplet response time, τ, is defined as the time needed for a droplet to accelerate to 66% of the gas velocity and is :

$$\tau = \frac{\rho_l \, d^2}{18 \, \mu_g} = \frac{\rho_l}{\rho_g} \, \frac{d^2}{18 \, \nu_g} \tag{7}$$

where d is the droplet diameter under consideration. The mean flow timescales include the rate of acceleration, $T_{acceler}$, of the gas velocity in the centre part of the spray, figure 8a, given by :

$$T_{acceler} = \left(\frac{dU}{dz}\right)^{-1} = \frac{z_m - L_c}{U_{gm} - U_l} \tag{8}$$

where it is assumed that droplets at the edge of the liquid core had velocities equal to that of the liquid jet, U_l. For liquid core length, L_c, around $2D_l$, the values of $T_{acceler}$, U_{gm}, the velocity differences $(U_{gm} - U_l)$, $(U_g - U_l)$ and the maximum measured slip velocity along the centreline between the gas phase and the 105 μm droplets, $(U_{gc} - U_{lc})$, have been calculated from our measurements and are given in tables 5a and b. The residence time of the droplet up to an axial distance from the nozzle, z_m, where U_{gm} occurs, is :

$$T_{residence} = \frac{z_m}{U_l} \tag{9}$$

The timescale associated with the presence of a liquid core in the spray is :

$$T_c = \frac{L_c}{U_l} \tag{10}$$

where it was assumed that the velocity of the liquid is equal to U_l.

The turbulent timescale of the energy containing eddies of the gaseous flow, T_{turb}, is :

$$T_{turb} = \frac{\delta}{u'} \tag{11}$$

where $\delta = 1/8\ D_g$ is the lengthscale associated with the energy containing eddies and D_g is the diameter of the gaseous jet and u' is the rms fluctuations of the axial velocity of the gas flow. The turbulent timescale of the large eddies of the gaseous flow, $T_{large\ eddies}$, in the mixing layer is :

$$T_{large\ eddies} = \frac{\delta_m}{U_g - U_l} \tag{12}$$

as suggested by Crowe et al (1985) and Hardalupas et al (1992), where δ_m is the local width of the shear layer and $U_g - U_l$ the velocity difference of the two streams. The transit time, $T_{transit}$, of a droplet through a distance equal to the characteristic lengthscale of the gas flow, λ, is :

$$T_{transit} = \frac{\lambda}{| u_g - u_d |} \tag{13}$$

where u_d is the local droplet velocity and u_g is the local gas velocity and λ is either δ or δ_m.

An additional timescale is the total breakup time required for a droplet undergoing secondary breakup to reach to a stage that the droplet and all its fragments are stable and is defined as :

$$T_b = t_b \frac{d}{(U_{gc} - U_{lc})} \left(\frac{\rho_l}{\rho_g}\right)^{0.5} \tag{14}$$

where T_b is the dimensional time and t_b is the dimensionless time which is correlated with the local droplet Weber number as suggested by Pilch and Erdmann (1987) :

$$\begin{aligned}
t_b &= 6\,(We_{loc} - 12)^{-0.25} && 12 \le We_{loc} \le 18 \\
t_b &= 2.45\,(We_{loc} - 12)^{0.25} && 18 < We_{loc} \le 45 \\
t_b &= 14.1\,(We_{loc} - 12)^{0.25} && 45 < We_{loc} \le 351 \\
t_b &= 0.766\,(We_{loc} - 12)^{0.25} && 351 < We_{loc} \le 2760 \\
t_b &= 5.5 && 2670 < We_{loc}
\end{aligned} \tag{15}$$

for low viscosity liquids.

Ratios between a characteristic flow timescale and the response time of the droplet are defined as Stokes numbers and indicate the droplet response to the considered gas flow quantity. Thus, the acceleration Stokes number is defined as :

$$St_{acceler} = \frac{T_{acceler}}{\tau}, \qquad (16)$$

characterises the droplet response to the centreline flow acceleration and is most important in the quantification of secondary breakup. The lower the value of $St_{acceler}$, the larger the lack of response of the droplet to the acceleration of the flow so the larger the slip velocity. Also the residence Stokes number :

$$St_{residence} = \frac{T_{residence}}{\tau}, \qquad (17)$$

when much less than 1, means that the droplets do not have time to respond to the gas flow within the distance z_m. So the value of the local Weber number, defined as

$$We_{loc} = \rho_g \, d \, (U_{gc} - U_{lc})^2 / \sigma \qquad (18)$$

increases when $St_{acceler}$ and $St_{residence}$ are less than 1 and for We_{loc} larger than a critical value We_{crit} of 12 imply breakup (Clift et al, 1978; Pilch and Erdman, 1987; Lefebvre, 1989). Then the maximum stable diameter in a spray is defined as :

$$d_{max} = We_{crit} \, \sigma / \rho_g \, (U_{gc} - U_{lc})^2 \qquad (19)$$

According to tables 5a and b the lower the value of $T_{acceler}$, the larger the slip velocity between the gas phase and the droplets and the finer the atomization, which supports the suggested mechanism for secondary breakup.

The critical value of the Weber number may change according to :

$$We_{crit} = 12(1 + 1.077 \, On^{1.6}) \qquad (20)$$

where On is the Ohnesorge number :

$$On = \frac{\mu_l}{(\rho_l \, d \, \sigma)^{0.5}} \qquad (21)$$

and quantifies the viscous effects on the breakup of a droplet diameter d. For the present study the value of On is around 10^{-4}, and very small to affect the value of We_{crit}, which remains around 12. The value of the local Weber number in the measured sprays was around unity and below the critical value of 12 at the location of the measurements, which was always larger than 25 liquid tube diameter from the nozzle exit. So secondary breakup was complete upstream of the measurement location.

Our measurements have shown that most of the liquid content of the spray remains close to the centre where the droplet sizes are larger, do not disperse radially, have larger evaporation times, and are the major cause of reduced mixing between fuel and oxidiser. So the limiting characteristic for the performance of the injectors is the large droplet sizes close to the centre and reduction in their size implies reduction of the acceleration time of the gas flow. This is confirmed by figure 8b, which shows that case 3 has shorter acceleration time of the gas phase along the centreline and finer atomization according to figure 7b for the 10 mm annulus nozzle and table 5a. Figure 8b shows also that the centreline gas phase velocity, when no liquid jet is present, reaches a maximum immediately after the exit of the nozzle. So the most efficient injector would be that with the maximum possible value of slip velocity along the centreline, which is $(U_g - U_l)$, occurring just after the nozzle exit. For example, for sprays according to case 8 of the present study $(U_g - U_l) = 115.4$ m/s and equation (19) estimates a maximum stable diameter of the order of 35 μm.

The parameters affecting the value of $T_{acceler}$ include the distance from the nozzle exit, z_m, where the gas velocity is largest and is expected to be related to the gas-to-liquid momentum ratio and the nozzle geometry, which is known to affect mixing in coaxial gaseous jets, see for example Champagne and Wygnanski (1971) and Ribeiro and Whitelaw (1980). The maximum value of the gas velocity on the centreline, U_{gm}, is also important and may be related to the gas-to-liquid momentum, velocity ratio and nozzle geometry. However, the results in tables 5a and b suggest that the acceleration timescale $T_{acceler}$ of the gas phase and the maximum measured slip velocity $(U_{gc} - U_{lc})$ along the centreline are mainly affected by the momentum ratio for the same nozzle geometry, so the value of the momentum ratio could be used to evaluate the rate of acceleration in the sprays of the SSME and thus correlate the mean droplet sizes in the sprays and this is confirmed in figure 8c. Figure 8c shows that for increase of the gas-to-liquid momentum ratio above a value of around 80, has negligible effect on mean droplet sizes. However, for values of gas-to-liquid momentum ratio smaller than 60, the mean diameter increases and the atomization becomes poorer. The atomization characteristics of sprays from straight gaseous jet exit nozzle improve with the reduction of the annular width. It is expected that changes in the nozzle geometry affect the acceleration of the gas phase along the centreline and in this way the atomization process. The liquid to gas density ratio, ρ_l / ρ_g, and the gas viscosity, ν_g, affect the value of $St_{acceler}$ through the response time of the droplets and so affect the slip velocity between the droplets and the gas

and the atomization. The surface tension σ and the gas density affect the value of the local Weber number and so the maximum stable diameter, according to equation (19). So the above physical mechanism for secondary atomization in airblast coaxial atomizers is influenced by the gas-to-liquid momentum, velocity and density ratios, the gas density, the kinematic viscosity, the surface tension and the nozzle geometry.

The turbulent timescale can affect the rate of spread of the sprays and the equivalent turbulent Stokes number, St_{turb}, is :

$$St_{turb} = \frac{T_{turb}}{\tau} \qquad (22)$$

and, since the droplets carrying most of the liquid flowrate are larger than around 100 μm, their response time, τ, is around 33 ms, which is too large to allow them to respond to the 1 ms turbulence timescale of the flow. Also the turbulent Stokes number of the large eddies :

$$St_{large\ eddies} = \frac{T_{large\ eddies}}{\tau} \qquad (23)$$

is also very low, so the droplets cannot respond even to the larger eddies of the turbulent flow.

The transit Stokes number quantifies the droplet response to turbulence during the transit time through the eddy :

$$St_{transit} = \frac{T_{transit}}{\tau} \qquad (24)$$

and when it is smaller than 1 implies limited transport of momentum from the turbulent eddy to the droplets.

The turbulent and transit Stokes numbers increase with the distance from the nozzle (Hardalupas et al, 1989), so that the large droplets begin to respond to the gas flow turbulence and disperse away from the centreline. This explains the increased rate of spread of the sprays after a distance from the nozzle around $91D_{liquid}$. Also the low turbulent Stokes numbers close to the nozzle suggests that the initial droplet trajectories define the rate of spread in this region, which are affected by the interaction with the gaseous mean flow, and explains the effects of the converging gaseous jet exit, the liquid tube recess and the gas flowrate on the rate of spread. This observation has implications for the computer modelling of such sprays, since large droplets do not respond to the gas phase turbulence and there is no need to simulate the interaction with the gas phase turbulence in order to calculate the rate the spread in the region close to the nozzle.

The Stokes numbers associated with the liquid core and the breakup timescales are :

$$St_c = \frac{T_c}{\tau} \tag{25}$$

$$St_b = \frac{T_b}{\tau} \tag{26}$$

For values of St_c and St_b lower than 1, the droplets generated during primary and secondary breakup do not change their characteristics before the end of the liquid core and the secondary breakup respectively. For the atmospheric conditions of the sprays in the present study the values of both Stokes numbers are much smaller than 1 for droplets larger than around 50 μm. Increase of the gas pressure decreases the density ratio ρ_l / ρ_g and results in a decreased liquid core length proportional to the square root of the density ratio and decrease the droplet response time in proportion to the density ratio, so St_c increases as the square root of density ratio. So the droplets response starts earlier at high pressure. The effect of high pressure is also to increase St_b by a larger amount than St_c, so the droplets change their velocity characteristics during secondary breakup.

3.2 The effect of swirl in the gaseous stream on the spray characteristics

The results are presented separately for the low and high swirl numbers with the latter giving rise to a recirculation zone at the nozzle exit. The nozzle conditions of the examined sprays are given in tables 2 and 3 for the low and high swirl number respectively.

a) Low swirl number

The swirl of the gaseous stream was generated by four tangential inlets and was in the counter-clockwise direction. Nozzles with annular width of 10 mm with swirl numbers of 0.2 and 0.3 and annular width of 6 mm and swirl number of 0.1 were examined. The internal liquid jet diameter, D_{liquid}, was 2.3 mm and the external diameter 2.95 mm.

Figure 9 presents the mean diameters, the liquid flux, the mean and rms fluctuations of the axial, radial and tangential velocity components and the correlation coefficients $\overline{uv}/u'\,v'$ and $\overline{uw}/u'\,w'$ of the sprays produced by a nozzle with an annular width of the gaseous jet of 10 mm and swirl number of 0.3, according to case S1 of table 2, at axial distances z/D_{liquid} = 26, 52 and 91 from the nozzle. The above characteristics are qualitatively the same for all the examined sprays and are summarised below.

The Sauter mean diameter, figure 9a, was largest at the centre, where the liquid jet breaks up, and decreased to the edge of the spray, where the small droplets were again generated in the initial stage and due to the high shear at the interface with the fast moving gas jet and later due to secondary breakup of the larger droplets, which remain close to the centre. The effect of low swirl was small, so that the volume flux of the liquid droplets, figure 9b, had a maximum at the centre and was nearly uniform over larger area of the central region than for the axial gaseous stream sprays of figure 5. The radial position where the spray flux became half of its centeline value increased from around $2.5D_{liquid}$ at $z/D_{liquid}=26$ to around $16D_{liquid}$ at $z/D_{liquid}=130$, which was wider than with the axial gas flow. So the sprays produced with swirl resulted in better mixing between the gaseous fuel and the oxidiser.

The mean axial velocity profiles of the 9, 50 and 105 μm droplet sizes, figure 9c, show that there was no recirculation zone close to the nozzle exit, although there was a minimum on the axis and a maximum at the high shear region between the gaseous and the liquid jet stream. The 9 μm droplets moved faster than the larger droplets, at least in the central part of the spray, and the rate of acceleration of the larger droplets in the central part was higher than at the edge, and with no axial velocity minimum in the central region after $z/D_{liquid}=52$. The larger droplets moved faster than the gas flow at the edge of the spray and even at the centre after z/Dliquid=52, since they could not follow the gas phase motion and maintained their upstream velocity for a larger distance.

The mean radial velocity of the 9 μm droplets and so of the gaseous phase, figure 9d, was around 25% of the mean axial velocity close to the nozzle ($z/D_{liquid}=26$) and larger than that of the larger droplets due to the delayed response of the larger droplets to the gas flow characteristics. The radial velocity increased with the radial distance from the axis of symmetry and had a maximum at the edge of the spray for the larger droplets which was higher than that of the gas phase. Although the radial velocity of the gaseous phase reduced with the axial distance, as the gaseous jet expanded, the large droplets maintained their large radial component up to $z/D_{liquid} = 91$ and moved away from the centre of the spray for a larger distance than the gas phase. The mean tangential velocity, figure 9e, of the larger droplets lagged behind the gas phase close to the nozzle, but after $z/D_{liquid} =52$ all droplet sizes had similar mean tangential velocity component, which was not observed for the radial component. This difference between the behaviour of the radial and tangential velocity components of the large droplets was due to the centrifuging of the latter away from the axis of the spray by the tangential movement acquired by the gas phase. The centrifuging caused the large radial velocity component away from the axis, in agreement with observations in swirling kerosene burners (Hardalupas et al, 1990). The centrifuging of the large droplets was responsible for the faster spread of the spray and the uniform liquid flux distribution in the central region.

The rms of the fluctuations of the axial velocity, u', was higher than those of the radial, v', and tangential, w', velocity components, figures 9f, g and h, and the anisotropy increased with droplet size in accord with the 'fan spreading' effect. Since the large droplets cannot respond to the gas phase turbulence, they move with straight trajectories and maintain their upstream velocities over larger distances, which justifies the observed increase of the axial velocity fluctuations. With the radial or tangential rms velocities of the droplets, the differences were small through out the flow.

The correlation coefficients, $\overline{uv}/u'\,v'$ and $\overline{uw}/u'\,w'$, figures 9i and j, of the large droplets were larger than those of the gas phase and those of $\overline{uv}/u'\,v'$ were around unity indicating the deterministic motion of the droplets in support of the 'fan-spreading' effect. The values of $\overline{uw}/u'\,w'$ were much smaller than those of $\overline{uv}/u'\,v'$, indicating no correlation between the fluctuations of the axial and tangential velocity components for the large droplets after $z/D_{liquid} = 52$, which is expected since the droplets did not respond to turbulence and there is no mean flow effect similar to centrifuging, which affected the radial velocity, for the tangential velocity. The velocity characteristics of the 9 μm droplets agree qualitatively with the gas phase measurements of Ribeiro and Whitelaw (1980) and suggest a delay in the development of the gaseous flow close to the axis of the symmetry, because of the delayed momentum transfer from the gas jet to the liquid droplets.

b) High swirl number

The high swirl gaseous stream was generated by helical type swirlers and was in the clockwise direction, in contrast to the counter-clockwise direction of the low swirl. The characteristics of the spray produced by a nozzle with annular width of 10 mm and conditions according to case S4 of table 3 at axial distances from the nozzle exit $z/D_{liquid} = 1.3$ and 26 are presented below and are representative of the sprays produced by the 3 and 6 mm annular width nozzles.

The main difference between the low and high swirl number flows is the presence of a recirculation zone of the gas phase close to the exit of the nozzle, as indicated by the mean axial velocity profile at $z/D_{liquid}=1.3$, figure 10a. No measurements were obtained close to the axis of summetry and at the nozzle exit, because of the liquid jet. The reduced slip velocity inside the recirculation zone delayed the initial breakup of the liquid jet which began at around $10D_{liquid}$ with the liquid jet spreading out and breaking into ligaments at large radial distance from the axis and reaching outside the recirculation zone, where the fine droplets were generated as a consequence of the high velocity gaseous stream. The larger droplets followed partially the mean gas phase flow and recirculated moving towards the nozzle exit, figure 10a, where a large amount of liquid reached the wall of the gaseous jet and built a liquid film,

which reatomised at a later stage. At $z/D_{liquid} = 26$, the recirculation zone was limited to a small central region and all the droplets moved with similar velocities, suggesting that the development of flow was faster than for the previously examined sprays. The values of the radial and tangential velocity components at the exit of the nozzle, $z/D_{liquid} = 1.3$, figure 10b, were similar to that of the axial velocity in the free stream outside the recirculation zone, which agrees with the expectations for high swirl number flows. The large droplets had tangential velocities similar to those of the gas phase and higher radial velocity close to the edge of the spray indicating some centrifuging of the large droplets to the wall of the gaseous jet. The recirculation zones with annular widths of 3 and 6 mm were smaller, and the liquid core length was shorter and varied between 8 and $10D_{liquid}$.

The rms fluctuations of the axial velocity, figure 11, had large values at the shear layer between the recirculation zone and the free stream at $z/D_{liquid} = 1.3$ and 26. Although this is expected for the gas phase and so for the 9 μm droplets, it is not clear why the large droplets had similar characteristics, since they cannot respond to the turbulence of the gas flow. However, the probability density functions of the axial velocity of the large droplets in the shear layer were bimodal, with distinct maxima at velocities around zero and large positive values, causing the large values of the rms fluctuations. This was also observed by Hardalupas et al (1992) and it was a result of the partial interaction of droplets with the larger eddies of the gaseous flow. This phenomenon becomes important in reacting flows because large eddies can cause large temporal variations of the local liquid concentration (Crowe et al, 1985; Lazaro and Lasheras, 1989; Squires and Eaton, 1990) and so of the local mixture fraction, which can limit the ability of the mixture to react and affect the stability of the flame.

The centreline characteristics of the sprays are presented in figure 12 and show that the mean axial velocity of the droplets after the breakup of the liquid jet was large and positive, but soon decelerated by the gas phase recirculation zone, which extended at the central part of the spray after z/D_{liquid} around 20. The large droplets although decelerated, they had low but positive mean axial velocity at the same region. Farther downstream the centreline values indicated that the recirculation zone ended, but that was because of some asymmetry of the flow and some precession of the central region, since the radial profiles of mean axial velocity indicated a recirculation zone still existing off the centreline. The mean diameter along the centreline was large close to the nozzle where the liquid jet broke up and large droplets existed in the flow which broke up or moved away from the centreline quickly, resulting in a nearly constant value of around 80 μm along the centreline.

It should be noted that the flow at the exit of the helical swirler was not uniform, but three distinct jets existed at the exit of its three grooves. The gas flow downstream of the nozzle exit developed as three distinct jets, which spreaded out following a spiral motion and interacted with the increase of the axial distance from the nozzle exit. The radial profiles were measured on a Cartesian coordinate system and thus indicated the stage of development of

these jets at different distances from the nozzle, and thus can generate a misleading conclusion that large asymmetries existed in the sprays, which were symmetrical around their geometrical axis if a cylindrical coordinate system was considered. In order to provide more information on the development of the three distinct jets with the distance from the nozzle exit, the following mean diameter and flux radial profiles are presented in the x and r directions of the Cartesian coordinate system, which formed a cross. Small asymmetries in the spray can be caused only due to small differences in the gas flowrate through each of the three helical grooves of the swirler.

The Sauter mean diameter, figure 13, had a maximum at the central region close to the nozzle exit, $z/D_{liquid} = 1.3$, and reduced at the edge. This is because the liquid jet was still breaking up in this region of the flow and larger droplets existed which moved away from the centre as the mean radial velocity, figure 10b, indicated. Some of the large droplets followed partially the gas phase recirculation zone and moved towards the nozzle exit, where they reached the wall of the gaseous tube and generated a liquid film, which disintegrated by the shear of the gas flow and reatomized causing the local maxima of the SMD at $r/D_{liquid} = 6$. Farther downstream, the droplet sizes broke up due to shear by the high velocity gaseous stream and the spray had a minimum SMD at the centre and a maximum value of around 100 μm away from the centre. The liquid flux profiles, figure 13b, indicated a hollow cone type spray with a net transfer of a small amount of liquid towards the nozzle at the centre, while most of the liquid was away from the axis of symmetry of the spray and moved away from the nozzle. The liquid flux profiles were normalised with the measured maximum value at each axial distance, G_{max}. The differences between the x and r direction of the flow show asymmetries but the characteristics of the sprays were the same in both directions.

Figure 14a and b shows the Sauter mean diameter and the liquid flux profiles respectively for the 3 mm annulus nozzle (case S6 of table 3). This nozzle was used for the later study of the interaction between multiple sprays. The symmetry of the spray close to the nozzle was improved relative to the 10 mm annulus nozzle, because of the smaller dimensions of the nozzle. The values of the SMD were higher than those of case S4 by around 20%, but the rate of spread of the sprays was similar. The spray was hollow cone type, but the net liquid flux remained always positive indicating no strong effect of a gas recirculating region at the central part of the spray. Similar characteristics were observed for the 6 mm annulus nozzle (case S5 of table 3).

c) Comparison between sprays with swirling and axial gaseous stream.

Comparison between sprays produced by nozzles with axial only and low swirl number gaseous streams, figure 15, suggests that for the same gas and liquid flowrates there was no improvement of the atomization with the increase of the swirl number, as the results

close to the nozzle exit suggests, where the SMD was less affected by the spreading of the sprays. For the small swirl number of 0.2, a reduction in the atomization was observed relative to the axial gaseous stream. This is justified by the lower centreline values of the gas velocity, figure 15b, caused by the faster spread out of the swirling gaseous jet relative to the axial flow jet, resulting in lower $T_{acceler}$, which, according to our suggestion in the previous section, results in reduced secondary breakup and is correlated with poorer atomization. Also, calculations by Lian and Lin (1990) suggest that the swirling gas stream has two counteracting stabilising and destabilising effects on the liquid jet and under certain conditions the stabilising mechanism can become dominant and reduce the efficiency of the primary atomization. The large differences between the SMD for different cases on the centreline downstream of $z/D_{liquid} = 80$ were caused by the differences in the rate of spread of the sprays as shown in figure 15c.

The main advantage of the swirling gaseous stream sprays is that the rate of spread is larger, mainly due to the centrifuging of the larger droplets, figure 15c. Nevertheless, a minimum swirl number of 0.2 is required to be able to centrifuge the droplets, since for a swirl number below that value the rate of spread is slightly reduced relative to the case without swirl. The small reduction in the rate of spread of the sprays may be explained by the decrease of the gas pressure in the central region induced by the swirling motion, which cause some of the generated droplets after the breakup of the liquid jet to move initially towards the centre and then spread out and in this way reduce the rate of spread. This mechanism is similar to the stabilising effect of swirl on atomization suggested by Lian and Lin (1990).

The radial profiles of the SMD at z/D_{liquid}=52 and 91, figure 16, are presented to explain why the centreline development of the SMD for a swirl number of 0.3, figure 15a, decreased fast after z/D_{liquid}=60. At z/D_{liquid} =52 the values of the SMD were similar for both the axial and swirling gaseous streams. Farther downstream, a large number of droplets with SMD around 70 μm existed in the swirling spray in a region outside the boundary of the axial gaseous stream spray. So these droplets were dispersed faster by centrifuging due to the swirl acquired by the gas flow within this axial distance from the nozzle and reduced dramatically the SMD on the centreline.

Sprays with high swirl number gaseous stream appears to be the best choice over the rest of the sprays examined till now. Figure 17 shows that the SMD of high swirl sprays at $z/D_{liquid} = 26$, so quite close to the nozzle, was much smaller than that of the rest of the sprays and the rate of spread was much larger since the maximum of the liquid flux existed outside the centreline. So the high swirl sprays improved atomization and mixing relative to the low swirl number and axial gaseous stream sprays. The gas flowrate required in the high swirl sprays to atomize sufficiently the liquid jet was lower than that in the low swirl, which allows more flexibility to control the gas-to-liquid mass flowrate ratio and so the gas-to-oxidiser ratio of each individual nozzle. However, it should be noted that the liquid core length for the high

swirl sprays was longer than that of the other sprays, but this is not considered to be a limiting factor for the performance of the preburners in the SSME. Also the build up of liquid at the wall at the exit of the gaseous stream, because of the recirculation zone at the exit of the nozzle, could cause local overheating problems in the preburner.

d) Atomization in coaxial airblast nozzles with swirling gaseous stream.

The mechanism causing the atomization in swirling gaseous stream nozzles will be examined in the following section.

For low swirl numbers, the mechanism is the same as for the axial gaseous stream nozzles. The large droplet sizes remain on the central part of the flow and are still the limiting factor on the performance of the atomizers. The secondary breakup is again mainly influenced by the acceleration of the gaseous flow along the centreline. Since the swirl does not change significantly the development of the gas phase flow along the centreline small differences are observed in the atomization characteristics of these sprays.

An additional timescale affecting the swirling sprays is that associated with the tangential velocity. If we consider a swirling vortex the associated timescale T_{swirl} is :

$$T_{swirl} = \frac{1}{\omega} \tag{27}$$

where ω is the angular velocity of the swirling vortex. The corresponding centrifuge Stokes number is then defined as :

$$St_{\omega} = \frac{T_{swirl}}{\tau} = \frac{18\ \mu_g}{\rho_l\ \omega\ d^2} \tag{28}$$

which was suggested by Dring and Suo (1978) and quantifies the centrifuging effect in the swirling gaseous stream sprays. τ in equation (28) was replaced by its value from equation (7). Assuming that the radius of the swirling vortex is R_g, the radius of the gaseous jet, and that the tangential velocity W was as measured, $\omega = W / R_g = 15 / 11.5 = 1.3$ ms. When St_{ω} is less than one, then the droplets will be centrifuged. The centrifuging effect increases the rate of spread of the sprays possibly without improving the atomization characteristics. However, the gas jet expands and the tangential velocity W is reduced with the distance from the nozzle. So the ability of the droplets to acquire tangential velocity component large enough for centrifuging depends on their residence time through the flow, which is :

$$T_{residence} = \frac{z}{U_l} \tag{29}$$

where z is the axial distance from the nozzle. The equivalent transit Stokes number :

$$St_{residence} = \frac{T_{residence}}{\tau} \qquad (30)$$

should be around 1 for droplets to acquire significant tangential velocity, so for example, for the case S1 of table 2, 100 μm droplets which have response time around 33 ms will travel a distance $z=U_l \tau$ = 3.6 m/s x 33 ms = 120 mm from the nozzle exit before acquiring tangential velocity components, which corresponds to $z/D_{liquid}=52$. This is the reason that there is a critical swirl number of around 0.2 associated with the examined sprays, below which no centrifuging occurred, because the initial tangential velocity of the gas flow was small and reduced with the distance from the nozzle and the droplets required a distance of $z/D_{liquid}=52$ to acquire it. However, this mechanism alone cannot explain the reduction of the rate of spread observed for swirl number around 0.2 and the low gas pressure generated by the swirling motion close to centre, as explained earlier in the text, may explain this effect. So there are two counteracting mechanisms affecting the rate of spread, the centrifuging of the droplets due to swirl, which increases the rate of spread and the gas pressure gradient in the radial direction, which decreases it. For swirl number lower than 0.2 the latter mechanism is dominant.

An alternative way to improve secondary atomization is to make the large droplets to spread away from the centreline in the high velocity gaseous stream, close to the nozzle and before the gaseous stream decelerates with jet expansion, where the slip velocity is large. The nozzle with converging gaseous jet exit examined in section 3.1 attempted to use the above effect by increasing the radial velocity close to the nozzle but was limited because the high axial velocities made the droplets move along slightly inclined trajectories relative to the vertical direction without allowing them to spread quickly in the high speed gas stream. The introduction of high swirl succeeded, because the recirculation zone at the nozzle exit delayed primary breakup of the liquid jet, caused spreading and directed the ligaments away from the centreline. The resulting droplets spread rapidly with better mixing between the gas and the liquid. The centrifuge Stokes number quantified the centrifuging of droplets by the swirling vortex, as explained above, or the centrifuging of droplets by the recirculating zone if it is considered as a vortex with a representative angular velocity. The latter use of the centrifuge Stokes number can quantify the amount of liquid reaching the wall of the gaseous jet.

3.3 Spray impingement on a flat disc

The sprays produced by 10 and 3 mm annulus nozzles with 2.3 mm liquid tube diameter were arranged to impinge on a flat disc with 50 mm diameter at z/D_{liquid} = 93.5 from

the nozzle exit according to the geometry of figure 3. The conditions corresponded to case 2 for the 10 mm annulus and to cases 14 and 19 for the 3 mm annulus, as in table 1a. The characteristics of the free spray were measured at $z/D_{liquid} = 91$, and the impinging spray at distances from $z/D_{liquid} = 87$ to 92.2 upstream of the disc, corresponding to 15 and 1.5 mm from the disc surface respectively, and on the side and downstream of the disc from $z/D_{liquid} =$ 93.5 to 95.2, corresponding to the level of the disc and 4 mm downstream of its surface respectively. The effects of gas and liquid flowrates were examined in terms of mean diameter, liquid flux and concentration distributions and correlations between size and axial and radial velocity components and the shear stress $\overline{uv}$. This section presents and compares the characteristics of free and impinging sprays and evaluates the mechanisms for secondary breakup during impingement.

a) Characteristics of free and impinging sprays.

i) Free Spray

The radial development of the free spray is required for comparison to the spray striking the disc and the profiles of the mean axial velocities of droplets in the 9, 50 and 105 μm size ranges, Sauter mean and Median diameter, liquid flux and liquid concentration are presented in figure 18 at $z/D_{liquid} = 91$. The maximum Sauter mean diameter was about 150 μm on the centreline and reduced to around 80 μm at the edge. The flux profile, which is normalised with the centreline value, shows that most of the liquid content of the spray remains close to the centre and the flux half width was around $3.5D_{liquid}$. The concentration of the liquid content of the spray, expressed as the volume of liquid per unit volume of space and normalised by the centreline value, C_m, was similar to the flux profile with a concentration half width of around $3D_{liquid}$. The axial mean velocity of the 9 μm droplets, which approximates that of the gaseous flow, was about 50 m/s on the centreline and the slip velocity between the gas and the 50 or 105 μm droplets there was negligible. The gas velocity decreased with the radial distance from the centre, while the 50 and 105 μm droplets maintained their velocity for longer distances and moved faster than the gas phase away from the axis of symmetry of the spray. In the following section, it will be assumed that the free spray characteristics were unchanged between $z/D_{liquid} = 87$ and 95 and the profiles at z/D_{liquid} =91 will be used for comparisons between the free and impinging sprays.

ii) Spray striking the disc

There are three regions in the impinging spray, where the characteristics are affected by different mechanisms. The region upstream of the disc, before $z/D_{liquid} = 89.6$, the near disc region, between $z/D_{liquid} = 89.6$ and 93.5, and the region downstream and on the side of the disc, between $z/D_{liquid} = 93$ and 95.

In the first region, the disc is bound to cause a gaseous jet to spread faster than the free jet before reaching the disc (Bearman, 1972) and so the deflection of the spray by the disc is the dominant mechanism which changes the spray characteristics. The gas flow can disperse certain droplet sizes from the axis faster than in the free spray, and this effect was identified in the calculations of a Diesel spray impinging on a wall made by Naber and Reitz (1988), although without a strong coflowing gaseous stream as in our case. The flux and concentration measurements confirmed this effect with figures 19a & b showing that the flux and concentration half width of the spray increased by around 25% as it approached the disc, from z/D_{liquid} 87 to 89.6, while their radial profiles remained similar to that of the free spray. The arrows on the graphs indicate the position of the edge of the disc which is at r/D_{liquid}=10.9, and show that the spread of the free spray at this distance from the nozzle resulted in a diameter larger than that of the disc, so that some of the droplets outside the region of the disc came directly from the nozzle and not only after deflection by the disc and carried little liquid flux. The Sauter mean and Median diameters of the impinging spray were reduced on the centreline by around 10% and increased by around 20% at the edge, figure 19c, relative to the free spray, figure 18, suggesting that some droplets were deflected from the axis of the spray due to the disc. The mean axial velocity of the 9 μm droplets, which indicated the gas phase flow, was slightly reduced on the centreline relative to the free spray, figure 19d, and the larger droplets in the central region moved faster than the gas phase, while the opposite was observed in the free spray. However, the slip velocity between large droplets and the gas phase remained negligible on the centreline and the same as in the free spray at the edge. The mean radial velocity of the 9 μm droplets increased in this region, figure 19e, while that of the 50 and 105 μm droplets remained unchanged and suggested that the deflection of the spray by the disc, resulting in the larger rate of spread, was due to droplets smaller than 50 μm. The rms of the fluctuations of the axial velocity of the 9 μm droplets was larger than that of the radial velocity, figures 19f and g, and indicated anisotropy of the order of 70%, as expected for a gaseous jet flow, and of the order of 50% for the larger droplets, in agreement with the 'fan-spreading' effect (Hardalupas et al, 1989). The sign of the correlation coefficient $\overline{uv}/u'v'$ of the 9 μm droplets, figure 19h, followed the gradient transport according to the axial velocity gradient of the gas phase and was of the order of 0.6, while the larger droplets had larger coefficients in agreement with their deterministic trajectories suggested by the 'fan-spreading' effect. At z/D_{liquid} =89.6, however, the correlation coefficient of the gas phase decreased, as the influence of the disc became important and the correlation coefficient of the 50 μm droplets changed sign close to the edge for reasons discussed below.

The region close to the disc was characterised by large redistribution of droplets and change of their size due to reatomization. Radial profiles were measured at z/D_{liquid}=90.9, 92.2 and 92.8. The flux measurements have been separated into positive and negative

components, figure 19a, depending on whether the instantaneous axial velocity component was directed towards, or away from, the disk and the net flux, being the algebraic sum of the two previous components, indicates the net transport of liquid. The profiles have been normalised by the centreline value of the net flux, G_m, or the maximum value, G_{max}, where the centreline value was not measured because of the limited optical access. The arrow on the graphs corresponds to the position of the edge of the disc, which is at r/D_{liquid} =10.9. The net flux was larger than that of the free spray at the edge of the disc, figure 18, and the measurements extended to around r/D_{liquid} = 25, indicating that the width of the spray was broader as a result of striking the disc. The flux of negatively-directed droplets (presented as the modulus of the flux value) exists mainly at r/D_{liquid} > 10 at z/D_{liquid} =90.9 but, as the spray approached the disc, the maximum value of negative flux at z/D_{liquid} =92.2 was above the disc area and between r/D_{liquid} 5 and 11. The negative flux decreased outside the disc area because droplets with initial negative axial velocity were deflected and gradually moved downstream of the disc, either by the gas flowing around the disc, or by gravity, which acted in the positive axial direction. The positive flux was larger than the negative flux at z/D_{liquid} =92.2, so that the net transport of liquid was towards the disc but, father downstream, at z/D_{liquid} =92.8, the negative flux became larger at the edge of the disc and the net transport of droplets was away from the disc surface. Close to the surface of the disc there was a net transport of reatomized droplets from the disc and sideways, because of the direction of the gas flow above its surface. The maximum measured value of negative flux was about half the centreline value and occurred at r/D_{liquid} > 8 and, because this flow was near axisymmetric, represented a substantial flow rate of reatomized liquid, given that negatively-directed droplets could only arise because of impingement of the spray on the disc.

The liquid concentration profiles of figure 19b were not similar to the flux profiles in this region and indicated high values close to the edge of the disc, where most of the reatomized droplets existed. This suggests the existence of an oxidiser-rich region at the edge of the disc, which was not indicated by the flux profiles, and can influence the location where ignition can occur close to the turbopump dome in the preburner of the SSME. It also emphasizes the importance of concentration measurements to identify fuel rich or lean regions, when droplets with either positive or negative velocities exist. Also, the motion of the droplets close to the disc is important in identifying the mechanism that modified the concentration profiles and is examined in detail in the next section.

The flow pattern that can be inferred from the mean axial and radial velocity component of the droplets in the 9, 50 and 105 μm size range, figures 19d and e, is consistent with the flux and concentration profiles. The mean axial velocity of the 9 μm droplets was reduced relative to the free spray at the area above the disc surface and small negative mean values appeared away from the centreline between r/D_{liquid} =5 and 10 at z/D_{liquid} =92.2, which coincided with the region of maximum negative flux and identified locations where

reatomized droplets were most likely to appear. The low values of axial velocity of the 9 μm droplets near the surface of the disc were due partly to the decrease of the axial velocity component as the gas approached the surface of the disc, which also slows the 9 μm droplets and partly to the generation of bimodal velocity pdfs, as discussed below, with pronounced low velocity peaks. The mean axial velocity of the larger droplets was also reduced by a smaller amount than the 9 μm droplets, which may be due to droplet deceleration by the gaseous flow, although the corresponding velocity probability distribution functions (pdf) were bimodal and suggest that the mean velocity value was reduced by the reatomized low velocity droplets which coexist with the high velocity droplets from the incoming spray. The mean radial velocity of the droplets increased by around three times the value in the region farther upstream of the disc, as expected by the side movement of the gas flow above the disc, indicating a net radial transport of droplets from the area of the disc, which explains the maximum of the flux. However, the large droplets lagged the gas mean radial velocity, since their response time did not allow them to accelerate as fast as the gas. So the initial droplets from the free spray strike the disc and reatomize and are then transfered radially from the disc area by the radial motion of the gaseous flow.

The rms of the fluctuations of the axial velocity of the 9 μm droplets, figure 19f decreased close to the disc, while those of the radial velocity increased, figure 19g, in agreement with measurements of gaseous jets impinging on a flat wall, for example, Özdemir and Whitelaw (1992). This occurs because the turbulent fluctuations in the axial direction are suppressed by the presence of the wall, while those in the radial direction are enhanced (Bradshaw and Wong, 1972), due mainly to the modification of the lengthscale of the turbulent eddies, which is reduced in the axial direction and increased in the radial direction (Wei and Miau, 1992). The large droplets had much higher axial velocity rms fluctuations than the gas phase, due to their bimodal axial velocity pdfs and the 'fan-spreading' effect rather than their response to turbulence. This is confirmed by their reduced rms fluctuations of the radial velocity component relative to the gas phase, which can only be acquired by the response to the gas phase. The correlation coefficient $\overline{uv}/u'\,v'$ of the 9 μm droplets, figure 19h, changed sign away from the axis of symmetry, as the flow approached the disc, and became negative for $r/D_{liquid} > 5$. This was caused by the transition of the jet flow, which had a positive correlation coefficient, to a wall jet flow, which had a negative correlation coefficient. The correlation coefficient of the large droplets had similar characteristics, since close to the axis of symmetry most of the droplets came directly from the nozzle, while those away from the axis were mainly reatomized and transfered from the centre than directly from the nozzle.

More direct evidence of secondary atomization is provided by the shape of the probability distribution function of the axial velocity component. For the purposes of subsequent comparison, the pdf of axial velocity of droplets in the 9 μm, 50 μm and 105 μm

size ranges as well as the pdf of all the droplet sizes of the free spray are shown in figure 20 for locations on the axis of symmetry and at the edge, at (r/D_{liquid}, z/D_{liquid}) = (0, 91) and (8.7, 91). The corresponding axial velocity probability distribution functions (pdf) for (r/D_{liquid}, z/D_{liquid}) = (0, 92.2) and (8.7, 92.2) and for (r/D_{liquid}, z/D_{liquid}) = (0, 90.9) and (8.7, 90.9) are shown in figures 21 and 22 a & b respectively and were typical of the region close to the disc. The comparison shows that the velocity distribution was bimodal in the impinging spray and the high velocity peak stemmed from droplets directly from the nozzle, without having come into contact with the surface of the disc. In contrast, the low velocity peak was generated by secondary atomization of droplets close to, and on the surface of, the disc and extended into negative axial velocities. The separation between the two peaks decreased with decreasing size, mainly because of the decrease in the magnitude of the velocity associated with the high velocity peak with decreasing size, caused by the stronger deceleration of smaller droplets due to the rapid deceleration of the gas as the disc was approached. The size - velocity correlation of droplets in the free spray at z/D_{liquid}=91 was negligible on the axis of the spray, and, thus, could not have influenced the observed reduction of the high velocity part of the bimodal pdf as a function of size in the impinging spray. The existence of a bimodal distribution, as see also Dementhon (1992) and Hardalupas et al (1992), is a useful indicator of reatomization and will be used below.

Examination of the axial velocity pdfs at different locations shows that reatomized droplets with low velocity and diameters up to around 120 μm at the centre and up to 180 μm at the edge existed at z/D_{liquid}=90.9 and up to around 160 μm at the centre and up to 230 μm at z/D_{liquid} = 92.2, which confirms a reduction of droplet size due to reatomization. Also the number of reatomized droplets was larger towards the edge of the disc. Thus, larger reatomized droplets remained closer to the surface of the disc than the smaller droplets and at the region close to the edge the reatomized droplets could move farther away from the disc. This motion of the reatomized droplets was due partly to gravity, which increased its importance with droplet size, and partly to local gas velocity at the centre and at the edge of the disc.

The average trajectory of reatomized droplets and droplets coming directly from the nozzle close to the disc surface can be examined by considering the pdfs of the velocity components along the directions ±45° measured by the method of Hardalupas and Liu (1992) and are presented for the same droplet sizes as above at one location (r/D_{liquid}, z/D_{liquid}) of (8.7, 90.9), as an example, in figure 23a & b for the +45° and -45° directions respectively. By considering separately the mean velocities of the high and low velocity peaks and assuming two dimensional flow, the velocity vector of the reatomized and the droplets directly from the nozzle can be evaluated. For example, for the location of figure 23, the inclination ϕ, as defined in figure 3, of the velocity vectors of the reatomized 33, 50 and 105 μm droplets relative to the horizontal was 0°, -8° and -8° respectively and that of the droplets directly from

the nozzle was 82°, 84° and 84° respectively, while the average trajectory of 9 μm droplets had ϕ around 45°, which should follow closely the gas flow passing around the disc at this location. So the angle between the incident and reatomized droplet trajectories at a location above the disc surface was of the order of 90°, with the reatomized droplets larger than 50 μm moving away from the disc surface and the axis of symmetry over a longer period of time than droplets smaller than 50 μm which followed the gaseous phase flow faster due to their shorter response time and moved parallel to the disc surface. The larger droplets did not travel far from the disc either because of gravity or because they broke up into smaller droplets due to shear. Figure 24 shows a drawing of the droplet trajectories close to the disc surface as indicated from the examination of the velocity pdfs at ±45° directions along the surface of the disc, which agrees with the observations of the trajectories of wind-blown grains above a grain bed by Bagnold (1956) and will be discussed later. The inclination of the trajectories directly from the nozzle show small changes as a function of size larger than around 40 μm, which suggests that the deflection of the spray was mainly caused by droplets smaller than 40 μm.

The Sauter mean diameter, figure 19c, decreased close to the disc by around 20% relative to the free spray for all the radial positions. The decrease of the SMD indicates a correlation between small droplet sizes and reatomized droplets, since the additional droplet sizes which reduced the mean diameters were generated close to the disc by reatomization. This was confirmed with the examination of the velocity pdfs of the droplets in different size ranges. The droplet sizes at the edge of the spray, which were mainly transported by the wall jet away from the surface of the disc as their axial and radial velocity indicated, had SMD around 70 μm at z/D_{liquid} =92.2 and suggested that the Sauter mean diameter of the reatomized droplets is of the order of 70 μm. However, this does not agree with the increased droplet sizes measured by Hardalupas et al (1992) after the impingement of a gasoline spray on a wall without coflowing gas stream, probably due to the larger impact velocity of the droplets on the wall and the high shear at the interface between the gaseous flow and the liquid film. The contribution of both these mechanisms on the reatomization of the droplets will be examined in the following section 3.3(b). It should be noted that the median diameter, which corresponds to the droplet size carrying 50% of the cumulative liquid flux, is presented only at locations where the negative flux of the droplets was small, at z/D_{liquid} =90.9 in figure 19c, because otherwise the estimation of the 50% of the cumulative net mass flux, although it can be defined mathematically, is affected by the correlation between droplet size and negative or positive flux and the corresponding diameter does not have any physical meaning. In this case the median diameter based on the liquid concentration may be a more useful quantity.

The last region identified during the spray impingement on a disc was that on the side and downstream of the disc surface, which was dominated mainly by reatomized droplets and measurements are presented at z/D_{liquid} = 92.8 and 94.8, however, not close to the centre

because of the limited optical access close to the surface of the disc at z/D_{liquid} =92.8 and because no droplet existed in the wake of the disc at z/D_{liquid} =94.8. The maximum of the net liquid flux and the concentration moved at larger radial position from r/D_{liquid} =14 at z/D_{liquid} =92.8 to r/D_{liquid} = 20 at z/D_{liquid} = 94.8, figure 19a & b, and was associated with an increase of the Sauter mean diameter from 65 to 85 μm, figure 19c. Close to the edge of the disc the Sauter mean diameter increased to around 120 μm, although the number of droplets there was small as indicated by the small liquid flux. This is a result of the reatomization of the liquid film at the edge of the disc due to the shear at the interface with the gas flow. Observations in this region suggest that some droplets with diameter of the order of a millimeter were dripping from the edge of the disc and fell due to gravity without being transported by the gas flow and without crossing the probe volume of the phase Doppler. So there was a considerable liquid flux removed by the disc surface in this way.

The mean axial and radial velocity components in this region, figures 19d & e, show that the droplets moved along trajectories inclined, relative to the horizontal, by an angle ϕ, defined in figure 3, of 20°, 15° and 29° at z/D_{liquid} = 92.8 and 27°, 23° and 20° at $z./D_{liquid}$ =94.8 for the 9, 50 and 105 μm respectively. So the droplets formed an umbrella-like flow around the disc with the gravity affecting the trajectories of the larger droplets more than the smaller droplets and in different ways at different axial distances from the disc. Downstream of the disc, at z/D_{liquid} = 94.8, single peak velocity distributions were found for all droplet size ranges up to radial distances of r/D_{liquid} =26, which indicated that these droplets were mainly reatomized and then deflected away from the axis of the spray by the wall jet beyond the width of the free spray. Only close to the edge of the disc some bimodal velocity pdfs were detected, because of the coexistence of droplets directly from the nozzle which avoided the disc and reatomised droplets. The rms fluctuations of the axial and radial velocity components, figures 19f & g, were mainly defined by the deterministic trajectories of the droplets, rather than the response to the gas phase turbulence. This was also confirmed by the large correlation coefficients, figure 19h, of the large droplets indicating deterministic trajectories. The sign of the correlation coefficient was negative following the characteristics of the wall jet flow.

Summarising the observations, the presence of a disc in the spray produced by a coaxial airblast atomizer with axial gaseous stream causes a part of the spray to deflect before reaching the disc, reatomization of initial droplets during their impingement on the disc, which results in smaller droplets being produced relative to the free spray and increase of the spread of the spray with the droplets forming an umbrella-like flow around the disc after their impingement. The results suggest that impingement of a liquid spray on the turbopump dome in the preburner of the SSME could result in liquid oxidiser with reduced droplet size moving sideways towards the inlet of the turbine and increasing the chances of ignition and combustion on the turbopump dome and in the first stage of the turbine blades.

b) Secondary breakup during the spray impingement process.

The fluxes and mean diameters in the flow over the disc are affected by at least two mechanisms. One is the deflection of the droplets by the gaseous flow over the disc surface, resulting in a part of the spray flowing around the disc without striking the solid surface. The second effect is the impaction of the droplets on the disc which, in general, resulted in some of the incident flux being lost to form a liquid film. In turn, this liquid was returned to the flow by reatomization caused by the mechanisms explained below.

The droplet sizes which are more likely to be deflected by the gas flow can be estimated by the following arguments. The time of flight of a droplet past the disc is of the order of

$$T_f = \frac{D_d}{U_0} \tag{31}$$

where D_d is the diameter of the disc and U_0 is a representative droplet approach velocity. For the droplet to avoid collision with the disc, it must be able to acquire a radial component of velocity from the gaseous flow and hence T_f must be large compared to the Stokesian response time, $\tau = \rho_l d^2 / 18 \mu_g$, defined in equation (7). Thus the Stokes number,

$$St_f = \frac{T_f}{\tau} \tag{32}$$

should be of the order of about 10 (Ingham et al, 1990). A typical value for t_f is of the order of 1.5 ms, so that droplets larger than about 10 μm are incapable of satisfying the Stokes number criterion. This order of magnitude estimate suggests that all the droplets above 40 μm will strike the disc and hence contribute to secondary atomization, and the deflection of the spray is mainly casued by the small droplet sizes, which agrees with our observations. Some large droplets were found to have avoided impaction on the disc and the preceding arguments suggest that these are likely to have come from the edge of the incident spray. The droplets striking the disc form a liquid film on the surface and contribute to the reatomized droplets by splash reatomization.

There are three mechanisms, which can modify the droplet sizes approaching the disc :
i) shear breakup before the droplets reach the wall,
ii) splash reatomization as the droplets hit the liquid film on the disc surface,
iii) reatomization of the liquid film on the disc surface due to shear with the gas flow,
and there will be examined separately in the following paragraphs which quantifies their contribution on the droplet reatomization.

Shear breakup can occur due to the relative velocity between the droplets and the gas phase. At a distance from the nozzle z/D_{liquid} around 90, the secondary breakup of droplets in the free spray has been completed, since their slip velocity was very small. However, for the spray striking the disc, the gas phase decelerated and close to the disc its mean velocity was around zero. So the deceleration time of the gas flow

$$T_{decel} = \left(\frac{dU}{dz}\right)^{-1} = \frac{L}{U_{cg}} \tag{33}$$

with U_{cg} the centreline gas velocity at a distance L upstream of the disc surface where the velocity was equal to that of the free spray. The corresponding deceleration Stokes number is:

$$St_{decel} = \frac{T_{decel}}{\tau} \tag{34}$$

and when less than 1 the droplets cannot respond to the gas phase flow. Our measurements have shown that it is only in the last 12 mm of the flow approaching the disc that the gas flow decelerated from its initial velocity of 45 m/s, rather than the one bluff body diameter of Bearman (1972), so T_{decel} = 12mm/45m/s = 0.27 ms. The droplets cannot respond to this sudden deceleration of the gas flow and maintain their initial velocity, increasing the relative velocity between the gas and the droplets, which can break up the droplets before they reach the disc surface. The value of the local Weber number close to the disc based on our measurements for a 200 μm droplets is around 3, which is of the same order as the critical Weber number of 12, indicating that some effect from shear breakup on the large droplets could exist after considering the rms of the fluctuations of the gas and liquid velocities. This effect becomes more important in the preburner of the SSME, because the surface tension between the oxygen droplets and the hydrogen gas is one order of magnitude smaller than that for the water/air interface used here, which will result in an order of magnitude increase of the local Weber number. A useful parameter is the ratio of the breakup time to the residence time of a droplet :

$$St_{br} = \frac{T_b}{T_{residence}} \tag{35}$$

where T_b is calculated from equations (14) and (15) and $T_{residence} = z / U_d$. When St_{br}=1, then the distance z travelled by a droplet during its breakup can be estimated and indicates whether a droplet can breakup due to shear before striking the disc.

Another mechanism causing shear breakup is the large radial velocity component of the gas flow close to the disc surface which is equal to the relative velocity between the gas and the droplets in the radial direction, since the droplets directly from the nozzle had negligible

small radial velocity. Then the local Weber number based on the slip velocity in the radial direction for a 200 μm droplet is around unity. The same mechanism can breakup droplets generated after the splashing of the free spray droplets on the disc, since the gas flow there moves with large radial velocity component.

Finally, the shear of the gas flow could break up droplets suspended in the flow close to the stagnation point when the viscous forces become larger than the surface tension, which could probably apply to the reatomized droplets after splashing on the liquid film. This mechanism would distort the droplets in the direction parallel to the disc, as observed by Taylor (1934) and discussed by Hinze (1955), and the droplets would breakup when the value of the generalised Weber number

$$We_{shear} = \frac{\mu_l S d}{\sigma} \qquad (36)$$

becomes around unity. S is the shear rate of the flow, d is the droplet diameter σ is the surface tension and μ_l is the viscocity of the liquid. S was taken equal to $(\ln X_2 - \ln X_1)/T_{decel}$ according to Taylor (1934), after the assumption that the time taken to travel from locations X_1 to X_2 along the centreline of the flow was equal to the deceleration time defined in equation (33), while X_1 and X_2 were equal to 3 and 15 mm respectively, so $S=6$ ms^{-1}. The value of the shear Weber number of equation (36) was of the order of 0.001 for a droplet diameter of 200 μm, too low for breakup to occur.

Splash reatomization occurs because the droplets hit either a solid surface or a surface covered with a liquid film. Many studies of droplets impinging on a surface have shown that the droplet sizes generated after the splashing varies according to the droplet size and velocity, liquid film thickness, surface temperature (Gallily and La Mer 1958; Wachters and Westerling 1966; Chandra and Avedisian 1991). Although it is difficult to evaluate the size, velocity and number of reatomized droplets due to splash atomization in our complex conditions experiment, the reatomized droplet velocity vectors confirm that this occurs.

Liquid film reatomization occurs due to the shear of the gas flow at the interface with the liquid film. Woodmansee and Hanratty (1969) suggested that droplets are produced from the surface of the liquid film for values of the Weber number :

$$We_{film} = \frac{\rho_g (V_g - C)^2 h}{\sigma} \qquad (37)$$

larger than around 1.5, where C is the wave velocity on the surface of the film, h is the height of the base film, V_g is the radial velocity of the gas flow above the film and ρ_g and σ are the density of the gas and the surface tension respectively. Assuming that C is zero and that h is around 1 mm, the value of the Weber number for our experiment was around 14, which was

larger than the critical value of 1.5, although this was the absolute maximum value and in reality is expected to be smaller. So some generation of droplets from the surface of the liquid film may occur, given enough time for the gas to generate waves on the liquid film surface. However, it is not expected that liquid film reatomization can occur from the break up of surface waves along the radius of the disc, because the distance was too short for the amplitude of these waves to develop for the gas velocity along the surface at the present experiment. So the liquid film breaks up into ligaments and droplets mainly at the edge of the disc, which were of the order of hundreds of μm and did not follow the gas flow and did not cross the probe volume of the phase Doppler. This observation agrees with the results of Rizk and Lefebvre (1980), which, for the flow conditions of our experiment, gas velocity of the order of 30 m/s and liquid film thickness of the order of 500 μm, measured droplet sizes with SMD larger than 500 μm.

The dominant mechanism generating reatomized droplets during the present study remains to be identified. It is believed that the shear breakup of the incoming droplets prior to the surface of the disc was not important, but it could result in breakup after impingement and, although the liquid film reatomization was argued earlier to be small, the liquid film reatomization and the splashing of the droplets on the liquid film can be responsible for the generation of reatomized droplets. It is helpful to establish the inclination angle of a reatomized droplet trajectory at the time of its generation on the disc surface. It is expected that splashing reatomization would produce droplets with initial inclination around the vertical direction, while the liquid film atomization would produce droplets with small inclination relative to the surface of the disc. Our velocity measurements show that droplets close to the axis of symmetry moved away from the wall at distances around 6 mm above the surface. The radial velocity component of the gas flow at this region was negligible and so unable to cause liquid film atomization, so reatomized droplets around the axis of symmetry were due to splash atomization. At the edge of the disc there were also reatomized droplet trajectories directed away from the wall even at a distance of 9 mm from the disc surface, which can only be justified by splash reatomization, since liquid film atomization would generate droplets with trajectories nearly parallel to the wall. So splash atomization appears to be the main mechanism of generation reatomized droplets in this experiment. These droplets were carried from the disc surface by the gaseous flow following the trajectories of figure 24. The initial inclination angle ϕ of the trajectory of a splash reatomized droplet was of the order of -90° and, assuming that different droplets size were generated with similar velocities, their trajectories were different, as figure 24 shows, for the following reasons. Trajectories of small droplets, which follow the gas flow quickly after their generation, rapidly became parallel to the wall and trajectories of medium size droplets, which do not follow the gas flow fast because of their long response time but gravity is not important, moved from the wall for a longer period of time. Trajectories of large droplets, which do not respond to the gas flow and gravity can

affect their motion, remained close to the wall and could strike the disc again generating new reatomized droplets. This description of droplet trajectories agrees with that of Bagnold (1956) for trajectories of grains above a wind blown grain bed. Only at the edge of the disc liquid film atomization becomes important by generating large droplets and even some of the order of one millimeter which are dripping away. So splash reatomization appears to be the main mechanism of generating droplets in the current experiment.

3.4 Multiple spray interaction

Here we examine the interaction between three sprays with gaseous jet diameter D_{gas} = 8.95 mm, 3 mm annular width of the gaseous stream and 2.3 mm internal diameter of the liquid tube separated by 18 mm in a triangular arrangement as in figure 4. The liquid tube was not recessed. The following two sections examine axial flow and the consequences of gas respectively and quantify the effects of the variations of the flowrates. The SSME has around 250 nozzles supported on the faceplate of the preburner and, as Ferrenberg et al (1985) suggested, their characteristics may be very different than those produced by the single nozzles.

a) Interaction between sprays produced by nozzles with axial gaseous stream.

i) Spray characteristics

The spray characteristics, corresponding to case 12 and 17 of table 1a, were measured at axial distances from the nozzles of z/D_{gas} = 13.4, 23.5 and 33.5, where D_{gas} is the diameter of the gaseous jet of the single nozzle. Since the flow was not axisymmetric, the measurements were along the x direction and along the r direction for different values of x, as in figure 4, but only the profiles in the x direction (r/D_{gas} = 0), and in the r direction at x/D_{gas} =1.68 will be presented. The arrows on the graphs indicate the location of the axis of symmetry of each nozzle and the zero value in the x direction corresponds to the axis of symmetry of nozzle 1, while the axes of nozzles 2 and 3 were at positions (r/D_{gas}, x/D_{gas}) = (-1, 1.68) and (1, 1.68) respectively.

The mean diameters with conditions according to case 12 along the r direction at x/D_{gas} = 1.68, figure 25a, show maxima of around 170 and 200 μm for the SMD and the MMD respectively, which occurred on the axis of symmetry of the individual nozzles. The value of the mean diameter at the region between nozzles 2 and 3, which is the most likely region for spray interaction, decreased but was still larger than that close to the edge, suggesting that the two sprays merge and result in a larger mean diameter. The liquid flux profiles of figure 25b show that very few droplets existed at z/D_{gas}=13.4 and between the nozzles, $-1 < r/D_{gas} < 1$, but, as the individual sprays spread, the liquid flux in this region increased to about 0.7 of the

maximum value observed at z/D_{gas} =33.5. The liquid flux maxima again concided with the axis of symmetry of the nozzles showing that the individual sprays could be identified even at large axial distance.

The mean axial velocity of droplets in the 9, 50 and 105 μm size ranges is compared with the gas single phase flow, when no liquid was injected through the liquid tube in figure 25c, in terms of profiles normalised by the velocity of the gas averaged over the area of the annulus of the gaseous jet, U_{gas}, of each nozzle. In the region between the axes of the nozzles the droplet velocities reached a maximum which decreased with increase of droplet size. Local velocity minima existed on the axes of the nozzles at z/D_{gas} = 13.4, and gradually disappeared with the distance. The larger droplets moved faster than the 9 μm droplets at the edge since they were not affected by the gas phase flow and, at z/D_{gas} = 33.5, all droplets had accelerated so that the characteristics of the individual nozzles had disappeared and a single maximum existed in the central part of the flow, while the larger droplets still moved faster than the 9 μm droplets and so the gas phase at the edge. Although the individual sprays could not be identified in terms of the velocity field, the mean diameter and liquid flux profiles show that the characteristics of the individual sprays still existed. Thus the velocity characteristics of the droplets were not a good indication of the development and this occurs because the lack of interaction with the gas turbulence led the droplets to remain in the region where they were initially generated and so close to the axes of symmetry.

The 9 μm droplets followed closely the gas phase when the liquid jets were present, so comparison between their velocity characteristics and the single phase velocity identifies the effect of liquid jets on the development of the gas flow. The single phase flow developed much faster and the presence of individual jets could only be identified at z/D_{gas}=13.4. Farther downstream the single phase velocity was similar to that of a single jet, with a maximum at the centre and decreasing at the edge. At the edge of the flow the velocity of the 9 μm droplets followed that of the single phase, suggesting that the gaseous flow there was unaffected by the presence of the liquid jet. However, most of the liquid content of the sprays existed in the central region where the gas flow was much slower than the single phase flow, since the gas flow momentum was used to accelerate the droplets. At z/D_{gas} = 33.5 all the droplets had accelerated and the gas phase velocity was close to the single phase, while the characteristics of the individual nozzles had disappeared.

The mean diameters in the x direction, r/D_{gas} =0, on the axis of symmetry of nozzle 1 were a maximum, figure 26a, and similar to those for the axes of symmetry of nozzle 2 and 3, which supports the argument that the main region of interaction between the sprays was between the nozzles and at the centre of the flow. The second maximum of the mean diameter occurred at around x/D_{gas} = 3, which was farther from the axes of symmetry of the other two nozzles at x/D_{gas} =1.68, but always remained smaller than that on the axis of symmetry of the nozzles, with values of SMD and MMD around 130 and 170 μm respectively. The liquid flux

in the x direction was dominated mainly by that of nozzle 1 at z/D_{gas} = 13.5, figure 26b, but a gradual increase occurred farther downstream at around x/D_{gas}=2 due to the interaction between the other sprays.

The maximum mean axial velocity of the droplets occurred between nozzles 2 and 3 at x/D_{gas} = 1.5, figure 26c, with a minimum on the axis of nozzle 1 at z/D_{gas} = 13.4 with gradual acceleration with the axial distance as the three sprays interacted. The single phase axial velocity, in agreement with the observations in the r direction at x/D_{gas} =1.68, figure 25c, was a single jet-like flow after z/D_{gas}=13.4 with its axis of symmetry at around x/D_{gas} =1, which was around the centre of the region between the axes of symmetry of the three nozzles. The velocity of the 9 μm droplets was closer to that of the single phase in the region of the interaction between nozzles 2 and 3, where the liquid content of the flow was lower and the gas phase could accelerate faster. However, in the region of the axis of symmetry of nozzle 1 the gas velocity was lower than that of the single phase as far as z/D_{gas}=33.5.

Thus the interaction between the three sprays was strong in the region between the axes of symmetry and gradually developed to a velocity maximum. However, the mean diameter and liquid flux characteristics of the individual sprays tend to exist beyond the mean velocity field and distinct maxima remain in the region of the axes of the nozzles as far as z/D_{gas} = 33.5. In the central region between the axes of symmetry of the nozzles, the spray interaction resulted in increased mean diameter and liquid flux relative to the single spray resulting in an oxidiser-rich region.

ii) Effect of liquid flowrate.

The effect of the reduction of the liquid flowrate was examined with the conditions of case 17 of table 1a and the measurements are presented along the r direction at x/D_{gas} = 1.68; observations in the other directions showed similar effects. The mean diameters of the sprays were reduced with the reduction of the flowrate, following the observations for the single sprays. The two distinct maxima on the axes of symmetry of nozzles 2 and 3 of the mean diameter and liquid flux profiles, figure 27a & b, disappeared after z/D_{gas}=23.5 earlier than for the higher liquid flowrate and at z/D_{gas} = 33.5 the mean diameter profile was flat in the region between the axes of symmetry of the nozzles with SMD and MMD around 110 μm and 140 μm respectively, which decreased towards the edge, while the liquid flux was a maximum at the same region. The mean axial velocities of the 9, 50 and 105 μm droplets,figure 27c, had only one maximum at the centre at z/D_{gas}=23.5 and the velocity profile of the droplets was similar to that of the single phase. The faster modification of the spray characteristics with the reduction of the liquid flowrate occurred because the rate of spread of the individual sprays increased, as indicated in section 3.1, and the interaction began earlier. Thus, a decrease of the liquid flowrate by 50% increased the interaction between the sprays, which started closer to the nozzle exit and resulted in the individual spray characteristics to disappear at a distance

30% less than for the higher liquid flowrate and the three sprays behaved like a single spray produced by a nozzle located between the axes of symmetry of the nozzles.

iii) Comparison between the single and the three sprays.

The characteristics of the three sprays at z/D_{gas}=23.5 were compared with those of the single nozzle in the same region by plotting the single spray characteristics, so that their axis of symmetry coincides with that of the nozzles in the three spray arrangement. Figure 28 shows that the results for the single and the three sprays at the edge of the flow were identical. The mean diameter decreased in the three interacting sprays on the axes of symmetry of the nozzles, relative to the single spray, because the smaller droplets at the edge of the neighbouring sprays affected the local size distribution by increasing the number of small droplet sizes. Comparison between the single and three sprays shows that there is no effect on the atomization of each individual nozzle due to the interaction from the others. The modification of the spray characteristics is caused mainly by the merging of the sprays, as they move downstream.

b) Interaction between sprays produced by nozzles with swirling gaseous stream.

The rotation of the swirling motion in the three sprays, S8 and S9 of table 3, was clockwise and the following section examines the consequences of the interactions in terms of liquid flowrate. The characteristics of the gaseous phase, when no liquid flowrate was supplied to the nozzle, are also presented and are referred as single phase characteristics in the text.

i) Spray characteristics

Profiles of droplet size, volume flux and axial, radial and tangential velocity components were measured in the cross stream direction at axial distances from the faceplate of the nozzles of z/D_{gas} = 13.4 and 23.5. The characteristics of the sprays were measured Measurements were made in the x and r directions, as shown in figure 4, and the profiles in the x direction, r/D_{gas} = 0, and in the r direction at x/D_{gas} =0, 0.84 and 1.68 are presented here. As in the previous section, the arrows on the graphs indicate the location of the axis of symmetry of each nozzle, and the zero value in the x direction corresponds to the axis of symmetry of nozzle 1, while the axes of nozzles 2 and 3 were at positions (r/D_{gas}, x/D_{gas}) = (-1, 1.68) and (1, 1.68) respectively.

The interaction of the three sprays with conditions as in case S8 of table 3, at z/D_{gas} = 13.4 and 23.5, figure 29 and 30, show that the flow was not symmetric as for the sprays produced by nozzles without swirl. There are three distinct streams of droplets, each the result of the breakup of the three liquid jets after being deflected as shown in figure 31 and the

liquid fluxes of figures 29a and 30a have distinct maxima which correspond to each of these droplet streams. For example, at z/D_{gas}=13.4, the flux maxima at positive r/D_{gas} values of the profiles at x/D_{gas}=0, 0.84 and 1.68 correspond to the droplet stream produced by the liquid jet of nozzle 1. Those at x/D_{gas}=5 at r/D_{gas} =0 and at negative r/D_{gas} for x/D_{gas}=1.68 correspond to the liquid jet of nozzle 3 and those at negative r/D_{gas} for x/D_{gas} =0.84 and 0 and at negative x/D_{gas} for r/D_{gas}=0 correspond to that of nozzle 2. It is also clear that there was a liquid flux minimum in the central region of the sprays. At z/D_{gas}=23.5, the liquid flux maxima can be observed in regions farther from the axes of the sprays.

The mean diameters associated with the three distinct droplet streams were around 160 and 220 μm respectively for the SMD and the MMD, figures 29b and 30b. The central region between the axes of the sprays, where the liquid flux was a minimum, had smaller diameters corresponding to SMD and MMD around 130 and 175 μm respectively at z/D_{gas} = 13.4 and farther downstream, at z/D_{gas}=23.5, the droplets spreaded and more distinct minima appeared, for example at x/D_{gas}=0. Thus the regions outside the three droplet streams were associated with lower mean diameters, since only smaller droplets could disperse and be entrained in these regions, while larger droplets moved on deterministic helical trajectories.

The mean axial, radial and tangential velocity of droplets in the 15, 50 and 105 μm size ranges are compared with the gas single phase flow in figures 29 and 30c & d and are normalised by the velocity of the gas averaged over the area of the annulus of the gaseous jet, U_{gas}, of each nozzle. It should be noted that the mean diameter of the droplets in the smaller size range increased from 9 to 15 μm, in order to increase the number of small droplets and improve the accuracy when calculating the mean velocity. The number of measurements of small droplets decreased with the wider spray and where the droplet density was sufficient to reduce the signal to noise ratio of the Doppler signals. However, the 15 μm droplets are still expected to follow the mean gas phase velocity closely.

The three droplet streams associated with the large liquid flux had large velocity components in all three directions. The axial velocity of the larger droplets was higher than that of the gas phase in these regions and, although all droplets had similar tangential velocity components, their radial velocity increased with droplet size due to the increased centrifuging with droplet size, as discussed in section 3.2. The radial velocity component of the large droplets was larger than their tangential component, which shows that the trajectories of the large droplets were directed away from the central region and never completed a 360° turn within the examined distance from the nozzle, because their axial velocity was large. They would not do so even in a larger distance because the centrifuging brings them to a region of the spray where the gas velocity was very low and gravity dominated their motion. The velocity of the droplets was a minimum in the central region between the three droplet streams, where the droplets were small. The velocity profiles become more uniform at z/D_{gas}=23.5, in

contrast to the liquid flux and mean diameter profiles, although the distinct characteristics of the droplet streams moving in helical trajectories were still present.

The single phase flow developed much faster than in the presence of the liquid jets and comparison shows that the gas flow developed in a different way. The single phase axial velocity was a maximum in the central region where most of the gas was entrained and the characteristics of the three nozzles could not be identified by z/D_{gas}=13.4. The tangential velocity component indicates that the axis of rotation was around x/D_{gas}=2 and did not coincide with that of the gas phase in the spray. The profiles show that the droplets reached larger radial distances than the single phase flow, because of the centrifuging of the large droplets, which entrained gas and resulted in a wider gaseous jet. Farther downstream, at z/D_{gas}=23.5, the single phase velocity was similar to that of a single swirling jet, with its axis at x/D_{gas} =2, while the gas phase flow in the spray retained a minimum at the centre, where the gas entrainement was reduced relative to the single flow because of the high momentum droplet streams away from the centre.

A simplified explanation of the behaviour of the three interacting swirling nozzles can be obtained, if the swirling motion is simulated by three irrotational vortices with their axes coinciding with the axes of symmetry of the three nozzles although, in reality, the swirling motion at the exit of the nozzle is a forced vortex. Since the direction of swirl in each nozzle is clockwise, the velocity induced by the two vortices on the centre of the third one has a direction which tends to deflect the liquid jet from its centre, as shown in figure 31b. The circulation Γ of each vortex is of the order of 1 m^2/s, so the velocity induced by each vortex on the centre of another, $w=\Gamma / 2\pi y$, is around 9 m/s and the combined induced velocity by the two vortices on the centre of the third is around 15 m/s. This velocity is strong enough to cause deflection of the liquid jet and the generation of the three droplet streams in the spray.

The interaction between the three sprays was strong and affected the breakup process of the liquid jets resulting in a different spray rather than a merging between the three individual sprays, as for the case of the three axial gaseous stream sprays. The mean diameter and liquid flux remained high at the edge of the spray with small droplets and a low liquid flux region formed at the centre of the flow. Thus, multiple injectors with swirling gaseous flow can lead to strong interactions when close together and modify the atomization and the flux distribution of the injected liquid by single nozzles.

ii) Effect of liquid flowrate.

The effect of liquid flowrate was examined by comparing sprays produced by nozzles with conditions S8 and S9 of table 3, that is a 50% increase of the liquid flowrate. The liquid flux, mean diameter and axial velocity profiles of the 15 and 105 μm droplets are compared at distances from the faceplate of the injectors of z/D_{gas}=13.4 and along the direction r/D_{gas}=0 and z/D_{gas}=23.5 and along the direction x/D_{gas}=1.68 in figures 32a & b respectively. The

liquid fluxes suggest that the structure of the three droplet streams initiated by the liquid jets of each nozzle remains at the high liquid flowrate and the mean diameters of the sprays increasedby around 20% with the 50% increase of the liquid flowrate, as for the single sprays. It should be noted that the atomization in a single nozzle with conditions S9 was poorer than for the three sprays and resulted in very large droplets existing at large distances from the nozzle. This shows that the interaction between the three sprays can result in better atomization in certain cases, because the deflection of the liquid jet brings the liquid in the high velocity gas and the combination of the initial instability of the liquid jet and the gas flow shear breaks it up closer to the nozzle. However, droplet secondary breakup in the sprays of S9 occurred up to around $z/D_{gas}=6$ inside the three distinct droplet streams. The mean axial velocity of droplets in the 15 and 105 μm size ranges was lower for the high liquid flowrate and as for the single sprays was a result of the required higher momentum transfer from the gas to the liquid to accelerate the droplets. Thus, the increase of the liquid flowrate by 50% did not affect the pattern of the sprays, but did result in mean diameters larger by 20%.

iii) Comparison between the single and the three sprays.

The characteristics of the three sprays produced by nozzles with conditions of case S8 were compared with those of the single nozzle of case S6 at $z/D_{gas}=13.4$ by plotting the single spray characteristics, so that its axis of symmetry coinciding with that of one of the nozzles in the three spray arrangement. It should be noted that the gas flowrate from each nozzle in the three spray arrangement, case S8, was higher than that of the single nozzle, case S6. Figure 33 shows that the width of the sprays was comparable and both sprays had a liquid flux minimum at the central region, although at different positions. The mean diameters were higher with the three interacting sprays than with single nozzle, although this may have been caused by the lower gas flowrate used in the former case. However, as mentioned earlier increase of the liquid flowrate in the single nozzle resulted in poorer atomization than in the three sprays, because of the difference in the atomization mechanism. In the single nozzle sprays, the liquid jet broke up on the axis of symmetry and increase of the liquid flowrate delays the breakup of the liquid jet and resulted in poorer atomization as the breakup length became longer than the recirculation zone length. In the three sprays, the liquid jet was deflected away from the axis of symmetry of each nozzle before breaking up in the high velocity gas region, which is less affected by the liquid flowrate, so the atomization was better. The axial velocities of the 9 and 105 μm droplets in the single and the three sprays was similar, which suggests that differences in the slip velocity cannot be responsible for differences in the atomization and supports that the difference in the mean diameters is caused by the different atomization mechanisms in the single and three sprays.

3.5 Design of the high pressure/supercritical conditions atomization facility

The design of a high pressure facility to allow study of atomization of coaxial sprays at high pressure and supercritical conditions have been prepared by Vafidis and Whitelaw (1991) and is included in the appendix B.

4. IMPLICATIONS FOR THE SPRAYS OF THE SPACE SHUTTLE MAIN ENGINE

The present study suggested that the local Weber number on the centreline of the sprays is the main parameter affecting secondary atomization. This is affected by the acceleration Stokes number $St_{acceler}$, which is related with the rate of acceleration of the gas velocity along the centreline $T_{acceler}$, the gas density, the surface tension and the nozzle geometry. It is important to be able to evaluate the value of the local Weber number on the centreline of the sprays in the Space Shuttle Main Engine (SSME) and the following paragraphs attempt to do this without considering differences between the nozzle geometry in the SSME and the present study.

The value of $St_{acceler}$, equation (16), defines the slip velocity between the gas and the droplets on the centreline and depends on $T_{acceler}$, equation (8), and the droplet response time τ, equation (7). Tables 5a and b suggest that $T_{acceler}$ and the maximum measured slip velocity (U_{gc} - U_{lc}) along the centreline are mainly affected by the momentum ratio and there is little effect of the velocity difference between the two streams at the exit of the nozzle. So the value of the gas-to-liquid momentum ratio of the sprays of the SSME, which was estimated to be around 10.6, could be used to evaluate the rate of acceleration of the gas phase on the axis of symmetry of these sprays. According to tables 5a and b, the cases 1, 5, 12, 35, 40 and 44 have momentum ratios varying from 8.9 to 13.6 around the value of 10.6 for the SSME and, although the nozzle geometry changes, the values of $T_{acceler}$ vary from 2.5 to 3.9 ms and of maximum slip velocity, max(U_{gc} - U_{lc}), from 8.2 to 12.8 m/s. A good expectation for the sprays of the SSME is that $T_{acceler} \approx 3$ ms. The droplet response time is affected by the liquid to gas density ratio, ρ_l / ρ_g, and the gas viscosity, ν_g, according to equation (7) and the quantity $\rho_l / \rho_g \nu_g$ increases from 56×10^6 $m^2 s^{-1}$ for the present study to around 140×10^6 $m^2 s^{-1}$ for the sprays in the SSME and, thus the droplet response time increases by a factor of 2.5 in the SSME. So the value of $St_{acceler}$ for similar droplet diameters decreases by around 2.5 in the SSME, thus the droplet response to the gas phase flow is delayed and the slip velocity increases by around a similar factor. According to tables 5a and b the value of max(U_{gc} - U_{lc}) is around 10 m/s for the present study and for momentum ratio around 10.6 and is expected to increase by 2.5 times in the SSME to 25 m/s.

The local Weber number, equation (18), depends on the slip velocity, which was evaluated for the SSME in the previous paragraph, and the ratio ρ_g / σ. The local Weber number for a 300 μm droplet in the present study is around 0.5 and ρ_g / σ is around 15 s^2m^{-3} In the SSME the ratio ρ_g / σ is around 2980 s^2m^{-3}, so an increase by a factor 200, thus the local Weber number of a 300 μm droplet in the SSME is expected to be around 100. The Ohnesorge number in the SSME is around $4x10^{-5}$ according to equation (21), so the critical Weber number We_{crit} from equation (20) is around 12 in the SSME. So the Weber number of a 300 μm droplet is larger than We_{crit} and will breakup. So the maximum local Weber number of the droplets in the SSME is around 120 for a maximum droplet size of 360 μm and their breakup will occur in the regimes of vibrational, bag, bag-and-stamen and sheet stripping as the local Weber number increases, according to Pilch and Erdman (1987), and not in the catastrophic breakup regime, which occurs for values of the Weber number larger than 350, and the resulting droplet size after breakup is independent of the initial value of the Weber number.

The maximum stable diameter in the SSME can be calculated according to equation (19) and is around 10 μm. However, the value of the maximum stable diameter is calculated without considering the breakup time of the droplets, which can allow droplets produced during breakup to be accelerated by the gas flow and reduce their slip velocity and survive without breaking up again. This effect is evaluated by the breakup Stokes number, St_b, according to equation (26). The breakup time evaluated by equations (14) and (15) for a 300 μm droplet with $We_{loc} = 100$ is around 2.7 ms, while its response time is around 700 ms, so St_b is very small for the initial droplet to accelerate during breakup. However, droplets produced during breakup, for example, 30 μm droplets have response time around 7 ms and can partially accelerate during breakup and may survive breakup increasing the maximum stable diameter calculated by equation (19). However, the maximum stable diameter in the SSME is not expected to be larger than 50 μm.

The length of liquid core of the initial liquid jet is mainly affected by the square root of the density ratio ρ_l / ρ_g according to equation (6). So the length of the liquid core is reduced by a factor of 5.5 in the SSME. This means that the liquid core Stokes number, equation (25), in the SSME is reduced by a factor of 14, because the timescale of the liquid core is reduced by 5.5 times while the droplet response time increases by 2.5. So smaller droplet sizes than in the present study generated during the primary atomization of the liquid jet in the SSME cannot modify their velocity characteristics before the primary atomization is completed. So their slip velocity becomes larger and can initiate secondary breakup closer to the nozzle exit resulting in improved atomization in the SSME.

An additional effect on the droplet size of the sprays in the SSME is the acceleration of the gas flow during combustion. Ferrenberg et al (1985) suggested that this effect reduces the droplet sizes and our model can explain it, since the acceleration of the gas flow will increase

the slip velocity and the rate of acceleration $T_{acceler}$, resulting in larger values of the local Weber number and improved secondary atomization.

The rate of spread of the sprays in the preburner of the SSME is also considered below. The residence time of the droplets in the preburner of the SSME is reduced because their initial velocity is larger than that of this study. So the droplets reach the turbopump dome, which is at approximately 200 mm from the faceplate, in a maximum time $T_{residence}$=200 mm / 30.5 m/s=6.5 ms. So the residence Stokes number $St_{residence}$, equation (17), for 40 μm droplets is around 1, which means that droplets larger than around 40 μm do not have enough time to respond to the gas flow and disperse. So the rate of spread of the sprays close to the nozzle in the SSME is mainly affected by the initial conditions and the high momentum gaseous stream there, as observed during this study. Farther downstream, there are two opposing influences on the rate of spread. First, the increase in the droplet response time by a factor of 2.5 delays the droplet response to turbulence and reduces the rate of spread. Second, as discussed in the previous paragraph, the droplet sizes in the SSME are reduced relative to this study, which will cause an increase in the number of droplets able to respond to the gas flow turbulence and disperse. So the difference between the rate of spread of the sprays in this study and the SSME farther downstream from the nozzle should be small, although it is not clear which of the two competing mechanisms will dominate the rate of spread.

The residence time of the droplets in the combustion chamber and their size quantifies their ability of striking the turbopump dome. Since their residence time in the preburners of the SSME is shorter than that of the present study increases the probability of striking the wall. Nevertheless, their size is smaller in the SSME which reduces the probability of surviving in liquid form up to the wall and thus, during the steady operation of the sprays in the SSME the probability of the spray striking the wall is low. Since cracks have been observed on the turbopump dome and the first and second blades of the turbine, liquid oxidiser reaches the wall probably due to poor atomization during the unsteady period of the startup process, before the gas and the liquid obtain their steady flow conditions. In this case, reatomization of the spray striking the wall will result in finer droplets in the SSME, because the local Weber number close to the wall will increase by around 200 due to the change of the ratio ρ_g / σ as shown in the previous paragraph. So the finer droplets close to the turbopump dome wall are likely to ignite and cause the observed cracks on the wall due to overheating.

5. SUMMARY

Phase Doppler measurements of size, velocity, liquid flux and concentration in sprays produced by airblast coaxial nozzles were obtained over a wide range of gas and liquid flowrate conditions and different nozzle geometries. The sprays covered a range of Weber

number at the nozzle exit from 200 to 3500, of gas-to-liquid momentum ratio from 2 to 110, gas-to-liquid velocity ratio from 10 to 85, gas-to-liquid mass flowrate ratio from 0.2 to 1.3, liquid jet Reynolds number from 10000 to 55000 and gaseous jet Reynolds number from 90000 to 190000. The main findings were :

i) The droplet size characteristics were determined by the local Weber number based on the local slip velocity and the droplet diameter rather than the exit Weber number, based on the slip velocity at the exit and the diameter of the liquid tube. A physically based model of the secondary atomization was suggested to predict the size characteristics of sprays from coaxial airblast atomizers which showed that the atomization precess was affected by the gas-to-liquid momentum ratio at the nozzle exit, the liquid to gas density ratio, the gas density ratio and the surface tension. The effects of gas mean and turbulent flow on the droplet motion were quantified in terms of Stokes numbers, defined as the ratio of the characteristic timescale to the droplet response time.

ii) Increase of the gas flowrate improved atomization but reduced the rate of spread, showing a trade off between improved atomization and mixing. Increase of the liquid flowrate reduced the atomization and the rate of spread.

iii) The effects of nozzle geometry on atomization were as follows :
- reduction of the liquid tube diameter by 50% improved the atomization of sprays with the same gas-to-liquid velocity ratio by 25%.
- a converging exit of the gaseous jet with a half angle of 28° improved atomization by around 20% and 10% for gas-to-liquid velocity ratios of 24 and 41 respectively relative to a straight exit nozzle, while no effect existed for gas-to-liquid velocity ratios larger than 45.
- recess of $2D_l$ of the liquid tube inside a straight exit nozzle improved atomization by 15%, but a recess of $3D_l$ reduced it again. The effect of a liquid tube recess with the converging exit nozzle was to reduce atomization by 10% and 15% for recesses $2D_l$ and $3D_l$.with greater reductions for gas-to-liquid velocity ratios higher than 40.

iv) The effects of nozzle geometry on the rate of spread were as follows :
- reduction of the liquid tube diameter by 50% reduced the rate of spread by 20% for sprays with similar gas-to-liquid velocity ratios.
- A converging exit of the gaseous jet with a half angle of 28° improved the rate of spread by 20% for gas-to-liquid exit velocity ratios up to around 45 relative to the straight exit nozzle. For gas-to-liquid velocity ratios higher than 45 the rate of spread of the sprays was reduced close to the nozzle.
- the recess of the liquid tube improved the rate of spread of the sprays by around 40%

v) The swirling gaseous stream had the following effects :
- For swirl numbers up to 0.67 no recirculation zone existed at the nozzle exit. The atomization remain unchanged and the rate of spread reduced for swirl number up to 0.2 and increased due to droplet centrifuging for swirl number higher than 0.2.
- For swirl numbers higher than 0.67, a recirculation zone was established at the nozzle exit resulting in improved atomization and rate of spread. The breakup length of the initial liquid jet increased and broke up in ligaments close to the stagnation point of the recirculation zone which dispersed outwards resulting in finer atomization and hollow cone type sprays. The high swirl number gaseous stream is the most effective mechanism to improve the atomization and the rate of spread of coaxial airblast atomizer sprays.
The centrifuging mechanism affecting the rate of spread of the sprays was quantified with a centrifuge Stokes number, defined as the ratio of the timescale of the swirling vortex to the response time of the droplet.

vi) The impingement of the sprays on a flat disc resulted in reatomization which produced finer droplets and wider spatial distribution of the liquid droplets. The main mechanism causing reatomization was the splashing of the droplets on the disc and the trajectories of reatomized droplets as a function of size were evaluated close to the disc surface.

vii) The interaction between three sprays produced by more identical coaxial airblast atomizers was strong and modified the size and flux spatial distribution of the droplets.
- For three nozzles with axial external gas stream, the droplet size and the flux increased in the region between the sprays while at the outer region remained unchanged and the same as for the single nozzle spray. However, this effect was mainly due to the merging of the sprays rather than a modification of the atomization mechanism.
- For nozzles with swirling external gas stream, the atomization mechanism was affected by the induced velocity of the two swirling vortices of the two nozzles on the liquid jet on the axis of the third and resulted in deflection of each liquid jet and breakup due to shear in the fast gaseous stream away from its axis of symmetry. This mechanism resulted in completely different spray characteristics than the single nozzles with three helical streams of droplets originated by each liquid jet directed at the outer region with larger droplet sizes and carrying most of the liquid than the low liquid flux and small droplet size central region between the spray axes.

ACKNOWLEDGEMENTS

The authors wish to acknowledge financial support from NASA Marshall Space Flight Center, under grant number NAS8 - 38872. Mr. J.R.Laker designed and constructed the electronics of the phase Doppler instrument. Mr. P. Trowell constructed the experimental facility. We are grateful to Mr. H. Struck and Dr. H. McDonald for many useful discussions during the conduct of this research.

REFERENCES

Bachalo W.D., Rudoff R.C. and Brena de la Rosa A. 1988. Mass flux measurements of a high number density spray system using the phase-Doppler particle analyzer. AIAA-paper-88-0236.

Bagnold R.A. 1956. The flow of cohesionless grains in fluids. Proc. Roy. Soc. Lond, A249, 235-297.

Beér J.M. and Chigier N.A. 1972. Combustion Aerodynamics. Applied Science Publishers Ltd, London.

Bearman P.W. 1972. Some measurements of the distortion of turbulence approaching a two-dimensional bluff body. J. Fluid Mech., 53, 451-467.

Bradshaw P. and Wong F.Y.F. 1972. The reattachment and relaxation of a turbulent shear layer. J. Fluid Mech., 52, 113-135.

Burick R.J. 1972. Atomization and mixing characteristics of gas/liquid coaxial injector elements. J. of Spacecraft and Rockets, 9, 326-331.

Caré I. and Ledoux M. 1991. Study of an air blast coaxial atomizer: experiments and modelisation. Proceedings of the 5th International Conference on Liquid Atomization and Spraying Systems (ICLASS), Gaithersburg, MD, USA, paper 85, 763-770.

Champagne F.H. and Wygnanski I.J. 1971. An experimental investigation of coaxial turbulent jets. Int. J. Heat Mass Transfer, 14, 1445-1464.

Chandra S. and Avedisian C.T. 1991. On the collision of a droplet with a solid surface. Proc. R. Soc. Lond. A, 432, 13-41.

Chehroudi B., Onuma Y., Chen S.-H. and Bracco F.V. 1985. On the intact core of full-cone sprays. SAE paper no. 850126.

Clift R., Grace J.R. and Weber M.E. 1978. Bubbles, drops and particles. Academic Press, London.

Cossali E. and Hardalupas Y. 1992. Comparison between laser diffraction and phase Doppler velocimeter techniques in high turbidity, small diameter sprays. Experiments in Fluids, 13, 414-422.

Crowe C.T., Gore R.A. and Troutt T.R. 1985. Particle dispersion by coherent structures in free shear flows. Particulate Science and Technology, 3, 149 - 158.

Dementhon J-B.1992. L'injection essence dans un moteur a etincelle: mesures granulometriques par la methode des phases Doppler et phénomnes de pulverisation. PhD Thesis, Université de Rouen, Rouen, France.

Dodge L.G., Rhodes D.J. and Reitz R.D. 1987. Drop-size measurement techniques for sprays : comparison of Malvern laser-diffraction and Aerometrics phase/Doppler. Appl. Optics, 26, 2144 - 2154.

Dring R.P. and Suo M. 1978. Particle trajectories in swirling flows. J. Energy, 2, 232 - 237.

Eroglu H. and Chigier N.A. 1991. Initial drop size and velocity distributions for airblast coaxial atomizers. Journal of Fluids Engineering, 113, 453-459.

Eroglu H., Chigier N.A. and Faragó Z. 1991. Coaxial atomizer liquid intact lengths. Phys. Fluids A3, 303-308.

Faeth G.M. 1983. Evaporation and combustion of sprays. Progr. Energy Combust. Sci., 9, 1-76.

Faeth G.M. 1987. Mixing, transport and combustion in sprays. Progr. Energy Combust. Sci., 13, 293-345.

Faeth G.M. 1990. Structure and atomization properties of dense turbulent sprays. In Proc. 23rd Symposium (International) on Combustion, The Combustion Institute, 1345-1352.

Falk A.Y. 1975. Coaxial spray atomization in accelerating gas stream. NASA CR-134825.

Faragó Z. and Chigier N.A. 1991. Classification of round liquid jet disintegration in coaxial air streams. In Proceedings of International Conference on Liquid Atomization and Spraying Systems (ICLASS), paper 73, 661 - 668, Gaithersburg, U.S.A.

Ferrenberg A., Hunt K. and Duesberg J. 1985. Atomization and mixing study. NASA CR-178751.

Gallily I. and La Mer V.K. 1958. On the behavior of liquid droplets after impinging on solid surfaces. J. Phys. Chem., 62, 1295 - 1299.

Glass M. and Kennedy I.M. 1977. An improved seeding method for high temperature laser Doppler velocimetry. Combustion and Flame, 29, 333 - 335.

Hardalupas Y. and Taylor A.M.K.P. 1989. On the measurement of particle concentration near a stagnation point. Exp. in Fluids, 8, 113 - 118.

Hardalupas Y., Taylor A.M.K.P. and Whitelaw J.H. 1989. Velocity and particle flux characteristics of turbulent particle-laden jets, Proc. Roy. Soc. Lond., A426, 31 - 78.

Hardalupas Y., Taylor A.M.K.P. and Whitelaw J.H. 1990. Velocity and size characteristics of liquid-fuelled flames stabilised by a swirl burner. Proc. Roy. Soc. Lond., A428, 129 - 155.

Hardalupas Y., Okamoto S., Taylor A.M.K.P. and Whitelaw J.H. 1992. Application of a phase-Doppler anemometer to a spray impinging on a disc. In Proceedings of the 6th Int. Symp. on Applications of Laser Techniques to Fluid Mechanics, paper 25.2, Lisbon, Portugal.

Hardalupas Y., Taylor A.M.K.P. and Whitelaw J.H. 1992. Particle dispersion in a vertical round sudden expansion flow. Phil. Trans. Roy. Soc. Lond., A341, 411-442.

Hardalupas Y., McDonald H. and Whitelaw J.H. 1992. Two fluid mixing. In Proceedings of Advanced Earth-To-Orbit Propulsion Technology, R.J. Richmond and S.T. Wu (Eds.), NASA Conference Publication 3174, Vol. II, 63-72.

Hardalupas Y. and Liu C.H. 1992. Size-discriminated velocity cross-correlation measured by a single channel phase Doppler velocimeter. In Proceedings of 6th Int. Symp. on Appl. of Laser Techn. to Fluid Mechanics, paper 18.2, Lisbon, Portugal.

Hardalupas Y. and Whitelaw J.H. 1993. The characteristics of sprays produced by coaxial airblast atomisers. AIAA paper no. 93-0698. Presented at the 31st Aerospace Sciences Meeting & Exhibit, Reno, U.S.A.

Hinze J.O. 1955. Fundamentals of the hydrodynamic mechanism of splitting in dispersion processes. AIChE J., 1, 289-295.

Ingham D.B., Hildyard L.T. and Hildyard M.L. 1990. On the critical Stokes' number for particle transport in potential and viscous flows near bluff bodies. J Aerosol Sci, 21, 935 - 946.

Joseph V., Ganesan V. and Shet U.S.P. 1987. Characteristics of open LPG jet flames in helical and tangential-slot swirl burners. J. of the Institute of Energy, 60, 193-198.

Kim K. and Marshall W. 1971. Drop size distributions from pneumatic atomizers. AIChE J., 17, 575 - 584.

Kliafas Y., Taylor A.M.K.P. and Whitelaw J.H. 1990. Errors due to turbidity in particle sizing using laser Doppler anemometry. Trans. of the ASME, J. Fluids Engin., 112, 142-148.

Law C.K. 1982. Recent advances in droplet vaporization and combustion. Progr. Energy Combust. Sci., 8, 171-201.

Lazaro B.J. and Lasheras J.C. 1989 Particle dispersion in a turbulent, plane, free shear layer. Phys. Fluids, A1(6), 1035 - 1044.

Lefebvre A.H. 1989. *Atomization and Sprays*. Hemisphere Publishing Corporation, New York.

Lian Z.W. and Lin S.P. 1990. Breakup of a liquid jet in a swirling gas. Phys. Fluids A2(12), 2134-2139.

Lorenzetto G. and Lefebvre A.H. 1977. Measurements of droplet size on a plain jet airblast atomizer. AIAA J., 15, 1006 - 1010.

Naber D. and Reitz R.D. 1988. Modelling engine spray/wall impingement. SAE paper no. 880107.

Nurick W.H. and Clapp S.D. 1969. An experimental technique for measurement of injector spray mixing. J. of Spacecraft and Rockets, 6, 1312-1315.

Nurick W.H. 1971. Analysis of sprays from rocket engine injectors. J. of Spacecraft and Rockets, 8, 796-798.

Özdemir I.B. and Whitelaw J.H. 1992. Impingement of an axisymmetric jet on unheated and heated flat plates. J. Fluid Mech., 240, 503-532.

Pilch M. and Erdman C.A. 1987. Use of breakup time data and velocity history data to predict the maximum size of stable fragments for acceleration-induced breakup of a liquid drop. Int. J. Multiphase Flow, 13, 741-757.

Priem R.J. and Heidman M.F. 1959. Vaporization of propellants in rocket engines. ARS Journal, 29, 836-842.

Ribeiro M.M. and Whitelaw J.H. 1980. Coaxial jets with and without swirl. J. Fluid Mech., 96, 769-795.

Rizk N.K. and Lefebvre A.H. 1980. The influence of liquid film thickness on airblast atomization. Trans. ASME, J. Eng. Power, 102, 706-710.

Sankar S.V., Brena de la Rosa A., Isakovic A. and Bachalo W.D. 1991. Liquid atomization by coaxial rocket injectors. AIAA paper no. 91-0691.

Sankar S.V., Wang G., Brena de la Rosa, Rudoff R.C., Isakovic A. and Bachalo W.D. 1992. Characterisation of coaxial rocket injector sprays under high pressure environments. AIAA paper no. 92-0228.

Simmons H.C. 1977. The correlation of drop-size distributions in fuel nozzle sprays. Part I: The drop-size/volume-fraction distribution. Trans. ASME : J. of Engineering for Power, 309-314.

Squires K.D. and Eaton J.K. 1990. Particle response and turbulence modification in isotropic turbulence. Phys. Fluids A2(7), 1191 - 1203.

Taylor G.I. 1934. The formation of emulsions in definable fields of flow. Proc. Roy. Soc. Lond., A146, 501-523. Also in : the Scientific papers of Sir Geoffrey Ingram Taylor, vol. IV, Mechanics of fluids : Miscellaneous papers, G.K. Batchelor (Ed.), Cambridge University Press, 1971, 107-125.

Taylor G.I. 1940. Generation of ripples by wind blowing over a viscous fluid. In the Scientific papers of Sir Geoffrey Ingram Taylor, vol. III, Aerodynamics and the mechanics of projectiles and explosions, G.K. Batchelor (Ed.), Cambridge University Press, 1963, 244-254.

Vafidis C. and Whitelaw J.H. 1991. A test facility for the study of liquid jet atomization under supercritical pressure conditions : preliminary study. Imperial College, Mechanical Engineering Department, Thermofluids Section, Report TF/91/32.

Wachters L.H.J. and Westerling N.A.J. 1966. The heat transfer from a hot wall to impinging water drops in the spheroidal state. Chemical Engineering Science, 21, 1047 - 1056.

Wall T.F. 1987. The combustion of coal as pulverized fuel through swirl burners. In : Principles of combustion engineering for boilers, Lawn C.J. (Ed.), Academic Press, London.

Wang T.-S. 1991. Computational analysis of the three-dimensional steady and transient SSME fuel preburner combustor. Proceedings of IUTAM symposium on Aerothermodynamics in Combustors, June 3-5, Taipei, Taiwan.

Wanhainen J.P., Parish H.C. and Conrad E.W. 1966. Effect of propellant injection velocity on screech in 20,000-pound hydrogen-oxygen rocket engine. NASA TN D-3373.

Wei C.Y. and Miau J.J. 1992. Stretching of freestream turbulence in the stagnation region. AIAA J., 30, 2196-2203.

Weiss M.A. and Worsham C.H. 1959. Atomization in high velocity airstreams. ARS Journal, 29, 252-259.

Woodmansee D.E. and Hanratty T.J. 1969. Mechanism for the removal of droplets from a liquid surface by a parallel air flow. Chemical Engineering Science, 24, 299-307.

Zaller M.M. and Klem M.D. 1991. Coaxial injector spray characterization using water / air as simulants. Presented at the 28th JANNAF Combustion Meeting, San Antonio, Texas.

APPENDIX A

Includes a copy of the following papers :

Hardalupas Y., McDonald H. and Whitelaw J.H. 1992. Two fluid mixing. In Proceedings of Advanced Earth-To-Orbit Propulsion Technology, R.J. Richmond and S.T. Wu (Eds.), NASA Conference Publication 3174, Vol. II, 63-72.

Hardalupas Y. and Whitelaw J.H. 1993. The characteristics of sprays produced by coaxial airblast atomizers. AIAA paper no. 93-0698. Presented at the 31st Aerospace Sciences Meeting & Exhibit, Reno, U.S.A.

NASA Conference Publication 3174, Vol. II

Advanced Earth-to-Orbit Propulsion Technology 1992

Edited by
R. J. Richmond
George C. Marshall Space Flight Center
Marshall Space Flight Center, Alabama

S. T. Wu
The University of Alabama in Huntsville
Huntsville, Alabama

Proceedings of a conference held at
NASA George C. Marshall Space Flight Center
Marshall Space Flight Center, Alabama
May 19–21, 1992

NASA
National Aeronautics and
Space Administration
Office of Management
Scientific and Technical
Information Program
1992

TWO FLUID MIXING

Hardalupas Y., McDonald H.* and Whitelaw J.H.
Imperial College of Science, Technology and Medicine
Mechanical Engineering Department
London SW7 2BX, United Kingdom.

ABSTRACT

Measurements of droplet size, velocity, liquid flux and concentration were carried out in sprays produced by a coaxial type airblast atomiser using a phase Doppler anemometer. The coaxial atomiser comprised a liquid jet with exit diameter 0.090" and length to diameter ratio of 22 positioned in the centre of a gaseous annular stream. The experiments were designed to simulate the characteristics of the SSME preburner sprays, by using water instead of liquid oxygen and air instead of hydrogen. Nozzles with annular width of 3, 6 and 10 mm were examined and the sprays covered a range of Weber number at the exit of the nozzle from 200 to 3500, of gas-to-liquid momentum ratio from 2 to 26, velocity ratio from 10 to 42, mass flowrate ratio from 0.2 to 1.2, liquid jet Reynolds number from 20000 to 55000 and gaseous jet Reynolds number from 90000 to 190000. The sprays were injected at atmospheric pressure and their development was examined up to 130 liquid jet diameters from the exit of the nozzle. The results show that the increase of the gas flowrate in the annulus for constant liquid flowrate resulted in better atomisation and reduced rate of spread of the spray, so there is a compromise to be made between finely atomised sprays and larger rate of spread. The increase of the liquid flowrate for constant gas flowrate resulted in poorer atomisation and reduced rate of spread.

INTRODUCTION

It is important to be able to control the droplet sizes and the spray width of airblast atomisers, since both parameters affect the mixing of the fuel with the oxidiser and can improve the combustion efficiency. For example, the atomisers of the preburners of the SSME atomise the liquid oxygen jet by a high velocity coaxial hydrogen jet. The ignition of the mixture, particularly during the startup process of the preburners, can be delayed with combustion occurring on the first and second stage blades of the gas turbine and the turbopump dome[1] and eventually the high temperature causes cracks on housings, sheetmetal, nozzles and blade shunks. So the characteristics of the airblast atomiser sprays are important for the liquid oxygen droplet evaporation and mixing with hydrogen.

An extensive review on airblast atomisation[2] and suggests that the influencial parameters of the atomisation are the exit Weber number, the Reynolds numbers of the gas and the liquid jet, the mass flowrate and the momentum flux ratio between the gas and the liquid jet, and the geometry of the nozzle. Most studies have made use of complex-geometry atomisers, where the effects of the parameters were difficult to separate. Also the sprays were mainly characterised by the spray angle and mean droplet size averaged over all the spray rather than local values.

The droplet sizes of sprays produced by simple-geometry coaxial airblast atomisers have recently been measured with a laser diffraction instrument[3], which provides the droplet mean diameter averaged over the line of sight of the laser beam interacting with the spray, and found that the Sauter mean diameter increases with the radial distance from the axis of the spray. However, the measurements with the laser diffraction technique can be misleading if they are not deconvoluted to provide local size information in the sprays[4]. The phase Doppler anemometer can provide local spray characteristics with high spatial resolution and has been used successfully to characterise dense Diesel and gasoline sprays[5,6,7]. Recently, the instabilities causing the atomisation process in airblast atomisers have been studied for exit Weber numbers up to 200 and liquid jet Reynolds numbers up to 4500 using photographic and imaging techniques[8,9] and the local spray characteristics close to the same nozzle were measured using a phase Doppler instrument[10] and it was found, in contrast to[3], that the radial distribution of the Sauter mean diameter has

---

* Formerly President SRA

two maxima one at the centre and one towards the spray boundary. However, the development of these sprays downstream of the nozzle was not examined and the values of Weber number and liquid Reynolds number used for their study were low relative to those used in the SSME preburner sprays.

This work examines the local size characteristics of coaxial atomiser sprays and the way the velocity characteristics of different droplet sizes develop with distance from the nozzle using a phase Doppler instrument. The values of the exit Weber number were between 200 and around 3500, the liquid Reynolds number between 20000 and around 55000 and the gas Reynolds number between 90000 and 190000 for different nozzle geometry dimensions. The next section presents the experimental arrangement, section 3 describes the results and section 4 summarises the main conclusions and describes the future work.

EXPERIMENTAL ARRANGEMENT

A single airblast coaxial atomiser was constructed and figure 1a shows the experimental arrangement with the basic dimensions. The atomiser operates at atmospheric pressure with air simulating hydrogen and water simulating liquid oxygen. A central tube provides the liquid to the nozzle and consists of a 10 mm diameter tube which is reduced to external diameter of 2.95 mm and an internal diameter of 2.3 mm (0.090") close to the exit of the nozzle. The length to diameter ratio of the thin part of the liquid tube at the exit of the nozzle was 22 and the diameter of the exit of the liquid tube is similar to that of the liquid oxygen tubes in the SSME. The liquid tube can easily be adjusted, so that its exit is either upstream or downstream of the exit of the gaseous jet, and can easily be changed so that different nozzle geometries can be examined.

The axial gas is supplied to the nozzle by four gas inlets with their axes normal to that of the nozzle (figure 1a). Flow straightners were used downstream of these inlets to remove any swirling motion of the gas and ensure axisymmetric flow. Since swirl is one of the parameters affecting atomisation, four additional tangential inlets could provide swirling gas flow. The gas flow was accelerated by a conical shape contraction before the exit of the nozzle to reduce possible flow asymmetries. Different nozzles, as shown in figure 1b, could be attached at the exit of the contraction resulting in annular widths of the gaseous jet of 3, 6 and 10 mm respectively, when a liquid jet tube with external diameter of 2.95 mm was used.

The axial and swirling gas were supplied by a compressor and metered separately by rotameters before passing to separate settling chambers. From each chamber four tubes supplied gas to the axial and tangential inlets of the experimental arrangement of figure 1a. The liquid was supplied by a tank using a powerful pump required by the pressure losses along the small diameter liquid tube. The liquid flowrate through the liquid tube was adjusted by a regulator existing on the return line of the excess liquid to the tank. The liquid content of the spray was collected in a tank while an exhaust system removed the gas with the mist of the small droplets generated by the spray. Flow straightners were used before the exhaust to ensure that the spray was not disturbed. The results presented here are for sprays without swirling gas and their parameters are summarised in table 1, although more cases have been examined and will be presented in a later communication.

TABLE 1 : Parameters of the sprays

annular width (mm)	gas velocity (m/s)	liquid velocity (m/s)	Reynolds number gas	Reynolds number liquid	Weber number	momentum ratio gas/liquid	velocity ratio gas/liquid	mass flowrate ratio
10	85	7.6	129100	20560	208	13.6	11.2	1.20
6	112	7.6	110810	20560	378	9.8	14.7	0.66
6	123	7.6	121698	20560	462	11.4	16.2	0.70
3	158	7.6	93590	20560	780	6.5	20.8	0.31
3	182	7.6	107800	20560	1050	8.6	23.9	0.35
3	266	7.6	157560	20560	2315	18.3	35.0	0.52
3	315	7.6	186580	20560	3275	25.5	41.4	0.61
3	266	10.0	157560	27060	2270	10.5	26.6	0.38
3	266	13.2	157560	35720	2215	6.0	20.1	0.30
3	266	16.8	157560	45460	2150	3.7	15.8	0.24
3	266	20.0	157560	54120	2097	2.6	13.3	0.20

3	315	16.8	186580	45460	3080	5.2	18.8	0.28
3	315	20.0	186580	54120	3015	3.7	15.8	0.23

The Reynolds number of the gaseous jet was based on the area averaged velocity at the exit and the exit diameter. The Weber number was estimated as $We = \rho_a U_{rel}^2 D / \sigma$, where ρ_a is the gas density U_{rel} is the relative velocity between the gaseous and the liquid jets at the exit, D is the diameter of the liquid jet exit and σ is the surface tension.

The velocity, diameter, flux and number density of the fuel droplets were measured by the phase-Doppler velocimeter[11,12] which comprised transmitting optics based on a rotating grating as beam splitter and frequency shifter and integrated receiving optics which collected the light scattered from the measuring volume in the forward direction. The receiving optics were arranged to collect light at a forward scattering angle of 30° on the bisector plane of the two laser beams to ensure that refraction through the droplets dominated the scattered light. The collected light was focused to the centre of a 100 μm slit and passed through a mask with three evenly spaced rectangular apertures before reaching the three photodetectors. The optical arrangement allowed the measurement of droplet diameters up to 360 μm. The optical characteristics of the instrument are given in table 2.

TABLE 2 : Optical characteristics of the phase Doppler instrument

Transmitting optics		
Laser: He-Ne laser		
operating power	35	mW
wavelength	632.8	nm
Beam intersection angle	3.024	deg.
Measurement volume length at $1/e^2$ intensity	4.88	mm
Measurement volume diameter at $1/e^2$ intensity	129	μm
Fringe spacing	11.991	μm
Number of fringes	11	
Frequency shift	0-3	MHz
Receiving optics		
Focal length of collimating lens	500	mm
Location of receiving optics from forward scatter angle	30	deg.
Equivalent aperture at collimating lens:		
dimension of rectangular aperture	67 x 10.6	mm
separation between aperture 1 and 2	13.3	mm
separation between aperture 1 and 3	26.6	mm
Magnification	1/2	
Spatial filter slit width	100	μm
Effective length of measuring volume	312.5	μm
Phase angle-to-diameter conversion factor for channel 1 and 3	0.973	μm/deg

The measured size distributions and the mean diameters estimates at each point were based on 20000 measurements resulting in statistical uncertainties of less than 2%[13] and the sizing accuracy of the instrument was less than 2 μm for droplets larger than 20 μm. The uncertainty is larger for the smaller droplets due to the tolerance of the phase-measuring electronic circuit and the oscillations of the phase shift remaining on the calibration curve of the instrument[11]. Droplet velocities were obtained in 60 size classes, with a 6 μm range in each size class. The uncertainties were less than 1% and 5% for the mean and rms values respectively, based on the average sample size of at least 1000 in each class for the smaller sizes and increased at the larger droplets due to the smaller sample size. The reduced number of measurements in the larger droplet size bins is due to the low number density of large droplets in the spray. The volume flux and number density of the liquid droplets were measured according to the method of[9]. The uncertainty of the flux measurements was around 30% in the dilute region of the spray due to uncertainties in the evaluation of the area of the probe volume for each size class and the rejection of measurements due to the validation procedure of the instrument[14,15,16] and higher in the dense region due to attenuation of the laser beams resulting in decreased signal to noise ratio and the occurrence of multiple droplets in the probe volume. The rate of spread of the spray was evaluated using the measured flux half width at each axial station from the nozzle, namely the radial

position where the liquid flux was half the value on the axis of the spray at each axial station. The droplet sizes carrying the 10%, 50% and 90% of the cumulative mass flux at each point and the spread of the size distribution were estimated.

RESULTS

This section describes the characteristics of the sprays, shows the effect of the gas and liquid flowrate on the atomisation and the rate of spread of the sprays and scales the results with the Weber number at the exit of the nozzle and the momentum ratio of the gas to liquid jet. The velocity characteristics of droplet sizes in the range of 6-12 μm, 48-54 μm and 102-108 μm, which are going to be referred to as 9, 50 and 105 μm in the rest of the text, are presented separately. These sizes were chosen, since the smaller droplets followed faithfully the mean and turbulent flow characteristics of the continuous phase, the 50 μm droplets corresponded to a value close to the most probable diameter in a large part of the spray and the 105 μm droplets indicated the motion of the large droplets in the spray, which carry a large fraction of the volume flux. The mean velocity and the rms of the fluctuations of the velocity were normalised by the liquid velocity averaged over the area at the exit of the liquid tube, U_{liquid}. The radial profile of volume flux of the droplets was normalised by the local centreline value of the flux, G_m. The radial distance from the axis of the spray, r, and the axial distance, z, from the exit of the nozzle were normalised by the diameter of the liquid jet exit, D.

SPRAY CHARACTERISTICS

Figure 2 presents the characteristics of coaxial atomiser sprays for an annular width of the gaseous jet of 10 mm, exit Weber number of 208 and momentum ratio of 13.6 at axial distances z/D=26, 52, 91 and 130 from the nozzle. These characteristics are qualitatively the same for all the examined sprays. Figure 2a shows the radial variation of the axial velocity of the 9, 50 and 105 μm droplet sizes. The mean axial velocity was normalised with the area averaged velocity at the exit of liquid jet, U_{liquid}, to indicate the rate of acceleration of the droplets relative to their initial velocity. The low velocity of the droplets close to the axis of symmetry of the spray indicates the delayed acceleration of the gas at the central part of the spray, while the droplet velocity is higher away from the axis where the gas velocity is also higher and causes the droplets to accelerate. The droplets in the central part of the spray were accelerated relative to the initial liquid jet velocity U_{liquid}=7.6 m/s with the axial distance from the exit and eventually the velocity minimum at the central part of the spray disappeared after z/D=91. The small droplets moved faster than the larger droplets up to the shear layer of the gas jet and then decelerated faster than the larger droplets, as the gas jet expanded and the gas velocity decreased, due to their better response to the continuous phase. The large droplets at the edge of the spray moved faster than the gas since they could not follow the continuous phase motion and maintained their upstream velocity for a larger distance in the spray.

Figure 2b shows the radial variation of the rms of the fluctuations of the axial velocity, u'. The rms fluctuations of the smaller droplets indicate the turbulence characteristics of the gaseous phase and were smaller at the centre, where most of the liquid content of the spray existed, and a maximum in the shear layer of the jet. The rms fluctuations of the axial velocity of the large droplets were smaller than those of the gas phase but larger than their negligible response to the continuous phase turbulence would suggest due to the deterministic motion of droplets reaching at the measuring point from different upstream positions with a wide range of axial velocities, and is the 'fan-spreading' effect[17].

Figure 2c shows the radial variation of the arithmetic, Sauter mean diameter and the median flux diameter of the spray. The mean diameters at the centre were much larger than at the edge of the spray. The shear at the interface between the fast moving gas jet and the liquid jet generated small droplets and, as the gas flow developed and the liquid jet diameter reduced, the expanding gas jet broke up the liquid jet even in the region close to the centre. Since the relative velocity between the gas and the liquid at the centre decreased, as figure 2a shows at z/D=26 and 52, larger droplets were generated close to the centre and remained there for a longer distance without dispersing, resulting in the larger mean diameters. Smaller droplets were generated away from the center during the breakup or were dispersed away from the center by the continuous phase turbulence faster than the large droplets after the completion of the breakup and resulted in the smaller mean diameters at the edge of the spray. This indicates that the finding of[3] with a laser diffraction instrument, namely that the Sauter Mean Diameter (SMD) was a minimum at the centre, was erroneous and due to the averaging of the spray droplet diameters over the line of sight of the diffraction instrument.

The phase Doppler instrument, which measures the local spray characteristics, is more appropriate to examine the characteristics of such sprays. Also the observation of two maxima in the radial distribution of the SMD, one at the centre and one at the edge of the spray,[10] may be a characteristic of the near nozzle region at low exit Weber number condition, which does not correspond to the conditions of the sprays in the preburners of the SSME.

Figure 2d presents the radial distribution of the volume flux of the liquid droplets and shows that most of the liquid content of the spray remained close to the centre. The radial profile quantifies the radial position where the spray flux became half of its centeline value and this is defined in the rest of the text as the flux half width of the spray, which increased from around 1.5D at z/D=26 up to around 4D at z/D=130. The flux half width of the spray indicates the rate of spread of the spray which is an important parameter for the mixing of the liquid droplets with the surrounding gas.

The centreline characteristics of the spray are shown in figure 3. The velocity of the droplets increased along the centreline relative to the area averaged velocity at the exit of the liquid jet U_{liquid}, figure 3a, since the gas stream accelerated the droplets after the breakup. The gas phase velocity on the centreline reached a maximum at a distance of z/D=90, a larger distance than the initial breakup length distance of the spray which is implied by calculations of the spray characteristics[18]. In the far field, the gas phase again decelerated along the centreline, as expected from the development of the jet, while the large droplets, which did not respond to the gas flow, maintained their velocity for longer time and appeared to move faster than the gas in some other cases. The scaling parameter, which can characterise the response of the droplets to the gas flow, is the mean Stokes number, defined as the ratio of the mean gas flow timescale to the relaxation time of the droplets, which was shown to increase with the distance from the nozzle[17], justifying the better response of the droplets far downstream and the reduced relative velocity between different droplet sizes. The Sauter mean diameter along the centreline, figure 3b, increased as the smaller droplets dispersed faster leaving more larger droplets on the centreline. The preferential spread of the droplets was supported also by the lower Sauter mean diameter outside the centreline (figure 2c). The median diameter along the centreline indicates that droplets larger than 200 μm carry half of the liquid flowrate and, although their number is small, they are very important for the combustion efficiency of the liquid fuel in the preburners.

EFFECT OF GAS FLOWRATE ON SPRAY CHARACTERISTICS

Figure 4 shows the effect of gas flowrate on atomisation and the rate of spread of the sprays produced by nozzles with 3 mm annular width of the gaseous jet, while the liquid flowrate remains the same. The increase of the gas flowrate results in an increase of the Weber number and the gas-to-liquid jet momentum ratio, so the increase of the gas flowrate on the figures corresponds to an increase in both.

The 9 μm droplets indicate the gas phase velocity and were accelerated faster for the high gas flowrate, figure 4a, so that their maximum velocity occurred closer to the nozzle than for the low gas flowrate. The 105 μm droplets were also accelerated faster for the high gas flowrate and the results imply that the relative velocity between the gas phase and the 105 μm droplets close to the nozzle was larger for the high gas flowrate resulting in breakup of more larger droplets close to the nozzle and finer atomisation. At z/D=26, the local Weber number based on the droplet diameter and the relative velocity, was around unity for the larger droplets, lower than the critical Weber number value of 6 for breakup and suggests that higher values occurred closer to the nozzle and were responsible for the breakup of the larger droplets.

Figure 4b shows the effect of the increase of the gas flowrate on the atomisation and the development of the Sauter mean diameter along the centerline. The Sauter mean diameter was lower for the higher gas flowrate, indicating finer atomisation and supporting the arguments of the previous paragraph based on the local Weber number of the droplets. The Sauter mean diameter increased along the centreline up to a certain distance from the nozzle, as the small droplets dispersed away from the spray axis faster than the larger droplets. When the large droplets also dispersed away from the centreline, the Sauter mean diameter decreased again and the radial distribution of droplet sizes in the spray became more uniform. This occurred closer to the nozzle for the higher gas flowrate because the droplet sizes in the spray were smaller and could respond to the gas phase and disperse in a shorter distance.

Figure 4c shows that increase in the gas flowrate led to decrease of the rate of spread in contrast to the expectations due to the improved atomisation by the increased gas flowrate. The result suggest that the high momentum of the gas phase jet close to the nozzle for the higher gas flowrate limited the spread of the otherwise finer droplets and, although the atomisation was improved, the mixing of the fuel with the oxidiser was reduced. So there

is a compromise to be made between the finer atomisation of the liquid jet and mixing close to the nozzle. Far downstream, the differences in the spread of the spray became smaller and the results suggest that the sprays produced by the higher gas flowrate became wider, as expected because the gaseous jet expands and the small droplets disperse more than the larger droplets.

EFFECT OF LIQUID FLOWRATE ON SPRAY CHARACTERISTICS

Figure 5 shows the effect of liquid flowrate on atomisation and rate of spread of the sprays produced by nozzles with 3 mm annular width of the gaseous jet, while the gas flowrate remains the same. The increase of the liquid flowrate results in a negligible decrease of the Weber number, since the change in the relative velocity between the gas and the liquid jet is small, and a large decrease of the gas-to-liquid jet momentum ratio.

Figure 5a shows the centreline development of the mean axial velocity of the 9 and 105 μm droplets for two liquid flowrates. The rate of acceleration of the droplets along the centreline decreased with increase of the liquid flowrate, which suggests increased breakup length. The gas phase was accelerated faster for the low liquid flowrate case. The 105 μm droplets were also accelerated faster for the low liquid flowrate case and the results imply that the relative velocity between the gas phase and the 105 μm droplets close to the nozzle was larger for the low liquid flowrate resulting in finer atomisation. For the high liquid flowrate, the relative velocity between the gas phase and the 105 μm was small and constant along the centreline and resulted in poorer atomisation.

Figure 5b shows the effect of increase of the liquid flowrate on the atomisation and the development of the Sauter mean diameter along the centerline. The Sauter mean diameter was larger for the high liquid flowrate indicating poorer atomisation. The increase of the liquid flowrate for constant gas flowrate had small effect on the Weber number, but resulted in lower gas-to-liquid momentum ratios, suggesting that the decrease of the momentum ratio for constant Weber number would result in poorer atomisation. Here also, as in figure 4b for the increased gas flowrate case, the Sauter mean diameter increased along the centreline and then decreased again.

Figure 5c shows that increase of the liquid flowrate decreases the rate of spread as expected due to the poorer atomisation when the liquid flowrate increased and the inability of the larger droplets to disperse quickly away from the centreline. Far downstream, the mixing between the fuel and the oxidiser became worse with the increase of the liquid flowrate due to the smaller dispersion of the large droplets.

CONCLUSIONS

The characteristics of sprays produced by coaxial airblast atomisers operating at conditions similar to those of the preburner sprays of the SSME but at atmospheric pressure have been measured by a phase Doppler instrument. The results have shown the following:

1. The Sauter mean diameter of the sprays is maximum at the centre and decreases with the radial distance from the axis. The mean axial velocity of the droplets is maximum at the shear layer and minimum on the centreline. The gas phase velocity, as indicated by the 9 μm droplets, is higher than that of the larger droplets close to the nozzle. Farther downstream the gas jet expands and the larger droplets, which maintain their initial velocity over longer distances, move faster than the gas phase. Most of the liquid content of the sprays remains close to the centre and the rate of spread of the sprays, as quantified by the flux half width at each axial station from the nozzle, was less than around 6D at axial distances from the nozzle of 130D for all the examined cases.
2. Increase of the gas flowrate improves the atomisation but at the same time limits the rate of spread of the spray close to the nozzle, and so reduces the mixing of the liquid with the gas. Farther downstream the sprays with high gas flowrate spread faster than those with lower gas flowrate.
3. Increase of the liquid flowrate results in poorer atomisation and reduced rate of spread.
4. The sprays have been scaled according to their exit Weber number and the gas-to-liquid jet momentum ratio and increase of both parameters improves the atomisation.
5. Additional parameters affect the atomisation, such as the position of the exit of the liquid jet relative to the gaseous jet exit, the existence of the convergence at the exit of the gaseous jet, the diameter of the liquid jet tube, the presence of swirl at the gaseous jet, and have been examined. The work also extended to the study of the sprays impinging on a plate, simulating the impingement of the sprays on the turbopump dome in the preburner of the SSME. Also the study of the interaction of multiple sprays have started and is still continuing. In the future this

work will extend to the study of the evaporation of the droplets by heating the gaseous jet at known initial temperatures.

ACKNOWLEDGEMENTS

The authors wish to acknowledge financial support from NASA Marshall Space Flight Center, under grant number NRA-90-MSFC-1.

REFERENCES

1. Wang T.-S. 1991. Computational analysis of the three-dimensional steady and transient SSME fuel preburner combustor. Proceedings of IUTAM symposium on Aerothermodynamics in Combustors, June 3-5, Taipei, Taiwan.
2. Lefebvre A.H. 1989. *Atomisation and Sprays.* Hemisphere Publishing Corporation, New York.
3. Caré I. and Ledoux M. 1991. Study of an air blast coaxial atomiser: experiments and modelisation. Proceedings of the 5th International Conference on Liquid Atomization and Spraying Systems (ICLASS), Gaithersburg, MD, USA, paper 85, 763-770.
4. Cossali E. and Hardalupas Y. 1992. Comparison between laser diffraction and phase Doppler velocimeter techniques in high turbidity, small diameter sprays. Experiments in Fluids, in the press.
5. Hardalupas Y., Taylor A.M.K.P. and Whitelaw J.H., 1990. Unsteady sprays by a pintle injector. JSME Intern. J., Ser. II, 33, 177-185.
6. Hardalupas Y., Taylor A.M.K.P. and Whitelaw J.H., 1992. Characteristics of the spray from a Diesel injector. Int. J. Multiphase Flow, 18, 159-179.
7. Pitcher G. and Wigley G. 1989. Velocity and dropsize measurements in fuel sprays in a direct injection Diesel engine. Proceedings of 3rd International Conference on Mechanics of two phase flows, 291-298. Taipei, Taiwan.
8. Faragó Z. and Chigier N.A. 1991. Classification of round liquid jet disintegration in coaxial air streams. Proceedings of the 5th International Conference on Liquid Atomization and Spraying Systems (ICLASS), Gaithersburg, MD, USA, paper 73, 661-668.
9. Mansour A. and Chigier N.A. 1990. Disintegration of liquid sheets. Phys. Fluids A, 2, 706-719.
10. Eroglu H. and Chigier N.A. 1991. Initial drop size and velocity distributions for airblast coaxial atomisers. Journal of Fluids Engineering, 113, 453-459.
11. Hardalupas Y. 1989. Experiments with isothermal two phase flows. PhD thesis, University of London.
12. Hardalupas Y. 1990. Description of the fluids section 'model 2' phase Doppler counter. Imperial College, Mechanical Engineering Department, Report no. FS/90/29.
13. Tate R.W. 1982. Some problems associated with the accurate representation of drop-size distributions. Proceedings of the 2nd International Conference on Liquid Atomization and Spraying Systems, Madison, Wisconsin, 341-351.
14. Bachalo W.D., Rudoff R.C. and Brena de la Rosa A. 1988. Mass flux measurements of a high number density spray system using the phase Doppler particle analyser. AIAA paper 88-0236.
15. Dodge L.G., Rhodes D.J. and Reitz R.D. 1987. Drop-size measurement techniques for sprays : comparison of Malvern laser diffraction and Aerometrics phase Doppler. Appl. Optics 26, 2144 - 2154.
16. Hardalupas Y. and Taylor A.M.K.P. 1989. On the measurement of particle concentration near a stagnation point. Experiments in Fluids, 8, 113-118.
17. Hardalupas Y., Taylor A.M.K.P. and Whitelaw J.H., 1989. Velocity and particle flux characteristics of turbulent particle-laden jets. Proc. Roy. Soc. Lond., A426, 31-78.
18. Przekwas A.J., Lee J.-G., Gross K.W., Chigier N.A. and Eroglu H. 1991. Analytical and experimental study of primary atomization of water jets. Proceedings of the 5th International Conference on Liquid Atomization and Spraying Systems (ICLASS), Gaithersburg, MD, USA, paper 93, 831-838.

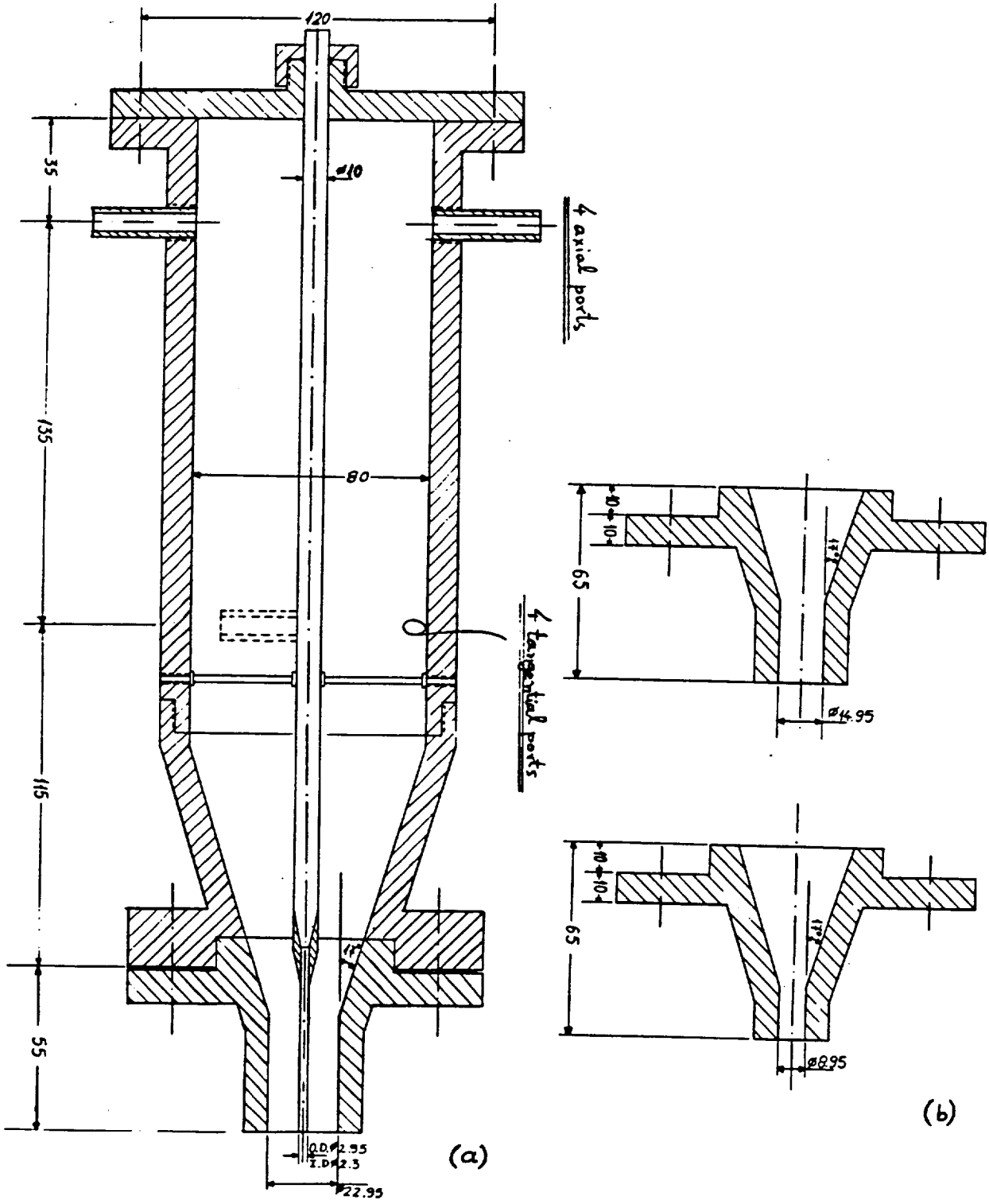

Figure 1. (a) Experimental arrangement of the coaxial atomiser with 10 mm annular width showing the basic dimensions; (b) nozzles used for the coaxial atomisers with 3 and 6 mm annular widths.

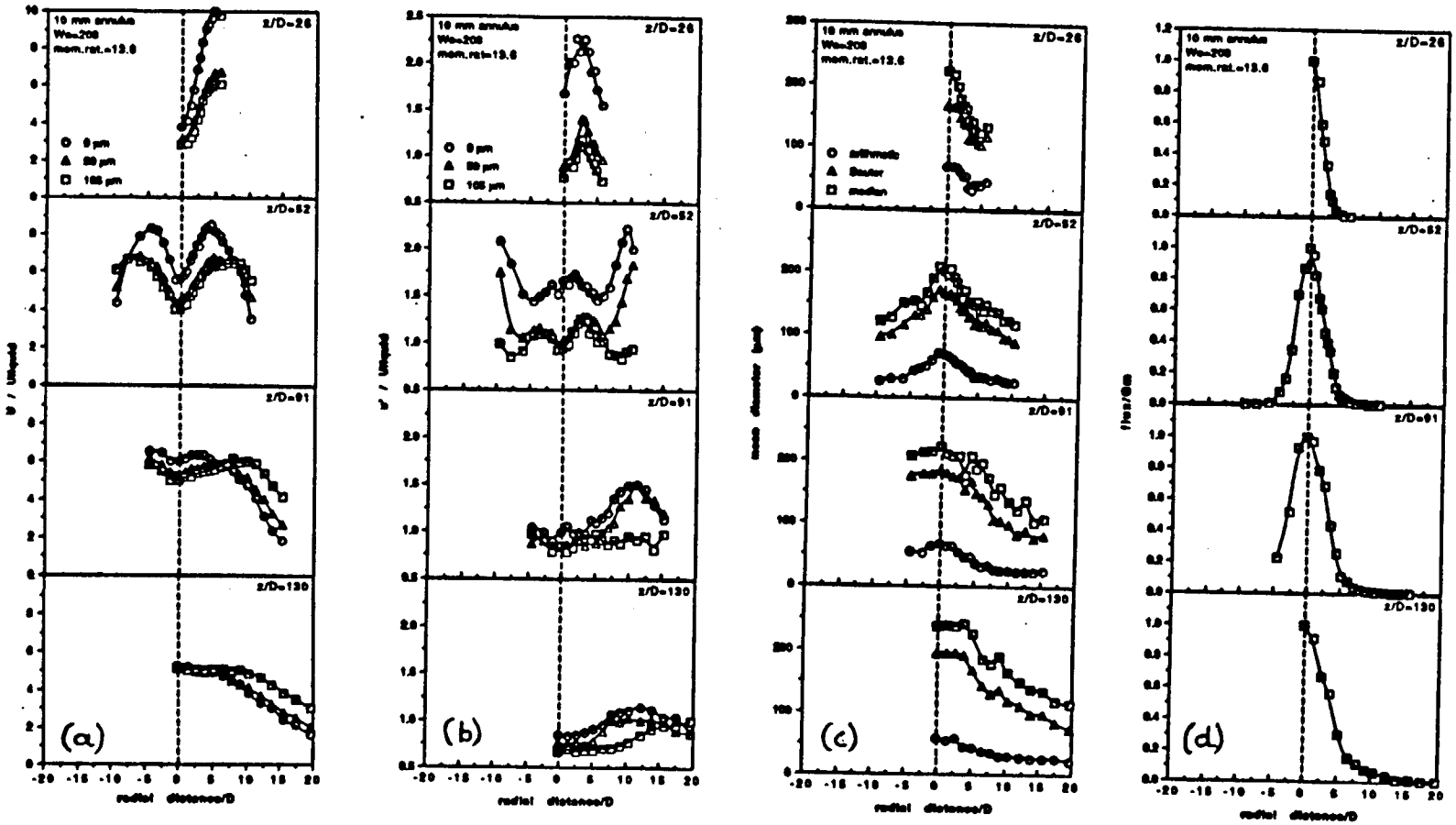

Figure 2. Radial profiles of the characteristics of a spray produced by a coaxial atomiser with annular width of 10 mm and exit Weber number=208 and gas-to-liquid momentum ratio=13.6 at axial distances from the nozzle z/D=26, 52, 91 and 130. (a) Mean axial velocity of 9, 50 and 105 μm droplets; (b) Rms of the fluctuations of the axial velocity of 9, 50 and 105 μm droplets; (c) arithmetic, Sauter and median diameter of the droplet size distributions; and (d) Volume flux of the liquid content of the spray.

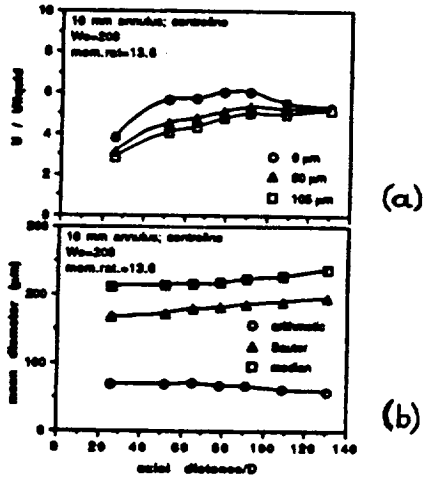

Figure 3. Centreline characteristics of a spray produced by a coaxial atomiser with annular width of 10 mm and exit Weber number=208 and gas-to-liquid momentum ratio=13.6. (a) Mean axial velocity of 9, 50 and 105 μm droplets; and (b) arithmetic, Sauter and median diameter of the droplet size distributions.

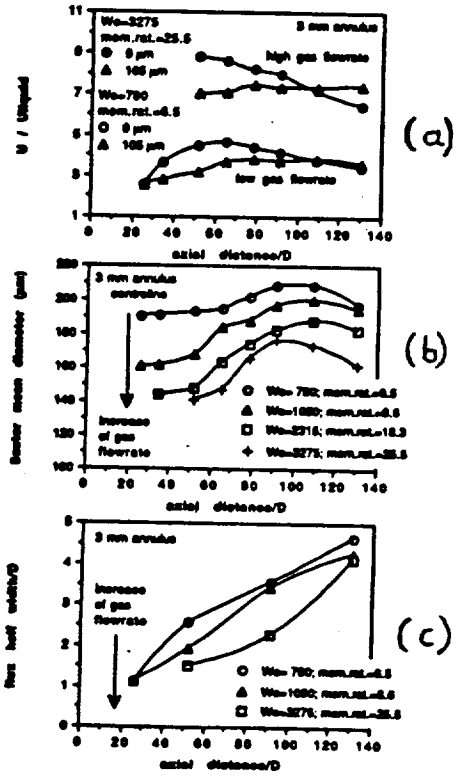

Figure 4. Influence of the gas flowrate on the spray characteristics, while the liquid flowrate remains constant. (a) Centerline development of the mean axial velocity of the 9 and 105 μm droplets; (b) centreline development of the Sauter mean diameter; and (c) change of the flux half width of the sprays with the axial distance from the nozzle.

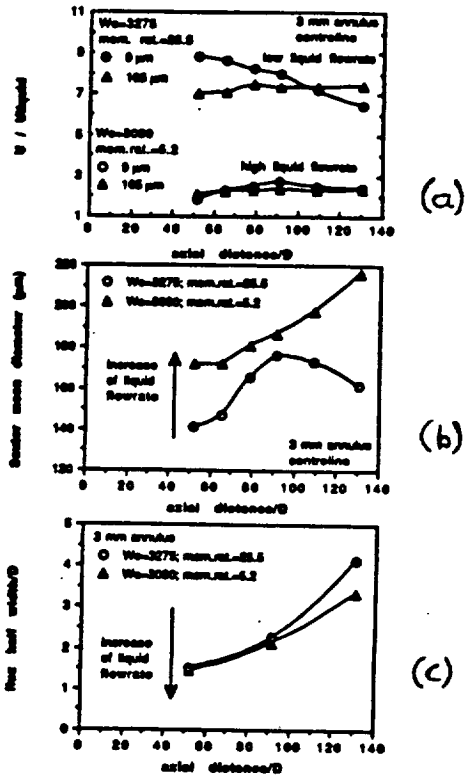

Figure 5. Influence of the liquid flowrate on the spray characteristics, while the gas flowrate remains constant. (a) Centerline development of the mean axial velocity of the 9 and 105 μm droplets; (b) centreline development of the Sauter mean diameter; and (c) change of flux half width of the sprays with the axial distance from the nozzle.

AIAA 93-0698

The Characteristics of Sprays Produced by Coaxial Airblast Atomisers

Y. Hardalupas and J.H. Whitelaw
Imperial College of Science, Technology and Medicine
Thermofluids Section
Mechanical Engineering Department
London SW7 2BX
United Kingdom.

31st Aerospace Sciences Meeting & Exhibit
January 11-14, 1993 / Reno, NV

THE CHARACTERISTICS OF SPRAYS PRODUCED BY COAXIAL AIRBLAST ATOMISERS

Hardalupas Y. and Whitelaw J.H.
Imperial College of Science, Technology and Medicine
Thermofluids Section
Mechanical Engineering Department
London SW7 2BX, United Kingdom.

Abstract

Measurements of droplet size, velocity, liquid flux and concentration were made in sprays produced by a coaxial airblast atomizer using a phase Doppler anemometer. The atomizer comprised a liquid jet with exit diameter varied between 1.1 and 2.3 mm positioned in the centre of a gaseous annular stream. The characteristics of the preburner sprays of the main engine of the space shuttle were simulated by using water and air respectively replacing liquid oxygen and hydrogen. The sprays covered a range of Weber number at the exit of the nozzle from 200 to 3500, of gas-to-liquid momentum ratio from 2 to 110, velocity ratio from 10 to 85, mass flowrate ratio from 0.2 to 1.3, liquid jet Reynolds number from 10000 to 55000 and gaseous jet Reynolds number from 90000 to 190000. Reduction of the diameter of the liquid tube was found to improve the atomization and reduce the rate of spread of sprays with similar gas-to-liquid velocity ratio. The presence of a converging nozzle at the exit of the gaseous jet improved the atomization and increased the rate of spread of sprays with gas-to-liquid velocity ratio up to around 45, but had no effect for higher velocity ratios. The recess of the liquid tube increased the rate of spread of the sprays for the straight exit jet and improved the atomization for $2D_l$ recess but reduced it for $3D_l$ recess.

1. Introduction

The atomization of liquid oxygen by a high velocity coaxial hydrogen stream is required in the preburner of the main engine of the space shuttle (SSME), and the characteristics of the sprays can influence the operation. The combustion stability of rocket engines has been shown to depend on the geometry of the coaxial injectors and on the gaseous and liquid injection velocity[1]. Also, the ignition of the mixture during the startup process of the preburner, can be delayed with combustion occurring even in the first and second stage blades of the gas turbine or the turbopump dome[2], causing cracks on housings, sheetmetal, nozzles and blade shunks. So it is important to be able to control the droplet sizes and the spray width of coaxial airblast atomizers, since both parameters affect the evaporation of the oxidizer and its mixing with the fuel and can limit combustion efficiency[3].

The characteristics of sprays produced by airblast atomizers have been reviewed[4,5] and results summarised by empirical correlations between the mean diameters of the sprays and the parameters of the atomization such as the exit Weber number, the Reynolds numbers of the gas and the liquid jet, the gas-to-liquid velocity, mass flowrate and the momentum flux ratio and the geometry of the nozzle. Most of these sprays were characterised mainly by their spray angle and mean droplet size averaged over the spray rather than local values, which makes it difficult to evaluate the effect of each parameters. So most of these correlations cannot characterise the spray characteristics over a wide range of conditions.

Early work on sprays produced by coaxial airblast injectors was performed by droplet capture and imaging techniques[6] and hot wax freezing[7], but accuracy was limited. Optical non-intrusive sizing techniques have allowed more accurate and detailed sizing measurements. Laser diffraction provides the droplet mean diameter averaged over the line of sight of the laser beam and has shown that the Sauter mean diameter increases with the radial distance from the axis of the spray[8], but such measurements can be misleading if they are not deconvoluted to provide local size information[9] and they do not provide the droplet velocity. The visibility/intensity interferometric technique measures the local size and velocity of sprays[4], but with limited accuracy of the size measurements particularly at the smaller droplets in the sprays. The phase Doppler anemometer provides local spray characteristics with high spatial resolution and has been used successfully to characterise sprays produced by coaxial injectors[10,11,12,13,14]. For exit Weber numbers up to 200 and liquid jet Reynolds numbers up to 4500, the radial distribution of the Sauter mean diameter has been shown to have two maxima, at the centre and towards the spray boundary[10], in contrast to[8]. Sprays produced from nozzles with gas and liquid flowrates close to the values of rocket engines, maximum values of mean diameter have been shown to exist close to the centre[11,13].

Although the effect of the geometry of the nozzle has been examined previously[11,14], the spray conditions were limited and the effect of the recess of the exit of the liquid tube upstream of the exit of the gaseous jet, for example, remains unclear. This work examines the effect of the nozzle geometry on the local size and velocity characteristics of coaxial atomizer sprays using a phase Doppler instrument. The effect of the liquid tube diameter, the liquid tube recess and the existence of a convergence at the exit of the gaseous jet has been examined. The conditions of the sprays were in the range of exit Weber number between 200 and 3500, liquid Reynolds number between 10000 and 55000 and gas Reynolds number between 90000 and 190000. The next section presents the experimental arrangement, section 3 describes and discusses the results and section 4 summarises the main conclusions.

2. Experimental arrangement

The airblast atomizer of figure 1a was constructed and operated at atmospheric pressure with air replacing the hydrogen and water the liquid oxygen of the SSME. A central tube provided the liquid to the nozzle and consisted initially of a 10 mm diameter tube which reduced to an external diameter of 2.95 mm with internal diameter D_l = 2.3 mm (0.090") and with length to diameter ratio 22; a second internal tube with external diameter 1.47 mm and internal diameter D_l = 1.1 mm with length to diameter ratio 45 was also used. The exit of the liquid tube could be adjusted, to be in the plane of the exit of the gaseous jet or recessed.

The gas flowrate was supplied to the nozzle by four gas inlets with their axes normal to that of the nozzle (figure 1a). Flow straighteners were used to remove residual swirling motion and ensure axisymmetric flow. Since swirl is one of the parameters affecting atomization, four additional tangential inlets could provide swirling gas flow, but there were not used during the reported work. The gaseous flow was accelerated by a conical shape contraction before the exit of the nozzle to reduce possible flow asymmetries. Nozzles with straight and converging exits, as shown in figure 1b, could be attached at the

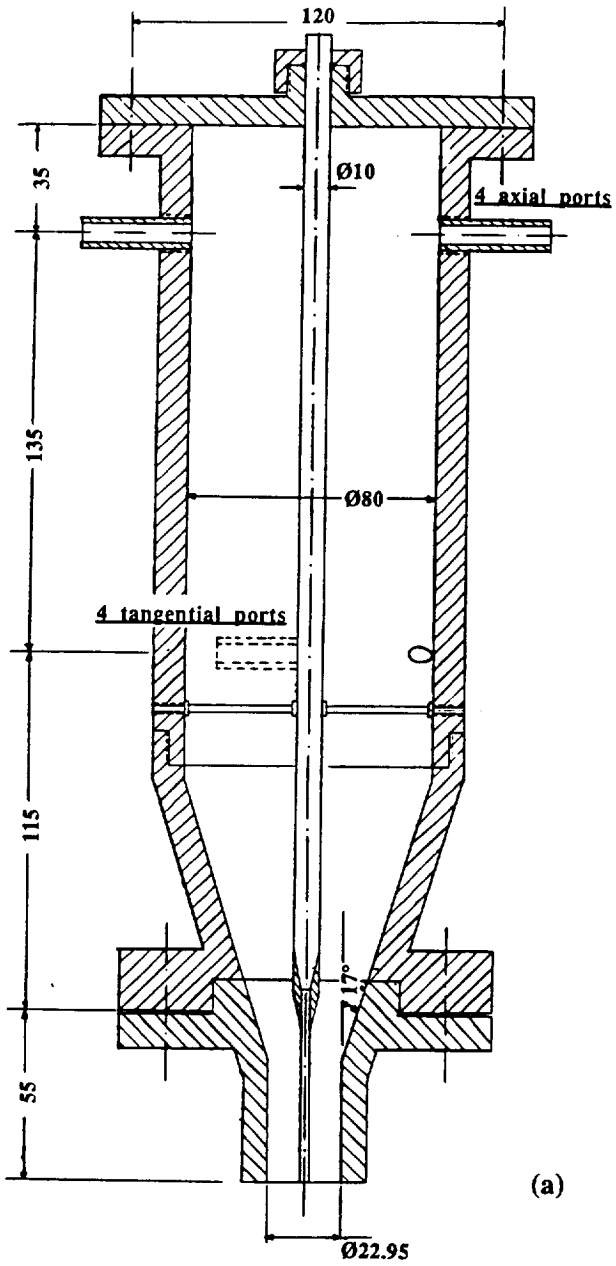

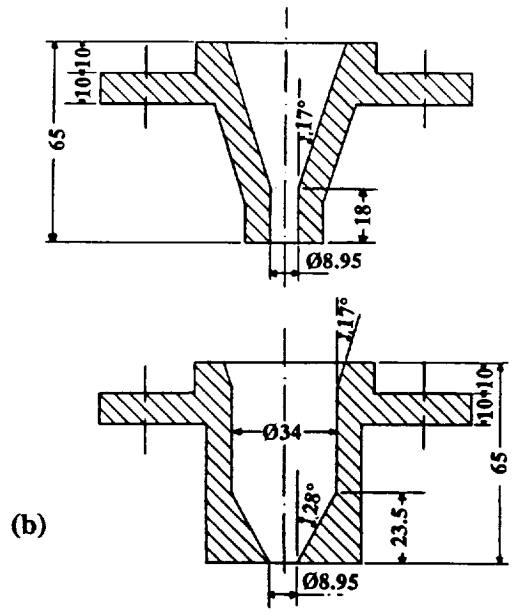

Figure 1. (a) Experimental arrangement of the coaxial atomizer with 10 mm annular width; (b) nozzles used for the coaxial atomizers with 3 mm annular widths with straight and converging exit.

exit of the gaseous jet with diameter of 8.95 mm resulting in annular widths of 3 mm and 3.74 mm when the liquid jet tube with external diameter of 2.95 mm and 1.47 mm was used. The length of the straight part of the nozzle was 18 mm and the converging nozzle had a half angle of 28° and length of 23.5 mm.

The axial and swirling gas flowrates were provided by a compressor and metered separately by rotameters before passing to separate settling chambers from which four tubes supplied gas to the axial and tangential inlets of the arrangement of figure 1a. The liquid was pumped from a tank and adjusted by a valve in the return line of excess liquid to the tank. The liquid content of the spray was collected in a tank while an exhaust system removed the gas with the mist of the small droplets generated by the spray. Flow straighteners were used to ensure that the spray was undisturbed. The results presented here are for sprays without swirling gas covering a range of Weber number at the exit of the nozzle from 200 to 3500, of gas-to-liquid momentum ratio from 2 to 110, velocity ratio from 10 to 85, mass flowrate ratio from 0.2 to 1.3, liquid jet Reynolds number from 10000 to 55000 and gaseous jet Reynolds number from 90000 to 190000. The Reynolds number of the gaseous jet was based on the velocity averaged over the area of the annulus at the exit and the exit diameter. The Weber number was defined as $We = \rho_g U_{rel}^2 D_l / \sigma$, where ρ_g is the gas density U_{rel} is the relative velocity between the gaseous and the liquid jets at the exit, D_l is the diameter of the liquid jet exit and σ is the surface tension.

The velocity, diameter, flux and number density of the fuel droplets were measured by the phase-Doppler velocimeter[15,16] which comprised transmitting optics based on a rotating grating, used as beam splitter and frequency shifter, and integrated receiving optics which collected the light scattered from the measuring volume in the forward direction. The receiving optics were arranged to collect light at a forward scattering angle of 30° on the bisector plane of the two laser beams to ensure that refraction through the droplets dominated the scattered light. The collected light was focused to the centre of a 100 μm slit and passed through a mask with three evenly spaced rectangular apertures before reaching the three photodetectors. The optical arrangement allowed the measurement of droplet diameters up to 360 μm. The optical characteristics of the instrument are given in the following table.

The measured size distributions and mean diameters at each point were based on at least 20000 measurements resulting in statistical uncertainties of less than 2%[17] and the sizing accuracy of the instrument was less than 2 μm for droplets larger than 20 μm. The uncertainty was larger for the smaller droplets due to the tolerance of the phase-measuring electronic circuit and oscillations of phase shift[15]. Droplet velocities were obtained in 60 size classes, with a 6 μm range in each size class. The uncertainties were less than 1% and 5% for the mean and rms values respectively, based on an average sample size of at least 1000 in each class for the smaller sizes and increased at droplets larger than 150 μm due to the smaller sample size. The reduced number of measurements in the larger droplet size bins was due to the low number density of large droplets in the spray. The volume flux and number density of the liquid droplets were measured according to the method of[20]. The uncertainty of the flux measurements was around 30% in the dilute region of the spray due to uncertainties in the evaluation of the area of the probe volume for each size class and the rejection of measurements due to the validation procedure of the instrument[18,19,20] and higher in the dense region due to attenuation of the laser beams resulting in decreased signal to

noise ratio and the occurrence of multiple droplets in the probe volume. The rate of spread of the spray was evaluated using the half width of the flux profile at each axial station from the nozzle, namely the radial position where the liquid flux was half the value on the axis of the spray at each axial station.

TABLE : Optical characteristics of the phase Doppler instrument

Transmitting optics		
Laser: He-Ne laser		
operating power	35	mW
wavelength	632.8	nm
Beam intersection angle	3.024	deg.
Probe volume dimensions at e^{-2} intensity length	4.88	mm
diameter	129	μm
Fringe spacing	11.991	μm
Number of fringes	11	
Frequency shift	3	MHz
Receiving optics		
Focal length of collimating lens	500	mm
Location of receiving optics from forward scatter angle	30	deg
Equivalent aperture at collimating lens: dimension of rectangular aperture	67 x 10.6	mm
separation between aperture 1 and 2	13.3	mm
separation between aperture 1 and 3	26.6	mm
Magnification	1/2	
Spatial filter slit width	100	μm
Effective length of measuring volume	312.5	μm
Phase angle-to-diameter conversion factor for channel 1 and 3	0.973	μm/deg

3. Results and Discussion

This section evaluates the effect of the diameter of the inner pipe, the existence of a converging nozzle at the exit of the gaseous jet and the influence of axial recess between the exit planes of the inner and outer pipes on atomization, rate of spread and velocity characteristics of the sprays. The velocity characteristics of droplet sizes in the range 6-12 μm and 102-108 μm, which are going to be referred to as 9 and 105 μm in the rest of the text, are presented separately. These sizes were chosen, since the smaller droplets followed faithfully the mean flow characteristics of the continuous phase and the 105 μm droplets indicated the motion of the large droplets in the spray, which carry a large fraction of the volume flux. The gas-to-liquid exit velocity ratio of the sprays will be referred as V.R. in the rest of the text. The diameter of the liquid tube will be referred as D_l or D_{liquid} in the text or in the figures and the diameter of the gaseous jet as D_{gas}.

Effect of liquid tube diameter

Figure 2a presents the radial variations of the axial velocity of the 9 and 105 μm droplet sizes of sprays produced by a coaxial atomizer with the gaseous jet diameter of 8.95 mm, the two inner tube diameters of 2.3 and 1.1 mm and a gas-to-liquid velocity ratio (V.R.) of around 25 at a distance z/D_{gas} = 13.4 from the nozzle. The radial and axial distances from the axis and the exit of the nozzle respectively were normalised by the diameter of the gaseous tube, D_{gas}, and the axial velocity of the droplets by the gas velocity averaged over the area of the annulus, U_{gas}, to allow comparison between sprays with different initial gas velocity. For the nozzle with D_l=2.3 mm, the low velocity of the 9 μm droplets close to the axis of symmetry indicates the delayed acceleration of the gas at the central part of the spray, while the 105 μm droplet velocity was higher away from the axis where the gas velocity was also higher and caused the droplets to accelerate faster than at the centre. The droplets of the spray from the nozzle with D_l=1.1 mm accelerated faster and there was no minimum axial velocity on the centreline at the examined location, because the initial

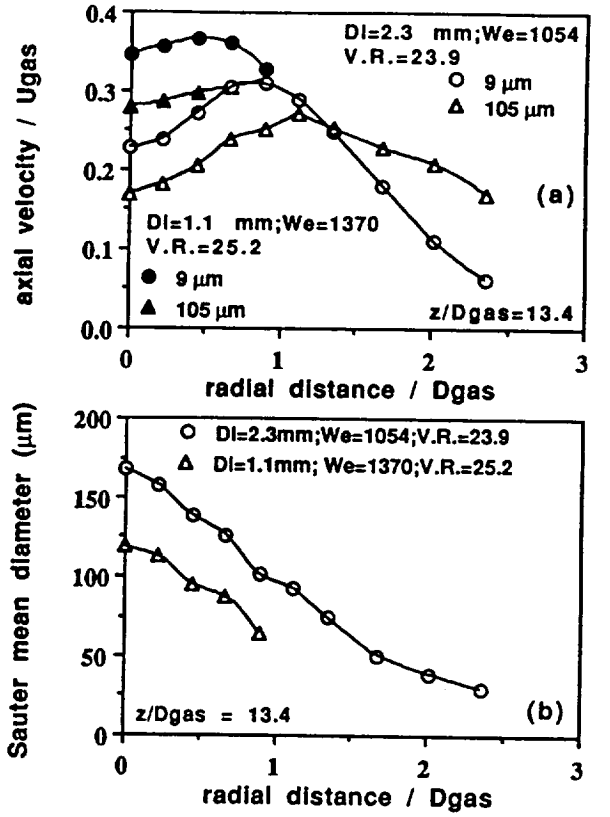

Figure 2. Radial profiles of velocity and SMD : D_{gas}=8.95 mm, and D_l=2.3 and 1.1 mm for V.R.=25 at axial distance from the nozzle z/D_{gas}=13.5. (a) Mean axial velocity of 9 and 105 μm droplets; (b) Sauter mean diameter.

diameter of the liquid jet was smaller and allowed the liquid jet to break up more rapidly. The droplets in the central part of the spray with D_l=2.3 mm continued to accelerate with axial distance from the exit and downstream of z/D_{gas} =13.5 the velocity minimum at the central part of the spray disappeared. The small droplets moved faster than the larger droplets up to the shear layer of the gas jet and then decelerated faster than the larger droplets, as the gas jet expanded and the gas velocity decreased, due to their better response to the continuous phase. The large droplets at the edge of the spray moved faster than the gas since they could not follow the continuous phase and maintained their upstream velocity for a larger distance. The relative velocity between the large droplets and the gaseous phase was responsible for the secondary atomization and the behaviour of the droplets and this information was absent in the results of the average velocity over all droplet sizes[11,12,14]. The local Weber number based on the droplet Sauter mean diameter and the relative velocity, was around unity for the larger droplets, lower than the critical Weber number value of 6 for breakup and suggests that higher values occurred closer to the nozzle and were responsible for the breakup of the larger droplets. The parameter, which can characterise the response of the droplets to the gas flow, is the mean Stokes number, defined as the ratio of the mean gas flow timescale to the relaxation time of the droplets, which was shown to increase with the distance from the nozzle[21] and, since the timescale of the gas phase increases, justifies the better response of the droplets downstream from the nozzle and the reduction of the relative velocity between small and large droplet sizes. However, the large droplets had straight trajectories determined by their initial conditions for most of the spray, without responding to the gas phase turbulence, and with a 'fan spreading' effect[21].

Figure 2b shows that the radial variation of the Sauter mean diameter (SMD) of the spray had a maximum at the centre and decreased with the radial distance. The shear at the interface

between the fast moving gaseous jet and the liquid jet generated small droplets which dispersed faster away from the axis and surrounded the developing sprays. The large droplets were generated at the centre after the break up of the liquid jet and remained there over a longer period of time. Comparison between the SMD of the sprays from the two nozzles shows that, with D_l=1.1 mm, atomization improved by around 25% for V.R.=25. The radial variation of the SMD indicates that the finding of[8] with a laser diffraction instrument, namely that the SMD was a minimum at the centre, was erroneous and caused by averaging of the spray droplet diameters over the line of sight of the diffraction instrument. Also the observation of two maxima in the radial distribution of the SMD, one at the centre and one at the edge of the spray[10], may be a characteristic of the near nozzle region at a low exit Weber number condition, which does not correspond to the conditions of the sprays in the preburners of the SSME.

The centreline value of the Sauter mean diameter close to the nozzle is an indication of the atomization efficiency of the nozzle, since this is the region where the spray had not dispersed. Figure 3 presents the centreline development of the SMD for the two nozzles and for V.R. of 14 and 25. The nozzle with D_l=1.1 mm produced consistently smaller droplets by around 25%. The SMD along the centreline increased as the smaller droplets dispersed faster leaving the larger droplets on the centreline. The preferential spread of the droplets was supported also by the lower SMD outside the centreline (figure 2b). It should be noted that the corresponding exit Weber number was larger for the large diameter liquid jet nozzle for V.R.=14 (figure 3a). When considered in isolation, this suggests better atomization for the large diameter liquid jet, which is opposite to our results. So the effect of the exit Weber number on the characteristics of the sprays was less important for nozzles with similar gas-to-liquid velocity ratios and this will

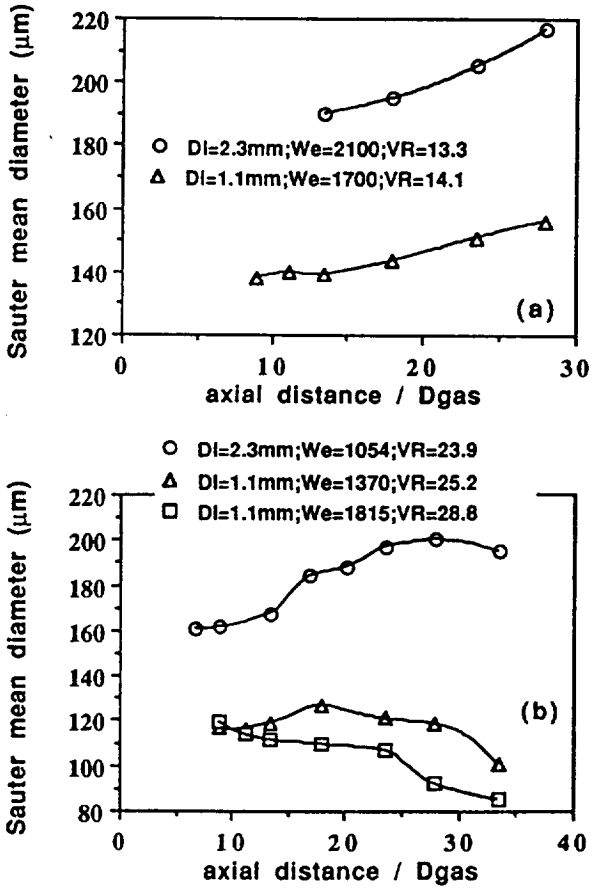

Figure 3. Centreline development of the Sauter mean diameter : D_{gas}=8.95 mm, and D_l=2.3 and 1.1 mm for (a) V.R.=14 and (b) V.R.=25.

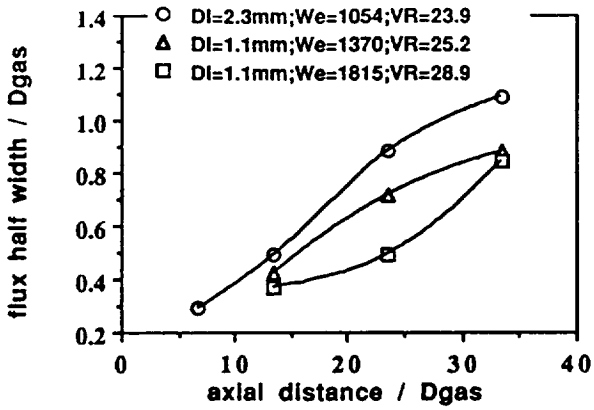

Figure 4. Flux half width of the sprays with the axial distance from the nozzle : D_{gas}=8.95 mm, and D_l=2.3 and 1.1 mm for V.R.=25.

be discussed in detail in another communication[22]. Comparison of figures 3a and b shows that the SMD increased with decrease of the gas-to-liquid velocity ratio, so that the atomization reduced with the reduction of the gas-to-liquid velocity ratio and justifies the observed correlation between sprays produced by low gas-to-liquid velocity ratio nozzles and combustion instability[1].

The flux half width of the sprays normalised by the diameter of the gaseous jet is presented in figure 4 and indicates that the spray from the larger liquid jet tube was wider by around 20%, while the atomization was reduced. So rate of spread and atomization characteristics of the sprays cannot be improved at the same time and there is a trade off between improving the atomization, which affects the vaporization of the oxidizer and the rate of spread, which affects the mixing of the fuel with the oxidizer. Figure 4 also shows that increasing the gas-to-liquid velocity ratio for the small liquid tube diameter nozzle by increasing the gas flowrate reduces the rate of spread of the spray close to the nozzle, which has also been observed for the large liquid jet diameter nozzle[13].

Summarising the results, the effect of the reduction of the liquid jet diameter by around 50% was to improve the atomization of sprays with the same gas-to-liquid velocity ratio, but the width of the spray was reduced by the reduction of the liquid tube diameter up to a distance of 30 D_{gas} from the nozzle. Reduction of the gas-to-liquid velocity ratio reduces atomization.

Effect of converging gaseous jet exit

The effect of a convergence with a half angle of 28° at the exit of the gaseous jet on the atomization and rate of spread of the spray was examined with the nozzle of figure 1b. The gaseous jet diameter, D_{gas}, was 8.95 mm and the liquid jet diameter, D_l, was 2.3 mm. The radial and the axial distances from the nozzle and the flux half width were normalised by the liquid jet diameter. Figure 5 shows the centreline development of the SMD for the converging and the straight exit nozzle, and that the effect of the converging nozzle on atomization was greater for low gas-to-liquid velocity ratios, and the atomization was improved by around 20% and 10% for gas-to-liquid velocity ratios of 23.9 and 41 respectively.

In order to understand the effect of low and high gas-to-liquid velocity ratio for the converging nozzle, the radial variation of the SMD and the axial velocity of the 9 and 105 μm droplets at a distance of z/D_l = 26 may be compared for the converging and the straight nozzle. The SMD for a spray with V.R. = 37.5 was 10% lower on the axis as well as at the edge of the spray, figure 6a, while there was no difference between the spray size characteristics, figure 6b, for V.R.=51. So the results suggest that the atomization improved with the converging nozzle when the gas-to-liquid velocity ratio was lower than 45. The axial velocity characteristics for the same velocity ratios, figure 7, show that the velocity in the central part

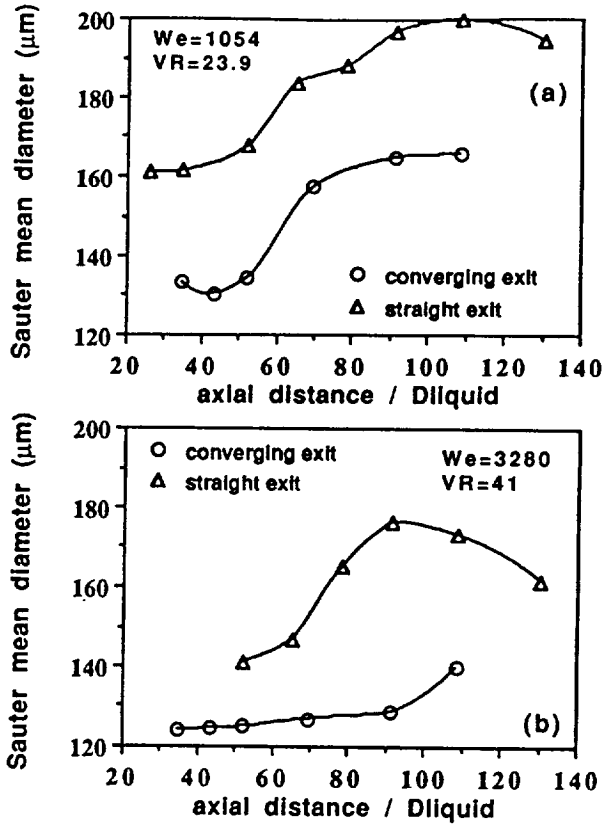

Figure 5. Centreline development of the Sauter mean diameter : D_{liquid} (or D_l) =2.3 mm with the straight and converging exit nozzle with D_{gas}=8.95 mm (a) We=1054 and V.R.=23.9 (b) We=3280 and V.R.=41.

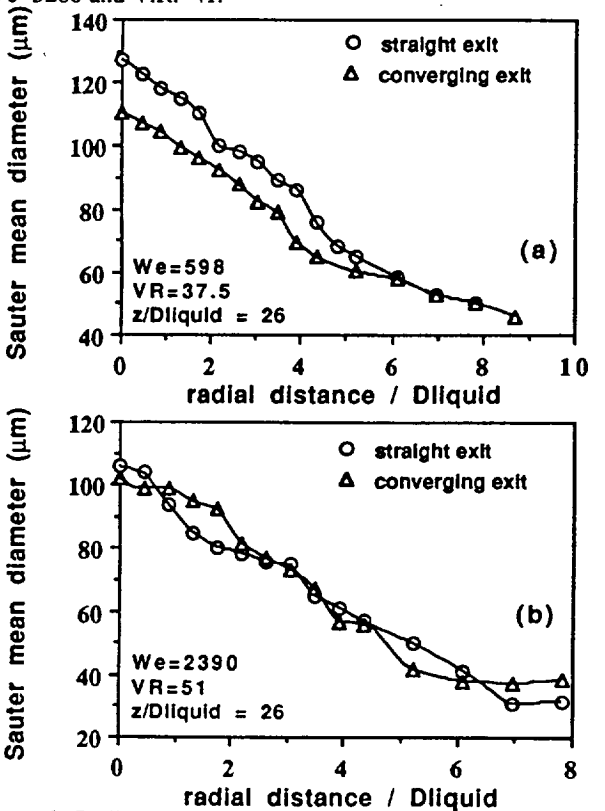

Figure 6. Radial profiles of Sauter mean diameter : D_l=2.3 mm with the straight and converging exit nozzle with D_{gas}=8.95 mm at axial distance from the nozzle z/D_l=26. (a) We=598 and V.R.=37.5 (b) We=2390 and V.R.=51.

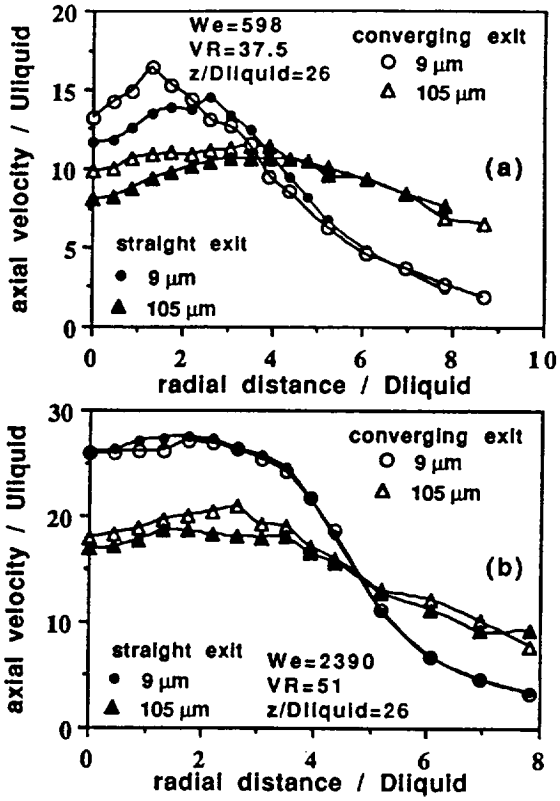

Figure 7. Radial profiles of axial velocity of 9 and 105 μm droplets : D_l=2.3 mm with the straight and converging exit nozzle with D_{gas}=8.95 mm at axial distance from the nozzle z/D_l=26. (a) We=598 and V.R.=37.5 (b) We=2390 and V.R.=51.

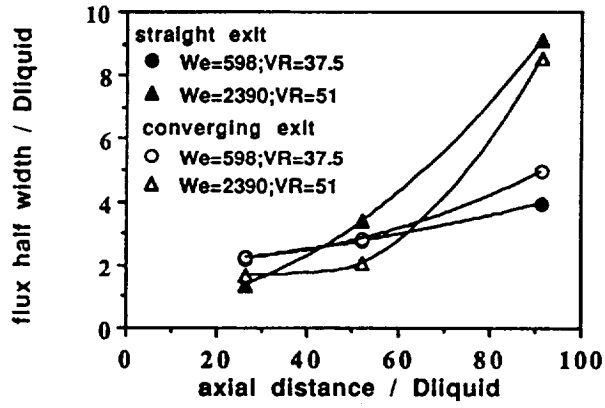

Figure 8. Flux half width of the sprays with the axial distance from the nozzle : D_l=2.3 mm with the straight and converging exit nozzle with D_{gas}=8.95 mm for We=598, V.R.=37.5 and for We=2390, V.R.=51.

of the spray increased with the converging nozzle relative to the straight exit nozzle for V.R.=37.5 and there was no difference for V.R=51. Since the converging nozzle had a half angle of 28°, the velocity vector at the exit of the nozzle is expected to be inclined by the same angle towards the liquid jet and so can break up the liquid jet faster for V.R lower than 45. For V.R. higher than 45 the shear between the gas and the liquid phase was sufficient to atomize the liquid jet without help from the directed gaseous jet.

Figure 8 shows that the flux half width increased by around 20% for the converging nozzle for V.R.=37.5. However, increasing the gas-to-liquid velocity ratio above 45 reversed this effect close to the nozzle, although at z/D_l =90 the

widths of the sprays were similar for both nozzles. It should be noted that both nozzles had lower rates of spread close to the nozzle as the velocity ratio increased and this suggests that the high momentum of the gas phase jet close to the nozzle for the higher gas flowrate limited the spread of the otherwise finer droplets and, although the atomization was improved, the mixing of the fuel with the oxidizer was reduced. So there is a compromise to be made between the finer atomization of the liquid jet and mixing close to the nozzle. Far downstream, the differences in the width of the spray became smaller and the results suggest that the sprays produced by the higher gas flowrate became wider, as expected because the gaseous jet expands and the small droplets dispersed more than the larger droplets.

Effect of liquid tube recess

This effect will be examined for the straight and the converging nozzles separately.

Straight gaseous jet exit nozzle.

Recesses of 0, 4.6 and 7 mm with the D_l=2.3 mm diameter liquid jet tube were examined, corresponding to 0, $2D_l$ and $3D_l$, and the centreline development of the SMD of the sprays, figure 9, shows that a recess of $2D_l$ improved atomization by around 15% independent of the gas-to-liquid velocity ratio over a range of 20 to 41. Increasing the recess to $3D_l$ reduced atomization for the V.R.=24, figure 9a, although, for values of z/D_l greater than 50, the SMD was reduced relative to that without recess, but it was always greater than for recess of $2D_l$. The improved atomization of the spray with the recess of the tube has been observed by other investigations[11] and it was also found to improve the combustion stability of rocket engines[1] which implied improved atomization. Improved atomization can be caused by the higher gaseous velocity at the initial interface between the liquid and the gaseous jet, when the tube is recessed, because the confinement of the flow does not allow the gaseous jet to expand as at the exit. However, this explanation cannot support the reduction in the atomization when the recess increased more than $2D_l$ or the findings of other workers[14], who found reduction of atomization with recess of the tube. The radial variation of the SMD, figure 10a and b, shows that for a recessed tube by $2D_l$, the mean diameters are lower at the centre but greater away from the axis from those without recess and this effect was stronger for higher V.R. So an area average droplet diameter over a plane of the spray may indicate no change in the atomisation characteristics and the observed differences on the centreline values of the SMD may be due to differences in droplet dispersion rather than improved atomization. However, for recess of $3D_l$, the radial variation of SMD of figure 10 shows that the mean droplet sizes were larger at the centre as well as at the edge of the spray relative to the recess of $2D_l$, and this observation can only be explained by reduced atomization.

The influence of the recess on the rate of spread of the sprays, figure 11, shows that the flux half width of the sprays increased by around 40% for all the cases with a recess and for V.R. between 20 and 41. So the rate of spread supports the argument of the previous paragraph, that the larger droplets dispersed faster away from the centreline when the liquid tube was recessed and justifies the centreline development and the radial profiles of the Sauter mean diameter, figure 9 and 10. This was caused probably by the atomization of the liquid jet upstream of the gaseous jet exit, so the droplets that existed at the exit of the gaseous jet could respond to the sudden expansion of the gaseous jet and dispersed away from the central part of the spray faster. Thus the improved combustion stability observed with the liquid tube recessed[1] could have been caused by improved mixing rather than improved atomization.

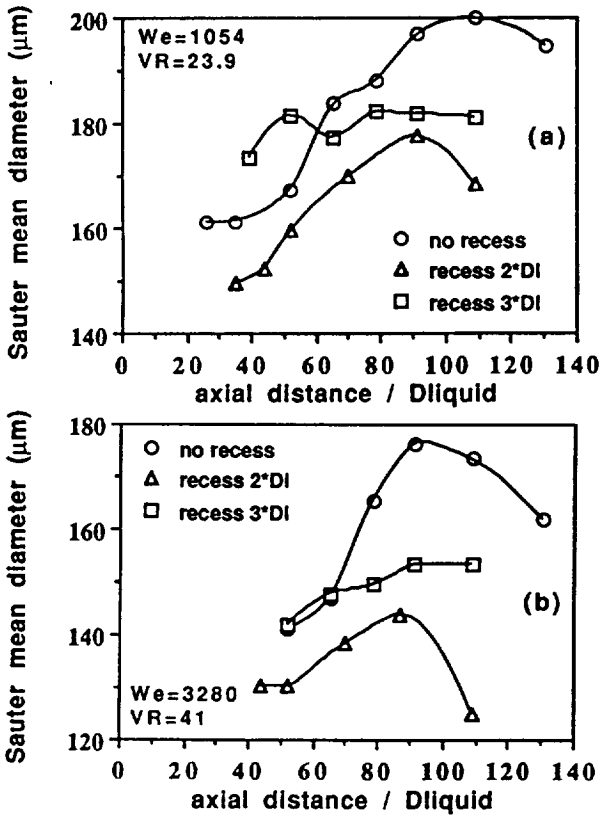

Figure 9. Centreline development of the Sauter mean diameter : D_l=2.3 mm with the straight exit nozzle with D_{gas}=8.95 mm as a function of the liquid tube recess. (a) We=1054 and V.R.=23.9, (b) We=3280 and V.R.=41.

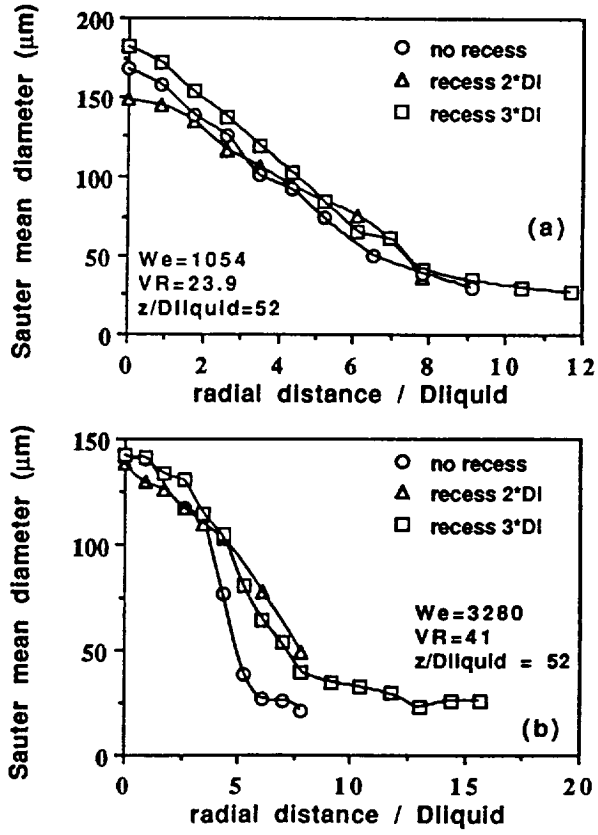

Figure 10. Radial profiles of Sauter mean diameter : D_l=2.3 mm with the straight exit nozzle with D_{gas}=8.95 mm at axial distance from the nozzle z/D_l=52 as a function of the liquid tube recess. (a) We=1054 and V.R.=23.9, (b) We=3280 and V.R.=41.

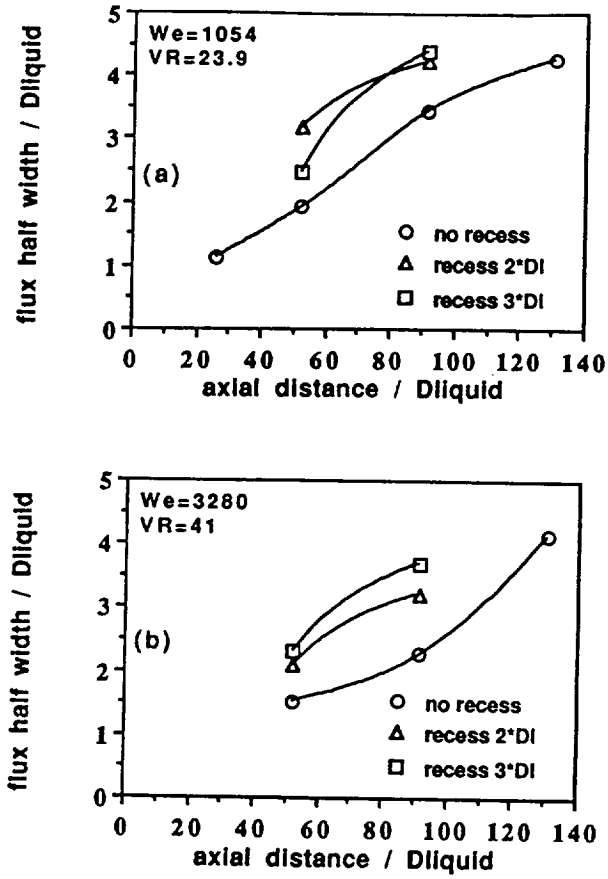

Figure 11. Flux half width : D_l=2.3 mm with the straight exit nozzle with D_{gas}=8.95 mm as a function of the liquid tube recess. (a) We=1054, V.R.=23.9 and (b) We=3280, V.R.=41.

Converging gaseous jet exit nozzle.

The effect of the recess of the liquid tube with diameter 2.3 mm by 0, 4.6 and 7 mm was examined for the converging exit nozzle, again corresponding to recesses 0, 2D_l and 3D_l respectively.

Figure 12 shows that the centreline atomization decreased with the recess, which caused the annular width of the tube at the exit of the liquid jet to be larger and, as a result, the local gaseous velocity to be lower. For V.R.=23.9, the effect of recessing the tube by 2D_l was negligible, probably because the effect of improving the atomization due to the converging nozzle, was eliminated by the reduction of the gas-to-liquid exit velocity ratio. For the larger recess, 3D_l, the reduction at the gas-to-liquid velocity ratio was larger and the atomization was reduced by around 15%. For larger V.R.=41, the atomization was clearly reduced by 10% and 15% for recess 2D_l and 3D_l respectively, which is less than expected, from the decrease of the gas velocity and the gas-to-liquid velocity ratio by 3 and 4 times for recesses of 2D_l and 3D_l respectively due to the increase in the area of the gaseous jet annulus at the exit of the liquid jet by the same amount. However, the gas velocity would still increase downstream of the exit of the recessed liquid tube due to the converging gaseous jet, so the gas velocity at the exit of the converging nozzle would be only 10% lower than for the case without recess, which could justify the small reduction in atomization.

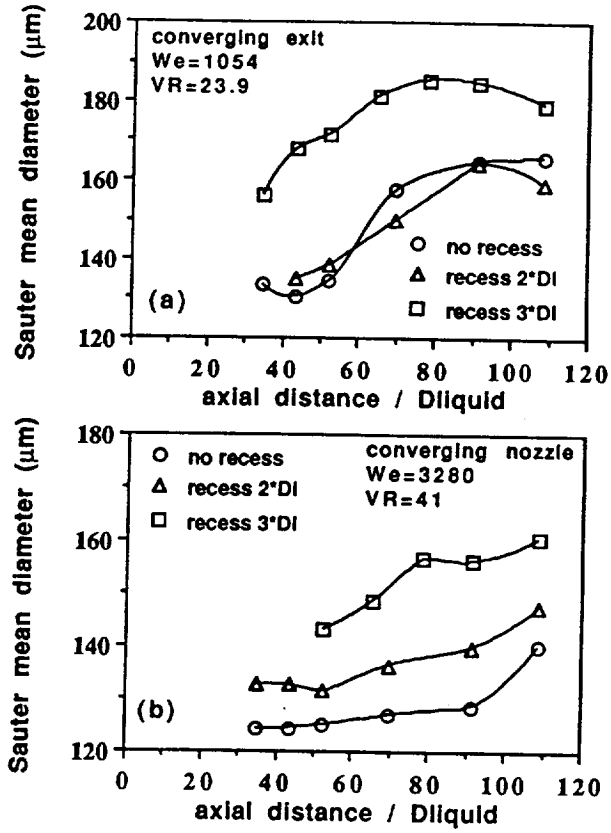

Figure 12. Centreline development of the Sauter mean diameter: D_l=2.3 mm with the converging exit nozzle with D_{gas}=8.95 mm as a function of the liquid tube recess. (a) We=1054 and V.R.=23.9, (b) We=3280 and V.R.=41.

4. Conclusions

The characteristics of sprays produced by coaxial airblast atomizers operating at atmospheric pressure with air and water have been measured by a phase Doppler instrument. The results have shown the following:

1. For sprays with the same gas-to-liquid exit velocity ratio, decrease of the diameter of the liquid tube by around 50%, improved the atomization by around 25%, but decreased the rate of spread of the sprays by 20%. So there is a trade off between improved atomization and rate of spread.
2. Atomization was improved when the gas-to-liquid velocity ratio increased, but the rate of spread close to the nozzle was reduced.
3. The use of a 28° half angle converging nozzle at the exit of the gaseous jet improved atomization by around 20% and 10% for velocity ratio of 24 and 41 respectively and rate of spread by 20% for gas-to-liquid exit velocity ratios up to around 45 relative to the straight exit nozzle. For gas-to-liquid velocity ratios higher than 45 atomization was not improved but the rate of spread of the sprays was rather reduced close to the nozzle relative to the straight exit nozzle.
4. The effect of a recess of 2D_l of the liquid tube with the straight exit nozzle was to improve atomization by 15% and to reduce it for a recess of 3D_l. However, the recess improved the rate of spread by around 40% which could justify the differences in the local sizing characteristics and could improve combustion stability as a consequence.
5. The effect of a liquid tube recess with the converging exit nozzle was to reduce atomization. The effect was larger for a gas-to-liquid velocity ratio higher than 40 for which atomization was reduced by 10% and 15% for recesses 2D_l and 3D_l.

Acknowledgements

The authors wish to acknowledge financial support from NASA Marshall Space Flight Center, under grant number NRA-90-MSFC-1. Mr. J.R. Laker designed and constructed the electronics of the phase Doppler instrument. Mr. P. Trowell constructed the experimental facility. We are grateful to Mr. H. Struck and Dr. H. McDonald for many useful discussions during the conduct of this research.

References

1. Wanhainen J.P., Parish H.C. and Conrad E.W. 1966. Effect of propellant injection velocity on screech in 20,000-pound hydrogen-oxygen rocket engine. NASA TN D-3373.
2. Wang T.-S. 1991. Computational analysis of the three-dimensional steady and transient SSME fuel preburner combustor. Proceedings of IUTAM symposium on Aerothermodynamics in Combustors, June 3-5, Taipei, Taiwan.
3. Priem R.J., Heidman M.F. 1959. Vaporization of propellants in rocket engines. ARS Journal, 29, 836-842.
4. Ferrenberg A., Hunt K. and Duesberg J. 1985. Atomization and mixing study. NASA CR-178751.
5. Lefebvre A.H. 1989. *Atomisation and Sprays*. Hemisphere Publishing Corporation, New York.
6. Weiss M.A. and Worsham C.H. 1959. Atomization in high velocity airstreams. ARS Journal, 29, 252-259.
7. Burick R.J. 1972. Atomization and mixing characteristics of gas/liquid coaxial injector elements. J. of Spacecraft and Rockets, 9, 326-331.
8. Caré I. and Ledoux M. 1991. Study of an air blast coaxial atomizer: experiments and modelisation. Proceedings of the 5th International Conference on Liquid Atomization and Spraying Systems (ICLASS), Gaithersburg, MD, USA, paper 85, 763-770.
9. Cossali E. and Hardalupas Y. 1992. Comparison between laser diffraction and phase Doppler velocimeter techniques in high turbidity, small diameter sprays. Experiments in Fluids, in the press.
10. Eroglu H. and Chigier N.A. 1991. Initial drop size and velocity distributions for airblast coaxial atomizers. Journal of Fluids Engineering, 113, 453-459.
11. Sankar S.V., Brena de la Rosa A., Isakovic A. and Bachalo W.D. 1991. Liquid atomization by coaxial rocket injectors. AIAA paper no. 91-0691.
12. Sankar S.V., Wang G., Brena de la Rosa, Rudoff R.C., Isakovic A. and Bachalo W.D. 1992. Characterisation of coaxial rocket injector sprays under high pressure environments. AIAA paper no. 92-0228.
13. Hardalupas Y., McDonald H. and Whitelaw J.H. 1992. Two fluid mixing. Presented at the 1992 conference on Advanced Earth-To-Orbit Propulsion Technology, NASA MSFC, Huntsville, Alabama.
14. Zaller M.M. and Klem M.D. 1991. Coaxial injector spray characterization using water / air as simulants. Presented at the 28th JANNAF Combustion Meeting, San Antonio, Texas.
15. Hardalupas Y. 1989. Experiments with isothermal two phase flows. PhD thesis, University of London.
16. Hardalupas Y. 1990. Description of the fluids section 'model 2' phase Doppler counter. Imperial College, Mechanical Engineering Department, Report no. FS/90/29.
17. Tate R.W. 1982. Some problems associated with the accurate representation of drop-size distributions. Proceedings of the 2nd International Conference on Liquid Atomization and Spraying Systems, Madison, Wisconsin, 341-351.
18. Bachalo W.D., Rudoff R.C. and Brena de la Rosa A. 1988. Mass flux measurements of a high number density spray system using the phase Doppler particle analyser. AIAA paper 88-0236.
19. Dodge L.G., Rhodes D.J. and Reitz R.D. 1987. Drop-size measurement techniques for sprays : comparison of Malvern laser diffraction and Aerometrics phase Doppler. Appl. Optics 26, 2144 - 2154.
20. Hardalupas Y. and Taylor A.M.K.P. 1989. On the measurement of particle concentration near a stagnation point. Experiments in Fluids, 8, 113-118.
21. Hardalupas Y., Taylor A.M.K.P. and Whitelaw J.H., 1989. Velocity and particle flux characteristics of turbulent particle-laden jets. Proc. Roy. Soc. Lond., A426, 31-78.
22. Hardalupas Y. and Whitelaw J.H. 1992. Scaling of sprays produced by coaxial airblast atomizers. In preparation.

APPENDIX B

Includes a copy of the report :

Vafidis C. and Whitelaw J.H. 1991. A test facility for the study of liquid jet atomization under supercritical pressure conditions : preliminary study. Imperial College, Mechanical Engineering Department, Thermofluids Section, Report TF/91/32.

IMPERIAL COLLEGE OF SCIENCE, TECHNOLOGY AND MEDICINE
Department of Mechanical Engineering
Thermofluids Section, Exhibition Road, London SW7 2BX, U.K.

A TEST FACILITY FOR THE STUDY OF LIQUID JET ATOMISATION UNDER SUPERCRITICAL PRESSURE CONDITIONS: PRELIMINARY STUDY

by

C. Vafidis and J.H. Whitelaw

November 1991

TF/91/32

ABSTRACT

This report proposes a laboratory experiment for the study of the atomisation process of a super-critical pressure, sub-critical temperature liquid jet in a supercritical pressure and temperature gaseous environment. The objective is to simulate the liquid oxygen atomisation process in the gaseous hydrogen environment of the SSME fuel preburner during the priming stage of its combustion chamber. It is shown that this process can be adequately simulated by the atomisation of super-critical pressure liquid Freon-12 in super-critical air, allowing the study of the liquid atomisation process under stationary flow conditions by means of Phase Doppler Anemometry in a relatively low pressure environment and at ambient temperatures.
Based on this simulation principle, a suitable test facility for the relevant study is proposed and its primary components are specified. The proposed experimental arrangement allows the variation of injector element geometry and of the main simulation parameters within the range of interest. It also provides for further simulations and studies of the liquid jet evaporation and transient atomisation/evaporation processes.

1 INTRODUCTION

The Space Shuttle Main Engine (SSME) is fuelled by gaseous hydrogen and uses liquid oxygen (LOX) as oxidiser. The SSME Powerhead assembly, shown schematically in Figure 1, consists of a main combustion chamber where fuel and oxidiser are mixed and burned to produce the required thrust. Hydrogen is pumped to the main injector bowl using a three stage High Pressure Fuel Turbopump (HPFTP) and liquid oxygen is supplied through an array of LOX tubes using a similar, single stage, pump (HPOTP). Both hydrogen and oxygen turbopumps are powered by axial turbines operating with hydrogen-rich fuel/oxidiser mixture which is burned in the corresponding preburners. The fuel preburner combustor consists of the Augmented Spark Igniter (ASI), a number of fuel injectors and the combustion chamber. Liquid oxygen and gaseous hydrogen are mixed by generating liquid oxygen sprays in order to produce a locally combustible mixture. Combustion is initiated by the ASI near the injector elements and the hot gases, which are hydrogen-rich combustion products, flow over the dome and into the stages of the axial turbine to power the HPFTP. The hot gases exiting from the axial turbine are directed through a 180^{o} turnaround duct to the hot gas manifold and then to the main injector bowl, via three (or two) transfer ducts. The hot gases from both turbopump preburners are used to pre-heat the liquid oxygen flowing through the LOX tubes of the main injector bowl and finally are mixed with it and burned into the main combustion chamber.
Despite the short duty cycle of the SSME powerhead, its extreme operating conditions, illustrated in the propellant flow schematic of Figure 2, cause significant structural and thermal loading of the SSME components, particularly in the, hotter, fuel side. In order to improve component life and

engine repair downtime, numerous studies have been undertaken to investigate anomalies observed in various SSME components. One of those, which forms the subject of the present preliminary study, is related to the fuel preburner and turbine hot parts. As has been reported [1] despite continuous improvement of the fuel preburner components of the SSME, several problems exist with its operation which include cracking of turbine blade shanks and fillets. These are primarily attributed to the extreme thermal environment during the engine start-up transient and, to a lesser extent, to inefficient LOX atomisation and possible unmixedness of the gaseous oxygen under steady state operating conditions which lead to locally excessive heating.
The objective of the present study is to investigate the possibility of understanding the LOX atomisation process in the SSME fuel preburner using relatively simple experiments in a suitable laboratory test facility. This study follows a recent, more fundamental, work [2] in which liquid jet atomisation studies under atmospheric conditions have been carried out using Phase Doppler Anemometry (PDA) in geometries similar to those of the LOX injector elements. The test facility proposed here aims to enable extension of these studies in high pressure environments and supercritical liquid jet conditions.
The following section outlines in greater detail the problem and sets the background for the proposed experimental investigation.

2 BACKGROUND

The start sequence of the fuel preburner, a schematic of which is shown in Figure 3, can be simply described as follows:
The combustion chamber and turbine blade passages are initially purged with nitrogen gas. After the start command, the fuel and oxidiser flow out from the ASI and the injector elements to prime the combustion chamber and turbine. This is the stage at which the fuel/oxidiser mixture is initially formed. The injector element geometry is shown in Figure 4 and consists of a coaxial tube arrangement with oxygen discharging through the central tube and hydrogen through the annulus. Both fuel and oxygen are injected into the combustion chamber at supercritical pressures (P_h/P_{hc}=26.25 and P_o/P_{oc}=6.75). The oxygen remains during injection at subcritical temperatures (T_o/T_{oc}=0.75) while the hydrogen fuel remains at high supercritical temperatures (T_h/T_{hc}=4.6). At each of the injector elements, therefore, the oxygen behaves like a liquid jet surrounded by an annular gaseous fuel flow. Mixing of the liquid oxygen with the gaseous fuel takes place through the atomisation of the liquid jets which brake into smaller droplets, increasing their area to improve evaporation. The gas temperature is higher than that of the liquid jet and, in fact, very close to its critical temperature (154 K). The liquid droplets are heated by the convective gas flow and, finally, evaporate to form a combustible mixture. Combustion is initiated by a swirling igniter torch issued from the ASI. The swirling motion of the torch acts like a flame holder and, by the time it reaches the turbine dome, the bulk of the

propellants is ignited. Combustion is then sustained by the continuous flow of fuel and oxidiser from the injector elements.
Combustion stoichiometry requires fuel/oxidiser mass flow rate ratio of 1/8=0.125. In fact the corresponding mass flow rates have an overall ratio of 1.154 (or 0.84 at the injector elements) indicating near ten times excess fuel. This should lead to full consumption of the available oxidiser but, according to the results of reference [1], an appreciable amount of oxidiser is left unburned and enters the turbine stages where it can cause chemical attack to the blade metal. Temperature peaks of the order of 1400 K have been calculated and measured near the turbine entry during the first 1 s of preburner operation, which are much higher than the expected average of 1100 K in the preburner, and are attributed to the mismatch of fuel and oxidiser flow rates and combustible mixture maldistribution prior to ignition.
A summary of the conditions prevailing during preburner operation is given in Table 1. All quantities are approximate and vary from engine to engine. Propellant properties are given in S.I. units and were obtained from references [3-5].
The above description of preburner operation highlights the complexity of the flow and combustion processes involved. Some aspects of these processes, mainly droplet evaporation and burning at elevated and near-critical pressure conditions have been theoretically studied in, for example, references [6-10]. Very few experimental studies have been reported in this field, particularly as far as the liquid atomisation process at elevated and super-critical pressures is concerned.
The present study will concentrate on the simulation of the liquid oxygen atomisation process prior to ignition, which corresponds to the critical stage of combustion chamber and turbine priming.

3 ATOMISATION AT ELEVATED PRESSURES

Ignoring the LOX droplet evaporation, the transient nature of the mixture formation and ignition process and the combustion process itself, one is left with the fundamental problem of liquid droplet atomisation from a matrix of coaxial liquid/gaseous jets in a supercritical pressure environment. Further simplification of the problem leads to a single coaxial liquid/gaseous jet arrangement issuing in an elevated pressure environment. Atomisation of a liquid under ordinary atmospheric conditions is governed by shear in the outer layer of the liquid core, characterised by the ratio of inertial to surface tension forces (Weber number, $We=\rho_g(U_g-U_l)^2 d/\sigma_l$), and by the momentum ratio between the liquid and gaseous phases, as well as by geometric details of the injector arrangement. The recent work of reference [2] examined in detail the atomisation of a water/air annular jet arrangement similar to that of Figure 4 under atmospheric conditions. This parametric study made use of Phase Doppler Velocimetry (PDA) to characterise the effect of We number and momentum ratio on water droplet size and velocity distribution along the centre-line and across several diameters of the coaxial jet arrangements shown in Figure 5. This study encompassed ranges

TABLE 1
Operating characteristics and propellant properties in the SSME fuel preburner

	FUEL (Hydrogen)	OXIDISER (Oxygen)	
Total mass flow rate	m_{ht}=35.47	m_{ot}=30.74	kg/s
Injector mass flow rate	m_h=0.113	m_o=0.134	kg/s
No. of injectors (estimate)	230		
Inlet temperature	T_h=154	T_o=116	K
Inlet pressure	P_{hi}=373x10^5	P_{oi}=407x10^5	N/m^2
Injector end pressure	P_h=340.5x10^5	P_o=340.5x10^5	N/m^2
Exit velocity	U_h=366	U_o=30.5	m/s
Central tube dia.		d=2.26x10^{-3}	mm
Annulus inner dia.	d_i=3.76x10^{-3}		
Annulus external dia.	d_e=4.928x10^{-3}		
Hydraulic diameter	Dh=1.168x10-3	Do=2.26x10-3	m
Flow area	A_h=7.966x10^{-6}	A_o=4.009x10^{-6}	m^2
Fuel/Oxidiser mass flow rate ratio	m_{ht}/m_{ot}=1.154		
Critical Pressure	P_{hc}=12.97x10^5	P_{oc}=50.43x10^5	N/m^2
Critical Temperature	T_{hc}=33.2	T_{oc}=154.58	K
Reduced Pressure	P_h/P_{hc}=26.25	P_o/P_{oc}=6.75	
Reduced Temperature	T_h/T_{hc}=4.64	T_o/T_{oc}=0.75	
State	Supercritical Gas	Supercritical Pressure Liquid	
Inlet density	ρ_{hi}=41.22	ρ_{oi}=1111	kg/m^3
Exit density	ρ_h=38.67	ρ_o=1098	kg/m^3
Exit volume flow rate	V_h=2.92x10^{-3}	V_o=0.122x10^{-3}	kg/s
Inlet viscosity	μ_{hi}=8.01x10^{-6}	μ_{oi}=1.674x10^{-4}	kg/ms
Exit viscosity	μ_h=7.76x10^{-6}	μ_o=1.581x10^{-4}	kg/ms
Inlet kinematic viscosity	ν_{hi}=1.943x10^{-7}	ν_{oi}=1.507x10^{-7}	m^2/s
Exit kinematic viscosity	ν_h=2.007x10^{-7}	ν_o=1.44x10^{-7}	m^2/s
Velocity of sound	a_h=1429		m/s
Surface tension	-	σ_o=13.2x10^{-3}	N/m
Exit velocity ratio	U_h/U_o=12		
Slip velocity	U_h-U_o=335.5		m/s
Density ratio	ρ_o/ρ_h=28		
Mass flow rate ratio	m_h/m_o=0.84		
Momentum ratio	J_h/J_o=10.6		
Reynolds Number at inlet	Re_{hi}=2.20x10^6	Re_{oi}=4.5x10^5	
Reynolds Number at exit	Re_h=2.13x10^6	Re_o=4.787x10^5	
Weber Number		We=7.45x10^5	
Mach Number	Ma_h=0.256		

of annular jet air velocities (U_a) up to sonic (330 m/s), air/water velocity ratios (U_a/U_w) from 17 to 45, air/water momentum ratios (J_a/J_w) from 4.5 to 30 and Weber numbers (We) between 550 and 3600. Ignoring the supercritical pressure environment at the exit of the injector elements of the SSME fuel preburner, the corresponding velocity and momentum ratios encountered at their exit are, as shown in Table 1, well within the above range. The range of Weber numbers covered by these experiments, however, is approximately two orders of magnitude lower. Further increase of the Weber number in these experiments would call for combinations of the following:

a) Higher air velocity (limited by the sonic condition at the annular jet exit)

b) Lower water jet velocity (limited by the requirement of turbulent flow in the central pipe)

c) Larger diameter of the water jet (which would cause a proportional increase of the annulus dimensions and flow rates)

d) Higher gas density

The most efficient method of increasing the Weber number appears to be the one under (d) above. This density increase of the gaseous phase could be achieved to a limited degree (factor of 4) by employing a heavier gas (e.g. a fluorocarbon refrigerant) or, more efficiently, by increasing the ambient pressure at the exit of the injector. Assuming similar air and water jet flow conditions, a mere increase of the discharge pressure at 10 bar would increase the Weber number by an order of magnitude and a further increase of discharge pressure to a reasonably high pressure of 50 bar would result in Weber numbers of the order of 1.8×10^5, which is only four times lower than those estimated for the SSME fuel preburner injector elements. The penalty for such an increase of discharge pressure would be the increased air and water pumping power requirements and test facility structural complexity.

The procedure outlined above forms a reasonable extension of the parametric study of [2] to encompass a wider Weber number range and to address the issue of liquid jet atomisation at elevated, but still sub-critical, pressures. The test facility proposed in the present preliminary design study should enable, to a certain extent, such experiments to be performed.

4 ATOMISATION AT SUPER-CRITICAL LIQUID PRESSURE

The water jet atomisation study of [2] was performed under ambient laboratory pressure and temperature conditions (say, $P_w=P_a=1$ bar abs, $T_w=T_a=290$ K). As shown in Table 2, both air and water were at sub-critical pressures, while air only was at super-critical temperature. As also shown in Table 2, the proposed extension of the atmospheric water jet experiments at pressures of the order of 50 bar will render the gaseous phase super-critical in terms of both temperature and pressure but the liquid phase will remain in the sub-critical regime.

TABLE 2
Reduced pressures and temperatures of air/water jet experiments

	AIR	WATER	
Critical pressure	$P_{ac}=37.74\times10^5$	$P_{wc}=221.19\times10^5$	N/m^2
Critical temperature	$T_{ac}=132.55$	$T_{wc}=647.4$	K
ATMOSPHERIC EXPERIMENTS			
Exit pressure	$P_a=1\times10^5$	$P_w=1\times10^5$	N/m^2
Exit temperature	$T_a=290$	$T_w=290$	K
Reduced pressure	$P_a/P_{ac}=0.026$	$P_w/P_{wc}=0.0045$	
Reduced temperature	$T_a/T_{ac}=2.19$	$T_w/T_{wc}=0.45$	
ELEVATED PRESSURE EXPERIMENTS			
Exit pressure	$P_a=50\times10^5$	$P_w=50\times10^5$	N/m^2
Exit temperature	$T_a=290$	$T_w=290$	K
Reduced pressure	$P_a/P_{ac}=1.32$	$P_w/P_{wc}=0.226$	
Reduced temperature	$T_a/T_{ac}=2.19$	$T_w/T_{wc}=0.45$	

In order to study the liquid phase atomisation process in a pressure and temperature environment simulating that of the combustion chamber priming stage of the fuel preburner of the SSME, the supercritical pressure of the liquid phase will have to be taken into account. In the following paragraphs, the principles of a proposed experimental arrangement to achieve this objective in a laboratory environment are reviewed.
The main requirements for the design of the proposed experimental arrangement are summarised below:

a) Adequate simulation of the atomisation process of interest.
b) Optical accessibility of the flow for the performance of PDA and other optical studies.
c) "Reasonable" pressure and temperature environments, compatible with requirement (b).
d) Safe operation of the test facility.
e) Practical and economical construction of the test facility.

All requirements above concern the choice of working fluids but requirements (b-e) are the limiting factors. For this reason a survey of the critical properties of commonly available chemical substances was conducted [3,4,11-13] and the results are summarised in Table 3.

Based on our experience in the design of high pressure windows (requirement b), an upper design pressure limit of 60 bar for the test section of the experimental arrangement is selected.

TABLE 3
Critical properties of common chemical substances

	T_c (K)	P_c x10^5Pa abs	Pc <43	T_c 385-430	T_c <200	Toxic Flam.	
Air	132.55	37.74	Y		Y		G
Allene C_3H_4	393.15	52.4		Y			
Ammonia NH_3	405.59	112.8		Y			
Argon Ar	150.75	48.6			Y		
Arsine AsH_3	373.05	66.0					
Boron Trichloride BCl_3	451.95	38.7	Y				
Boron Trifluoride BF_3	260.95	49.85					
1,3-Butadiene C_4H_6	425.15	43.27	Y	Y		F	(L)
n-Butane C_4H_{10}	425.15	37.96	Y	Y		F	(L)
1-Butene C_4H_8	419.55	39.25	Y	Y		F	(L)
cis-2-Butene C_4H_8	433.15	42.07	Y				
cis and trans-2-Butene C_4H_8	428.15	40.8	Y	Y		F	(L)
trans-2-Butene C_4H_8	428.15	40.8	Y	Y		F	(L)
Carbon dioxide CO_2	304.15	73.82					
Carbon monoxide CO	132.91	35.0	Y		Y	T	(G)
Carbonyl fluoride COF_2	295.95	57.6					
Carbonyl sulphide COS	375.00	58.77					
Chlorine Cl_2	417.15	77.0		Y			
Cyanogen C_2N_2	400.15	59.4		Y			
Deuterium D_2 or H_2	38.37	16.65	Y		Y	F	(G)
Diborane B_2H_6	289.85	39.8	Y				
Dichlorosilane SiH_2Cl_2	449.45	44.0					
1,-1 Difluoroethylene $C_2H_2F_2$	302.85	44.63					
Dimethylamine $(CH_3)_2NH$	437.65	53.1					
Dimethylether $(CH_3)_2O$	400.10	52.69		Y			
2,2-Dimethylpropane C_5H_{12}	433.78	31.96	Y				
Ethane C_2H_6	305.42	48.84					
Ethyl acetylene C_4H_6	463.65	47.12					
Ethylchloride C_2H_5Cl	460.35	52.7					
Ethylene C_2H_4	283.05	50.76					
Ethylene oxide C_2H_4O	468.93	71.91					
Fluorine F_2	144.3	52.15			Y		
Freon 11 CCl_3F	471.15	44.1					
Freon 12 CCl_2F_2	385.15	41.13	Y	Y			L
Freon 13 $CClF_3$	302.05	38.71	Y				
Freon 13B1 $CBrF_3$	340.15	39.6	Y				
Freon 14 CF_4	227.48	37.4	Y		Y		G
Freon 22 $CHCLF_2$	369.15	49.8					
Freon 23 CHF_3	299.05	48.3					
Freon 113 $C_2Cl_3F_3$	487.55	34.1	Y				
Freon 114 $C_2Cl_2F_4$	418.85	32.6	Y	Y			L
Freon 115 C_2ClF_5	353.15	31.5	Y				
Freon 116 C_2F_6	292.85	29.8	Y				
Freon 500	378.65	49.8					
Freon 502	355.35	40.7	Y				
Freon 503	292.65	43.6					
Germane GeH_4	308.00	55.5					

Helium He	5.2	2.28	Y		Y		G
Helium 3 ^3He	3.31	1.165	Y		Y		G
Heptane C_7H_{16}	540.2	27.36	Y				
Hexane C_6H_{14}	507.9	30.29	Y				
Hydrogen H_2	33.2	12.97	Y		Y	F	(G)
Hydrogen Bromide HBr	363.15	85.52					
Hydrogen chloride HCl	324.55	82.58					
Hydrogen fluoride HF	461.15	64.85					
Hydrogen idodide HI	423.95	83.0		Y			
Hydrogen selenide H_2Se	411.15	89.2		Y			
Hydrogen sulphide H_2S	373.15	89.37					
Isobutane C_4H_{10}	408.13	37.2	Y	Y		F	(L)
Isobutylene C_4H_8	417.85	40.01	Y	Y		F	(L)
Isopentane C_5H_{12}	460.35	33.3	Y				
Krypton Kr	209.4	55.02			Y		
Methane CH_4	190.53	45.96			Y		
Methyl acetylene C_3H_4	402.39	56.28		Y			
Methyl bromide CH_3Br	467.15	52.3					
3-Methyl-1 butene C_5H_{10}	444.65	32.65	Y				
Methyl chloride CH_3Cl	416.25	66.8		Y			
Methyl mercaptan CH_3SH	469.95	72.33					
Monoethylamine $C_2H_5NH_2$	456.55	56.29					
Monomethylamine CH_3NH_2	430.05	74.6		Y			
Natural gas	193.15	45.0			Y		
Neon Ne	44.40	27.65	Y		Y		G
Neon-20	44.15	27.6	Y		Y		G
Neon-22	44.15	27.6	Y		Y		G
Nickel carbonyl $Ni(CO)_4$	473.15	30.4	Y				
NItric oxide NO	180.15	64.0			Y		
Nitrogen N_2	126.2	33.9	Y		Y		G
Nitrogen dioxide NO_2	126.15	33.4	Y		Y	T	(G)
Nitrogen trifluoride NF_3	233.75	44.7					
Nitrous oxide N_2O	309.55	72.54					
Oxygen O_2	154.58	50.43			Y		
Pentane C_5H_{12}	469.80	33.7	Y				
Perfluoropropane C_3F_8	201.25	26.8	Y		Y		G
Phosgene $COCl_2$	455.15	56.74					
Phosphine PH_3	324.75	65.35					
Propane C_3H_8	369.95	42.0	Y				
Propylene C_3H_6	364.95	46.0					
Silane SiH_4	269.15	47.8					
Silicon tetrachloride $SiCl_4$	505.95	47.8					
Silicon tetrafluoride SiF_4	258.95	37.15	Y				
Sulphur dioxide SO_2	115.50	78.84			Y		
Sulphur hexafluoride SF_6	318.75	37.6	Y				
Sulphur tetrafluoride SF_4	364.00	-.-					
Sulphuryl fluoride SO_2F_2	364.95	51.17					
Trimethylamine $(CH_3)_3N$	433.30	40.8	Y	Y		T/F	(L)
Vinyl chloride C_2H_3Cl	429.65	55.90		Y			
Vinyl methyl ether C_3H_6O	436.75	46.66		Y			
Water H_2O	647.40	221.19					
Xenon Xe	289.73	58.40					

This implies that the critical pressure of both fluids should be below this value and, if the reduced pressures (P/P_C) quoted in Table 1 were to be simulated, the critical pressure of the gaseous phase should be $P_{gc}=(61/26.25)=2.32$ bar and that of the liquid phase $P_{lc}=(61/6.75)=9.04$ bar. The first condition is easily satisfied by Helium gas ($P_C=2.28$ bar) but the condition for the liquid phase is not satisfied by any of the commonly available chemical substances.
Considering the reduced temperatures of Hydrogen and Oxygen in Table 1, and assuming a test section temperature between 290 and 320 K, the critical temperatures of the gaseous and liquid phases should be $T_{gc}=60-70$ K and $T_{lc}=385-430$ K, respectively. None of the common substances of Table 3 satisfies the condition for the gaseous phase but several substances satisfy the one for the liquid phase.
Following the above observations and the data available from Table 3, the simulation principles were relaxed as follows:

	P/P_C	T/T_C
Liquid phase:	>1.4	~0.75
Gaseous phase:	>1.4	>1.4

Given a test section pressure P=60 bar and temperature T=290-320 K, both working fluids to be selected must have critical pressures $P_C<43$ bar. The critical temperature of the liquid phase should be $385\ K<T_{lc}<430\ K$ and that of the gaseous phase $T_{gc}<200$ K. At the same time, and in order to satisfy the safety requirement (d) above, the selected substances should not be toxic (T) or flammable (F). All these conditions are checked in Table 3 and the result is indicated in the last column: Substances marked with "G" are suitable for simulation of the gaseous phase and those marked with "L" can simulate the liquid phase. Those marked (G) or (L) within brackets are rejected on safety grounds.
From the data of Table 3, and as expected, it becomes clear that most of the substances which could be used for the simulation of the liquid phase fall within the category of flammable hydrocarbons and, therefore, are excluded. The remaining candidates are fluorocarbon refrigerants Freon 12 and 114. Freon 114 is advantageous from the lower critical pressure point of view, but Freon 12 will be preferred for the liquid phase simulation because it fulfills the requirement $T/T_C=0.75$ at ambient conditions. At the same time, the price ratio of Freon 114 to Freon 12 is of the order of 2.
The substances suitable for the gaseous phase simulation are, (in ascending critical pressure and temperature order), Helium, Neon, Nitrogen, Air and Freon 14. Although Helium or Neon gases are advantageous for simulation purposes, Air will be preferred for the proposed experimental arrangement on the grounds of the practicality and economy requirement (e) above.
It is concluded that the physics of the liquid oxygen atomisation process during the priming stage of the combustion chamber of the SSME fuel preburner can be studied in a laboratory environment using Freon 12 and air at moderate

pressures and temperatures to simulate the super-critical pressure and sub-critical temperature liquid jet atomisation in a super-critical gaseous environment. A similar conclusion was reached by the work reported in [14] which came to the authors' attention after the completion of this preliminary study. In this report it is proposed that the coaxial injector flow of the fuel preburner is simulated by Freon-12 injection into a nitrogen/helium (10/90) gaseous mixture.
The following section considers the operating conditions and working fluid properties in the proposed experimental arrangement and compares them with those of the SSME fuel preburner.

5 OPERATING CONDITIONS OF THE PROPOSED EXPERIMENTAL ARRANGEMENT

The main geometric and operating characteristics of the proposed experimental arrangement will be similar to those considered in [2] and as close as possible to those of the SSME fuel preburner. Provisions will also be made for their modification to allow parametric studies to be performed.

5.1 Injector Element Geometry

For given working fluid properties at the test section conditions, the Reynolds number at the annular injector element could be increased by either increasing the corresponding fluid flow rate or decreasing the injector dimensions, ($Re=\rho Ud/\mu \sim m/d\mu$). The Weber number will also increase with increasing gas mass flow rates and decreasing injector dimensions ($We=\rho U^2 d/\sigma \sim mU/d\sigma$). Considering that any increase in mass flow rate corresponds to a significant increase in pumping power requirements throughout the flow circuit ($W \sim m^3/\rho^2 D_p^4$, where D_p a typical piping diameter), it is concluded that the geometry of the injector element should remain as small as practical. Structural considerations for a high pressure vessel also favour this approach of reduced dimensions.
The inner tube diameter of the annular arrangement of [2] is very close to the one of the fuel preburner injector element (d=2.3 vs 2.26 mm), and as small as practical. The annular gap of the SSME injector, $((d_e-d_i)/2)$, however, is only 0.584 mm, which is considered too small to allow geometrical symmetry to be easily achieved. On the other hand, the range of annular gaps examined in [2] (10, 6 and 3 mm) would require high air flow rates through the annulus to ensure adequately high Reynolds and Weber numbers. A compromise is, therefore, proposed to employ an annular gap of 1.025 mm. This, combined with a standard (B.S. Gauge 11) central tube with external diameter of d_i=2.95 mm gives an annulus external diameter of d_e=5 mm which is very close to that of the SSME injector element (4.976 mm) and allows future reduction of the annular gap by increasing the inner tube wall thickness. (It should be noted here that the inner tube wall thickness may be an important parameter affecting atomisation from the annular jet arrangement and should form an additional parameter for investigation).

The upstream geometry of the annular arrangement will be kept similar to that used in [2] in order to maintain the same geometrical initial conditions for the two coaxial jets.
The base-line geometry of the proposed injector element is shown in Figure 6.

5.2 Operating Conditions

The exact simulation of the liquid oxygen atomisation process in the SSME fuel preburner would require similarity of Weber and Reynolds numbers as well as of mass flow rate and momentum ratios. In order the keep the pumping power requirements within reasonable levels, the simulation proposed here will be based on adequately high Reynolds and Weber numbers and similar momentum, mass flow rate and velocity ratios. Given the different flow areas and density ratios of the working fluids (28 vs 18 in the SSME and model, respectively), one only of these ratios can be simulated at a time. Although the mass flow rate ratio of fuel and oxidiser is essential for the combustion process, the momentum ratio is thought to be of greater importance in the atomisation process. For this reason, an example of operating conditions will be provided here based on a momentum ratio of Freon-12 and air equal to that of Oxygen and Hydrogen in the SSME fuel preburner.

For: $(J_a/J_f)=(J_h/J_o)=10.6$ and $\rho_f/\rho_a=18.19$ at 60bar and 290K

with $A_a=12.79\times10^{-6}$ m^2
$A_f= 4.15\times10^{-6}$ m^2 and $A_a/A_f=3.08$

it follows $(\rho_a U_a^2 A_a)/(\rho_f U_f^2 A_f) = 10.6$

and $U_a/U_f = 7.91$

The choice of the Freon-12 exit velocity is arbitrary but should ensure a Reynolds number in the central pipe corresponding to fully turbulent flow ($Re>2\times10^4$) and, at the same time, a reasonably low flow rate to minimise the pumping power requirements.

Since $Re_f=U_f d_f/\nu_f > 2\times10^4$ and $d_f=2.3\times10^{-3}$ m
$\nu_f=1.717\times10^{-7}$ m^2/s
@ 60 bar and 290 K

$$U_f > 2\times10^4(\nu_f/d_f) = 1.49 \text{ m/s}$$

Let us assume **$U_f = 2.0$ m/s**

This will result in **$Re_f= 2.68\times10^4$**

which ensures fully turbulent flow of Freon-12 in the central pipe.
The air velocity in the annular pipe must, therefore, be:

$U_a=7.91\ U_f$ ie **$U_a = 15.82$ m/s**

and the corresponding Reynolds number in the annulus:

$Re_a=U_a d_a/\nu_a$ with $d_a = (5-2.95)\times10^{-3}$ m and $\nu_a = 2.606\times10^{-7}$ m^2/s @ 60 bar and 290 K

$$\mathbf{Re_a = 1.24\times10^5}$$

which also ensures fully turbulent air flow in the annulus.

The hydrodynamic entrance length for fully developed turbulent flow in the annulus for $d_i/d_e=0.59$ must be $z_a > 26\ D_a$, [11]. For this case and for $6\times10^3<Re_a<3\times10^5$, the overall friction factor is given by:

$f_a=0.085\ (Re_a)^{-0.25} = 0.045$ and

$\Delta P=0.5\rho_a U_a^2[4f_a(L/D_a)+K]$ where K=0.2 (entry/exit loss factor)

and the overall pressure drop is

$\Delta P = 0.2\times10^5$ N/m^2

For the central tube, $z_f > 25\ D_f$ and from the Chen equation for friction in pipes, [15], assuming relative roughness $\varepsilon/D=0.0007$ (drawn stainless steel tubing), $1/D_f=26$ and including entrance and exit pressure losses (K=0.2), the overall pressure drop is estimated as:

$\Delta P=0.5\rho_f U_f^2[4f_f(1/D_f)+K] = 0.02\times10^5$ N/m^2

Given the small estimated pressure losses, the air and Freon-12 pressures and properties at inlet to the injector simulation are assumed to be equal to those at its exit.
Based on the above preliminary calculations, the various fluid properties and flow parameters in the test section of the Freon/Air simulation are calculated and presented in Table 4, using data from references [3,13,16] and in a format similar to that of Table 1 to assist comparisons.
These conditions represent the base-line flow configuration of the proposed experimental arrangement and can be considerably varied by adjusting air and Freon-12 flow rates and test section pressure or temperature.
For the base-line configuration above, the objective was to simulate the momentum ratio of the SSME preburner. This was achieved with fairly low air and Freon mass flow rates which resulted in adequately high Reynolds numbers but, as expected, much lower Weber number and considerably different velocity and mass flow rate ratios from those of the SSME case. However, the Weber number and various other quantity ratios of this simulation fall within the range of those examined in [2] and tests conducted under these conditions will clarify the effect of super- or sub-critical fluid state on its atomisation process.
Table 5 below summarises the values of the various parameters of interest within the test section, for three alternative cases where the momentum, mass flow rate and velocity ratios of the SSME preburner are individually simulated. In all these

TABLE 4
Operating characteristics and fluid properties in the Freon-12/Air simulation

	"FUEL" (Air)	"OXIDISER" (Freon-12)	
Total mass flow rate	m_{at}=0.015	m_{ft}=0.011	kg/s
Injector mass flow rate	m_a=0.015	m_f=0.011	kg/s
No. of injectors	1		
Inlet temperature	T_a=290	T_f=290	K
Inlet pressure	P_{ai}=60.5x10^5	P_{fi}=60.02x10^5	N/m^2
Injector end pressure	P_a=60x10^5	P_f=60x10^5	N/m^2
Exit velocity	U_a=15.82	U_f=2.0	m/s
Central tube dia.		d=2.3x10^{-3}	m
Annulus inner dia.	d_i=2.95x10^{-3}		m
Annulus outer dia.	d_e=5.0x10^{-3}		m
Hydraulic diameter	D_a=2.05x10^{-3}	D_f=2.30x10^{-3}	m
Flow area	A_a=12.79x10^{-6}	A_f=4.15x10^{-6}	m^2
Air/Freon mass flow rate ratio	m_{at}/m_{ft}=1.35		
Critical Pressure	P_{ac}=37.74x10^5	P_{fc}=41.13x10^5	N/m^2
Critical Temperature	T_{ac}=132.55	T_{fc}=385.15	K
Reduced Pressure	P_a/P_{ac}=1.59	P_f/P_{fc}=1.46	
Reduced Temperature	T_a/T_{ac}=2.19	T_f/T_{fc}=0.75	
State	Supercritical Gas	Supercritical Pressure Liquid	
Inlet density	ρ_{ai}=	ρ_{fi}=	kg/m^3
Exit density	ρ_a=73.15	ρ_f=1328	kg/m^3
Exit volume flow rate	V_a=0.205x10^{-3}	V_f=0.0083x10^{-3}	m^3/s
Inlet viscosity	μ_{ai}=	μ_{fi}=	kg/ms
Exit viscosity	μ_a=1.906x10^{-5}	μ_f=2.28x10^{-4}	kg/ms
Inlet kinematic viscosity	ν_{ai}=	ν_{fi}=	m^2/s
Exit kinematic viscosity	ν_a=2.606x10^{-7}	ν_f=1.717x10^{-7}	m^2/s
Velocity of sound	a_a=352		m/s
Surface tension	-	σ_f=10.36x10^{-3}	N/m
Exit velocity ratio	U_a/U_f=7.91		
Slip velocity	U_a-U_f=13.82		m/s
Density ratio	ρ_f/ρ_a=18.15		
Mass flow rate ratio	m_a/m_f=1.35		
Momentum ratio	J_a/J_f=10.6		
Reynolds Number at inlet	Re_{ai}=	Re_{fi}=	
Reynolds Number at exit	Re_a=1.24x10^5	Re_f=2.68x10^4	
Weber Number		We=3.1x10^3	
Mach Number	Ma_a=0.045		

cases the geometry and exit pressure/temperature of the injector arrangement as well as the mass flow rate of Freon-12 are kept the same as in the base-line case described above (Table 4).

TABLE 5
Operating parameters for various simulation modes

Simulated ratio	J_h/J_o=10.6	m_h/m_o=0.84	U_h/U_o=12.0
Re_a	$1.24x10^5$	$0.77x10^5$	$1.89x10^5$
Re_f	$2.68x10^4$	$2.68x10^4$	$2.68x10^4$
We	$3.10x10^3$	$1.01x10^3$	$7.86x10^3$
J_a/J_f	10.6	4.15	24.5
m_a/m_f	1.35	0.84	2.04
U_a/U_f	7.91	4.94	12.0

Table 5 illustrates the inter-relation between the various operating parameters and suggests that Weber numbers up to $7.9x10^3$ can be obtained with the proposed experimental arrangement, while maintaining moderate flow rates, temperatures and pressures.

5.3 Other operating modes

Due to the low mass flow rates involved in the proposed simulation, the temperature of the working fluids can be easily increased using heating elements or appropriate heat exchangers. This can be used, for example, in order to reduce the momentum and mass flow ratios of the third case shown in Table 5 without affecting the velocity ratio.
Alternatively, the test section pressure can be reduced to introduce similar changes of the operating parameters.
Other possibilities have also been considered, including the simulation of the evaporation process after the liquid atomisation. Since the critical temperature of Freon-12 is relatively high, it is proposed to replace it in the future with Freon-13. This has a critical pressure $P_{fc}=38.7x10^5$ N/m^2, which is near to that of Freon-12, but exhibits a critical temperature T_{fc}=302 K, which is only 10 K above ambient. With minor adjustments of the experimental arrangement operating conditions, evaporation of Freon-13 could easily be achieved after its atomisation and studied within the test section. That would constitute a further, even closer, simulation of the priming stage of the SSME fuel preburner.
The study of secondary atomisation from the impingement of the liquid spray on a flat or curved surface simulating the fuel pump turbine dome can also be contemplated. The unknown factor here is the extent to which the test chamber windows will be

fouled with the droplet cloud and inhibit the performance of the PDA measurements.
Finally, the possibility of extending the proposed stationary simulation of the liquid oxygen spray to that of a transient spray is also considered in section 7, below.

6 DESIGN OF THE TEST FACILITY

This section presents and discusses the principles and, to a certain extent, the details for the design of a test facility to enable the Freon-12/air simulation study outlined in section 5, above. It is noted that this is a preliminary design stage and only the basic details of the test facility are considered.

6.1 Basic Design Principles

The nature and cost of Freon-12 calls for a closed-loop-type facility. Air and Freon should be circulated from the test section (injection chamber) back to the injector element using suitable pumps. The whole circuit should be kept at pressures above P_{fc} (42×10^5 N/m^2) in order to maintain Freon-12 in the liquid phase and allow its separation from air by gravity after the injection process. The pressurised closed-loop concept has the additional advantage of minimising the required pumping power to that necessary to overcome the piping and injector pressure losses, as opposed to the power required to compress the working fluids from atmospheric to the required pressure.
The injection chamber should be equipped with, at least two, high pressure windows positioned 150^o apart along a cross section of the injection chamber to allow the application of Phase Doppler Anemometry (PDA) and other optical techniques for the study of the liquid Freon atomisation process. Strength and safety considerations suggest that the diameter and number of the high pressure windows must be kept to a minimum. PDA measurements of droplet velocity and size, however, must be obtained at various distances from the injector exit along its axis, (up to 250 mm) in order to study the axial spray development. This would require a number of window pairs or access holes along the test section, increasing cost and reducing reliability. For this reason, it is proposed to use one only pair of fixed windows and traverse the face plate with the injector element along the test section axis, in an arrangement similar to that of a piston-cylinder assembly.
The two windows must be easily removable for cleaning or replacement. They also have to be recessed with respect to the test section cylindrical wall to minimise fouling by liquid droplets.
The injector face plate must be removable and interchangeable with similar plates incorporating injector elements of different geometries, or even arrays or matrices of multiple injectors.
The cylindrical test section diameter must be as small as possible without interfering with the initial spray development. From the results of [2], a diameter of 160 mm is

selected which is nearly three times the atmospheric spray width 200 mm downstream of the injector. This diameter could, and should, be reduced if the measurement requirements in terms of axial spray development are relaxed.

6.2 Materials

The materials to be used in the construction of the test facility must be compatible with all working fluids. Freon-12 (and Freon 13) is compatible with most common metals with the exception of zinc and magnesium/aluminium alloys. The possibility of using water as the liquid phase, however, calls for the metallic parts to be made of corrosion resistant steel. All strength calculations below are carried out for steel with design stress higher than 120 N/mm^2. The recommended material for the construction of the test facility is austenitic stainless steel 316-S14(S) (BS 5500, [17]) which has a design stress at 50^oC f=147 N/mm^2 (>120) but requires special welding techniques.
The piping will be made of seamless stainless steel 316 tubing according to ASTM A269 and the pipe fittings will be of the double-ferrule compression type (eg Swagelok) with appropriate valves (eg Nupro or Whitey). Any flexible piping will be made of stainless steel-braided, PTFE-lined flexible hose with integral fittings, (eg Cajon).
Elastomer parts involved in the flow circuit, such as seals, gaskets and O-rings must exhibit minimum swelling in the presence of Freon-12. Table 6 below [13] may be used as a guidance. For the O-rings, in particular, compound CR (ISO 1629, chloroprene) is specifically recommended, [18].

TABLE 6
Swelling of Elastomers in Freon-12 at room temperature
Linear Swell per cent (%)

BUNA N	BUNA S	BUTYL	NATURAL RUBBER	NEOPRENE	VITON
2	3	6	6	0	9

6.3 Flow Circuit

A schematic of the proposed working flow circuit is shown in Figure 7 and identifies the main components of the Freon-12 and air circuits. A brief description of the test facility operation follows:
Freon-12 and air are injected into the vertical test chamber through the injector element at a pressure of $60x10^5$ N/m^2. Freon remains in the liquid phase and is collected at the bottom of the test chamber from where it is pumped using a (reciprocating) liquid pump. The pump outlet pressure is of the order of $5x10^5$ N/m^2 higher than that at the inlet. The outlet flow is directed via a specially designed T-piece to a nitrogen-charged diaphragm accumulator in order to damp the flow pulsations induced by the pump and compensate for

possible Freon leaks. This is followed by a pressure regulator and a water heat exchanger to control the pressure and temperature of the injected liquid. The Freon flow rate, pressure and temperature are then measured and finely adjusted using a flow metering device, a flow control valve and a precision pressure regulator near the injector element.
Air is drawn from the upper part of the test chamber using a reciprocating pump preceded by a droplet separator/filter. The outlet of the air pump is fed to a plenum chamber to damp the flow pulsations and, subsequently, through a pressure regulator, water heat exchanger and flow, pressure and temperature measuring devices, it is fed into the annular tube of the injector element. The presence of the heat exchanger in the air circuit is mandatory since the compression process in the air pump significantly increases the air temperature.
The system start-up procedure consists of initially charging the whole circuit by filtered air near the operating pressure. Zero-grade air is supplied in 9.7 m^3 cylinders at pressures of 200 bar and, therefore, the charging can be performed directly from the cylinder using a suitable pressure regulator.
Freon-12 is normally supplied in 70 kg cylinders at a pressure of 4 bar (@ 15^{o}C). Liquid Freon can be withdrawn by either using the appropriate supply valve or inverting the cylinder. Liquid Freon must be pressurised at the test chamber pressure which is 15 times higher than that of the cylinder. To achieve this, the bottom outlet of the test chamber is isolated and liquid Freon is pumped from the bottle using the Freon reciprocating pump.
After the end of the filling process the Freon cylinder is isolated and the air and freon pumps activated to initiate the injection process.
It is essential that both working fluid circuits incorporate particulate filters to avoid blockages in the small passages of the injector element. Flow, temperature and pressure metering and control must be of adequately high precision. Pressure relief valves must be installed in both flow circuits and in the test section.

6.4 Individual Component Design

6.4.1 *Injector head*

The injector head (Figure 8) is a 160 mm diameter by 380 mm length piston-like device incorporating the injector element, a plenum chamber upstream of the injector annulus and a set of piston seals and guide rings to allow it to slide along the axis of the cylindrical test section. This "piston" is preceded by a 300 mm length externally threaded hollow rod acting both as a positioning and locking device for the injector head as well as a feed-through pipe for the supply of the working fluids to the injector element.
Freon-12 is fed into the central tube of the injector element through a 10 mm dia stainless steel pipe, running along the hollow rod, which is reduced to the (2.95 mm O.D.-2.3 mm I.D.) tube 58 mm upstream of the injector element exit. This arrangement is supported and centered by a 3-spoke spider at the end of the larger diameter pipe.
Air is fed into the plenum chamber via four radial ports

drilled on the wall of the injector head, followed by a baffle and a 17° half-angle convergent nozzle leading to the injector element annulus. The geometry of the injector can be readily modified in terms of annulus diameter and face plate geometry by replacing its lower detachable part. The face plate geometry shown in Figure 8 is similar to that examined in [2] and shown in Figure 5.
The injector head assembly can slide along the cylindrical test section, by rotating the fixed nut at the top flange of the injection chamber around the thread of the hollow feed pipe, while maintaining the injection chamber sealing by a set of high pressure hydraulic seals. The seals proposed for the specific application are "Novathan U-rings T18", backed with anti-extrusion rings, and manufactured by MERKEL FRG.(Ref. No. 0521-269.443), or equivalent. The guide rings are also manufactured by MERKEL (Ref. No. 9297-204.644). This sealing arrangement is able to withstand pressures in excess of 400×10^5 N/m^2 at 350 K with near zero leakage, while their material (Bronze impregnated PTFE) is fully compatible with the working fluids.

6.4.2 *Injection chamber (Test section)*

The injection chamber (Figure 9) is essentially a vertically held cylinder with D=160 mm internal diameter, equipped with two externally protruding window housings positioned 150° apart, and sealed by the injector head at one end and a flange at the other. The injector head slides at its top half which is, for sealing purposes, internally ground to a surface roughness better than 0.3 μm.
The design pressure for the cylindrical test chamber is, according to BS 5500 [17], $P=160 \times 10^5$ N/m^2, which is the maximum pressure the air pump can deliver (see below) if the pressure regulating devices fail. According to BS 5500 section 3.5.1, the wall thickness (e) of the cylinder is calculated by:

$$e = PD/(2f-P)$$ where f the design stress

For f=120 N/mm^2 (material: austenitic steel) the resulting wall thickness e=12 mm.
The protruding window housings are welded on the injection chamber and are treated as "branch connections" to the high pressure vessel, (BS 5500, section 3.5.4). The window housings are designed for an internal diameter d=70 mm, which leads to a required wall thickness of 7 mm. The weakening of the tubular shell resulting from the two adjacent openings and associated welding is compensated by a local increase of shell thickness to 18 mm. Details of the recommended weld for the two window housings are shown in Figure 10 and are in accordance to BS 5500, Section E.2.
Care must be taken that the internal grinding of the top part of the cylinder takes place <u>after</u> the welding of the window housings in order to rectify the thermal distortion caused by the welding.
As shown in Figure 9 a set of conical baffles is arranged at a distance of 300 mm below the windows. These act like "splashers" aiming to collect the Freon droplets at the bottom

of the test section, thus assisting the Freon/air separation process and minimising the cloud of suspended droplets.
The bottom end of the test chamber is sealed by a 35 mm thick plate (BS 5500, section 3.5.5) and sealed with a 6.9 mm O-ring backed with an anti-extrusion ring. The plate is retained on the test section flange by 18 M16 bolts (austenitic Cr Ni steel 18/8). Alternatively, the bottom flange could have a torispherical domed shape with 50 mm height and only 12 mm thickness, (BS 5500 section 3.5.2.1). The end plate (or dome) is equipped with a drain pipe to collect and recirculate the liquid Freon-12 back to the injector element. Air is drawn from the test section below the window housings by means of four equally-spaced outlet pipes arranged so as to minimise the possibility of Freon droplets contaminating the air circuit.
The overall height of the cylindrical injection chamber is dictated by the extent to which the spray axial development needs to be studied. Assuming this to be of the order of 250 mm downstream of the injector exit, the required length of the ground cylindrical section above the window axes is L_1=250+380=630 mm, say 650 mm. The cylinder length below the windows is selected as L_2=850 mm, making a total test section height of $L=L_1+L_2$=1500 mm.
Despite the care taken during the preliminary sizing of the test section dimensions, it is strongly recommended that the proposed design is subjected to further inspection and the final test chamber is submitted for testing and approval by the appropriate authorities.

6.4.3 *High pressure windows*

The design of the high pressure windows, shown in Figure 10, is based on data from references [18-22]. The window is usually treated either as a clamped disk or as a simply supported disk, the latter being the least favorable case. The proposed design of Figure 10 ensures that the internal pressure load is taken up by a soft copper ring located on the outer surface of the window, while the sealing is obtained via an anti-extrusion backed O-ring housed in a similar copper ring. Additional sealing is provided by the outer O-ring between the housing and flange of the window. The window is also bonded within its flange by means of a Silastic potting compound (Dow Corning 3120 RTV Silicone Rubber) to ensure safe removal of the window/flange assembly for cleaning. This design can be treated as a "clamped window" but, due to the elastic inner support it will be considered, for safety, as "simply supported". The required window thickness (s) is given by [18]:

$$s=C\ d_m(P\ S/\sigma_b)^{0.5}$$ where

$C = 0.55$
$d_m = (d_o+d_i)/2$
P : operating pressure
S : safety factor
σ_b: tensile strength

The windows will be designed for $P=60\times10^5$ N/m^2 (not 160×10^5) with a safety factor S=8 and for clear fused silica (σ_b=50 N/mm^2, [19,20]) with d_o=100 and d_i=70 mm which yields a

BS 5500 : 1982

Issue 1, January 1982

WINDOW FLANGE

Suggested working form

Loose-type flange design

Design pressure		p	16 N/mm²	Gasket details SOFT COPPER	$b=b_o$ if $b_o \leq 6.3$ mm	N	15
Design temperature			20 °C			b_o	7.5
Flange material			AUSTENITIC S/S	Facing details Type:	$b=2.52\sqrt{b_o}$ if $b_o>6.3$ mm	b	6.9
Bolting material			CrNi 18/8	Gasket o.d.: 100		y	45
Corrosion allowance			— mm	$W'_{m2}=3.14bGy=$ 82870		m	3.5
Allowable bolt stress	Design temp.	S_b	200 N/mm²	$H_p=6.28bGmp=$ 58930			
	Atm. temp.	S_a	200 N/mm²	$H=0.785G^2p=$ 90746	$H_p+H=$ 150000		
Allowable flange stress	Design temp.	S_{FO}	>120 N/mm²	A_m = greater of $\frac{W'_{m2}}{S_a}$ or $\frac{H_p+H}{S_b}$ = 414 or 750 ≡ 10×M12			
	Atm. temp.	S_{FA}	>120 N/mm²	$A_b=A_m=$ 750			
				$W'=0.5(A_m+A_b)S_a=$ 150000			
All dimensions are shown in the corroded condition				$W'_{m1}=H_p+H=$ 150000			
				Gasket width check	$N_{min}=\frac{A_b\times S_a}{6.284yG}=6.2<15$		

Operating condition

$H_D=0.785B^2p=$ 61544	$h_D=0.5(C-B)=$ 27	$H_Dh_D=$ 1661700
$H_G=H_p=$ 58930	$h_G=0.5(C-G)=$ 19.5	$H_Gh_G=$ 1150000
$H_T=H-H_D=$ 29200	$h_T=0.5(h_D+h_G)=$ 23.25	$H_Th_T=$ 678900
		$M_{op}=$ 3490000

Bolting-up condition

$H_G=W'=$ 150000	$h_G=0.5(C-G)=$ 19.5	$M_{atm}=H_Gh_G=$ 2925000

M_o = greater of M_{op} or $M_{atm}\times\frac{S_{FO}}{S_{FA}}=$ 3490 | Apply factor C_F when $C_F=\sqrt{\frac{\text{bolt spacing}}{2(\text{bolt diameter})+6t/(m+0.5)}}\geq 1$ | $M=\frac{M_o\times C_F}{B}\simeq$ 49800

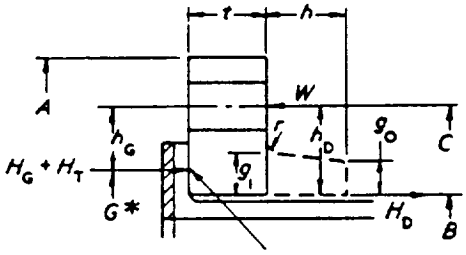

To be taken at mid-point of contact between flange and lap independent of gasket location

Shape constants

$K=\frac{A}{B}=$ 2.143

$Y=$ 2.7 [Fig. 3.83(3)]

$t=\sqrt{\frac{YM}{S_{FO}}}=$ 33.5 mm

$C_F=\sqrt{\frac{39}{2\times 12+\frac{6\times 33.5}{3.5+0.5}}}=0.72<1$

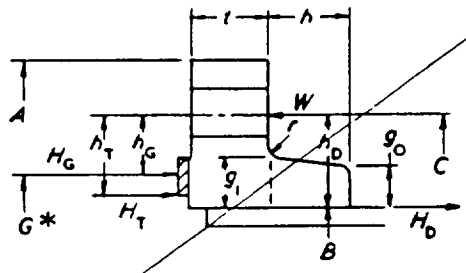

* G = (o.d. of contact face) − $2b$

Remarks:

A = 150 mm

B = 70

C = 124

G = 85

thickness s=43 mm. The high compressive strength of fused silica (1150 N/mm^2) ensures that the surface in contact with the outer copper ring is sufficient for the relevant surface stress (9 N/mm^2) and allows for adequate pre-loading of the window flange bolts to ensure sealing.
An alternative window material is thermally pre-stressed boro-silicate glass. The pre-stressing process of this common glass [18] increases its bending strength (60 N/mm^2) by a factor of 2.5 (but its surface compressive stress is only 100 N/mm^2). That would lead to significantly thinner windows but no real cost saving.
The window clamping (hollow) flange is designed for $160x10^5$ N/m^2 according to BS 5500 section 3.8.3.4 as a loose-type flange. According to the procedure of the attached working form, the minimum thickness of the 150 mm O.D. - 70 mm I.D. flange will be t=33.5 mm and will be held by 10xM12 bolts on PCD=124 mm.

6.5 Main Component Selection

In this section the characteristics of the primary commercially available components to comply with the operating requirements of the test facility are identified and provisional recommendations for specific products are made.

6.5.1 *Freon-12 pump*

The nominal operating characteristics of the liquid freon pump are the following:

State	liquid	
Suction Pressure	60	bar (abs)
Discharge Pressure	65	bar (abs)
Operating Temperature	20	degC
Mass Flow Rate	40	kg/hr
Density (at pump exit)	1.33	kg/l
Volume Flow Rate	0.5	l/min
Dymamic Viscosity	0.22	centipoise

Further to the above the pump should be able to charge the flow circuit from the initial cylinder pressure of 4 bar to the final 65 bar.
Based on the low flow, high pressure requirements above, the specified pump will be of the reciprocating type. The recommended pump is a Maximator MSF 22L air-driven single-acting liquid pump, manufactured by Schmidt, Kranz & Co. GmbH, capable of more than 0.5 l/min Freon-12 at 5 bar differential with an air drive consumption less than 10 Nm^3/hr at 2 bar. The maximum pressure obtainable from the pump, however, is 250 bar at zero flow and the maximum flow rate is 3 l/min at zero head thus making this arrangement ideal for the system charging process.

6.5.2 *Freon-12 pulsation damping*

The displacement volume of the reciprocating Freon pump is 4 cm^3 and its operating frequency for the specified flow rate is only 2 Hz. In order to minimise the resulting liquid flow

pulsations a 1.4 l branch-mounted Pulstone damping unit model SBO-140-1.4, manufactured by Hydac GmbH is recommended. This unit is in effect a diaphragm accumulator rated at 140 bar and will be operating with nitrogen pressure at 65 bar above its nitrile (NBR) diaphragm.
The Hodgson number (Ho) of this dumping unit (see 6.5.4 below) is estimated to be less than 0.03, which ensures more than adequate pulsation damping.

6.5.3 *Air pump*

The nominal air pump operating conditions are summarised below:

State	gas	
Suction Pressure	60	bar (abs)
Discharge Pressure	65	bar (abs)
Operating Temperature	60	degC (estimated)
Mass Flow Rate	55	kg/hr
Density (at pump exit)	0.07	kg/l
Volume Flow Rate	13	l/min
or	960	Nl/min

For this application a double-acting single-stage air-driven model DLE 15 gas booster (manufactured by Schmidt, Kranz & Co. GmbH) is selected. This reciprocating pump is capable of a maximum flow rate of 20 l/min (at exit conditions) for a pressure differential of 5 bar and a maximum pressure of 160 bar at zero head. Nominal air drive consumption is 120 Nm^3/hr at 7 bar. The compression ratio of the pump is 20:1 and its displacement is 225 cm^3.

6.5.4 *Air plenum chamber*

Given the air pump displacement an operating frequency of 1 Hz is deduced. In order to damp the associated air flow pulsations a plenum chamber of adequate volume, combined with the pressure loss of, approximately, 4 bar along the pressure regulators and piping is required. Based on data from BS 1042, [23], a minimum Hodgson (Ho) number of 2 is required for a pulsating flow to be damped sufficiently so as to give rise of 1% error in a differential pressure flow measuring device. Using this as a guideline, an adequately large plenum chamber volume can be deduced:

$$Ho = (\Delta P/P)(V_p/V_d)$$

where

ΔP: line pressure loss
P : line abs. pressure
V_d: pump displacement
V_p: plenum volume

For ΔP=4 bar, P=60 bar, V_d=225 cm^3 and Ho>2, a minimum plenum volume V_p=6.75 l is estimated.
The plenum chamber will be designed for a capacity of 8.0 l according to BS 5500.

6.5.5 *Heat exchangers*

During pump operation, the air and, to a lesser extent, Freon-12 temperatures will be continuously rising. For this reason, and in order to maintain constant fluid properties, both circuits should be equipped with appropriate heat exchangers and temperature controllers. Apart from maintaining constant fluid temperature, these heat exchangers will be selected so as to enable future intentional increase of working fluid temperatures in order to allow the proposed system to cover operating modes described in section 5.3. As an example, a typical double-pipe counter-flow heat exchanger configuration was considered which, for an air temperature increase of 40 K, yielded a required heat exchange area of the order of 1 m^2, [11,15].
The heat exchangers recommended for both fluid circuits will be operated with mains water (heated or not, see Figure 7) and controlled via two reverse-action PD temperature controllers (eg Eurotherm Type 104). The recommended exchangers are Heliflow Sizes 4-10 and 12-14L for the Freon-12 and air circuits, respectively (manufactured by Graham Ltd UK and rated at 400 bar). Cooling (or heating) water input will be controlled by solenoid valves operated by the two temperature controllers.

6.5.6 *Temperature measurement*

The temperature of the working fluids should be measured at various circuit locations (flow meters and injection chamber) and controlled at the injector inlet. The recommended sensors are resistance thermometers (PT 100, BS1904 Grade I) connected to an eight channel temperature monitoring unit (eg Eurotherm 141-70-467-19).

6.5.7 *Flow rate measurement*

The choice of devices for the measurement of the, relatively low, flow rates of liquid Freon-12 and air under the prevailing high pressure conditions has been considered very carefully. It was found that the best compromise in terms of cost, measurement accuracy and flexibility is offered by orifice plate flow meters for both fluid circuits, combined with electronic pressure transducers and PT100 sensors for the measurement of the differential and static pressures and fluid temperature, respectively.
The orifice plate flow meters will be designed according to BS 1042, [23], for an internal pipe diameter of 26.2 mm (1.25" O.D., 0.109" wall thickness) and differential pressures of the order of 0.2×10^5 N/m^2 with orifice/pipe area ratio m=0.4. This should result in net pressure loss across the flow meters of the order of 60% of the pressure differential, which is perfectly acceptable given the capacity of the fluid pumps selected in 6.5.1 and 6.5.3.
The pressure differential will be measured by low range wet/wet differential pressure transducers capable of withstanding line pressures of the order of 60 bar. The proposed transducers are the Sensotec Model Z (AD111), with SS-316 wetted parts, pressure range 0-5 psi (0-0.34 bar),

maximum line pressure 100 bar and accuracy and non-linearity of +/-0.25% and +/-0.15 FS, respectively.
The static pressure upstream of the flow meters will be measured with suitable absolute pressure transducers, one for each fluid circuit. The recommended transducers are the Sensotec Mode TJE (AP122) precision absolute transducers with 0-1500 psi (0-100 bar) range, +/- 0.1% accuracy, and 17-4 PH stainless steel wetted parts. It is proposed that the same transducers are used in order to monitor the fluid pressures in other points of the flow circuit and within the injection chamber using suitable selector valves (eg Whitey SS-43ZF2 5-way valves). All four transducers should be used in conjunction with the appropriate power supplies and pressure readout units, (eg Eurotherm 842 process indicators).
Care should be taken in the positioning of the transducers with respect to the pressure taps. The transducers in the liquid Freon side should be located below the pipework so that air is not trapped in their dead volumes and the ones in the air circuit should be located above the pipework. Vapour traps according to BS 1042 could also be installed at the orifice plate flow meters.
Fluid temperatures upstream of the orifice plate flow meters will be measured using the PT100 sensors described in 6.5.6, above. The flow metering devices described above will be able to measure volume and mass flow rates of the working fluids with an accuracy better than 1.5% of the actual.

6.5.8 *Pressure and flow control*

The line pressure within the working fluid circuits will be adjusted by means of appropriate high-pressure regulators (eg BOC Spectrol X87). The pressure regulators in the Freon circuit should be of the non-relieving type.
The flow rate of the working fluids will be controlled by a combination of air supply pressure to the air-driven pumps and suitable regulating valves (eg Whitey SS-6LRS6) in the individual fluid circuits. Shut-off valves will be equivalent to Whitey SS-6TS6.
Both working fluid circuits will incorporate filters for the removal of foreign particulates. Nupro type TF removable filter units with 2μm sintered filter elements are recommended for both circuits. At the nominal flow rates discussed above, these filters will cause a pressure loss of the order of 0.5 and 0.4 bar in the air and Freon circuits, respectively.
In order to prevent accidental mixing of air and Freon due to unbalanced exit pressures in the injector element, both circuits will be fitted with appropriate check valves near their exit. Nupro SS-4CA-3 check valves, or equivalent, are recommended.
For safety reasons a relief valve will be installed after the pump of each working fluid circuit as well as in the injection chamber. The relief valves recommended for all three positions are the Nupro Types 177-R3A-K1-C with externally adjustable cracking pressure in the range of 50-100 bar.

7 TRANSIENT ATOMISATION/EVAPORATION STUDIES

The experimental arrangement described in sections 5 and 6 could be modified to allow the study of super-critical liquid jet atomisation under transient flow conditions. For this purpose the diaphragm accumulator used for damping the Freon flow pulsations will be replaced with a bladder accumulator of larger capacity (units of 5 to 50 l are readily available) and the liquid Freon will be pressurised at 65 bar before its release through the injector element. Similarly, and if required, the 8 l plenum chamber of the air circuit can be replaced with a larger volume and higher pressure rating vessel (for instance the air cylinder itself) and discharged through the injector simultaneously with the Freon-12. Time-resolved PDA measurements of liquid droplet size and velocity can then be obtained with reference to the injection start time in order to study the transient characteristics of the liquid jet atomisation process.
The same experimental setup could be used for the study of the transient atomisation and evaporation of a super-critical liquid jet by replacing Freon-12 with Freon-13, as mentioned in section 5.3.

8 SUMMARY

This report has outlined a preliminary study regarding the feasibility of characterising the atomisation process of a super-critical pressure liquid in a super-critical pressure and temperature gaseous environment, under conditions simulating those during the priming stage of the SSME fuel preburner combustion chamber.
It was shown that by using Freon-12 and air as the liquid and gaseous phase, respectively, the atomisation process of liquid oxygen in supercritical hydrogen in the SSME fuel preburner could be adequately simulated under stationary flow conditions and reasonably low pressures and temperatures.
Based on this simulation principle, the main characteristics of a suitable test facility have been determined and, to a certain extent, the primary components designed or specified. The test facility allows optical access into the injection chamber for the application of Phase Doppler Anemometry techniques for the simultaneous measurement of liquid droplet size and velocity, thus allowing detailed study of the atomisation process.
The proposed test facility is flexible enough to accommodate various injector element geometries and allows the main simulation parameters to vary within the range of interest. Additionally, and with minor modifications of the proposed design, the transient nature of the SSME fuel preburner priming stage as well as the evaporation of the liquid phase after atomisation can be simulated and studied.

REFERENCES

1 - Wang Ten-See, (1991) "Computational analysis of the three-dimensional steady and transient SSME Fuel preburner combustor", IUTAM Symposium on Aerothermodynamics in Combustors, June 3-5, Taipei.

2 - Hardalupas, Y. and Whitelaw, J.H., (1991) "Characteristics of coaxial blast atomisers" Imperial College, Mech. Eng. Dept., Report in preparation.

3 - Vargaftik, N.B., (1975) *"Tables on th thermophysical properties of liquid and gases"*, 2nd edn., Hemisphere.

4 - Weast, R.C., Ed. (1989) *"CRC Handbook of chemistry and physics"*, 69th Edition, CRC Press.

5 - Reynolds, W.C., (1979) *"Thermodynamic properties in SI - Graphs, tables and computational equations for 40 substances"*, Dept. of Mechanical Engineering, Stanford University, Stanford CA 94305.

6 - Delplanque, J.-P. and Sirignano, W.A. (1991) "Transient vaporization and burning for an oxygen droplet at sub- and near-critical conditions" AIAA 29th Aerospace Sciences Meeting, Paper AIAA-91-0075.

7 - Chiang, C.H. and Sirignano, W.A. (1991) "Axisymmetric vaporizing oxygen droplet computations" AIAA 29th Aerospace Sciences Meeting, Paper AIAA-91-0281.

8 - Rosner, D.E. and Chang, W.S., (1973) "Transient evaporation and combustion of a fuel droplet near its critical temperature", Comb. Sci. Tech., 7, 145-158.

9 - Umemura, A., (1986) "Supercritical liquid fuel combustion", Proc. 21st Symposium (Int.) on Combustion, The Combustion Institute, 463-471.

10 - Litchford, R.J and Jeng, S.-M., (1990) "LOX vaporisation in high-pressure hydrogen-rich gas", Paper presented at AIAA/SAE/ASME/ASEE, 26th Joint Propulsion Conference, Orlando, FL.

11 - Rohsenow, W.M. and Hartnett, J.P., Eds. (1973) *"Handbook of heat transfer"*, McGraw Hill.

12 - BOC Ltd, Special Gases, (1986) "Special Gases Catalogue".

13 - ASRAHE, (1989) *"Fundamentals Hanbook (SI)"*.

14 - Cox, G.B. and Petersen, E.L., (1991) "Liquid stability mechanisms program summary", Report Pratt & Whitney/Government Engines & Space Propulsion, West Palm Beach, FL 33410-9600.

15 - Janna, W.S., (1988) *"Engineering Heat Transfer"*, SI Edition, Van Nostrand Reinhold.

16 - Dupont, (1967) "Surface tension of the Freon compounds", Technical Bulletin D-27.

17 - BS 5500, (1982) "Specification for: Unfired fusion welded pressure vessels", British Standards Institution, Issue 3, April 1984.

18 - DIN 7080, (1975) "Pressure resistant circular sight glasses for temperatures up to 300oC: No pressure limitation at low temperatures", Deutsches Institut Fur Normung, September 1975.

18 - Parker-Pradifa GmbH, (1986) "Precision O-ring handbook".

19 - Heraeus, (1985) "Transparent and opaque fused silica", Technical Bulletin Q-A 1/112.2.

20 - Quartz & Silice, (1987) "Optical Silica", Technical Note OPT 87-11.

21 - Wigley, G., (1987) "Laser anemometry measurement techniques in internal combustion engines", Proc. 2nd Int. Conf. on Laser Anemometry - Advances and Applications, 21-23 September 1987, Glasgow, UK.

22 - Vukobratovich, D., (1986) "Introduction to opto-mechanical design", S.P.I.E. Course 23-24 Feb. 1987, S.I.R.A., UK.

23 - BS 1042, (1964) "Methods for the measurement of fluid flow in pipes", British Standards Institution, Part 1.

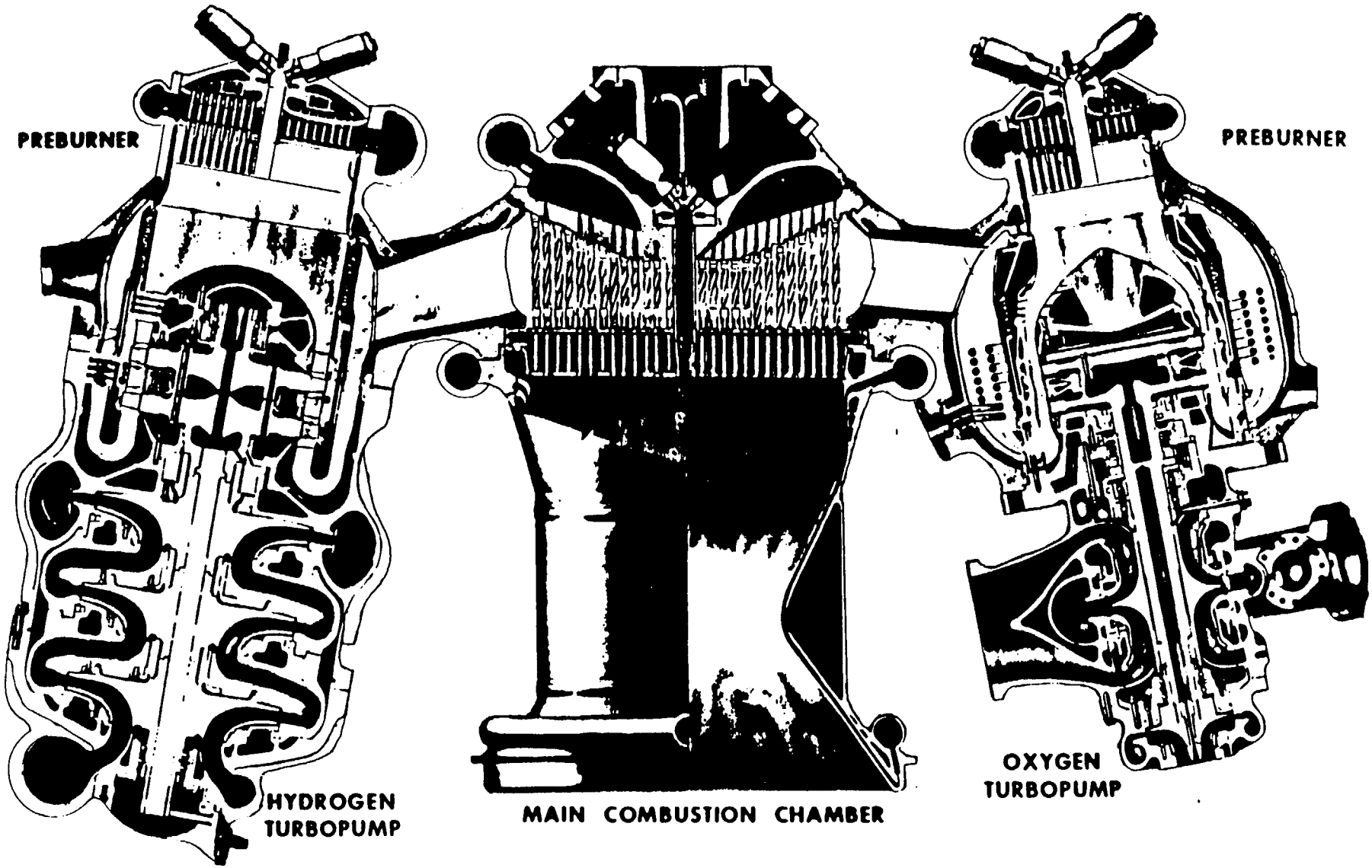

Figure 1. The SSME Powerhead assembly

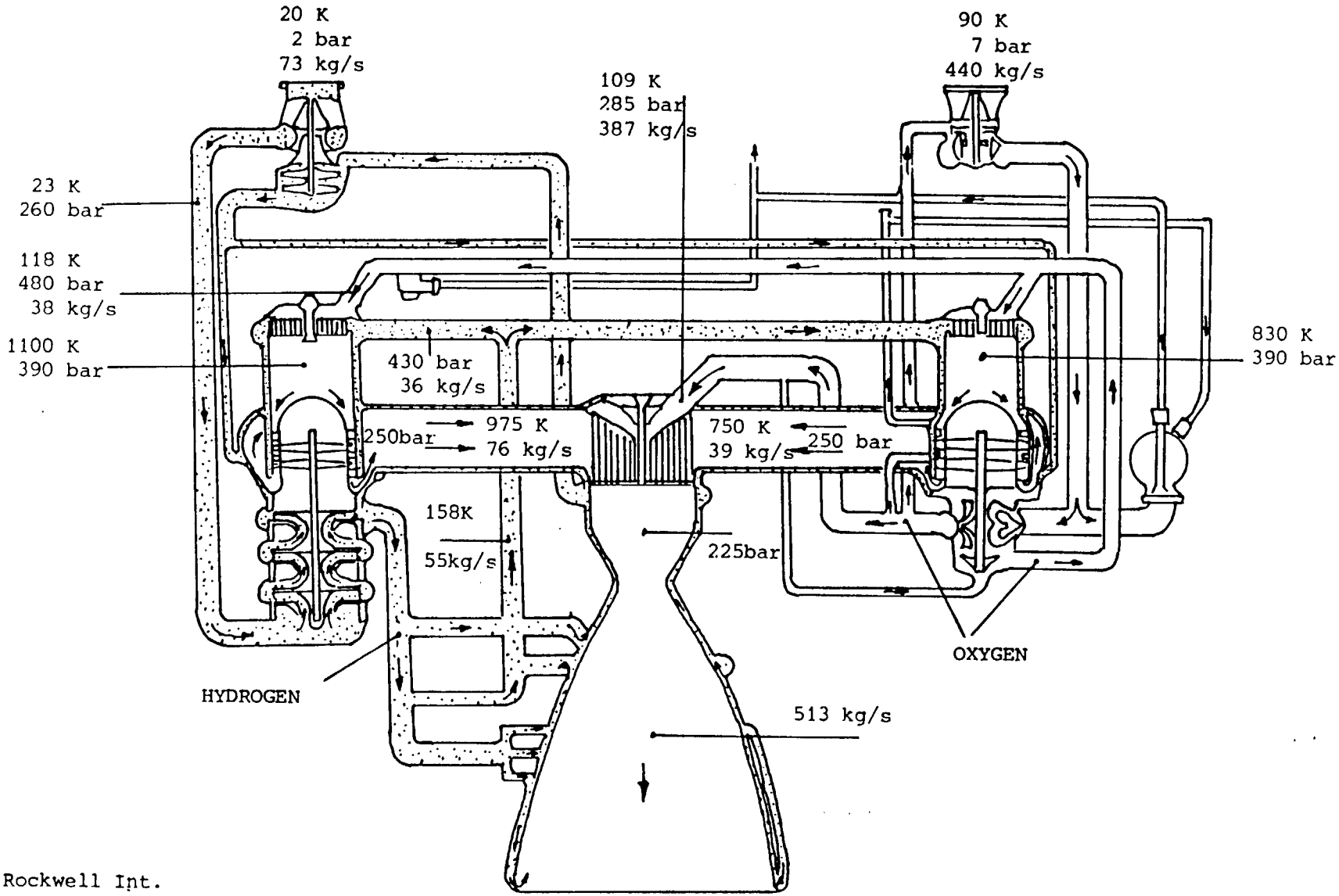

Source: Rockwell Int.
Rocketdyne Div.
LC 430-702

Figure 2. S.S.M.E. propellant flow schematic

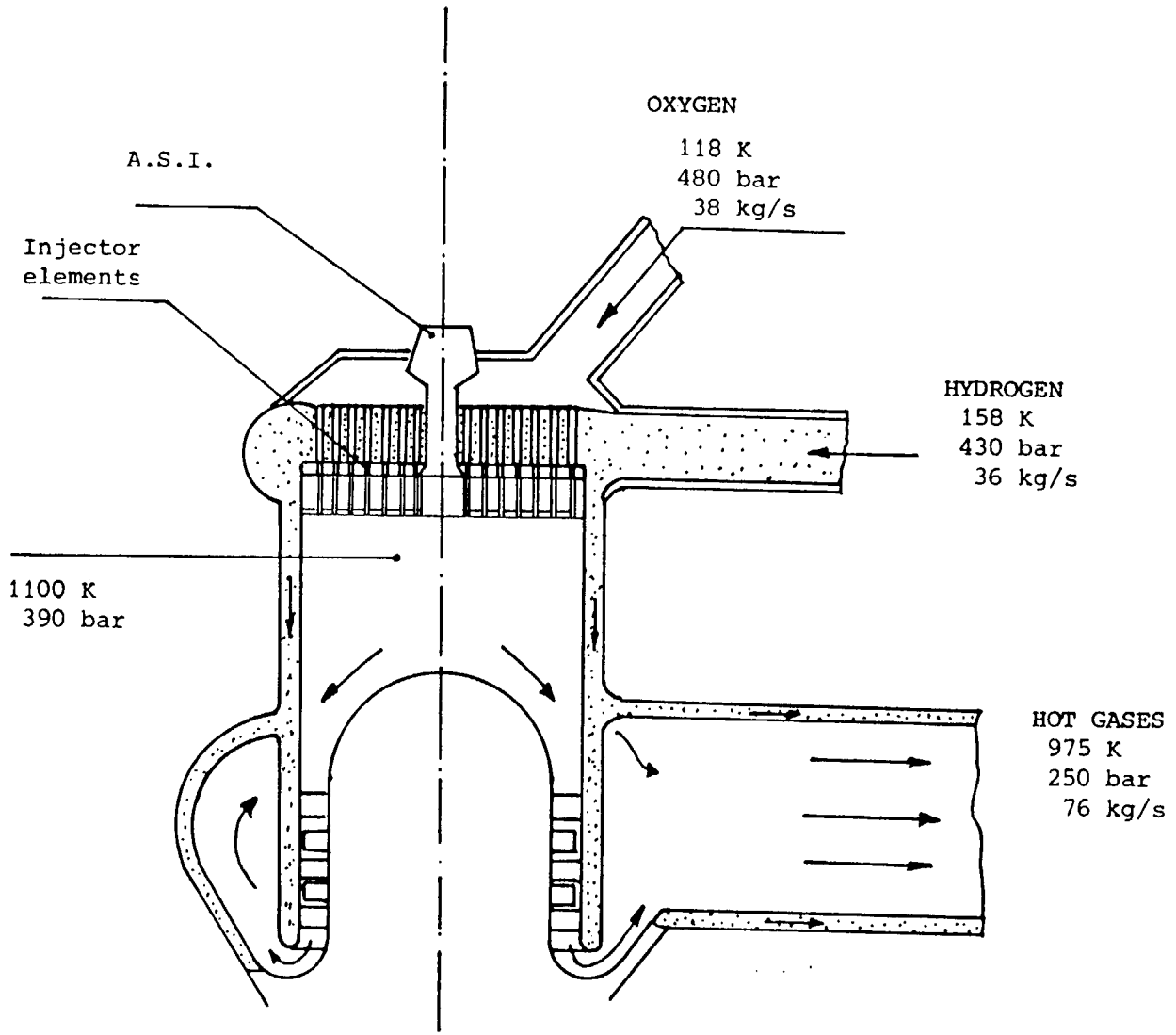

Figure 3. Schematic of the High Pressure Fuel Turbopump preburner

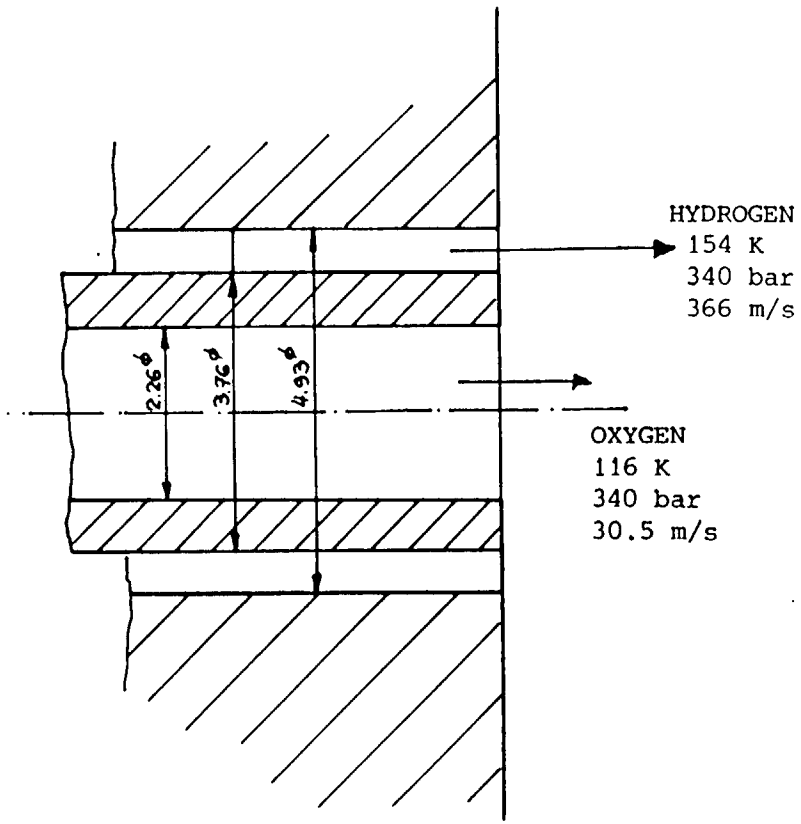

Figure 4. SSME injector element geometry (scale 10:1)

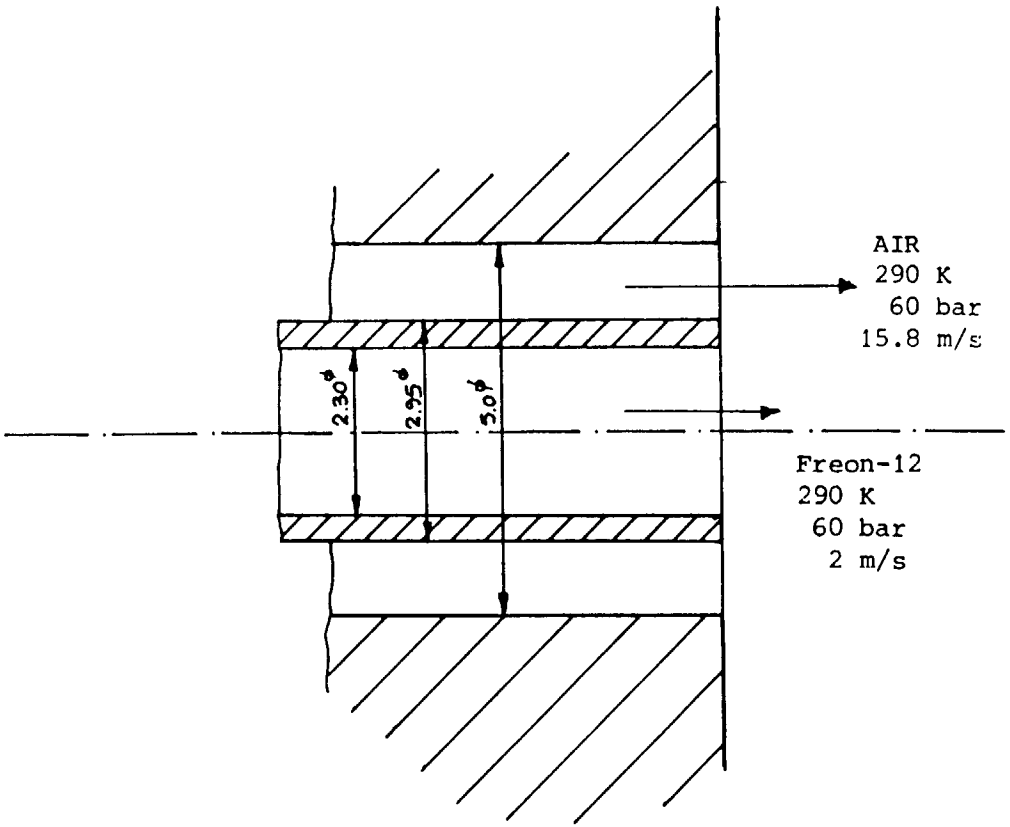

Figure 6. Proposed baseline injector element geometry (scale 10:1)

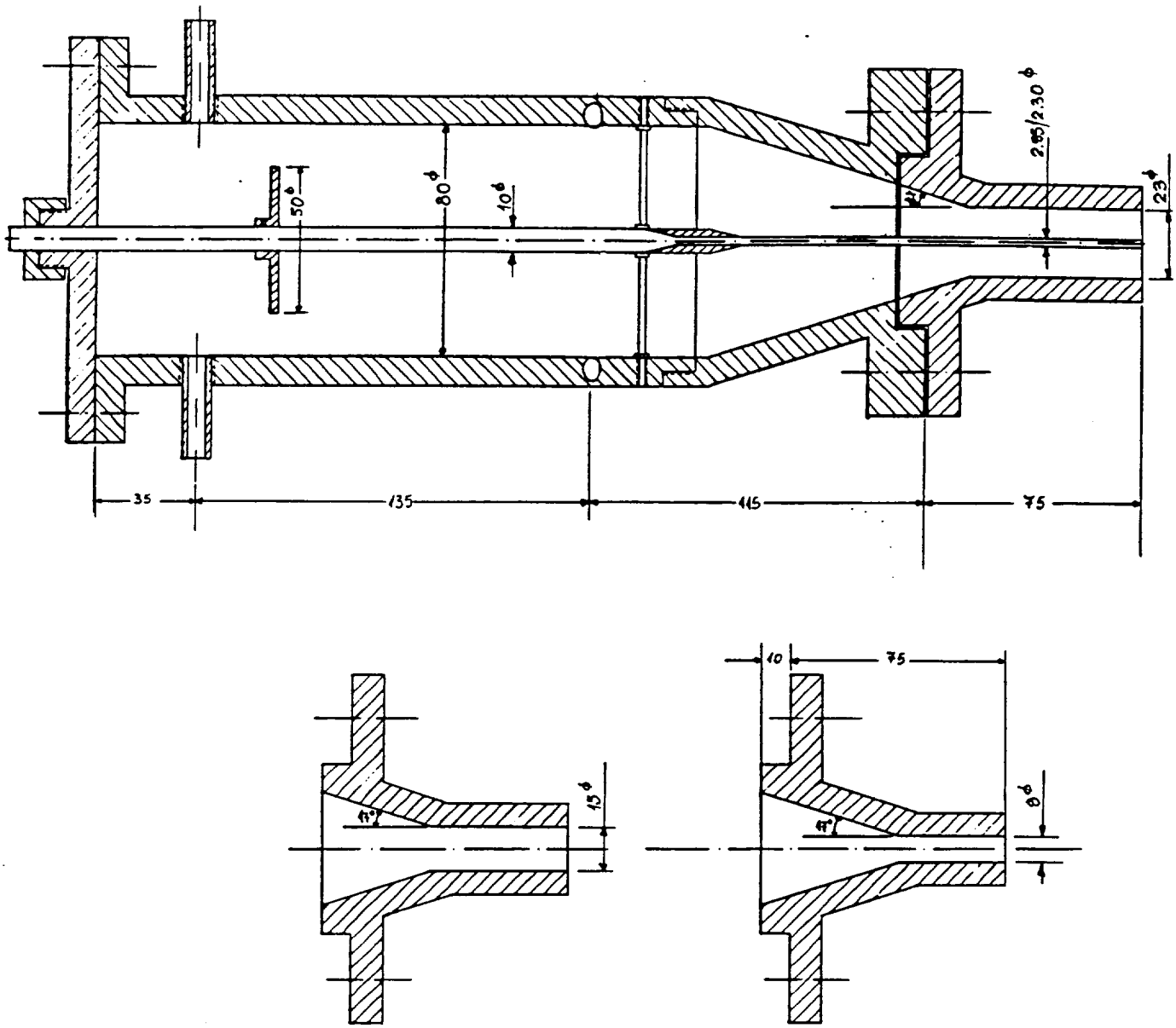

Figure 5. Atmospheric water/air injector geometry (from ref. [2]) with alternative annular duct external diameter nozzles

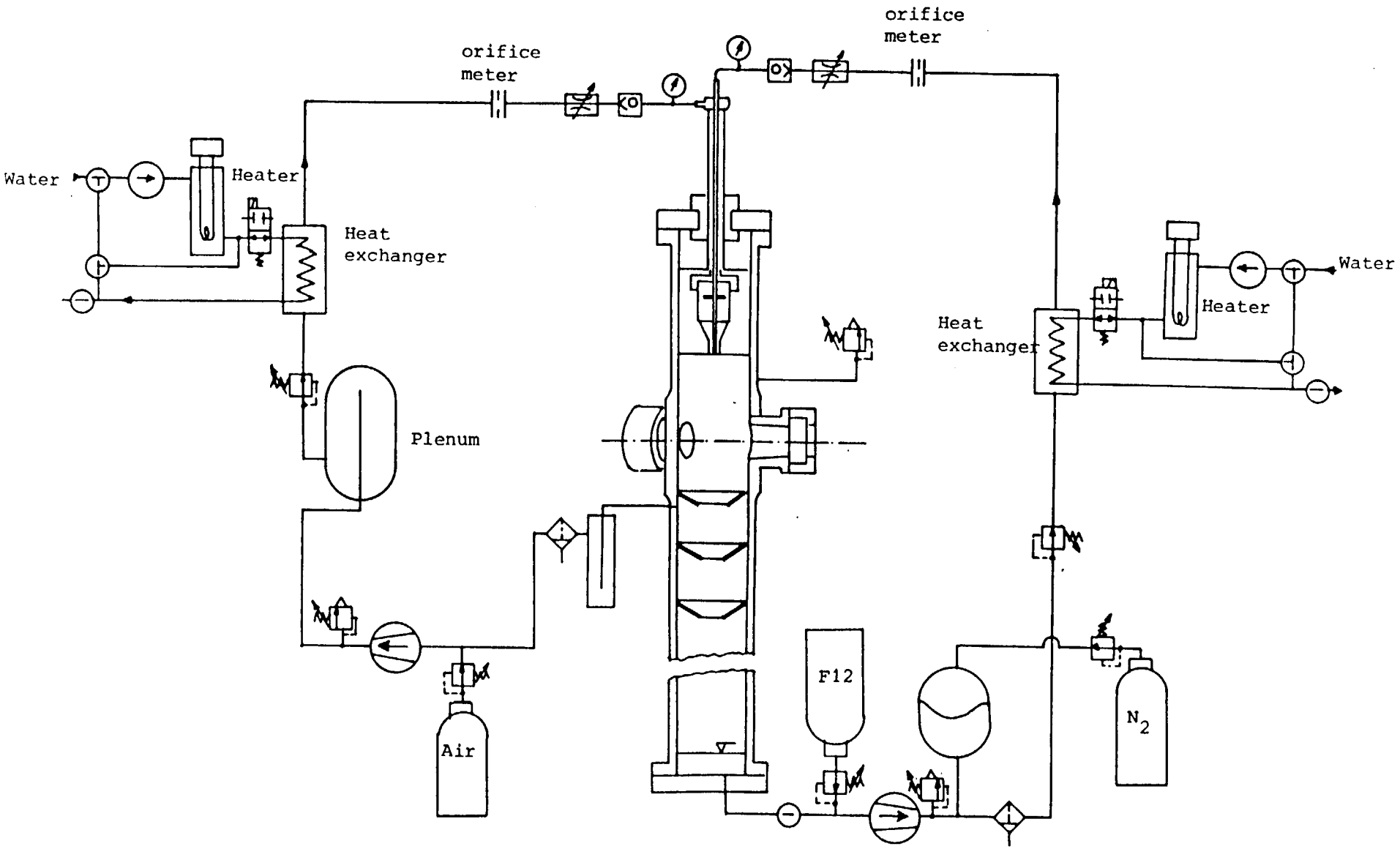

Figure 7. Flow circuit

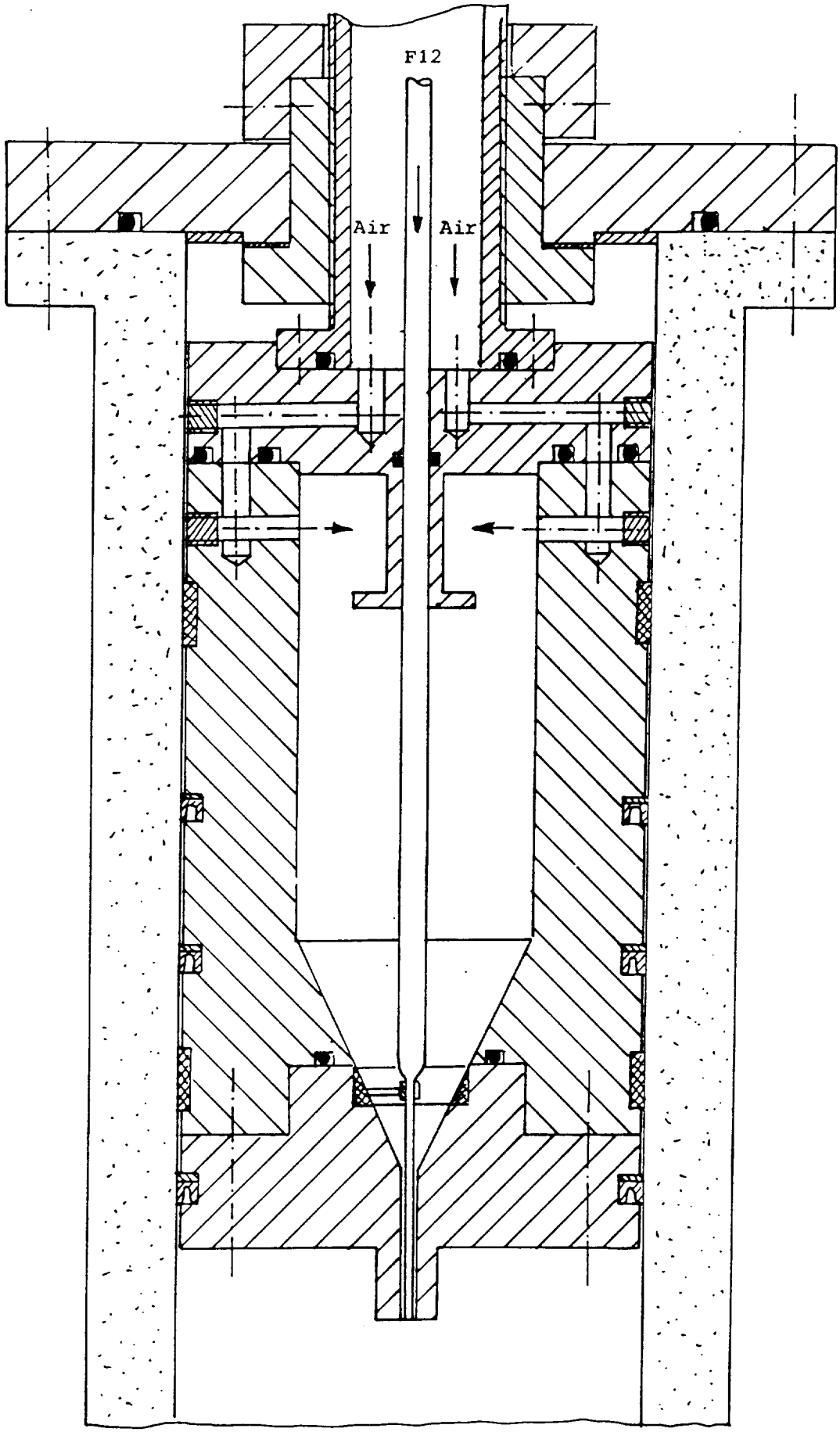

Figure 8. Injector head assembly (scale 1:2)

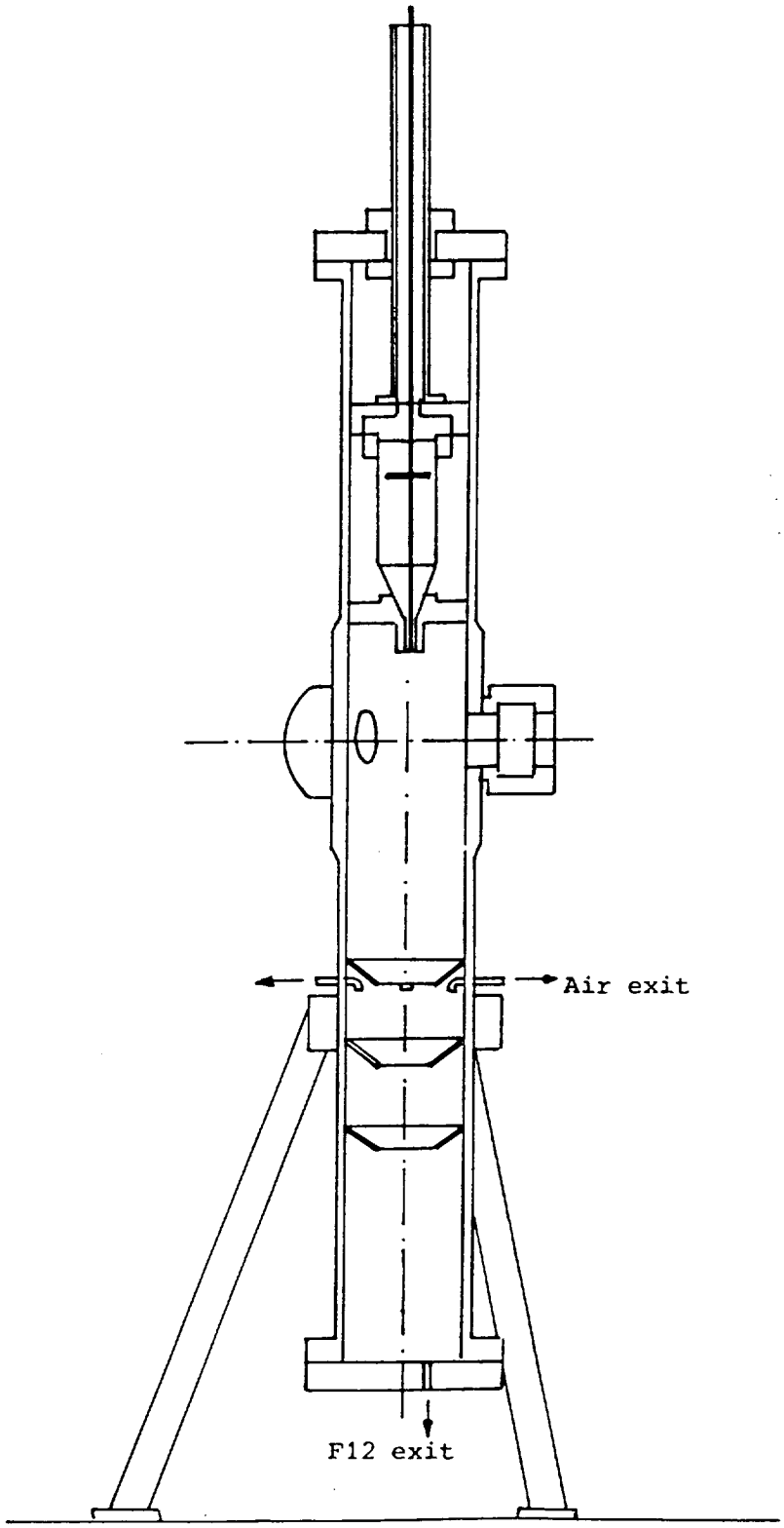

Figure 9. The injection chamber assembly (scale 1:10)

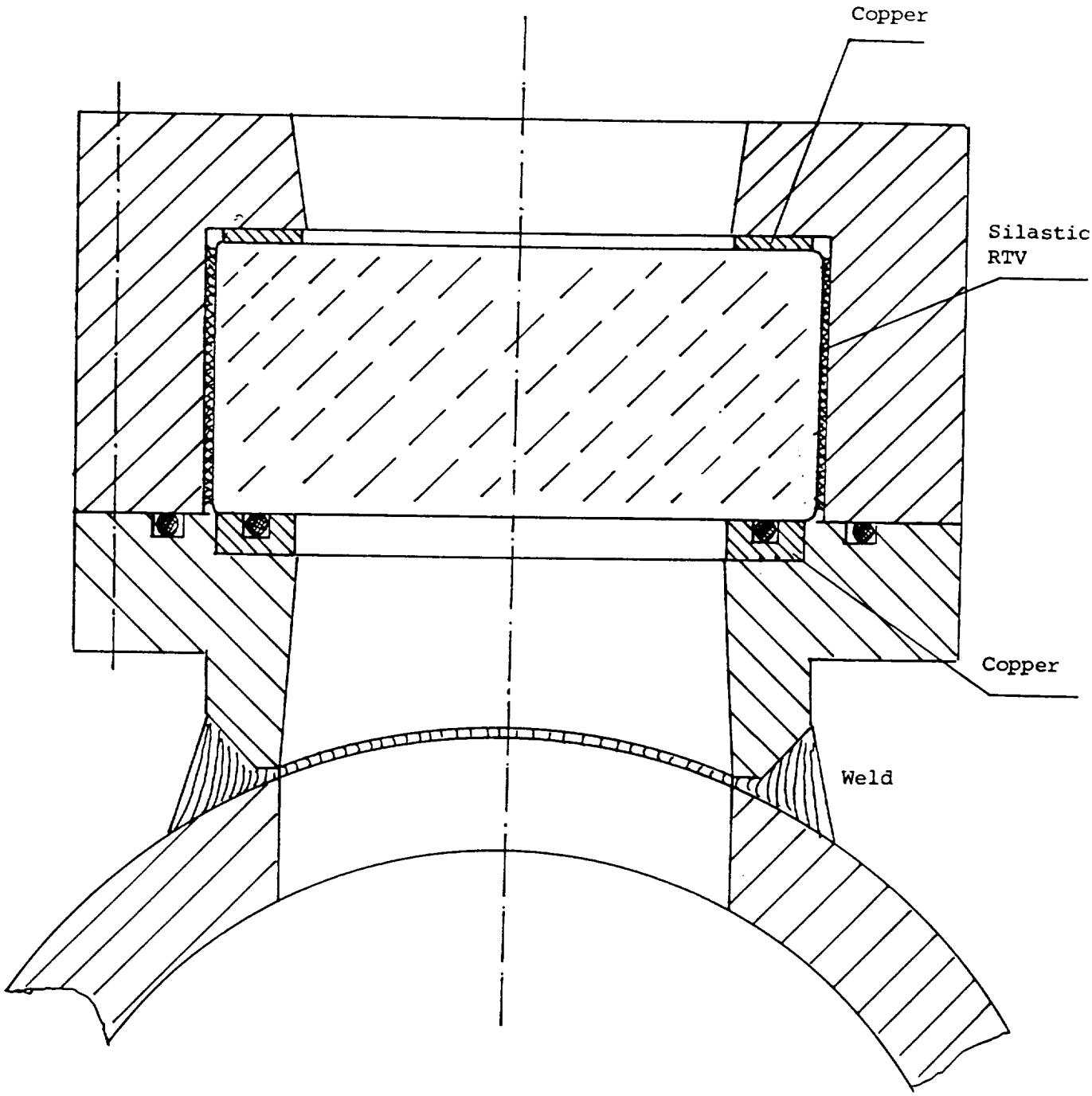

Figure 10. Window housing detail (scale 1:1)

TABLES

Table 1a. Parameters of the examined sprays produced by axial only gaseous stream nozzles with D_{liquid} = 2.3 mm.

Table 1b. Parameters of the examined sprays produced by axial only gaseous stream nozzles with D_{liquid} = 1.1 mm.

Table 2. Parameters of the examined sprays produced by swirling gaseous stream nozzles with D_{liquid} =2.3 mm. Swirl generated by tangential inlets.

Table 3. Parameters of the examined sprays produced by swirling gaseous stream nozzles with D_{liquid} =2.3 mm. Swirl generated by helical type swirlers.

Table 4. Optical characteristics of the phase Doppler instrument

Table 5a. Parameters affecting secondary atomization in sprays produced by axial only gaseous stream nozzles with D_{liquid} = 2.3 mm

Table 5b. Parameters affecting secondary atomization in sprays produced by axial only gaseous stream nozzles with D_{liquid} = 1.1 mm

TABLE 1a. Parameters of the examined sprays produced by axial only gaseous stream nozzles with D_{liquid} = 2.3 mm

case no.	annular width (mm)	gas velocity [1] (m/s)	liquid velocity [2] (m/s)	Reynolds number gas [3]	Reynolds number liquid [4]	exit Weber number [5]	momentum ratio gas/liquid [6]	velocity ratio gas/liquid [7]	mass flowrate ratio gas/liquid [8]
1	10	85	7.6	129100	20560	208	13.6	11.2	1.20
2	10	85	3.6	129100	9740	230	60.6	23.6	2.60
3	10	85	2.4	129100	6490	236	136	35.4	3.85
4	10	85	1.6	129100	4330	241	298	53.1	5.50
5	6	112	7.6	110800	20560	378	9.8	14.7	0.66
6	6	112	3.6	110800	9740	407	43.6	31.1	1.40
7	6	112	2.4	110800	6490	416	98	46.7	2.10
8	6	123	7.6	121700	20560	462	11.4	16.2	0.70
9	6	123	3.6	121700	9740	494	50.8	34.2	1.49
10	6	123	2.4	121700	6490	504	114	51.3	2.23
11	3	158	7.6	93590	20560	780	6.5	20.8	0.31
12	3	182	7.6	107800	20560	1050	8.6	23.9	0.35
13	3	266	7.6	157560	20560	2315	18.3	35.0	0.52
14	3	315	7.6	186580	20560	3275	25.5	41.4	0.61
15	3	135	3.6	79970	9740	598	21	37.5	0.56
16	3	158	3.6	93590	9740	826	28.7	43.9	0.65
17	3	182	3.6	107800	9740	1103	38.1	50.6	0.75
18	3	266	3.6	157560	9740	2386	81.3	73.9	1.10
19	3	315	3.6	186580	9740	3360	113	87.5	1.29
20	3	182	13.2	107800	35720	988	2.83	13.8	0.21
21	3	182	20	107800	54120	910	1.23	9.1	0.14
22	3	266	13.2	157560	35720	2215	6.0	20.1	0.30
23	3	266	20.0	157560	54120	2097	2.6	13.3	0.20
24	3	315	13.2	186580	35720	3160	8.4	23.9	0.35
25	3	315	16.8	186580	45460	3080	5.2	18.8	0.28
26	3	315	20.0	186580	54120	3015	3.7	15.8	0.23

TABLE 1b. Parameters of the examined sprays produced by axial only gaseous stream nozzles with D_{liquid} = 1.1mm

case no.	annular width (mm)	gas velocity [1] (m/s)	liquid velocity [2] (m/s)	Reynolds number gas [3]	Reynolds number liquid [4]	exit Weber number [5]	momentum ratio gas/liquid [6]	velocity ratio gas/liquid [7]	mass flowrate ratio gas/liquid [8]
27	10.74	85	8.2	129100	10600	204	51.1	10.4	4.9
28	10.74	85	12.3	129100	15900	183	22.7	6.9	3.3
29	10.74	85	16.8	129100	21750	161	12.2	5.1	2.4
30	6.74	112	8.2	110800	10600	373	37.3	13.7	2.73
31	6.74	112	12.3	110800	15900	345	16.6	9.1	1.82
32	6.74	112	16.8	110800	21750	314	8.9	6.7	1.33
33	6.74	123	8.2	121700	10600	457	45	15	3.0
34	6.74	123	12.3	121700	15900	425	20	10	2.0
35	6.74	123	16.8	121700	21750	390	10.7	7.3	1.46
36	6.74	143	8.2	141500	10600	630	61	17.4	3.5
37	6.74	143	12.3	141500	15900	592	27.1	11.6	2.3
38	6.74	143	16.8	141500	21750	552	14.5	8.5	1.7
39	3.74	155	8.2	91800	10600	747	25.2	18.9	1.33
40	3.74	155	12.3	91800	15900	706	11.2	12.6	0.89
41	3.74	155	16.8	91800	21750	662	6.0	9.2	0.65
42	3.74	207	8.2	122600	10600	1370	44.9	25.2	1.78
43	3.74	207	12.3	122600	15900	1315	20.0	16.8	1.19
44	3.74	207	16.8	122600	21750	1255	10.7	12.3	0.87
45	3.74	217	8.2	140400	10600	1815	59.3	28.9	2.05
46	3.74	217	12.3	140400	15900	1750	26.3	19.3	1.37
47	3.74	217	16.8	140400	21750	1680	14.1	14.1	1.
48	3.74	316	8.2	187200	10600	3285	105.2	38.5	2.73
49	3.74	316	12.3	187200	15900	3197	46.7	25.7	1.82
50	3.74	316	16.8	187200	21750	3100	25.0	18.8	1.33

[1] U_g, averaged over the area of the annulus of the gaseous jet

[2] U_l, averaged over the area of the liquid jet

[3] $Re_g = U_g D_{gas} / \nu_g$

[4] $Re_l = U_l D_{liquid} / \nu_l$

[5] according to equation (1a)

[6] according to equation (1d)

[7] according to equation (1e)

[8] according to equation (1b)

TABLE 2. Parameters of the examined sprays produced by swirling gaseous stream nozzles with D_{liquid} =2.3 mm. Swirl generated by tangential inlets.

case no.	annular width (mm)	gas velocity (m/s)	liquid velocity (m/s)	swirl number [1]	Reynolds number gas	Reynolds number liquid	exit Weber number	momentum ratio gas/liquid	velocity ratio gas/liquid	mass flowrate ratio gas/liquid
S1	10	85	3.6	0.3	129100	9740	230	60.6	23.6	2.60
S2	10	85	3.6	0.2	129100	9740	230	60.6	23.6	2.60
S3	6	138	3.6	0.1	136540	9740	630	63.6	38.3	1.66

[1] according to equation (2)

TABLE 3. Parameters of the examined sprays produced by swirling gaseous stream nozzles with D_{liquid} =2.3 mm. Swirl generated by helical type swirlers.

case no.	annular width (mm)	gas velocity (m/s)	liquid velocity (m/s)	velocity vector [2] angle (°)	swirl number [3] S'	Reynolds number gas	Reynolds number liquid	exit Weber number	momentum ratio gas/liquid	velocity ratio gas/liquid	mass flowrate ratio gas/liquid
S4	10	50.2	3.6	85	7.9	76250	9740	75	21.4	13.9	1.54
S5	6	80	3.6	82.2	5.3	79150	9740	202	21.5	22.2	0.97
S6	3	127	3.6	77	3.2	75230	9740	528	18.7	35.3	0.53
S7	3	185	3.6	77	3.2	109590	9740	1140	39.6	51.4	0.77
S8 [1]	3	112	3.6	77	3.2	66345	9740	407	14.6	31.1	0.47
S9 [1]	3	112	7.6	77	3.2	66345	20560	378	3.2	14.7	0.22

[1] cases used only for spray interaction
[2] angle between axis of symmetry of the swirler and vanes
[3] according to equation (2a)

TABLE 4. Optical characteristics of the phase Doppler instrument

Transmitting optics		
Laser: He-Ne laser		
operating power	35	mW
wavelength	632.8	nm
Beam intersection angle	3.024	deg.
Measurement volume length at $1/e^2$ intensity	4.88	mm
Measurement volume diameter at $1/e^2$ intensity	129	μm
Fringe spacing	11.991	μm
Number of fringes	11	
Frequency shift	0-3	MHz
Receiving optics		
Focal length of collimating lens	500	mm
Location of receiving optics		
from forward scatter angle	30	deg.
Equivalent aperture at collimating lens:		
dimension of rectangular aperture	67 x 10.6	mm
separation between aperture 1 and 2	13.3	mm
separation between aperture 1 and 3	26.6	mm
Magnification	1/2	
Spatial filter slit width	100	μm
Effective length of measuring volume	312.5	μm
Phase angle-to-diameter conversion factor		
for channel 1 and 3, without rotation of the plane of the beams	0.973	μm/deg
Phase angle-to-diameter conversion factor		
for channel 1 and 3, after rotation of the plane of the beams by ±45°	1.163	μm/deg

TABLE 5a. Parameters affecting secondary atomization in sprays produced by axial only gaseous stream nozzles with D_{liquid} = 2.3 mm

case no.	annular width (mm)	SMD at z=80 mm [1] (μm)	MMD at z=80 mm [1] (μm)	MMD/ SMD ratio	U_{gm} [2] (m/s)	$T_{acceler}$ [3] (ms)	(U_{gm}-U_l) [4] (m/s)	max (U_{gc}-U_{lc}) [5] (m/s)	(U_g - U_l) [6] (m/s)
1	10	170	212	1.24	45.9	3.2	38.3	12	77.4
2	10	130	163	1.25	56.2	2.4	52.6	16	81.4
3	10	120	145	1.20	65.6	1.3	63.2	20	82.6
4	10	107	125	1.17	71	1.2	69.4	22.5	83.4
5	6	166	212	1.27	40.4	3.9	32.8	10	104.4
6	6	139	175	1.25	49.2	1.7	45.6	14.5	108.4
7	6	110	130	1.18	63.9	1.2	61.5	19.5	109.6
8	6	153	196	1.28	47.4	3.3	40.1	12	115.4
9	6	118	146	1.23	59.7	1.4	56.1	17	119.4
10	6	96	111	1.16	73.7	0.8	71.3	21.5	120.6
11	3	190	235	1.23	35.4	4.4	27.8	10	150.4
12	3	165	199	1.20	41.3	3.4	33.7	11.5	174.4
13	3	142	172	1.21	50.4	2.7	42.8	11.4	258.4
14	3	137	164	1.19	67.1	1.9	59.5	14	307.4
15	3	127	158	1.24	41.9	1.4	38.3	13	131.4
16	3	114	137	1.20	62	1.0	58.4	25	154.4
17	3	96	109	1.14	81.4	1.0	81.4	30	178.4
18	3	90	103	1.15	95.5	0.61	91.9	33.3	262.4
19	3	90	100	1.12	108.2	0.53	104.6	30.4	311.4
20	3	198	240	1.21	30	9.2	16.8	5.7	168.8
21	3	226	263	1.16	31.5	13.4	11.5	3.2	162
22	3	170	210	1.23	41.4	7.3	28.2	6.5	252.8
23	3	175	227	1.29	37.3	11.8	17.3	2.9	246
24	3	152	181	1.19	45	6.4	31.8	4	301.8
25	3	171	205	1.20	45.6	7.1	28.8	6.3	298.2
26	3	165	206	1.25	39	10.7	19	1.7	295

1 values at axial distance 80 mm from nozzle exit
2 maximum gas velocity on the centreline
3 according to equation (8)
4 difference between maximum gas velocity and U_l
5 maximum measured slip velocity on the centreline
6 velocity difference at the nozzle exit

TABLE 5b. Parameters affecting secondary atomization in sprays produced by axial only gaseous stream nozzles with D_{liquid} = 1.1 mm

case no.	annular width (mm)	SMD at z=80 mm [1] (μm)	MMD at z=80 mm [1] (μm)	MMD/ SMD ratio	U_{gm} [2] (m/s)	$T_{acceler}$ [3] (ms)	$(U_{gm}-U_l)$ [4] (m/s)	max $(U_{gc}-U_{lc})$ [5] (m/s)	$(U_g - U_l)$ [6] (m/s)
27	10.74	141	168	1.19	62.6	2.3	54.4	15.3	76.8
28	10.74	165	204	1.23	53	3.9	40.7	11.2	72.7
29	10.74	175	210	1.20	52.6	4.6	35.8	9	68.2
30	6.74	125	153	1.22	61.6	1.9	53.4	14	103.4
31	6.74	142	169	1.19	55.5	2.3	43.2	13	99.7
32	6.74	165	200	1.21	52.5	2.9	32.6	11	95.2
33	6.74	122	147	1.20	68.3	1.9	60.1	16.6	114.8
34	6.74	139	170	1.22	58.7	2.5	46.4	13	110.7
35	6.74	147	180	1.22	57.3	2.9	40.5	10.8	106.2
36	6.74	103	125	1.21	86.2	1.0	78	24.6	134.8
37	6.74	121	159	1.31	73.2	1.9	60.9	14.9	130.7
38	6.74	135	170	1.25	67.7	2.3	50.9	14.5	126.2
39	3.74	130	156	1.20	58	2.0	49.8	12.8	146.8
40	3.74	151	184	1.22	52.1	2.5	39.8	12.8	142.7
41	3.74	170	205	1.21	50.6	3.0	33.8	9.8	138.2
42	3.74	116	136	1.17	73.6	1.1	65.4	19.4	198.8
43	3.74	130	162	1.24	60.8	1.6	48.5	15.3	194.7
44	3.74	151	186	1.23	56.7	2.6	39.9	8.2	190.2
45	3.74	110	137	1.25	96.5	0.9	88.3	25.2	208.8
46	3.74	120	142	1.18	80.3	1.1	68	27.4	204.7
47	3.74	138	163	1.18	66.3	2.1	50.1	10.7	200.2
48	3.74	170 *	208 *	1.22	115	0.8	106.8	11.4	307.8
49	3.74	150 *	187 *	1.24	106.2	1.1	93.9	18.3	303.7
50	3.74	139 *	167 *	1.20	89.4	1.7	72.6	10	299.2

* the mean diameters of cases 48, 49 and 50 show a decrease with increase of liquid flowrate. This is probably due to droplet breakup at the measurement location and the nonspherical droplets affect the sizing measurement.

LIST OF FIGURES

Figure 11. Characteristics of sprays produced by high swirl number gaseous stream nozzles with 10 mm annulus. Conditions according to case S4 of table 3. Radial profiles of the rms of the fluctuations of the axial velocity of 9, 50 and 105 μm droplets at axial distances from the nozzle of z/D_{liquid} = 1.3 and 26.

Figure 12. Characteristics of sprays produced by high swirl number gaseous stream nozzles with 10 mm annulus. Conditions according to case S4 of table 3. Centreline development of (a) mean axial velocity of 9, 50 and 105 μm droplets and (b) Sauter mean diameter.

Figure 13. Characteristics of sprays produced by high swirl number gaseous stream nozzles with 10 mm annulus. Conditions according to case S4 of table 3. Radial profiles at z/D_{liquid} = 1.3, 26 and 91 of (a) Sauter mean diameter and (b) liquid flux normalised by the maximum value for each axial location.

Figure 14. Characteristics of sprays produced by high swirl number gaseous stream nozzles with 3 mm annulus. Conditions according to case S6 of table 3. Radial profiles at z/D_{liquid} = 26, 52 and 91 of (a) Sauter mean diameter and (b) liquid flux normalised by the measured maximum value for each axial location.

Figure 15. Comparison between the characteristics of sprays produced by axial and low swirl number gaseous stream nozzles. Centreline development of (a) Sauter mean diameter; (b) mean axial velocity of the gas phase; (c) flux half width.

Figure 16. Comparison between the characteristics of sprays produced by axial and low swirl number gaseous stream nozzles. Radial profiles of the Sauter mean diameter at z/D_{liquid}= 52 and 91.

Figure 17. Comparison between the characteristics of sprays produced by axial and swirling gaseous stream nozzles. Radial profiles at z/D_{liquid} = 26 of (a) Sauter mean diameter; (b) liquid flux normalised by the maximum value of flux at the axial location.

Figure 18. The characteristics of the free spray produced by a nozzle according to the conditions of case 2 of table 1a at an axial distance from the nozzle of z/D_{liquid}=91. (a) Mean diameters; (b) normalised volume flux of the liquid content of the spray; (c) normalised concentration of the volume of liquid; (d) mean axial velocity of 9, 50 and 105 μm droplets and (e) rms fluctuations of the axial velocity of 9, 50 and 105 μm droplets.

Figure 19. Characteristics of the spray, produced by a nozzle with conditions according to case 2 of table 1a, striking a disc located at z/Dliquid = 93.5. Radial profiles at axial distances from the nozzle, z/D_{liquid} = 87, 88.3, 89.6, 90.9, 92.2, 92.8 and 94.8. (a) Normalised volume flux of the liquid content of the spray; (b) normalised concentration of the volume of liquid; (c) mean diameters; velocity characteristics of 9, 50 and 105 μm droplets for (d) mean axial velocity; (e) mean radial velocity; (f) rms fluctuations of axial velocity; (g) rms fluctuations of radial velocity; (h) correlation coefficient of $\overline{uv}$ /u'v'. The arrows on the graphs indicate the edge of the disc.

Figure 20. Probability density functions of the axial velocity of droplets in the 9, 50 and 105 μm size ranges and irrespective of diameter in the free spray of case 2 of table 1a at z/D_{liquid}= 91 at radial positions r/D_{liquid} of (a) 0 and (b) 8.7.

Figure 21. Probability density functions of the axial velocity of droplets in the 9, 50 and 105 μm size ranges and irrespective of diameter on the axis of symmetry, r/D_{liquid} =0, of the spray of case 2 of table 1a striking the disc, at axial locations of z/D_{liquid} (a) 90.9 and (b) 92.2.

Figure 22. Probability density functions of the axial velocity of droplets in the 9, 50 and 105 μm size ranges and irrespective of diameter at a radial position r/D_{liquid} =8.7, of the spray of case 2 of table 1a striking the disc, at axial locations of z/D_{liquid} (a) 90.9 and (b) 92.2.

Figure 23. Probability density functions of the velocity in directions (a) +45° and (b) -45° relative to the vertical of droplets in the 9, 50 and 105 μm size ranges and irrespective of diameter at a position (r/D_{liquid} , z/D_{liquid}) = (8.7, 90.9), of the spray of case 2 of table 1a striking the disc.

Figure 24. Drawing of reatomized droplet trajectories close to the surface of the disc.

Figure 25. Radial profiles of (a) mean diameters, (b) liquid flux and (c) mean axial velocity of 9, 50 and 105 μm droplets and single phase at axial distances z/D_{gas} = 13.4, 23.5 and 33.5 from the faceplate of three nozzles producing sprays according to case 12 of table 1a along the r direction at x/D_{gas} = 1.68.

Figure 26. Radial profiles of (a) mean diameters, (b) liquid flux and (c) mean axial velocity of 9, 50 and 105 μm droplets and single phase at axial distances z/D_{gas} = 13.4, 23.5 and 33.5 from the faceplate of three nozzles producing sprays according to case 12 of table 1a along the x direction at r/D_{gas} = 0.

Figure 27. Radial profiles of (a) mean diameters, (b) liquid flux and (c) mean axial velocity of 9, 50 and 105 μm droplets and single phase at axial distances z/D_{gas} = 13.4, 23.5 and 33.5 from the faceplate of three nozzles producing sprays according to case 17 of table 1a along the r direction at x/D_{gas} = 1.68.

Figure 28. Comparison between the Sauter mean diameter, the liquid flux and the axial velocity of the 9 and 105 μm droplets of the three interacting and the single sprays produced by nozzles according to case 12 of table 1a. (a) z/D_{gas} = 23.5, x/D_{gas}=1.68; (b) z/D_{gas}=23.5; r/D_{gas}=0.

Figure 29. Radial profiles along the directions r/D_{gas} = 0 and x/D_{gas}=0, 0.84 and 1.68 of (a) liquid flux, (b) mean diameter, (c) mean axial velocity and (d) mean tangential and radial velocity of the 15, 50 and 105 μm droplets and the single phase at axial distance z/D_{gas} = 13.4 from the faceplate of three nozzles producing sprays according to case S8 of table 3.

Figure 30. Radial profiles along the directions r/D_{gas} = 0 and x/D_{gas}=0 and 1.68 of (a) liquid flux, (b) mean diameter, (c) mean axial velocity and (d) mean tangential and radial velocity of the 15, 50 and 105 μm droplets and the single phase at axial distance z/D_{gas} = 23.5 from the faceplate of three nozzles producing sprays according to case S8 of table 3.

Figure 31. (a) Atomization mechanism in the three interacting sprays produced by nozzles with swirling gaseous stream. (b) The induced velocity by two irrotational vortices, nozzles 2 and 3, on the axis of the third, nozzle 1, explaining the deflection of the liquid jet.

Figure 32. Comparison between the liquid flux, the Sauter mean diameter and the axial velocity of the 15 and 105 μm droplets of the three interacting sprays produced by nozzles with 50% differences in the liquid flowrate according to cases S8 and S9 of table 3. **(a)** z/D_{gas} = 13.4, r/D_{gas}=0; **(b)** z/D_{gas}=23.5; x/D_{gas}=1.68.

Figure 33. Comparison between the Sauter mean diameter, the liquid flux and the axial velocity of the 9 and 105 μm droplets of the three interacting and the single sprays produced by nozzles according to case S8 and S6 of table 3 respectively. **(a)** z/D_{gas} = 13.4, r/D_{gas}=0; **(b)** z/D_{gas}=23.5; x/D_{gas}=1.68.

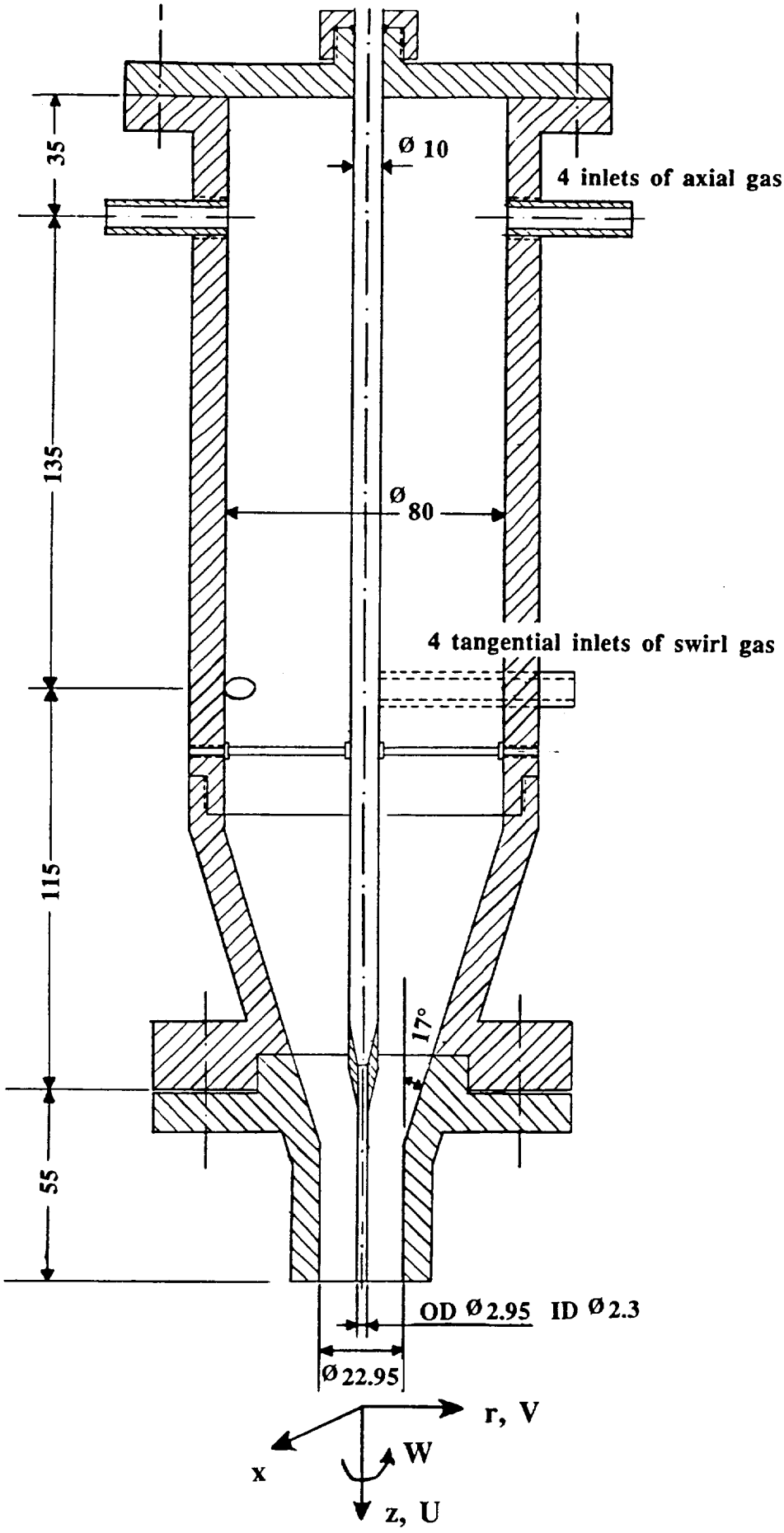

Figure 1. Geometry and main dimensions of the coaxial atomizer used during the experiments.

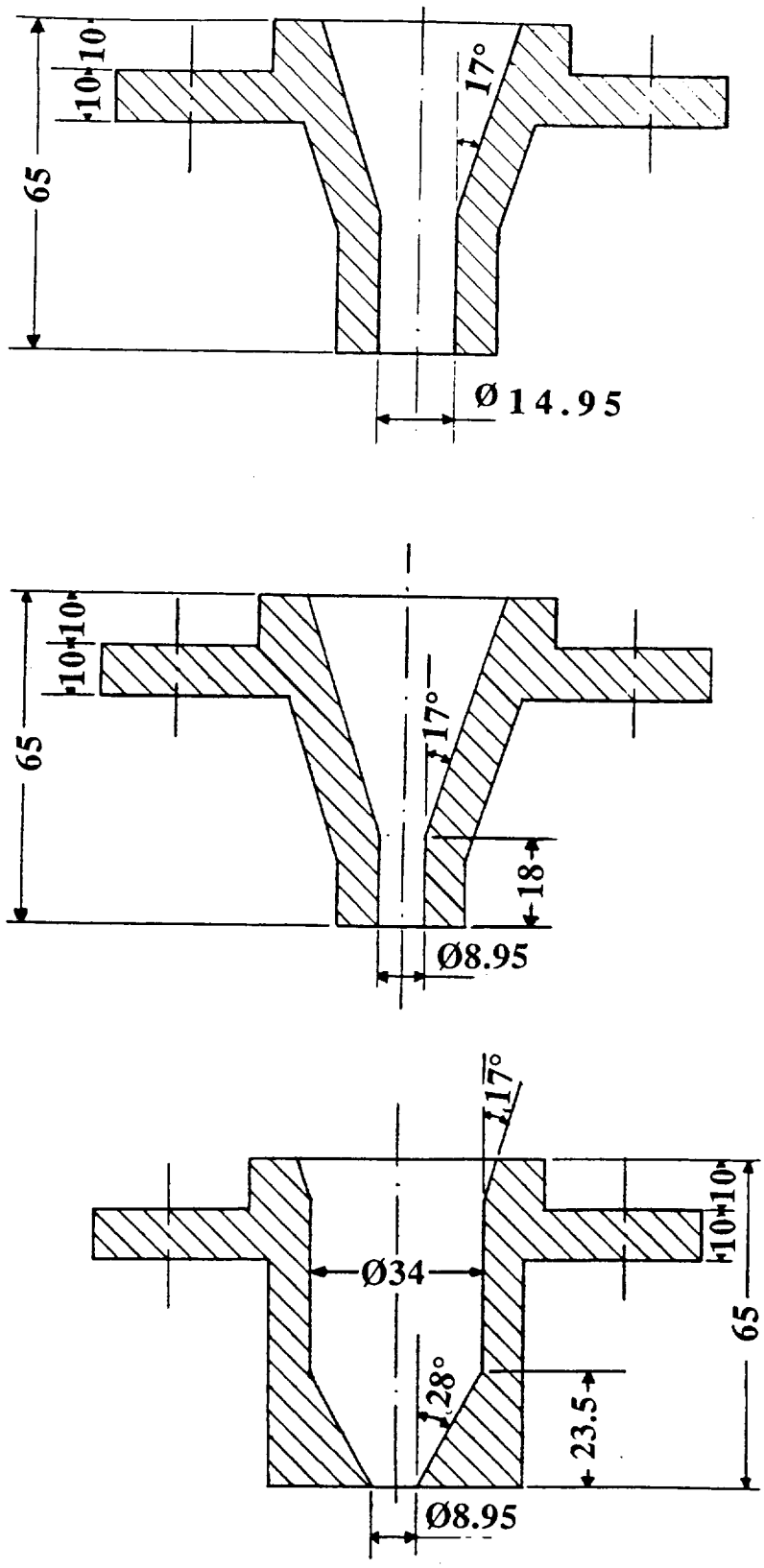

Figure 2a

Figure 2. (a) Nozzle geometries used during the experiments, which could be exchanged at the exit of the injector of figure 1. (b) The geometry of the nozzles when the helical type swirlers were used during the high swirl number experiments.

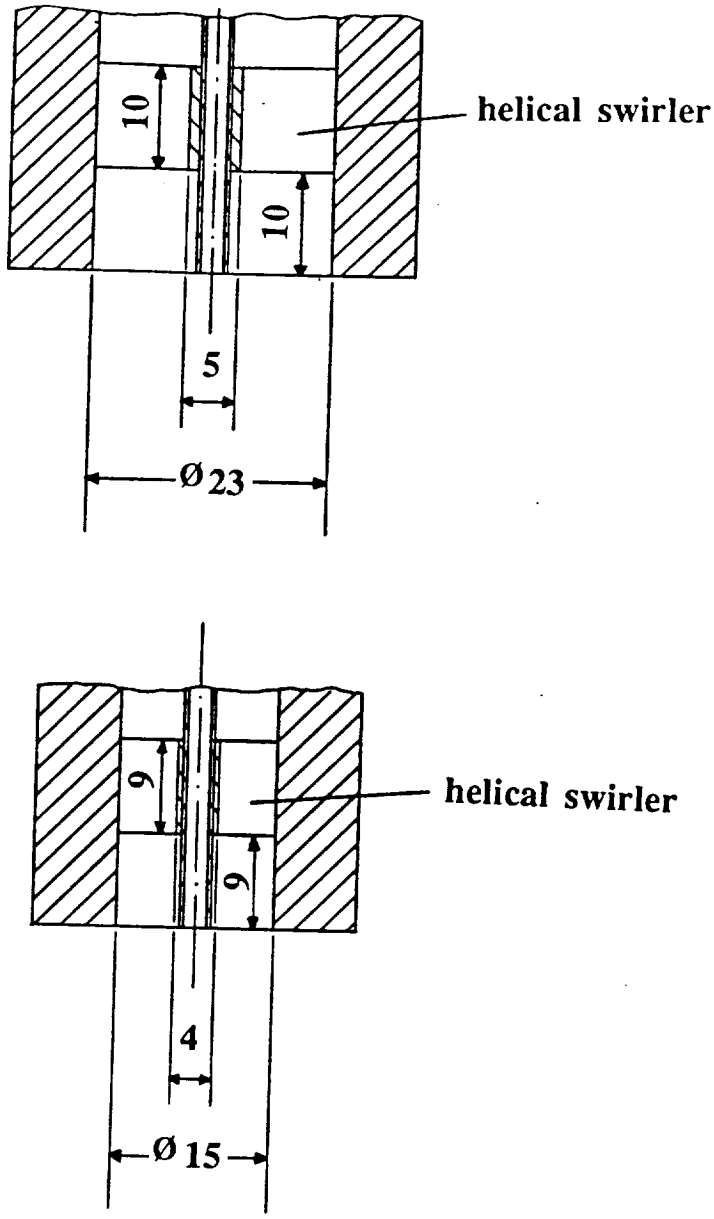
helical swirler
10
10
5
Ø23
helical swirler
9
9
4
Ø15
6
helical swirler
3
3.5
Ø9

Figure 2b

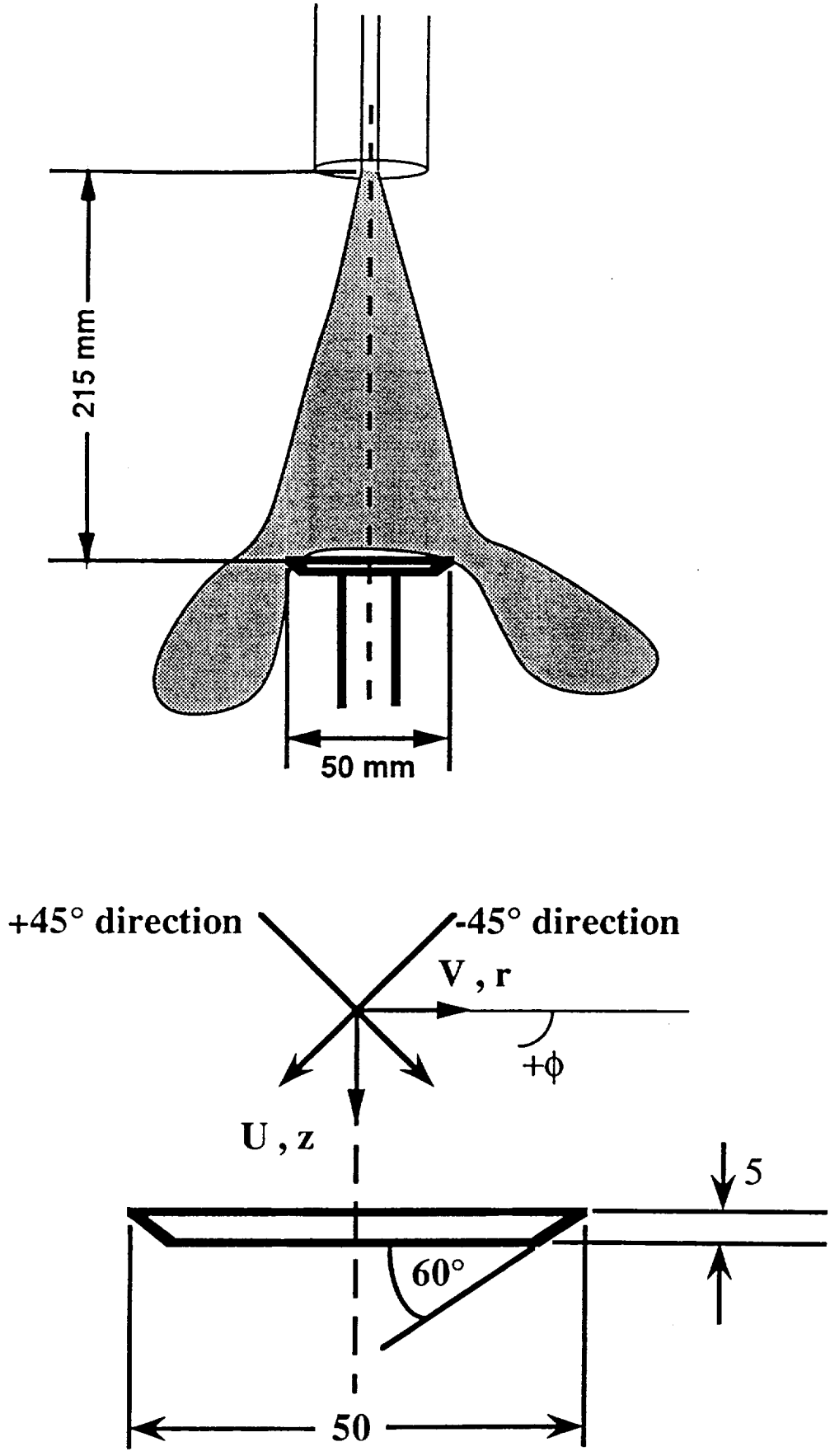

Figure 3. Experimental setup and coordinate system for the spray impingement on a flat disc.

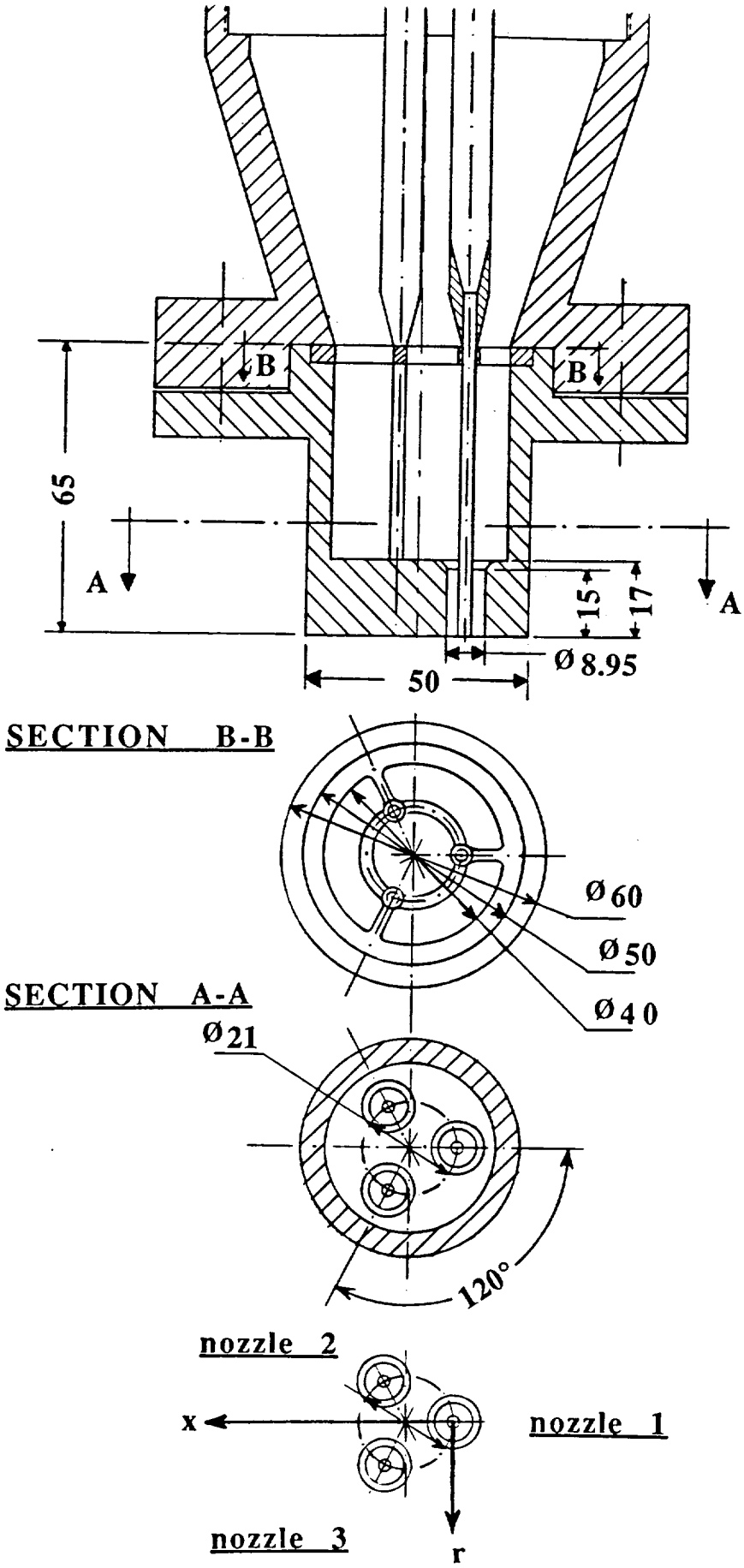

Figure 4. Geometry of the three identical nozzles and the coordinate system used for the study of the spray interaction with and without swirling gaseous stream.

Figure 5. Characteristics of sprays produced by axial gaseous stream nozzles with 10 mm annulus. Radial profiles at axial distances from the nozzle of z/D_{liquid} = 26, 52, 91 and 130. Conditions according to case 1 of table 1a. **(a)** Arithmetic, Sauter and Median diameter; **(b)** Liquid flux normalised by the centreline value at each position, G_m; **(c)** Mean axial velocity of 9, 50 and 105 μm droplets; **(d)** Rms of the fluctuations of the axial velocity of the 9, 50 and 105 μm droplets.

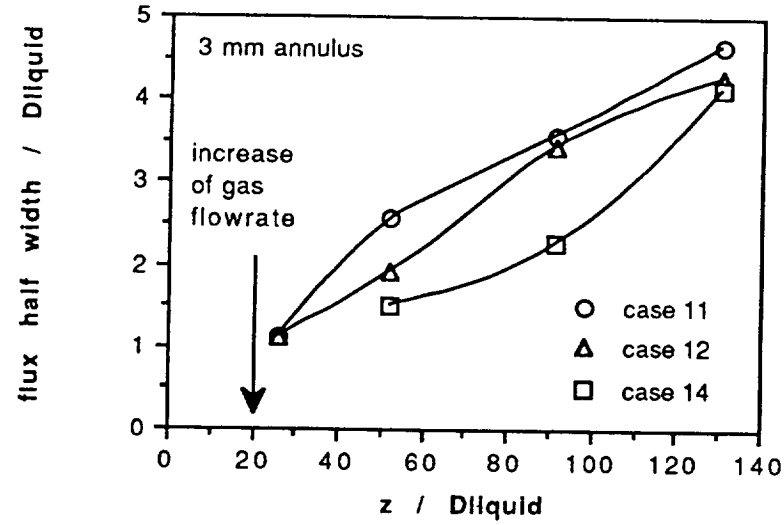
3 mm annulus
increase
of gas
flowrate
case 11
case 12
case 14
flux half width / Dliquid
z / Dliquid
0
1
2
3
4
5
0
20
40
60
80
100
120
140

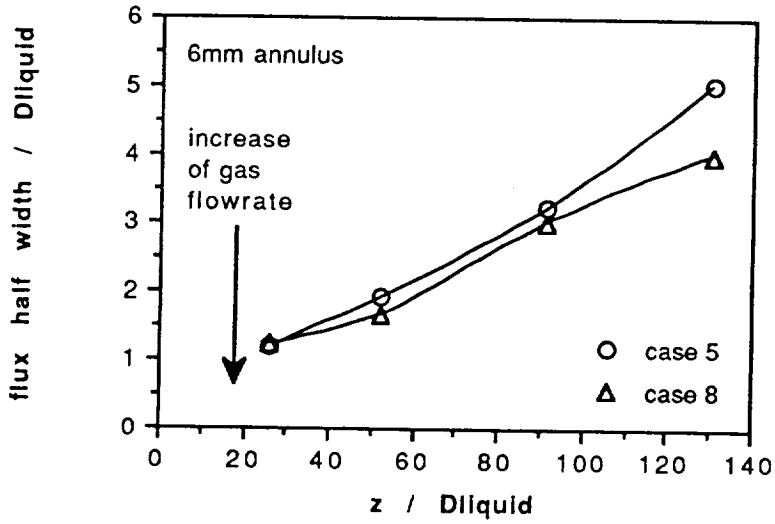
6mm annulus
increase
of gas
flowrate
case 5
case 8
flux half width / Dliquid
z / Dliquid
0
1
2
3
4
5
6
0
20
40
60
80
100
120
140

Figure 6b

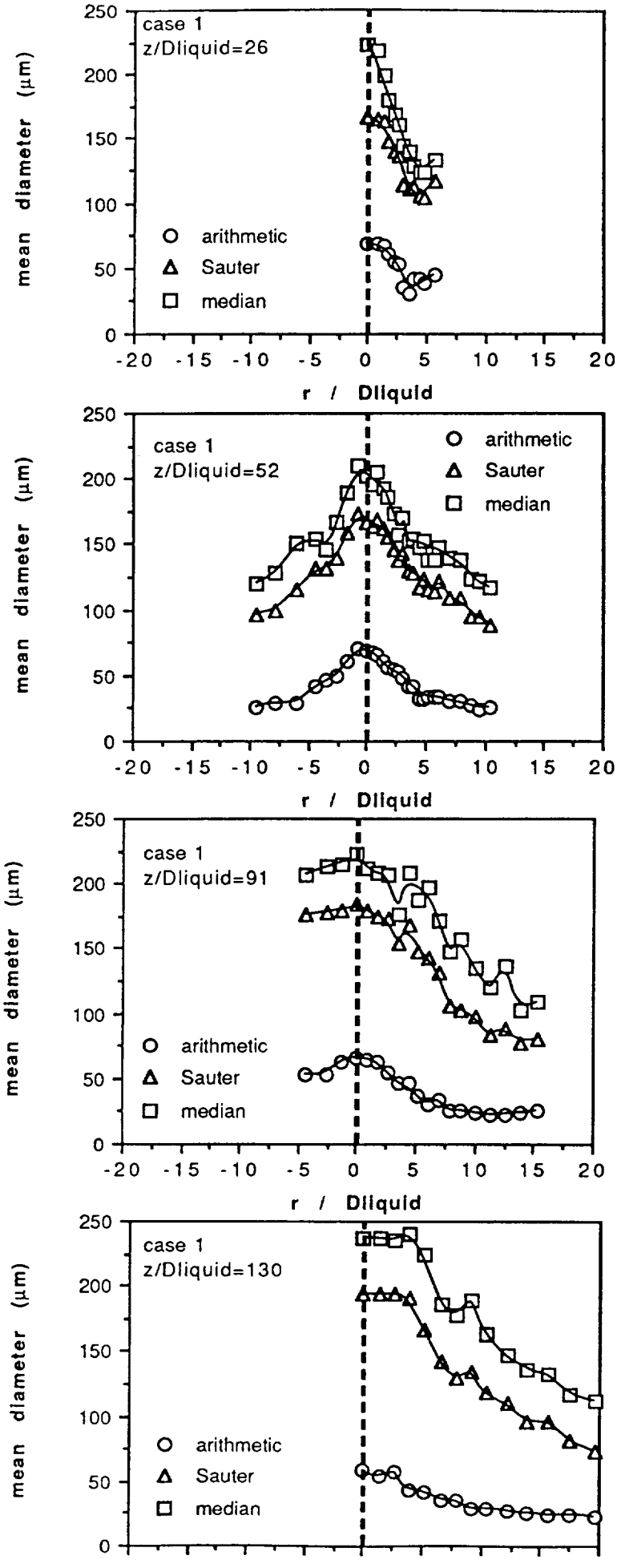
case 1
z/Dliquid=26
arithmetic
Sauter
median
mean diameter (μm)
r / Dliquid
case 1
z/Dliquid=52
case 1
z/Dliquid=91
case 1
z/Dliquid=130

Figure 5a

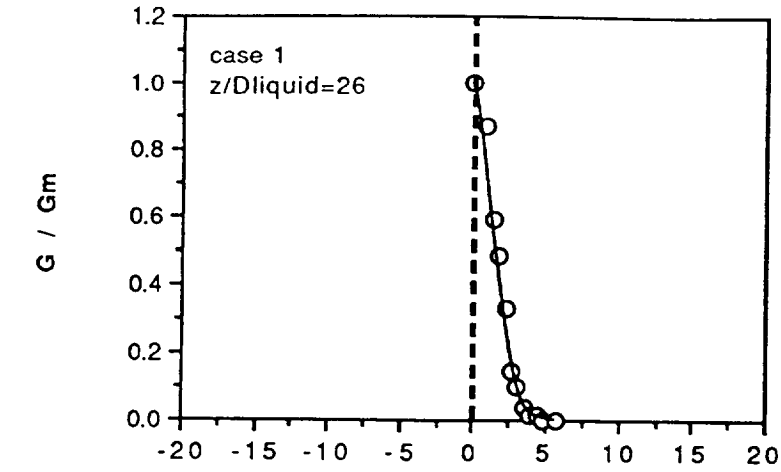
case 1
z/Dliquid=26
G / Gm
r / Dliquid

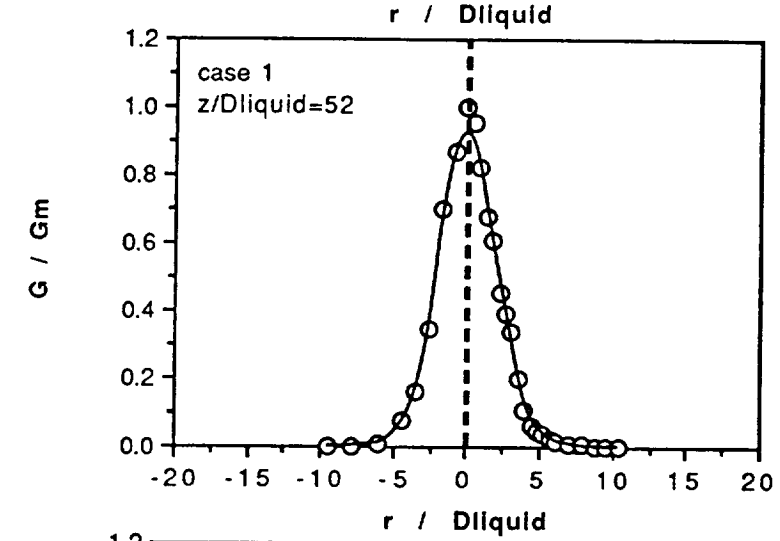
case 1
z/Dliquid=52
G / Gm
r / Dliquid

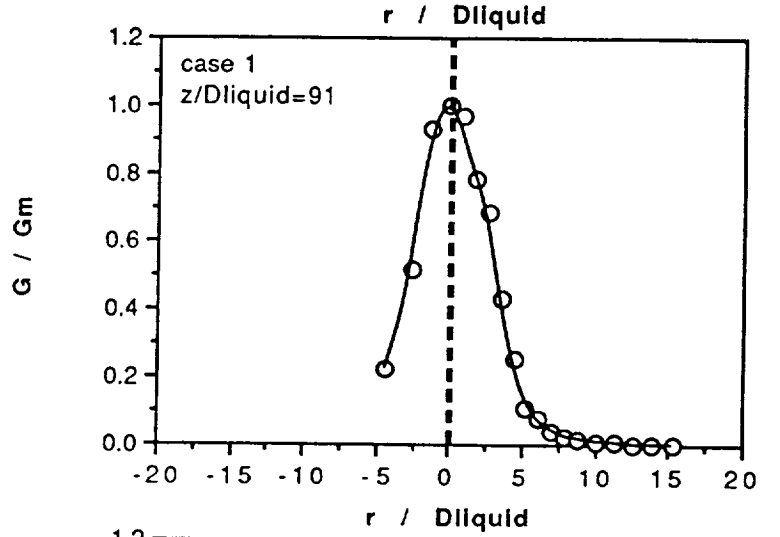
case 1
z/Dliquid=91
G / Gm
r / Dliquid

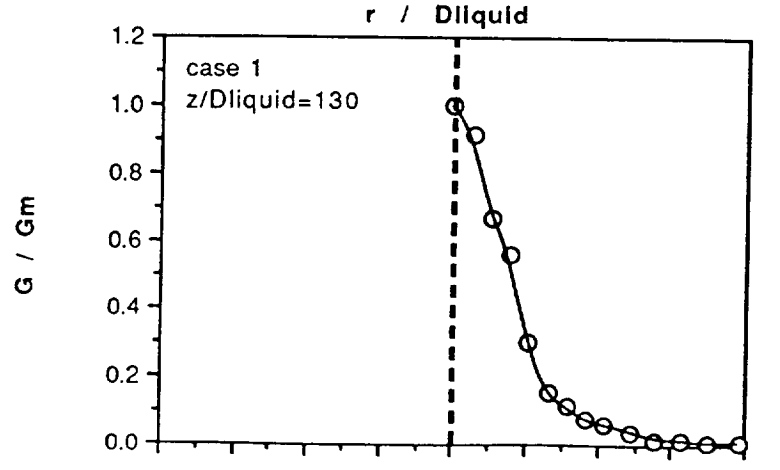
case 1
z/Dliquid=130
G / Gm

Figure 5b

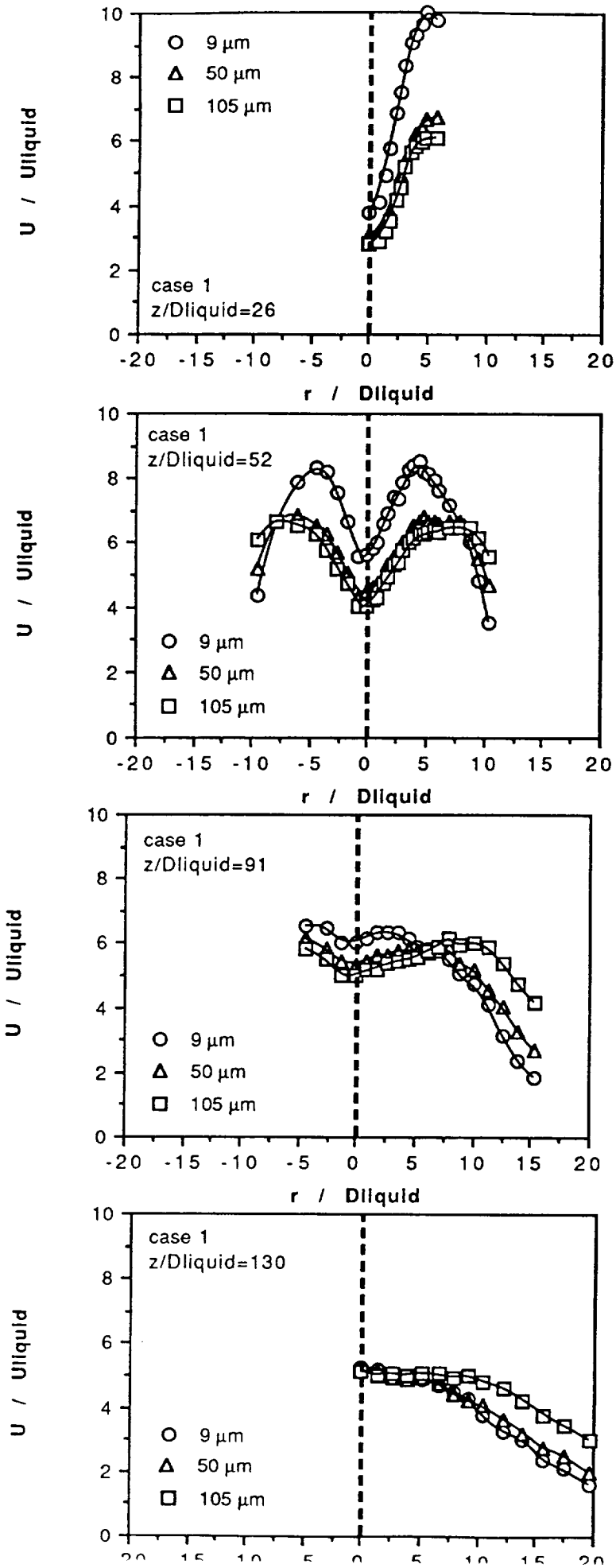
U / Uliquid
r / Dliquid
9 µm
50 µm
105 µm
case 1
z/Dliquid=26
case 1
z/Dliquid=52
case 1
z/Dliquid=91
case 1
z/Dliquid=130

Figure 5c

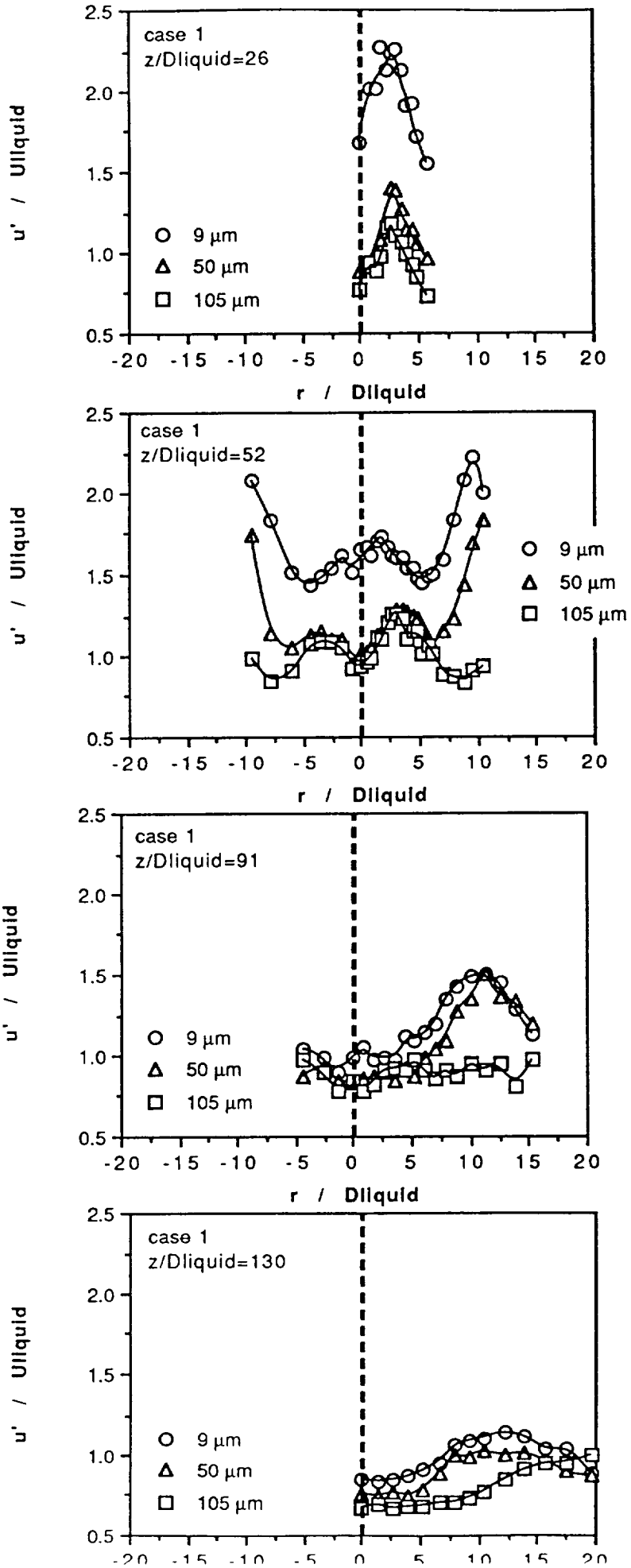
case 1
z/Dliquid=26
9 µm
50 µm
105 µm
u' / Ulquid
r / Dlquid
case 1
z/Dliquid=52
case 1
z/Dliquid=91
case 1
z/Dliquid=130

Figure 5d

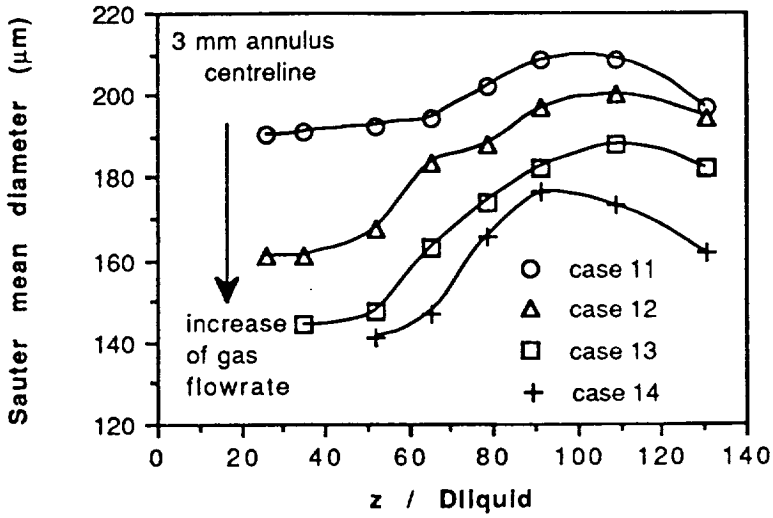

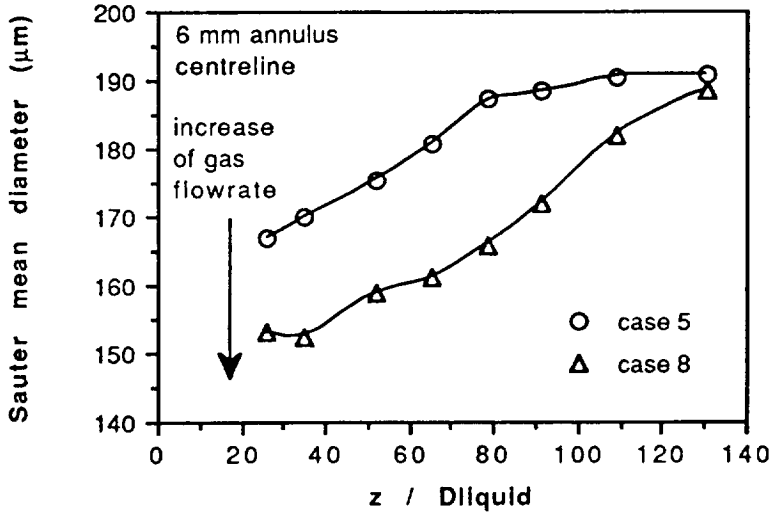

Figure 6a

Figure 6. Effect of the gas flowrate on the characteristics of sprays produced by nozzles with 3 and 6 mm annular widths. (a) Centreline development of the Sauter mean diameter; (b) Flux half width.

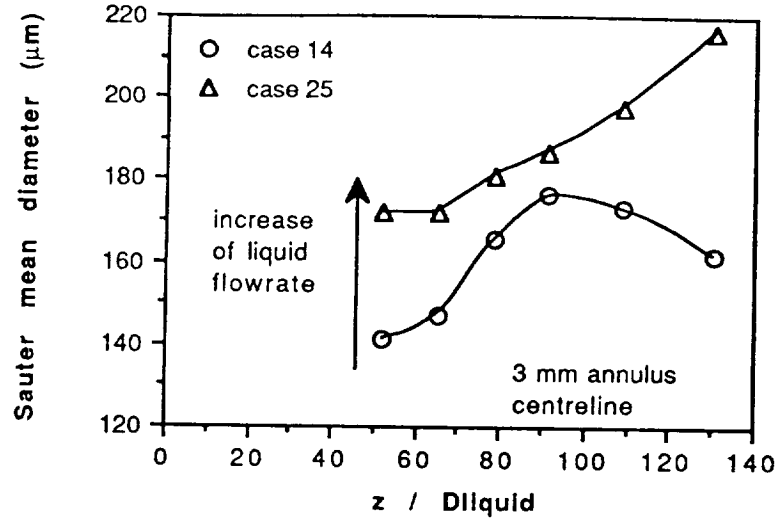

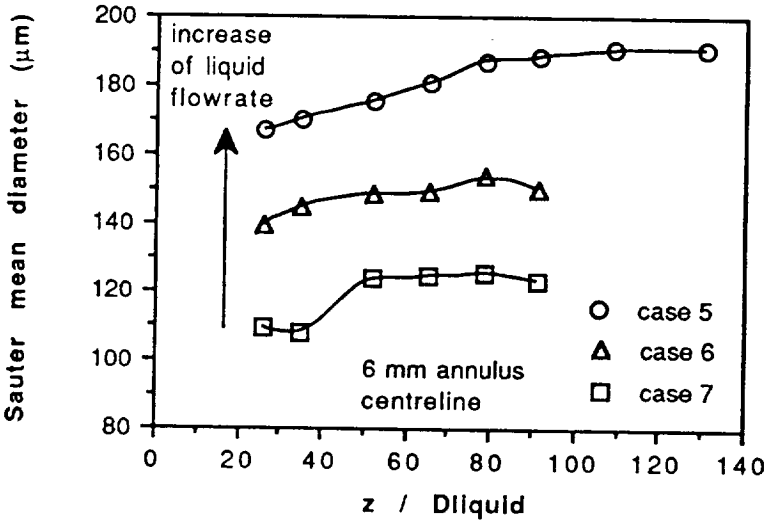

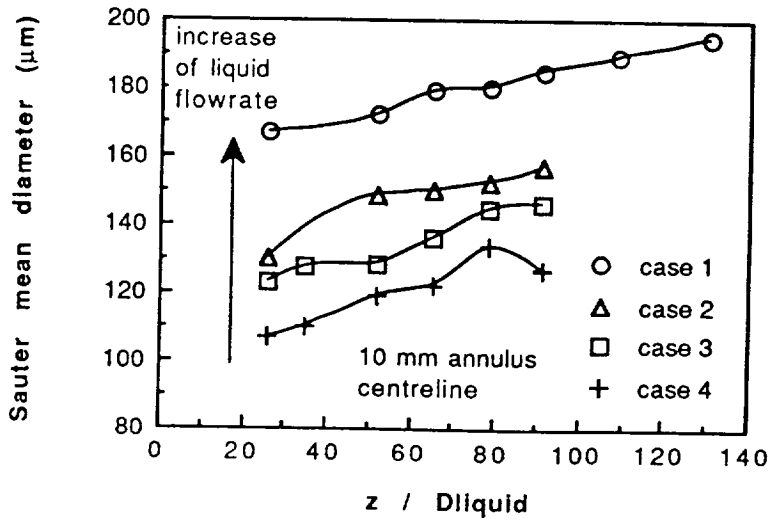

Figure 7a

Figure 7. Effect of liquid flowrate on the characteristics of sprays produced by nozzles with 3, 6 and 10 mm annular widths. (a) Centreline development of the Sauter mean diameter; (b) Flux half width.

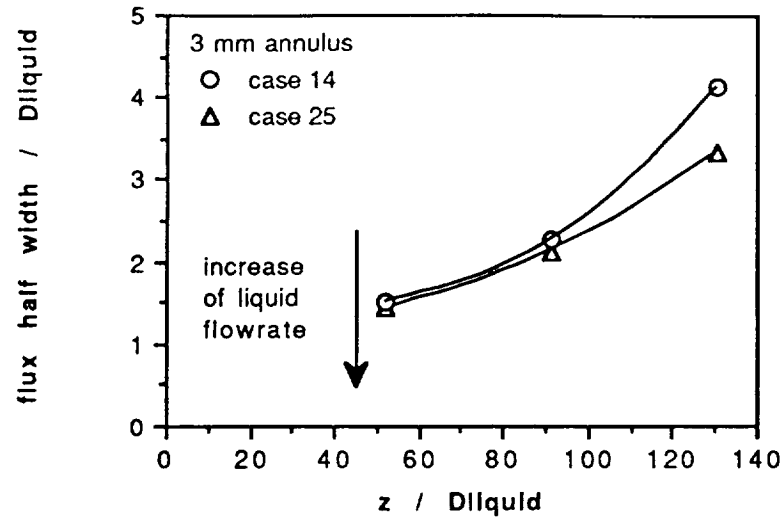
3 mm annulus
case 14
case 25
increase
of liquid
flowrate
flux half width / Dliquid
z / Dliquid
0
1
2
3
4
5
0
20
40
60
80
100
120
140

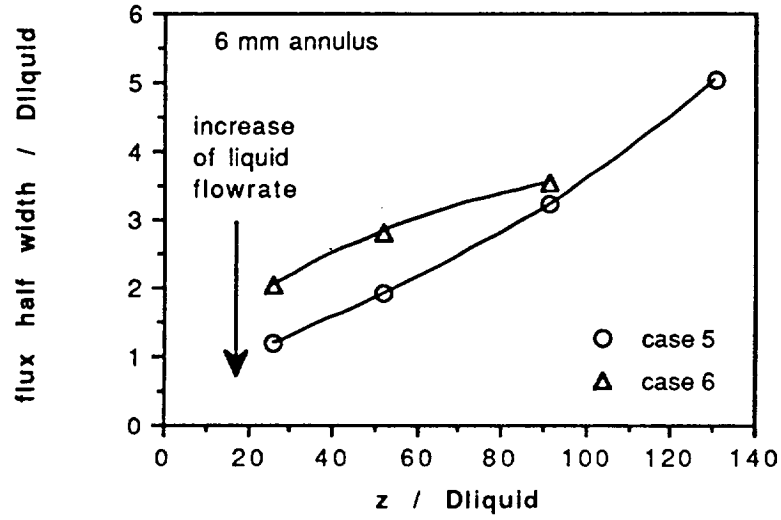
6 mm annulus
increase
of liquid
flowrate
case 5
case 6
flux half width / Dliquid
z / Dliquid
0
1
2
3
4
5
6
0
20
40
60
80
100
120
140

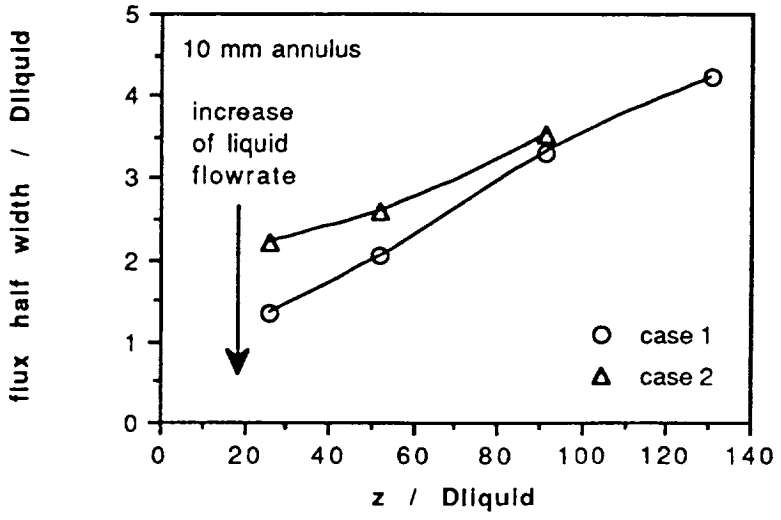
10 mm annulus
increase
of liquid
flowrate
case 1
case 2
flux half width / Dliquid
z / Dliquid
0
1
2
3
4
5
0
20
40
60
80
100
120
140

Figure 7b

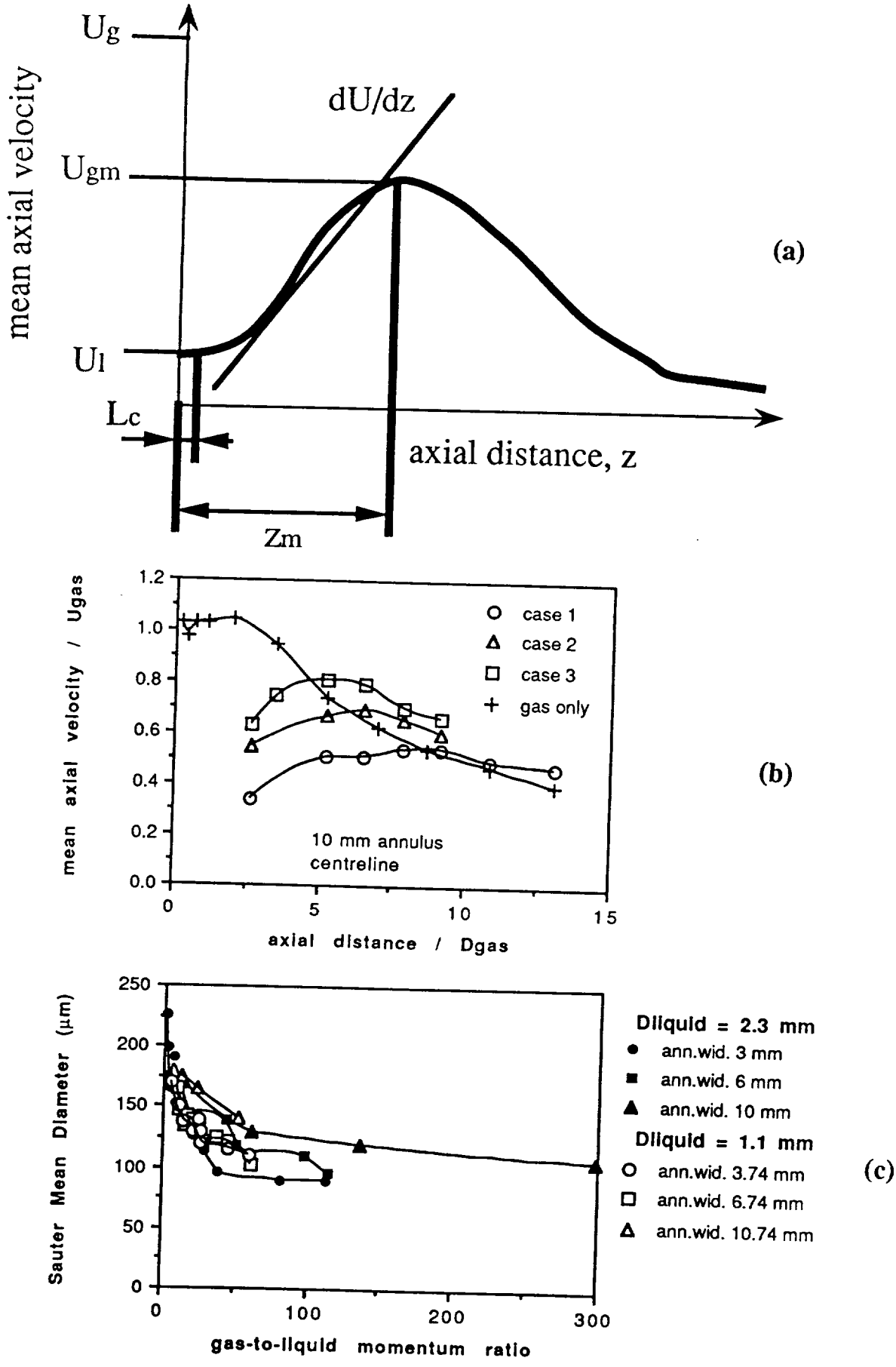

Figure 8. (a) Drawing showing the parameters used to explain the secondary breakup mechanism of the droplets in the coaxial atomizers. (b) Centreline development of the gaseous phase mean axial velocity in the sprays produced by a 10 mm annulus nozzles. (c) Correlation between the measured Sauter Mean diameter and the gas-to-liquid momentum ratio for the sprays produced by nozzles with straight exit and axial gaseous stream, which are summarised in tables 1 and 5.

Figure 9. Characteristics of sprays produced by low swirl number gaseous stream nozzles with 10 mm annulus. Radial profiles at axial distances from the nozzle of $z/D_{liquid} = 26$, 52 and 91. Conditions according to case S1 of table 2. (a) Sauter and Median diameter; (b) Liquid flux normalised by the centreline value at each position, G_m; (c) Mean axial velocity of 9, 50 and 105 μm droplets; (d) Mean radial velocity; (e) Mean tangential velocity; (f) Rms of the fluctuations of the axial velocity of the 9, 50 and 105 μm droplets; (g) Rms of the fluctuations of the radial velocity; (h) Rms of the fluctuations of the tangential velocity; (i) Correlation coefficient $\overline{uv}/u'v'$ of 9, 50 and 105 μm droplets; (j) Correlation coefficient $\overline{uw}/u'w'$.

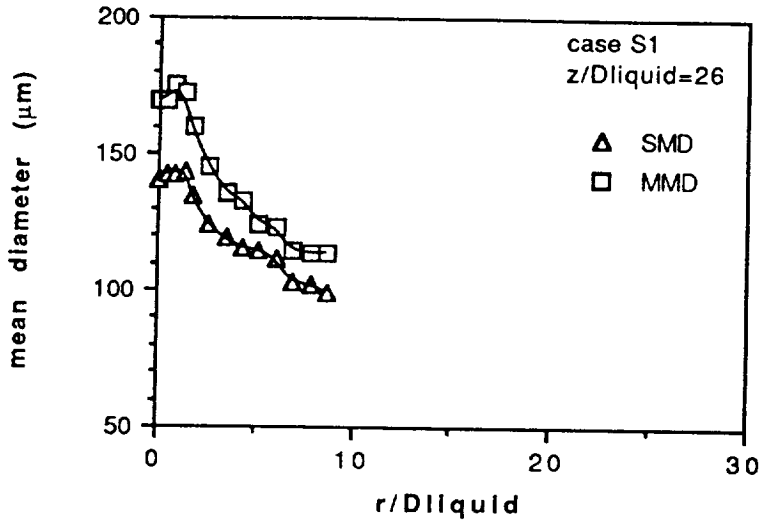
case S1
z/Dliquid=26
SMD
MMD
mean diameter (μm)
200
150
100
50
0
10
20
30
r/Dliquid

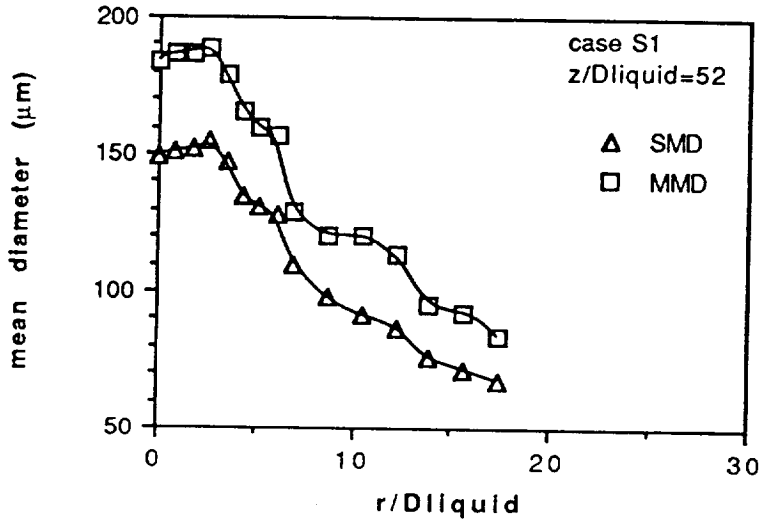
case S1
z/Dliquid=52
SMD
MMD
mean diameter (μm)
200
150
100
50
0
10
20
30
r/Dliquid

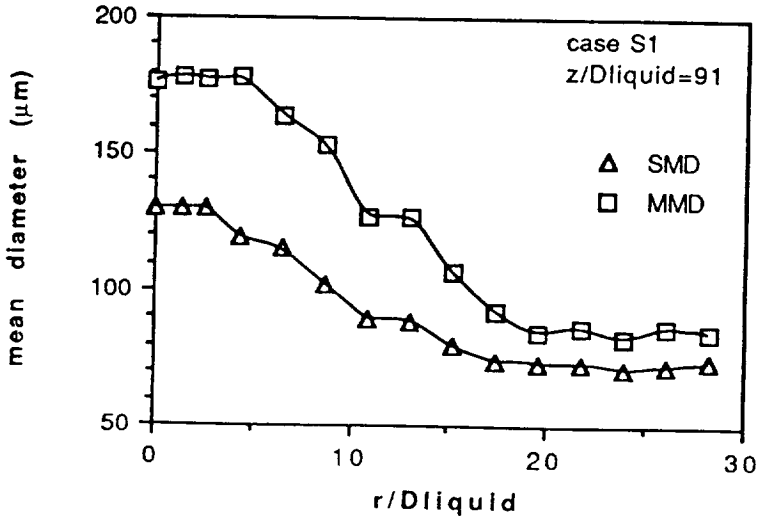
case S1
z/Dliquid=91
SMD
MMD
mean diameter (μm)
200
150
100
50
0
10
20
30
r/Dliquid

Figure 9a

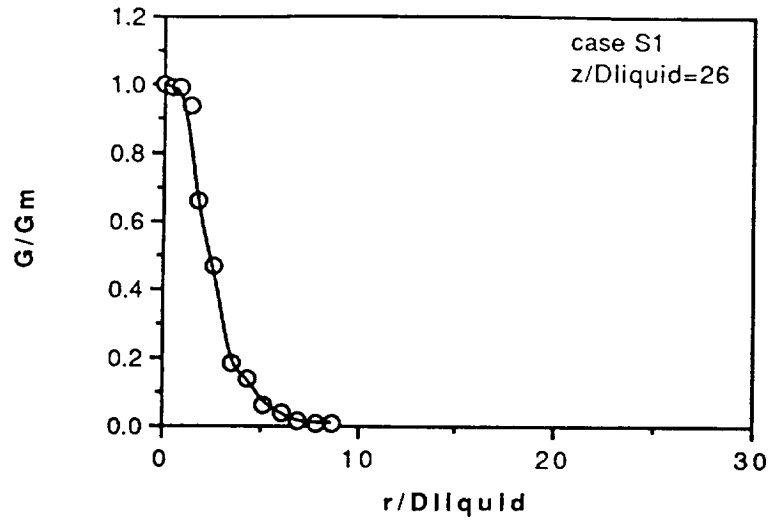
case S1
z/Dliquid=26
G/Gm
r/Dliquid
1.2
1.0
0.8
0.6
0.4
0.2
0.0
0
10
20
30

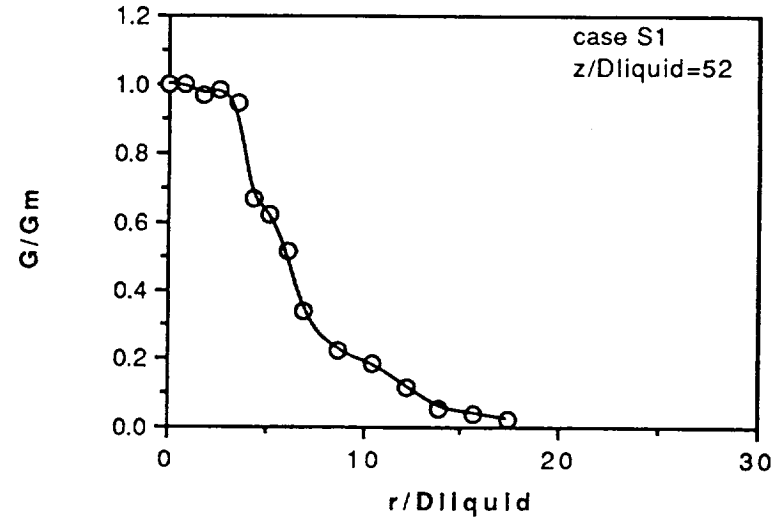
case S1
z/Dliquid=52
G/Gm
r/Dliquid
1.2
1.0
0.8
0.6
0.4
0.2
0.0
0
10
20
30

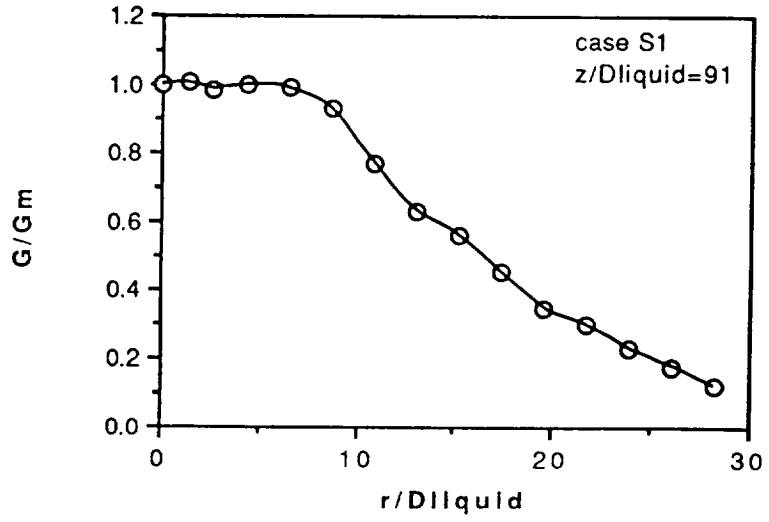
case S1
z/Dliquid=91
G/Gm
r/Dliquid
1.2
1.0
0.8
0.6
0.4
0.2
0.0
0
10
20
30

Figure 9b

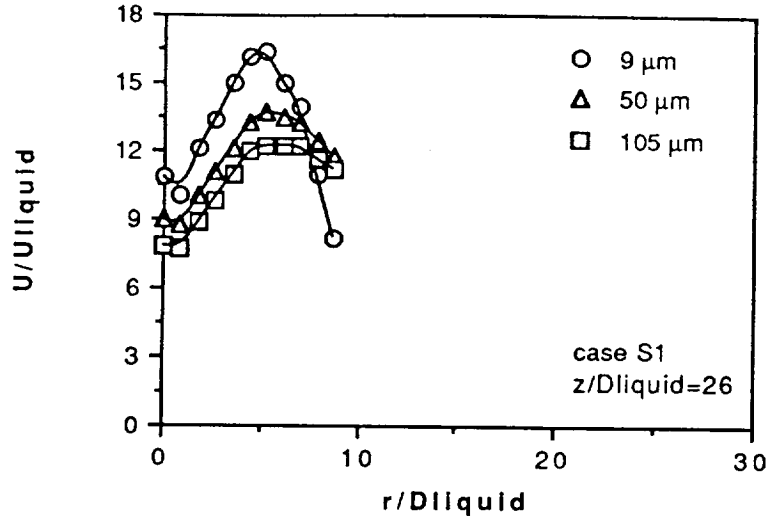
18
15
12
9
6
3
0
U/Ulquid
0
10
20
30
r/Dliquid
9 µm
50 µm
105 µm
case S1
z/Dliquid=26

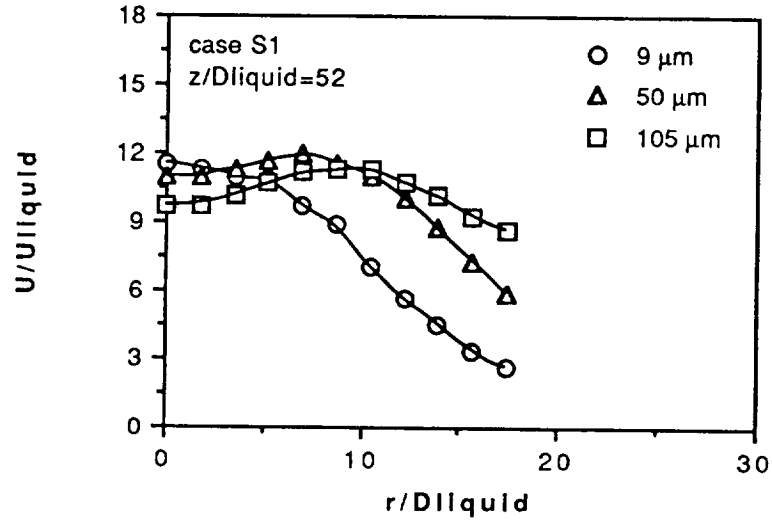
18
15
12
9
6
3
0
U/Ulquid
0
10
20
30
r/Dliquid
case S1
z/Dliquid=52
9 µm
50 µm
105 µm

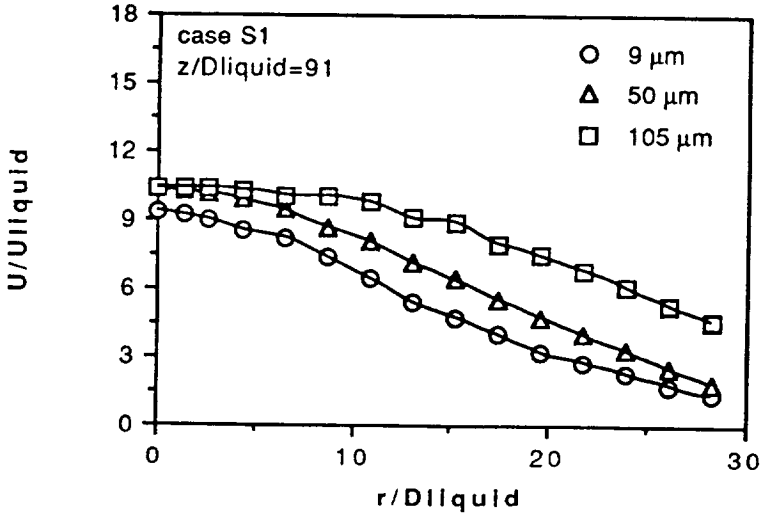
18
15
12
9
6
3
0
U/Ulquid
0
10
20
30
r/Dliquid
case S1
z/Dliquid=91
9 µm
50 µm
105 µm

Figure 9c

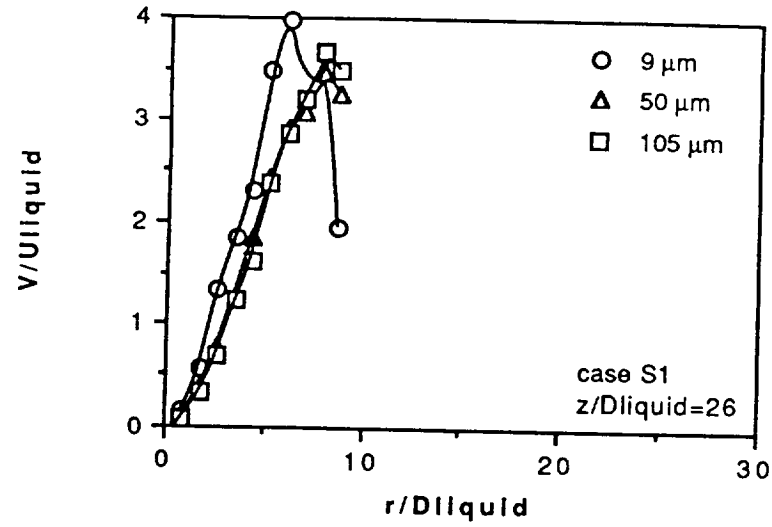
V/Ulliquid
r/Dliquid
9 µm
50 µm
105 µm
case S1
z/Dliquid=26

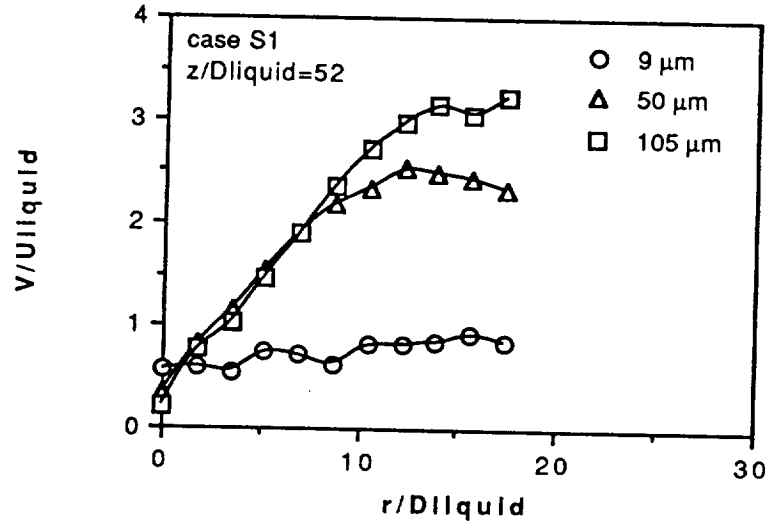
V/Ulliquid
r/Dliquid
case S1
z/Dliquid=52
9 µm
50 µm
105 µm

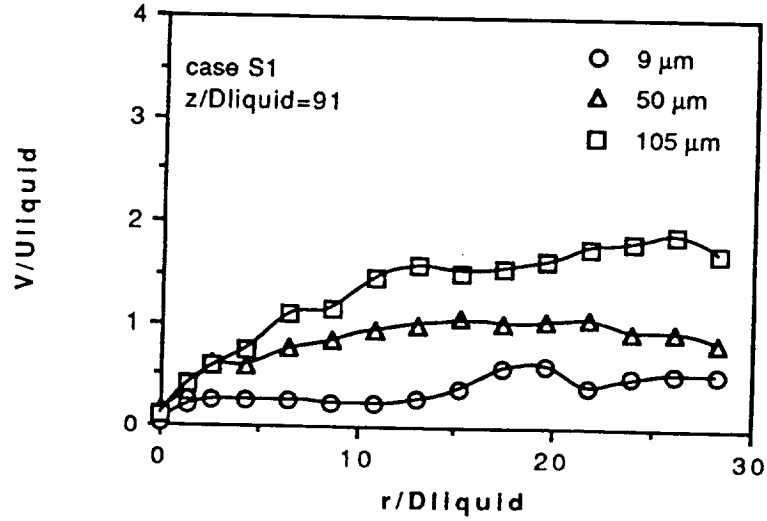
V/Ulliquid
r/Dliquid
case S1
z/Dliquid=91
9 µm
50 µm
105 µm

Figure 9d

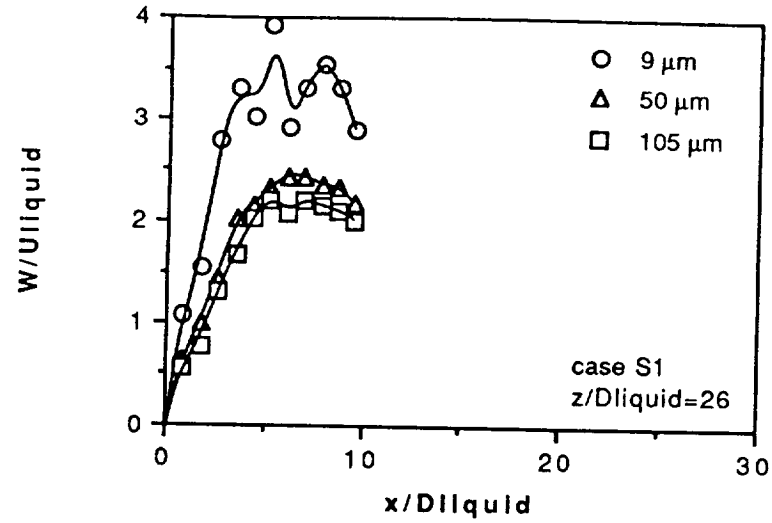
W/Ulliquid
x/Dliquid
9 µm
50 µm
105 µm
case S1
z/Dliquid=26

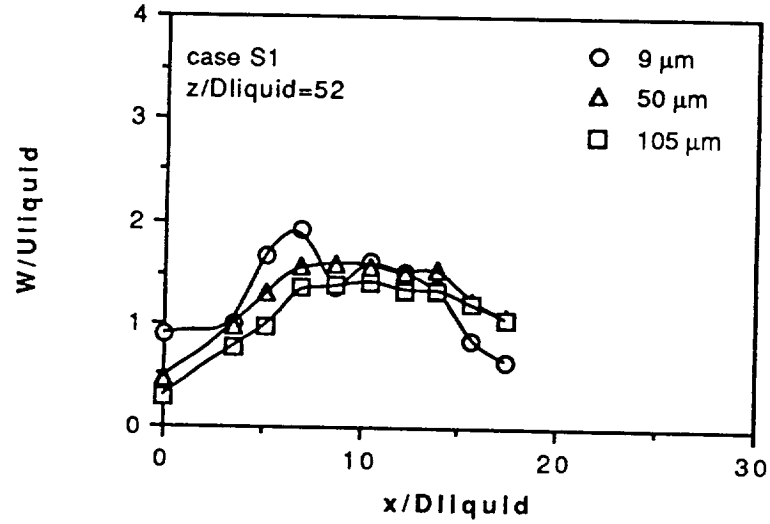
W/Ulliquid
x/Dliquid
case S1
z/Dliquid=52
9 µm
50 µm
105 µm

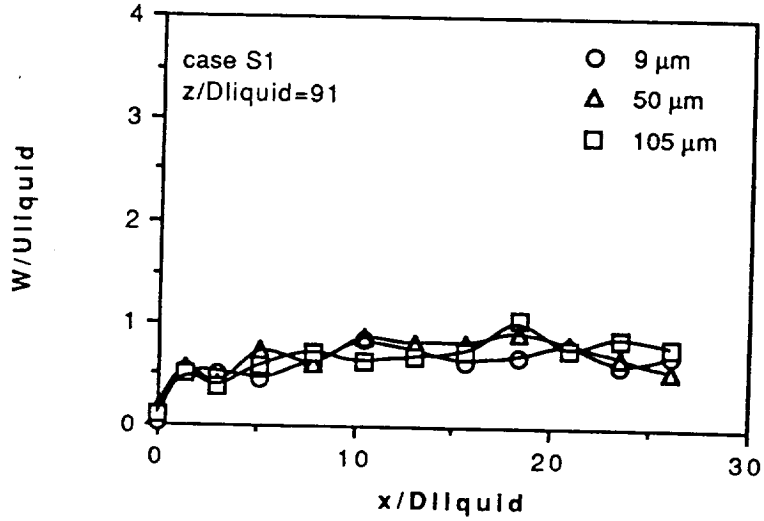
W/Ulliquid
x/Dliquid
case S1
z/Dliquid=91
9 µm
50 µm
105 µm

Figure 9e

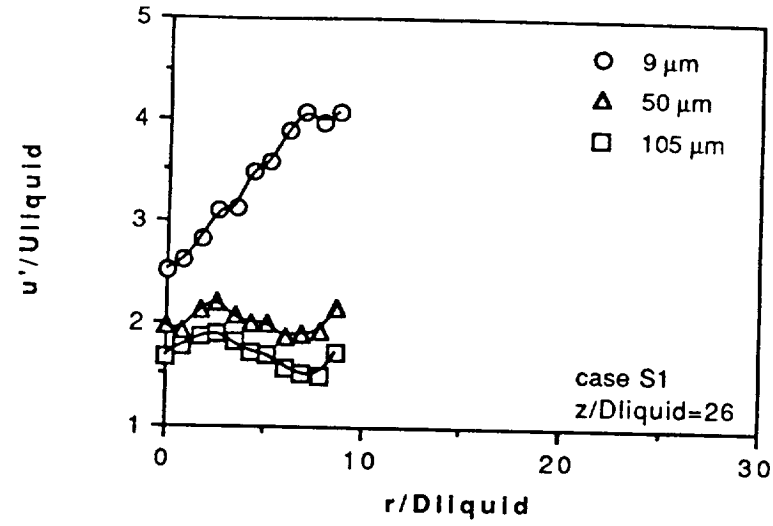
u'/Ulquid
r/Dliquid
9 µm
50 µm
105 µm
case S1
z/Dliquid=26

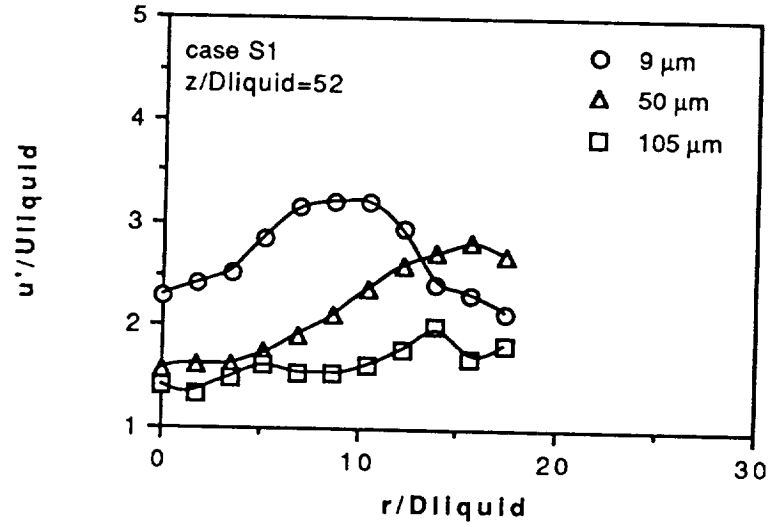
u'/Ulquid
r/Dliquid
case S1
z/Dliquid=52
9 µm
50 µm
105 µm

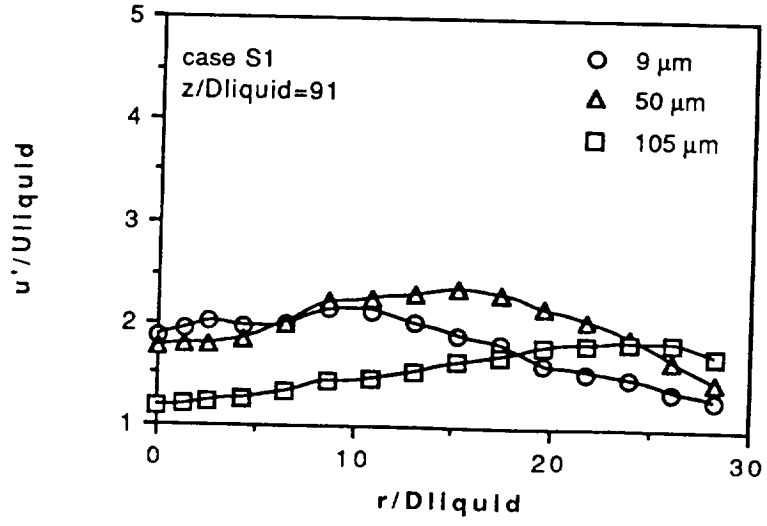
u'/Ulquid
r/Dliquid
case S1
z/Dliquid=91
9 µm
50 µm
105 µm

Figure 9f

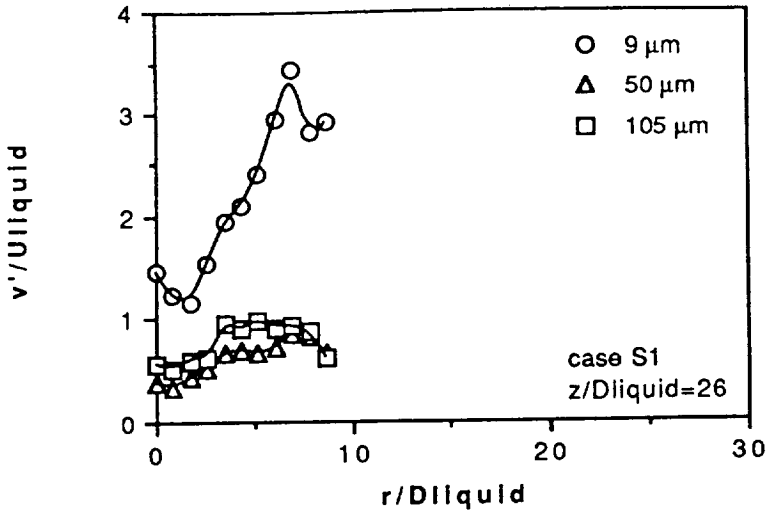
v'/Ulquid
r/Dliquid
9 µm
50 µm
105 µm
case S1
z/Dliquid=26

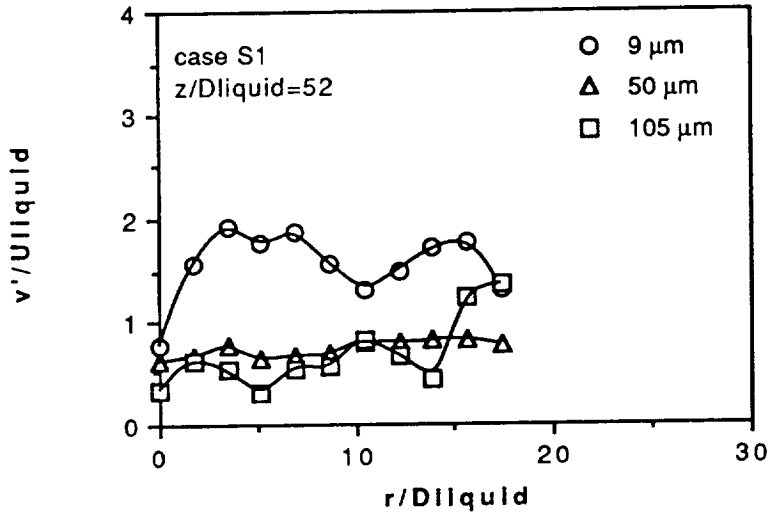
v'/Ulquid
r/Dliquid
case S1
z/Dliquid=52
9 µm
50 µm
105 µm

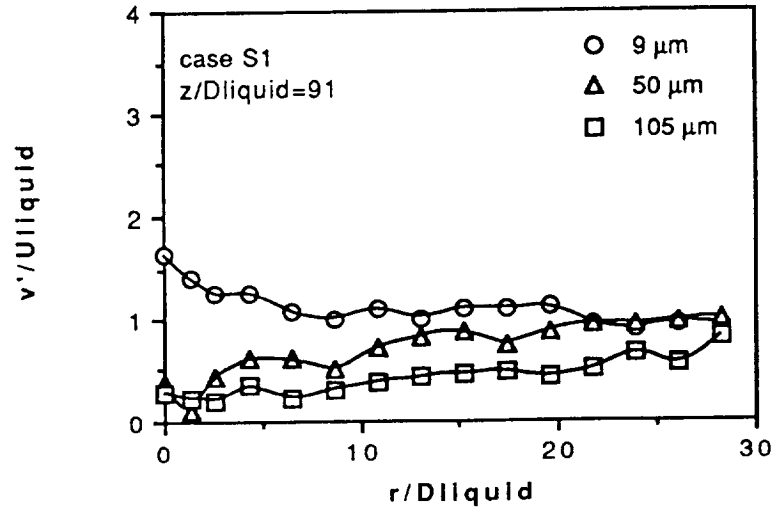
v'/Ulquid
r/Dliquid
case S1
z/Dliquid=91
9 µm
50 µm
105 µm

Figure 9g

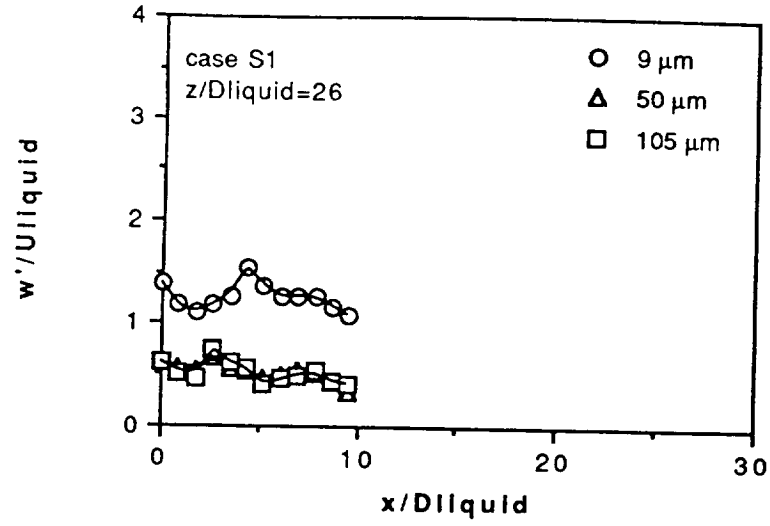
case S1
z/Dliquid=26
9 µm
50 µm
105 µm
w'/Ulquid
x/Dlquid
0
1
2
3
4
0
10
20
30

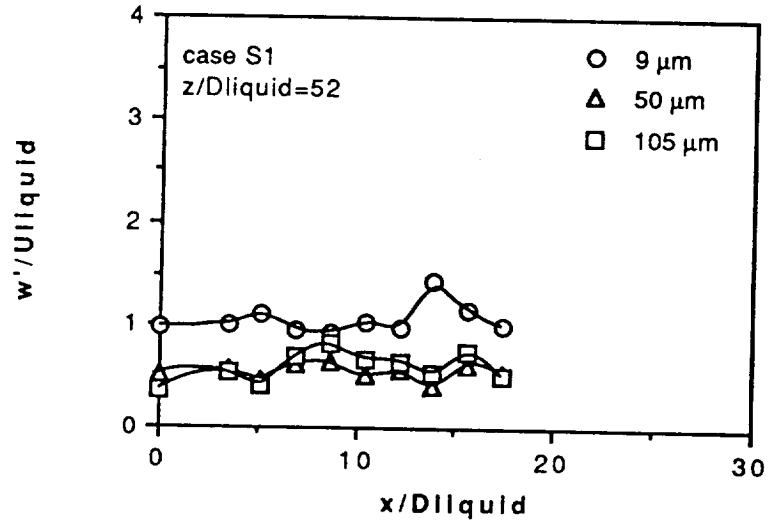
case S1
z/Dliquid=52
9 µm
50 µm
105 µm
w'/Ulquid
x/Dlquid
0
1
2
3
4
0
10
20
30

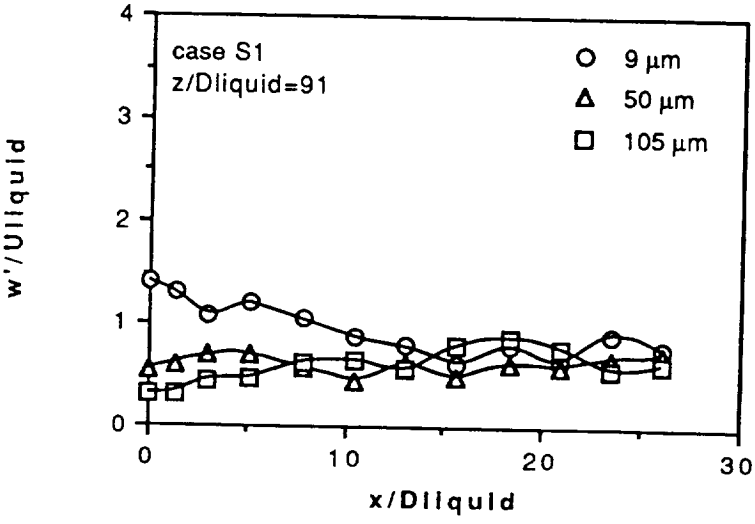
case S1
z/Dliquid=91
9 µm
50 µm
105 µm
w'/Ulquid
x/Dlquid
0
1
2
3
4
0
10
20
30

Figure 9h

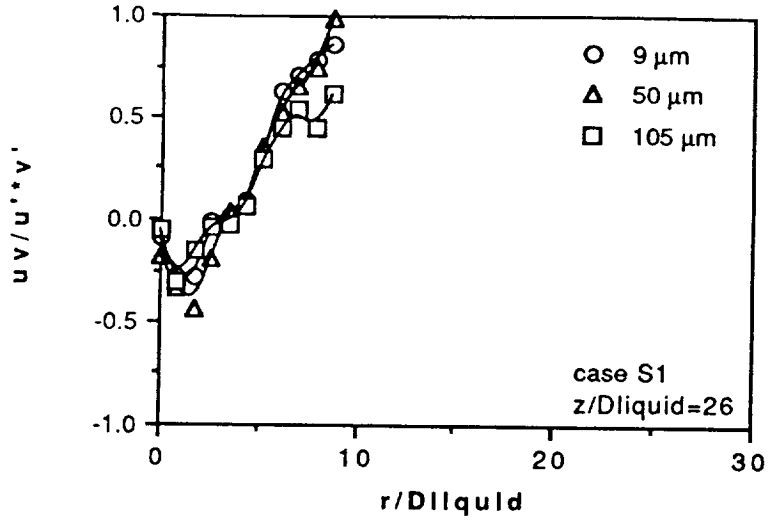
1.0
0.5
0.0
-0.5
-1.0
0
10
20
30
r/Dliquid
uv/u'*v'
9 µm
50 µm
105 µm
case S1
z/Dliquid=26

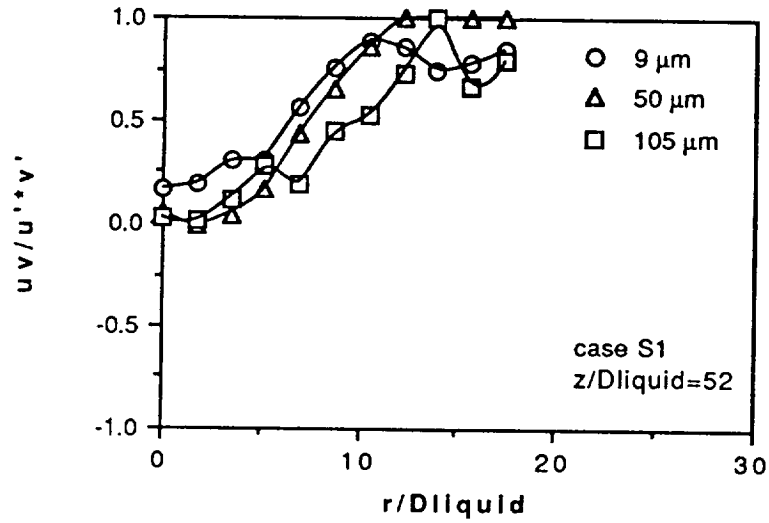
1.0
0.5
0.0
-0.5
-1.0
0
10
20
30
r/Dliquid
uv/u'*v'
9 µm
50 µm
105 µm
case S1
z/Dliquid=52

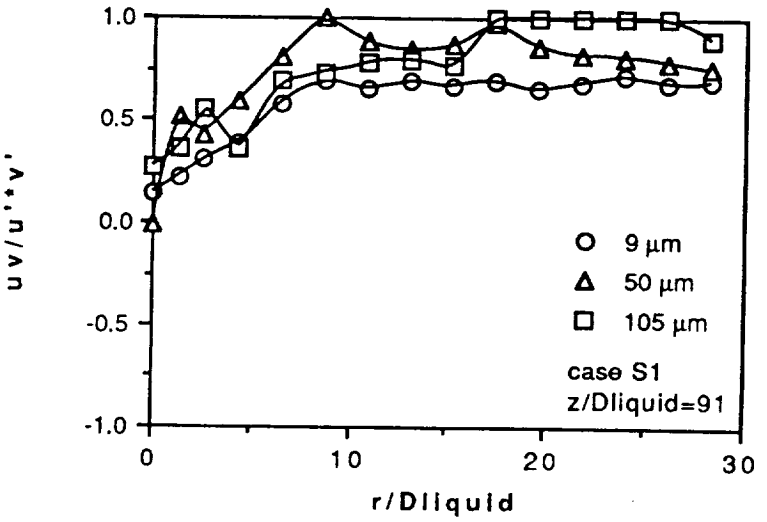
1.0
0.5
0.0
-0.5
-1.0
0
10
20
30
r/Dliquid
uv/u'*v'
9 µm
50 µm
105 µm
case S1
z/Dliquid=91

Figure 9i

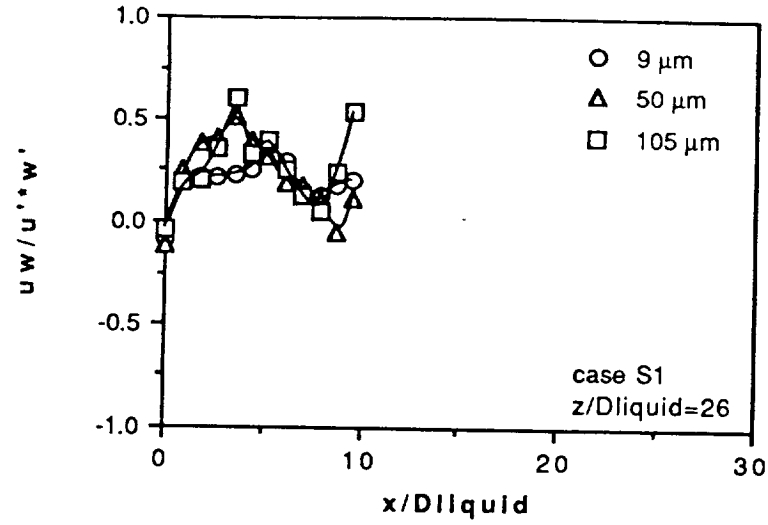
1.0
0.5
0.0
-0.5
-1.0
0
10
20
30
x/Dliquid
u'w'/u*u*
9 µm
50 µm
105 µm
case S1
z/Dliquid=26

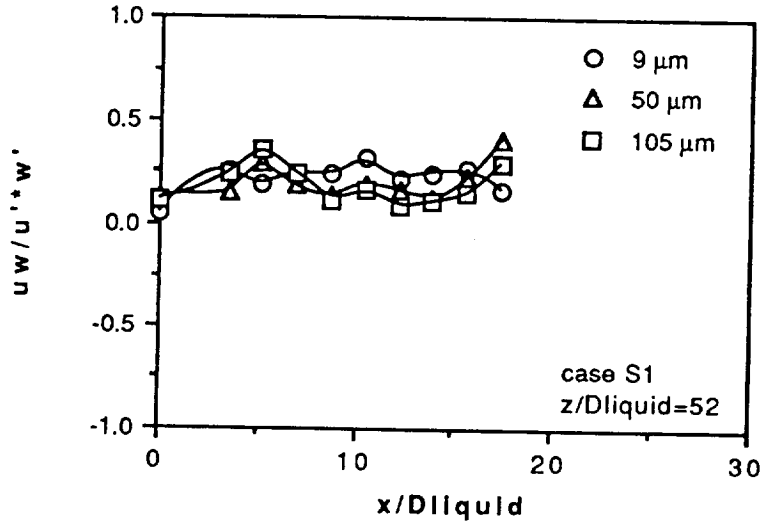
1.0
0.5
0.0
-0.5
-1.0
0
10
20
30
x/Dliquid
u'w'/u*u*
9 µm
50 µm
105 µm
case S1
z/Dliquid=52

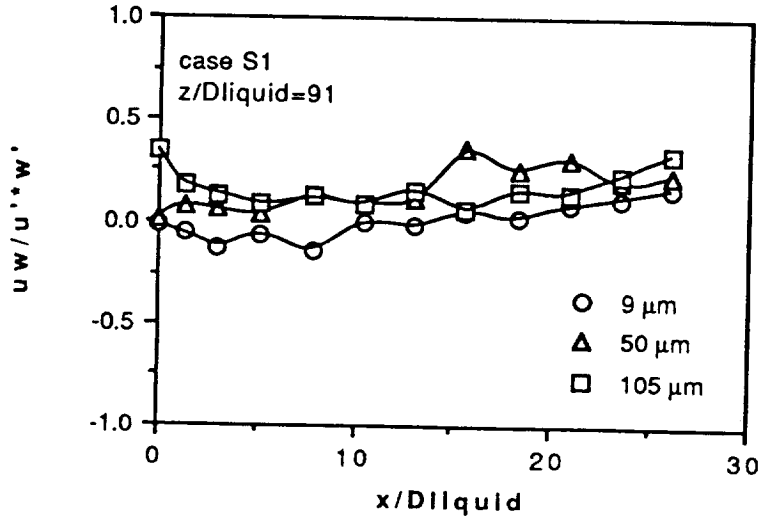
1.0
0.5
0.0
-0.5
-1.0
0
10
20
30
x/Dliquid
u'w'/u*u*
case S1
z/Dliquid=91
9 µm
50 µm
105 µm

Figure 9j

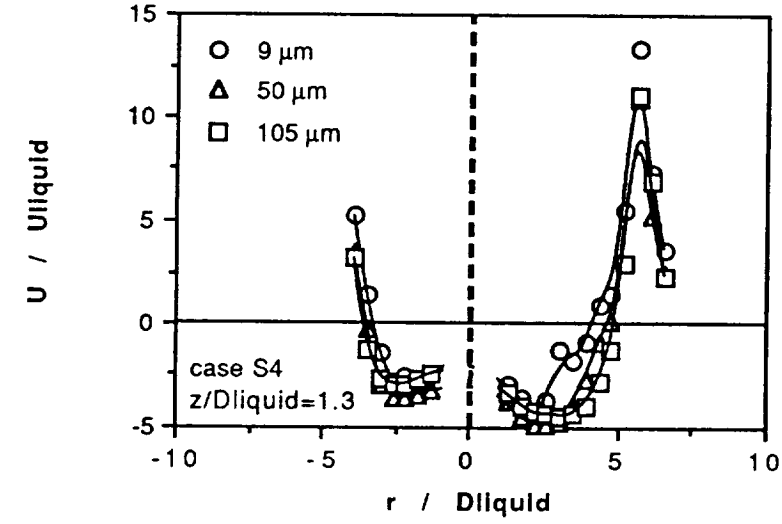

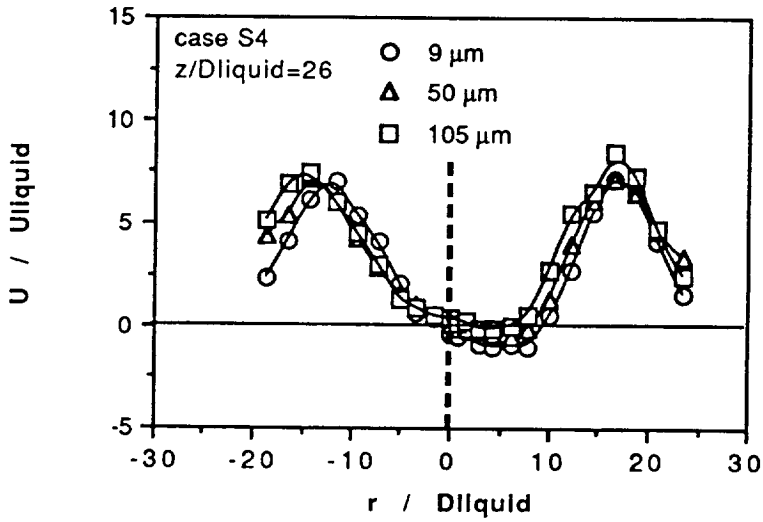

Figure 10a

Figure 10. Characteristics of sprays produced by high swirl number gaseous stream nozzles with 10 mm annulus. Conditions according to case S4 of table 3. Radial profiles of (a) mean axial velocity of 9, 50 and 105 µm droplets at axial distances from the nozzle of z/D_{liquid} = 1.3 and 26 and (b) mean radial and tangential velocity of the 9, 50 and 105 µm droplets at z/D_{liquid} = 1.3.

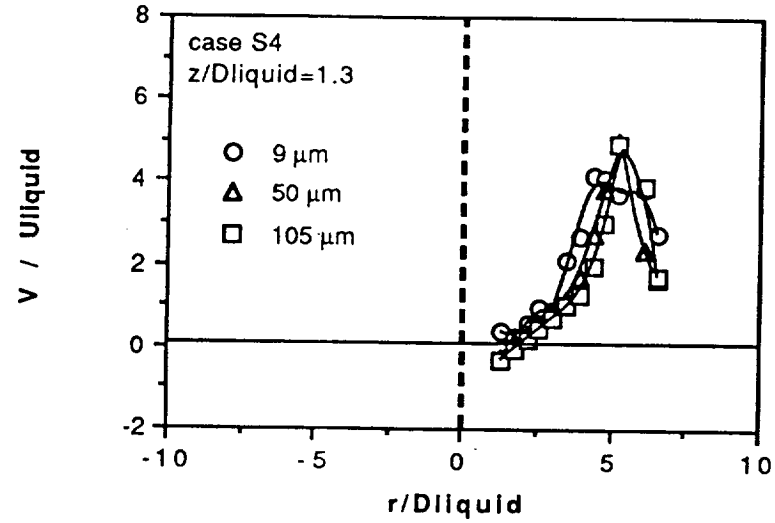
case S4
z/Dliquid=1.3
9 µm
50 µm
105 µm
V / Uliquid
r/Dliquid
8
6
4
2
0
-2
-10
-5
0
5
10

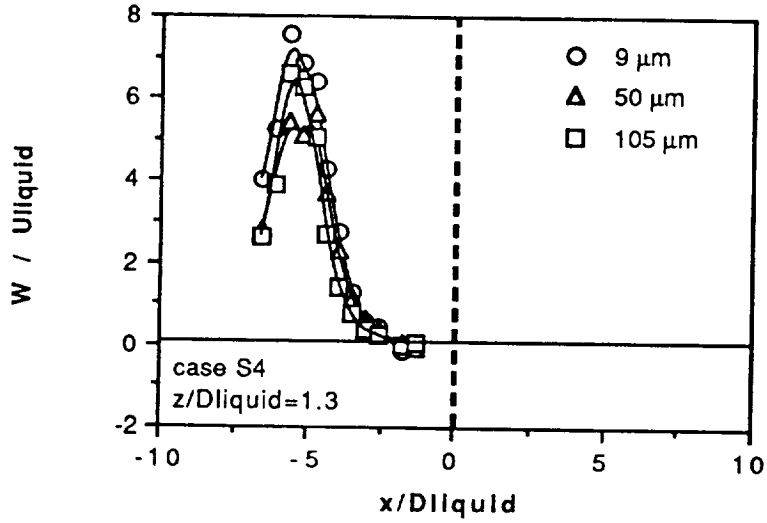
9 µm
50 µm
105 µm
case S4
z/Dliquid=1.3
W / Uliquid
x/Dliquid
8
6
4
2
0
-2
-10
-5
0
5
10

Figure 10b

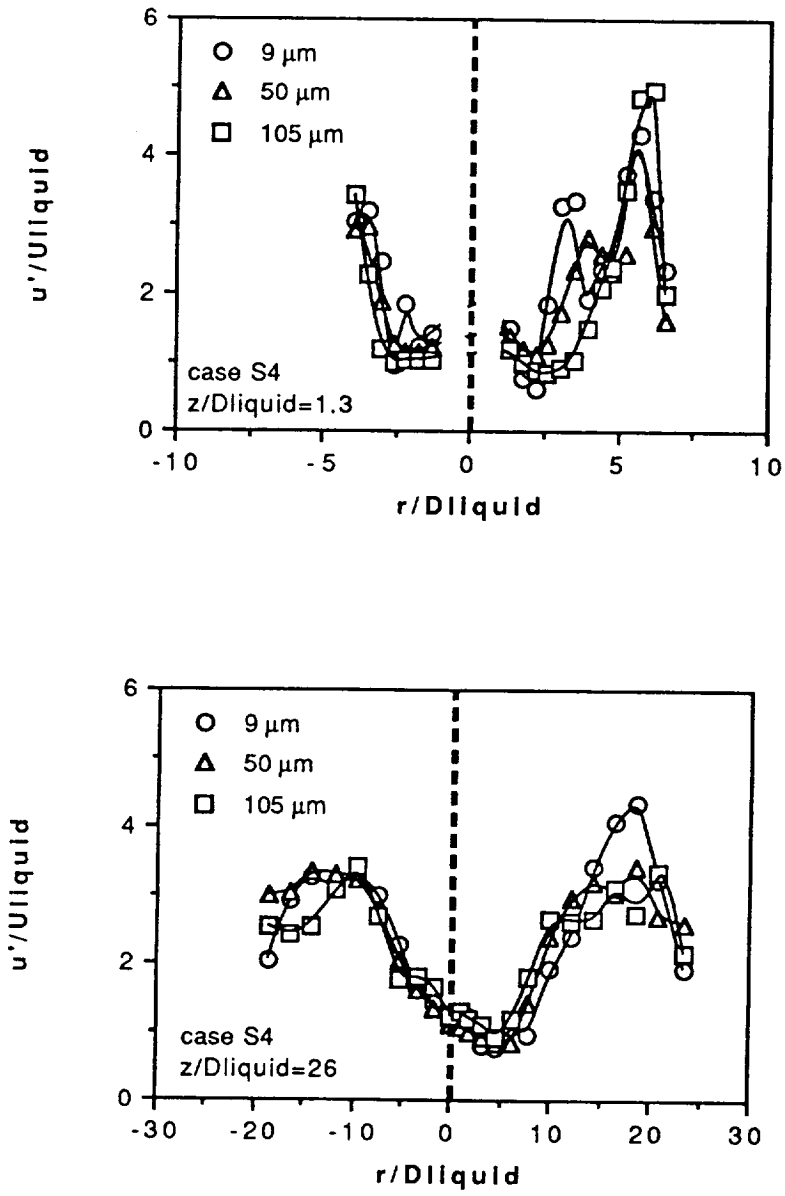

Figure 11. Characteristics of sprays produced by high swirl number gaseous stream nozzles with 10 mm annulus. Conditions according to case S4 of table 3. Radial profiles of the rms of the fluctuations of the axial velocity of 9, 50 and 105 μm droplets at axial distances from the nozzle of z/D_{liquid} = 1.3 and 26.

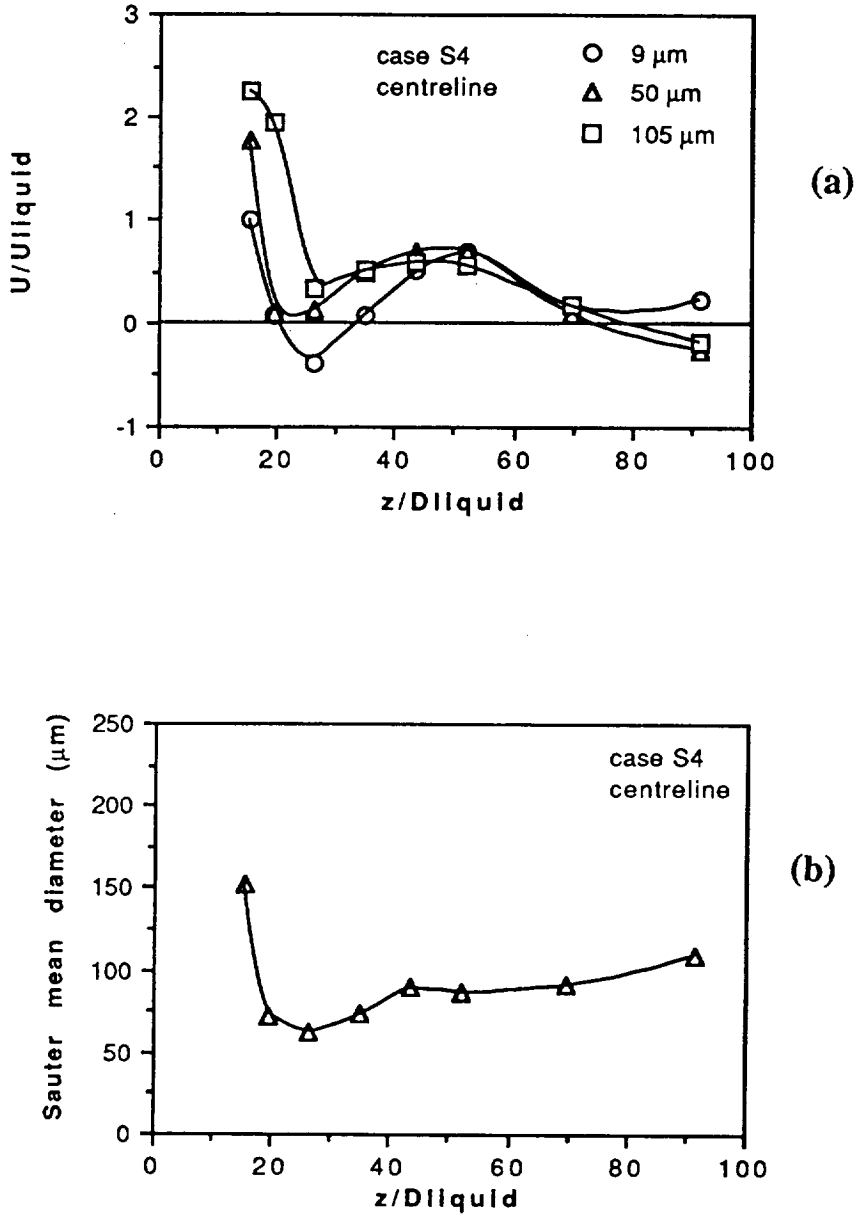

Figure 12. Characteristics of sprays produced by high swirl number gaseous stream nozzles with 10 mm annulus. Conditions according to case S4 of table 3. Centreline development of (a) mean axial velocity of 9, 50 and 105 μm droplets and (b) Sauter mean diameter.

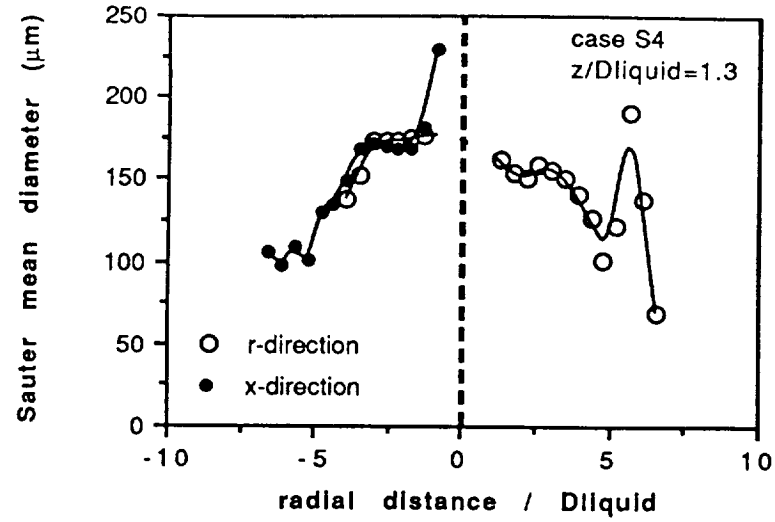

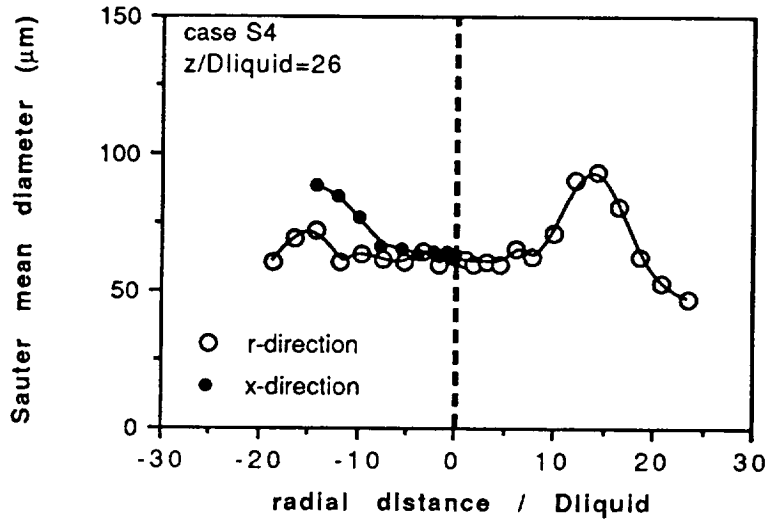

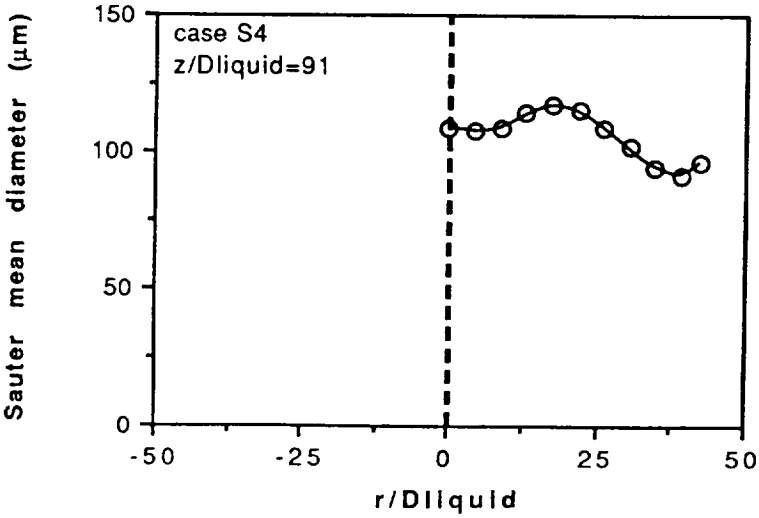

Figure 13a

Figure 13. Characteristics of sprays produced by high swirl number gaseous stream nozzles with 10 mm annulus. Conditions according to case S4 of table 3. Radial profiles at z/D_{liquid} = 1.3, 26 and 91 of (**a**) Sauter mean diameter and (**b**) liquid flux normalised by the maximum value for each axial location.

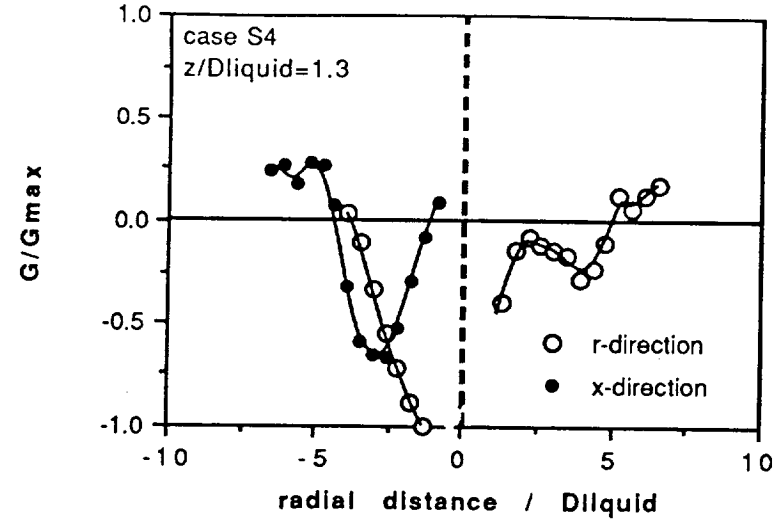
case S4
z/Dliquid=1.3
G/Gmax
1.0
0.5
0.0
-0.5
-1.0
-10
-5
0
5
10
r-direction
x-direction
radial distance / Dliquid

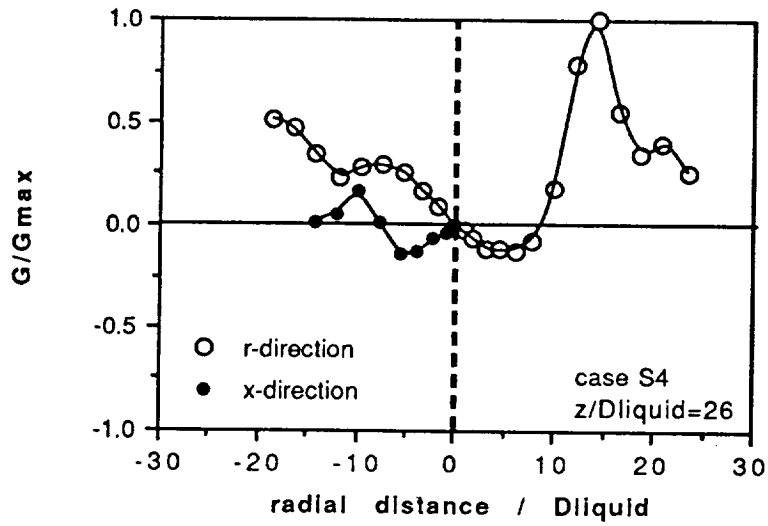
G/Gmax
1.0
0.5
0.0
-0.5
-1.0
-30
-20
-10
0
10
20
30
r-direction
x-direction
case S4
z/Dliquid=26
radial distance / Dliquid

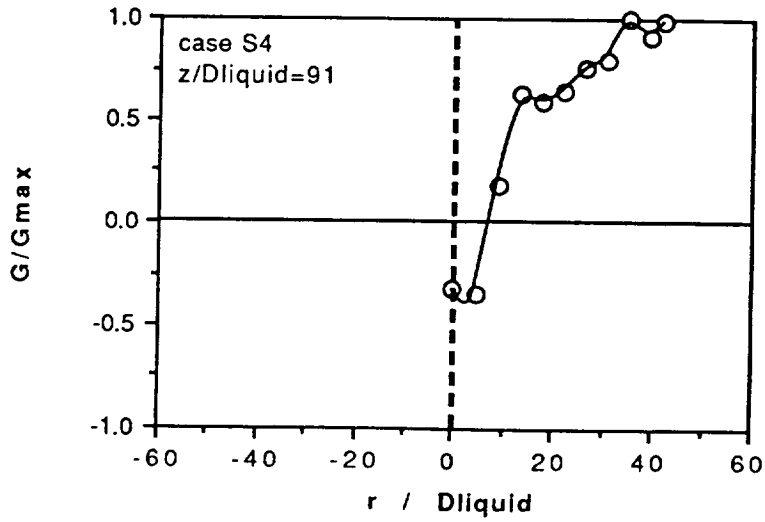
case S4
z/Dliquid=91
G/Gmax
1.0
0.5
0.0
-0.5
-1.0
-60
-40
-20
0
20
40
60
r / Dliquid

Figure 13b

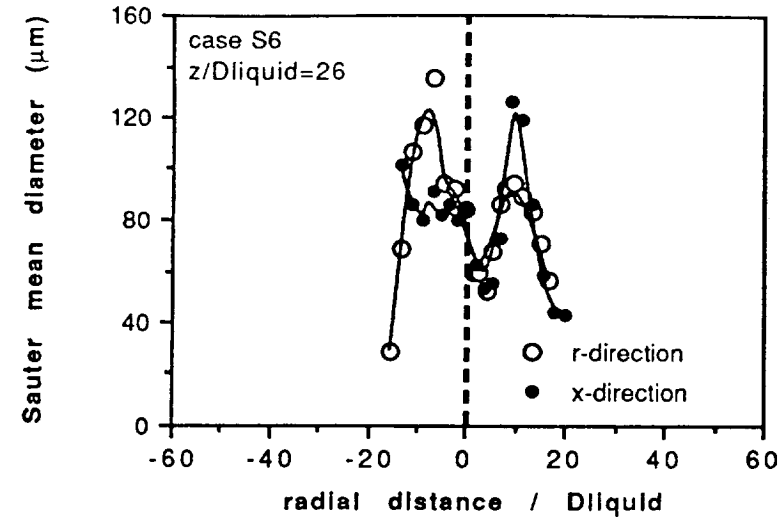

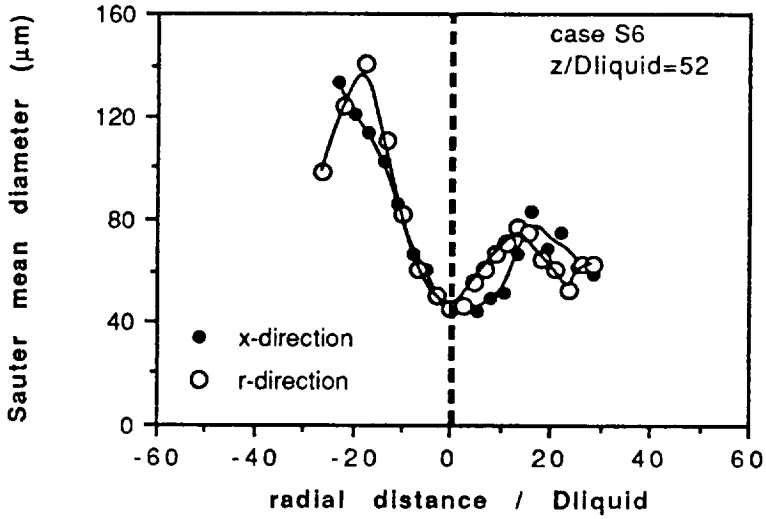

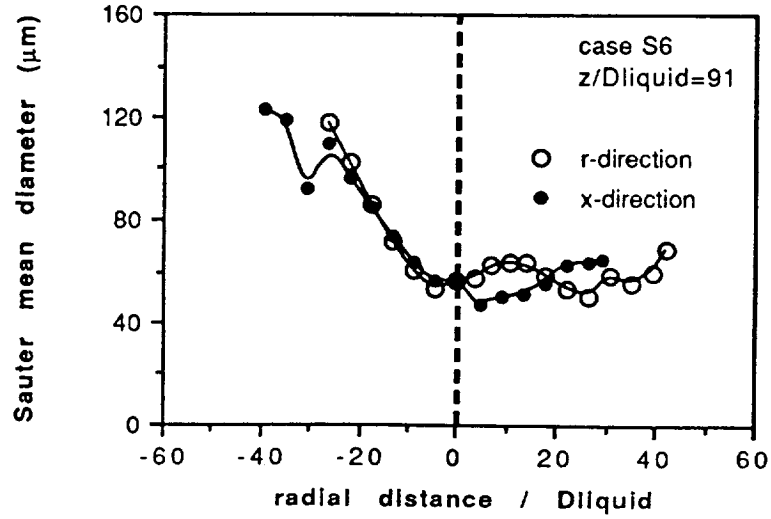

Figure 14a

Figure 14. Characteristics of sprays produced by high swirl number gaseous stream nozzles with 3 mm annulus. Conditions according to case S6 of table 3. Radial profiles at z/D_{liquid} = 26, 52 and 91 of (a) Sauter mean diameter and (b) liquid flux normalised by the measured maximum value for each axial location.

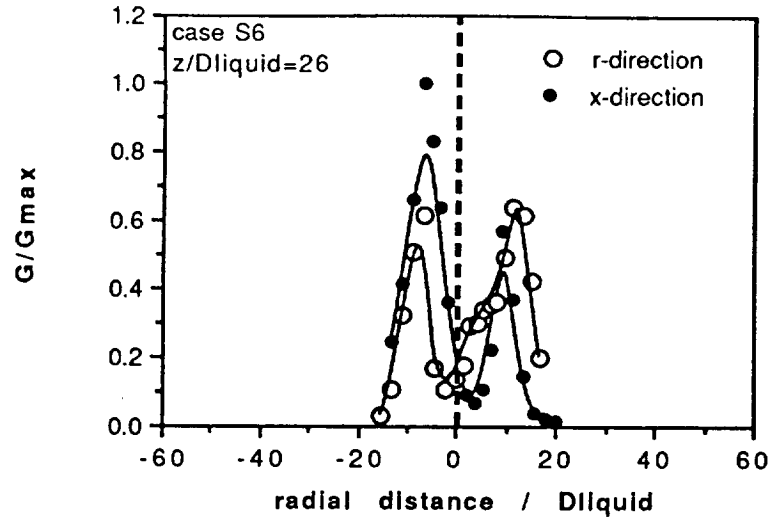
case S6
z/Dliquid=26
r-direction
x-direction
G/Gmax
radial distance / Dliquid

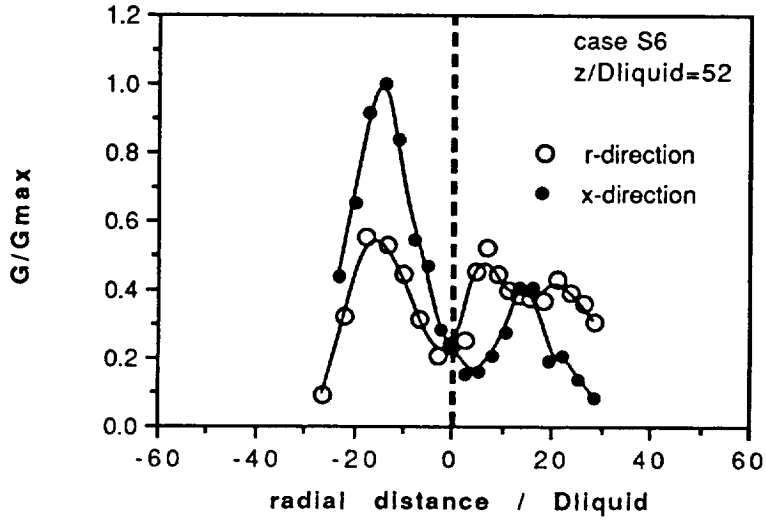
case S6
z/Dliquid=52
r-direction
x-direction
G/Gmax
radial distance / Dliquid

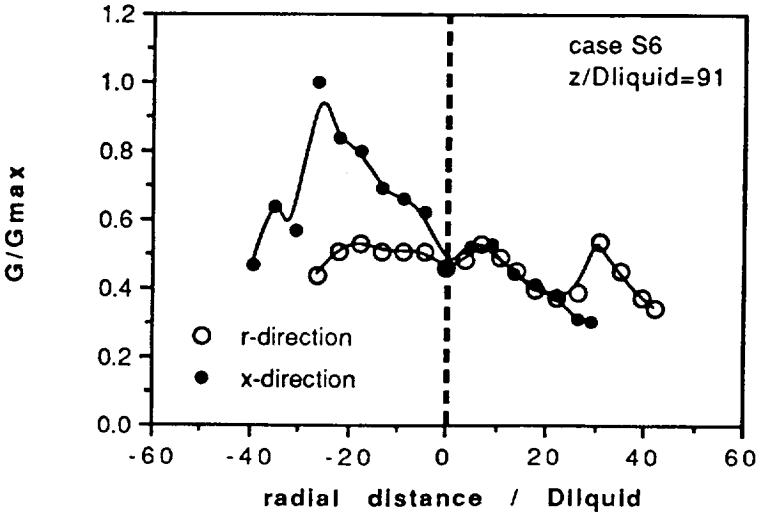
case S6
z/Dliquid=91
r-direction
x-direction
G/Gmax
radial distance / Dliquid

Figure 14b

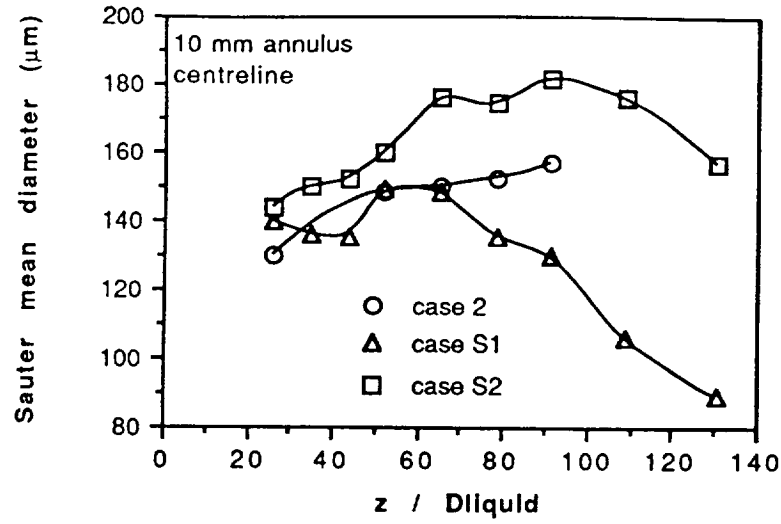

(a)

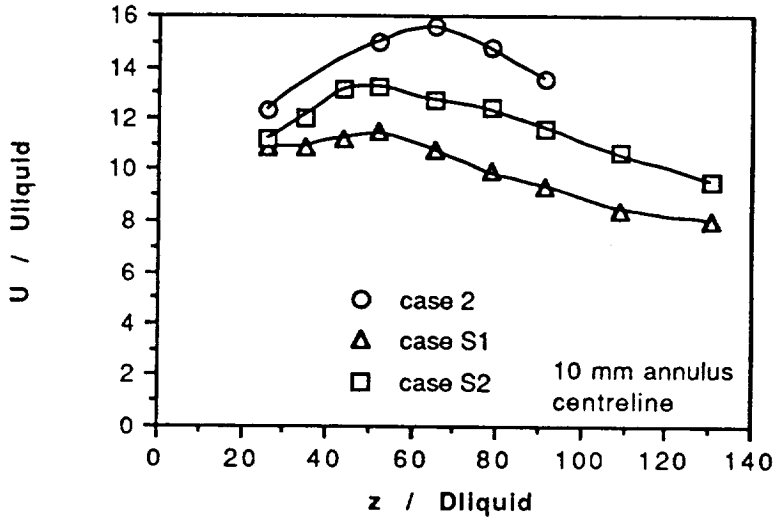

(b)

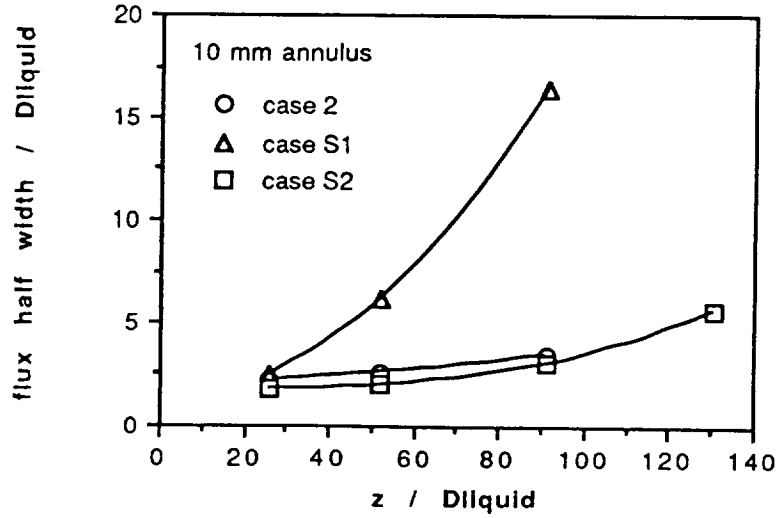

(c)

Figure 15. Comparison between the characteristics of sprays produced by axial and low swirl number gaseous stream nozzles. Centreline development of (a) Sauter mean diameter; (b) mean axial velocity of the gas phase; (c) flux half width.

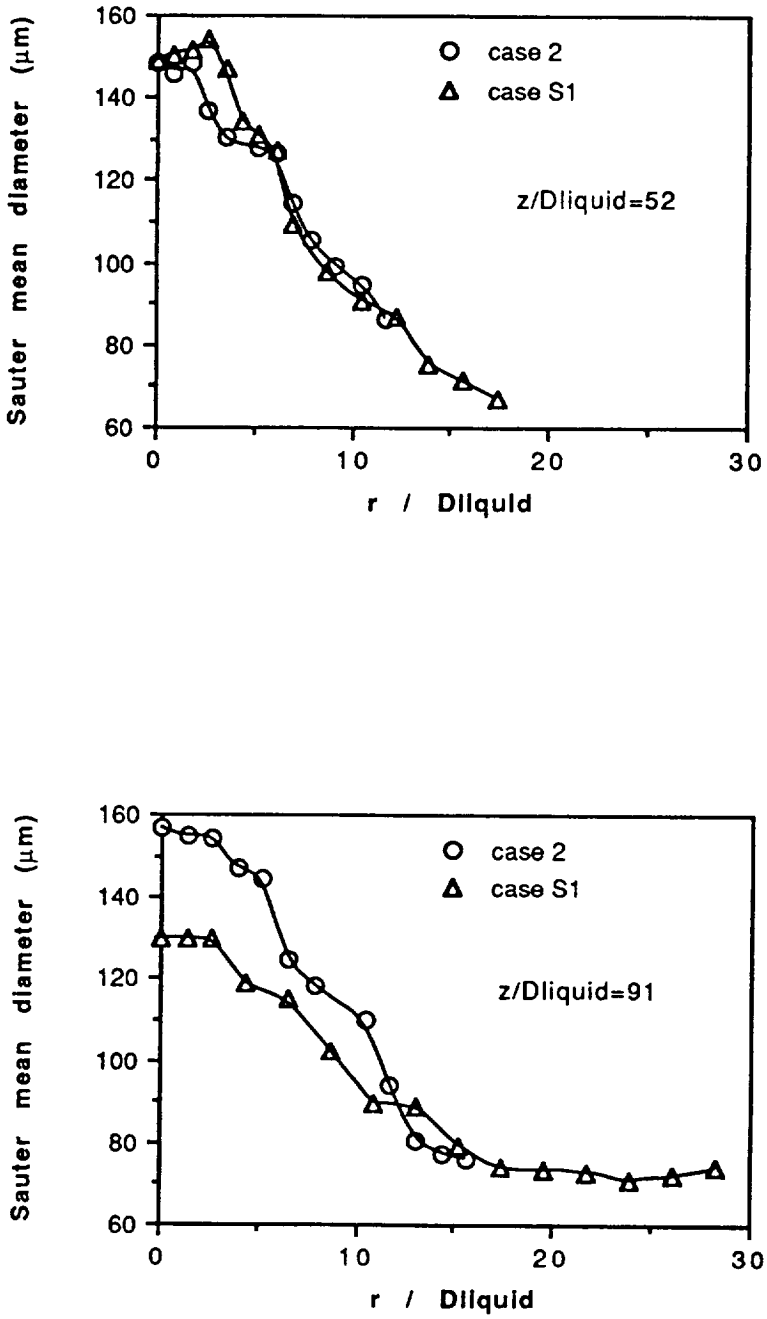

Figure 16. Comparison between the characteristics of sprays produced by axial and low swirl number gaseous stream nozzles. Radial profiles of the Sauter mean diameter at z/D_{liquid}= 52 and 91.

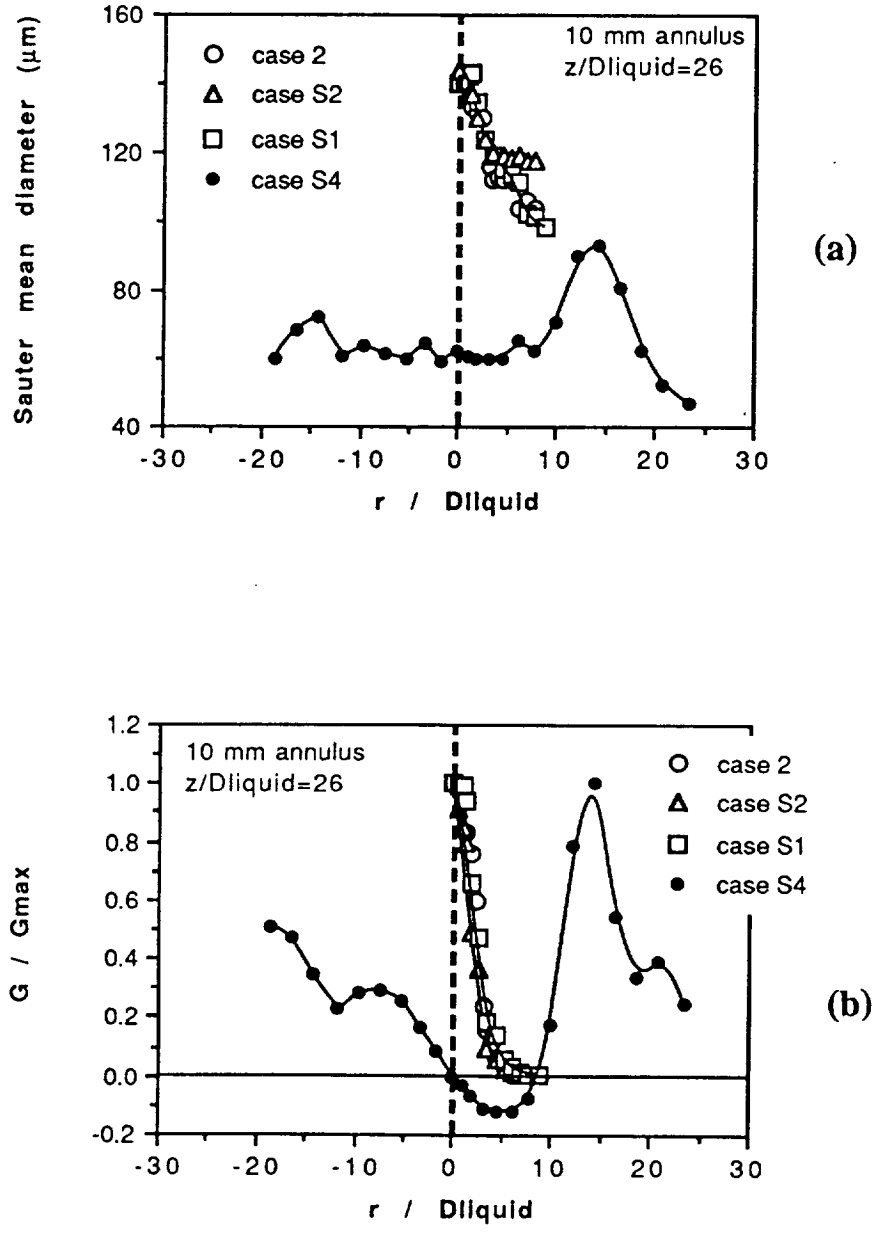

Figure 17. Comparison between the characteristics of sprays produced by axial and swirling gaseous stream nozzles. Radial profiles at $z/D_{liquid} = 26$ of (a) Sauter mean diameter; (b) liquid flux normalised by the maximum value of flux at the axial location.

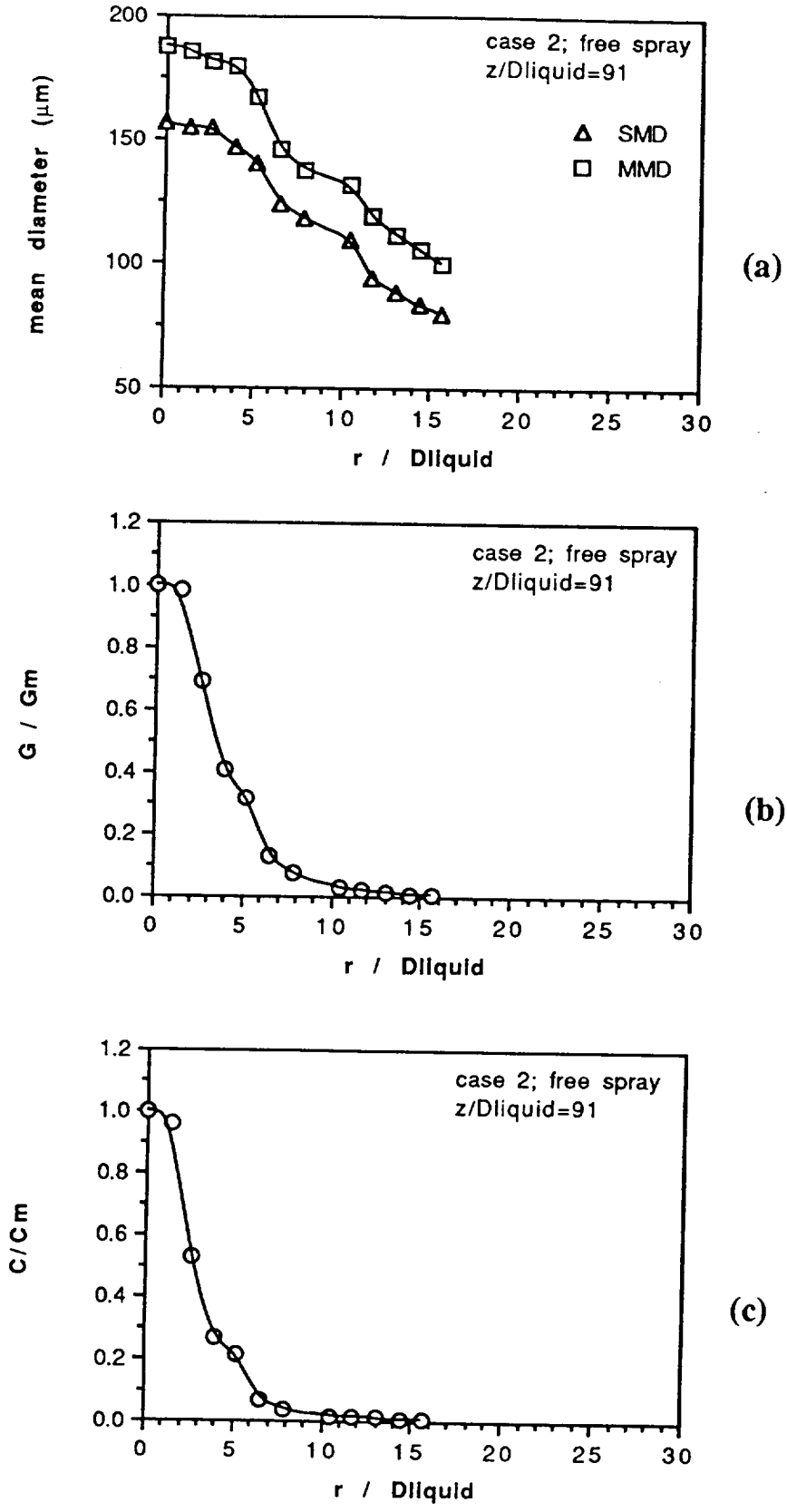

Figure 18. The characteristics of the free spray produced by a nozzle according to the conditions of case 2 of table 1a at an axial distance from the nozzle of $z/D_{liquid}=91$. **(a)** Mean diameters; **(b)** normalised volume flux of the liquid content of the spray; **(c)** normalised concentration of the volume of liquid; **(d)** mean axial velocity of 9, 50 and 105 µm droplets and **(e)** rms fluctuations of the axial velocity of 9, 50 and 105 µm droplets.

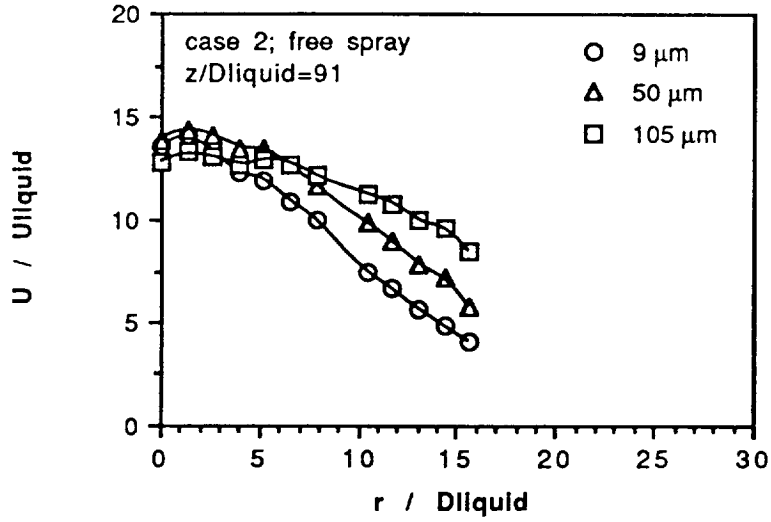
case 2; free spray
z/Dliquid=91
9 µm
50 µm
105 µm
U / Uliquid
r / Dliquid
0
5
10
15
20
25
30

(d)

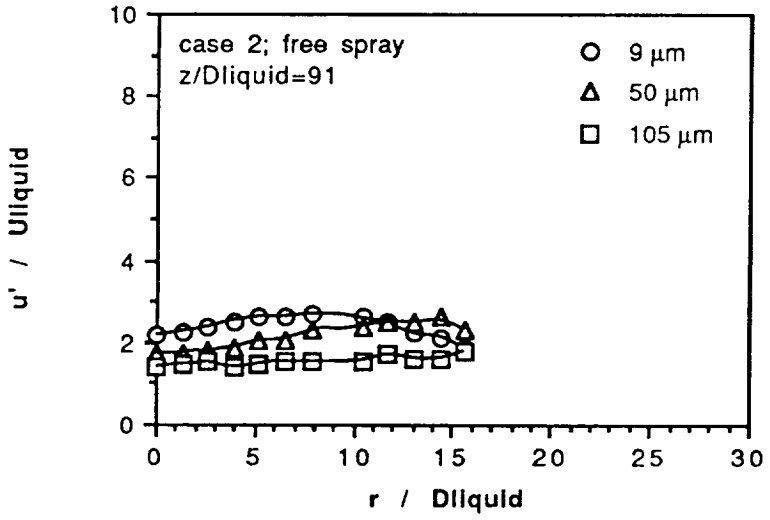
case 2; free spray
z/Dliquid=91
9 µm
50 µm
105 µm
u' / Uliquid
r / Dliquid
0
2
4
6
8
10
0
5
10
15
20
25
30

(e)

Figure 18.

Figure 19. Characteristics of the spray, produced by a nozzle with conditions according to case 2 of table 1a, striking a disc located at z/Dliquid = 93.5. Radial profiles at axial distances from the nozzle, z/D_{liquid} = 87, 88.3, 89.6, 90.9, 92.2, 92.8 and 94.8. (a) Normalised volume flux of the liquid content of the spray; (b) normalised concentration of the volume of liquid; (c) mean diameters; velocity characteristics of 9, 50 and 105 μm droplets for (d) mean axial velocity; (e) mean radial velocity; (f) rms fluctuations of axial velocity; (g) rms fluctuations of radial velocity; (h) correlation coefficient of $\overline{uv}/u'v'$. The arrows on the graphs indicate the edge of the disc.

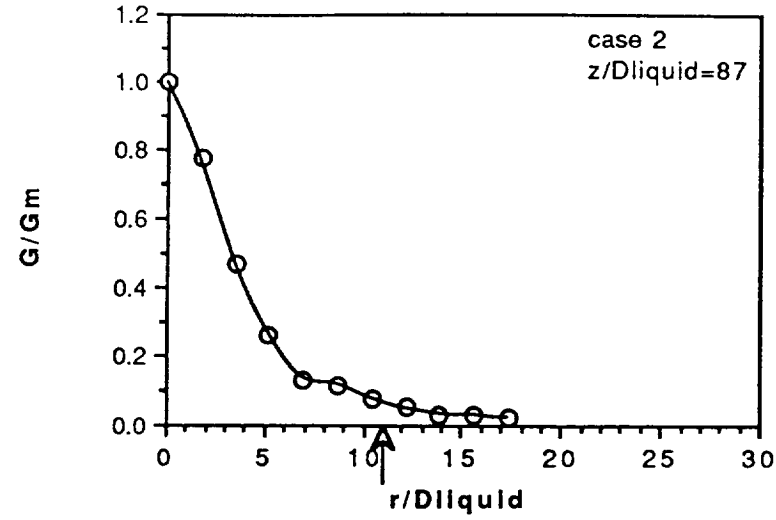
case 2
z/Dliquid=87
G/Gm
r/Dliquid
1.2
1.0
0.8
0.6
0.4
0.2
0.0
0
5
10
15
20
25
30

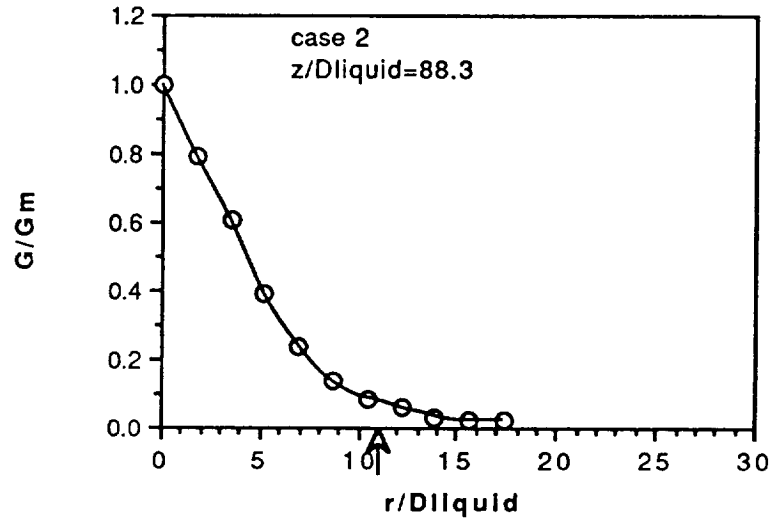
case 2
z/Dliquid=88.3
G/Gm
r/Dliquid
1.2
1.0
0.8
0.6
0.4
0.2
0.0
0
5
10
15
20
25
30

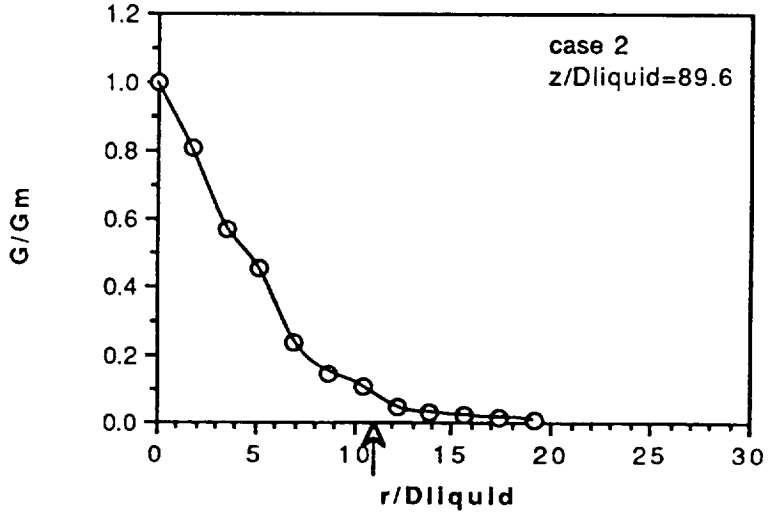
case 2
z/Dliquid=89.6
G/Gm
r/Dliquid
1.2
1.0
0.8
0.6
0.4
0.2
0.0
0
5
10
15
20
25
30

Figure 19a

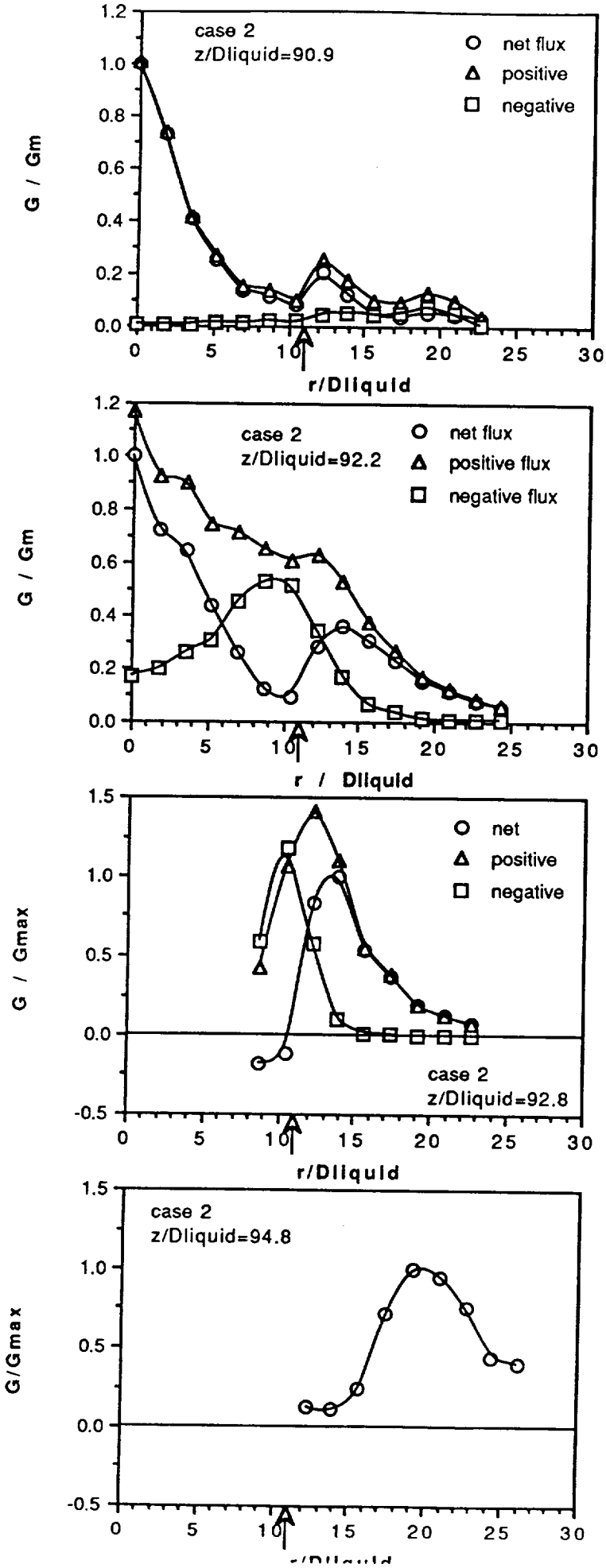
case 2
z/Dliquid=90.9
net flux
positive
negative
G / Gm
r/Dliquid
case 2
z/Dliquid=92.2
net flux
positive flux
negative flux
G / Gm
r / Dliquid
net
positive
negative
case 2
z/Dliquid=92.8
G / Gmax
r/Dliquid
case 2
z/Dliquid=94.8
G/Gmax

Figure 19a

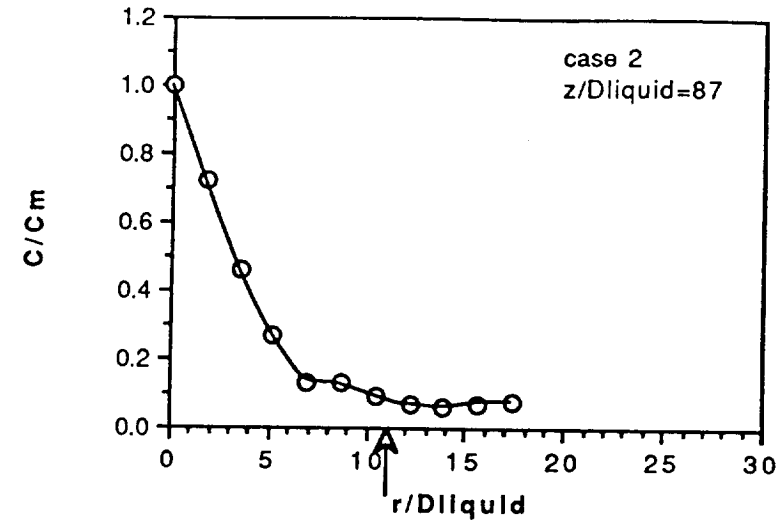
case 2
z/Dliquid=87
C/Cm
r/Dliquid
1.2
1.0
0.8
0.6
0.4
0.2
0.0
0
5
10
15
20
25
30

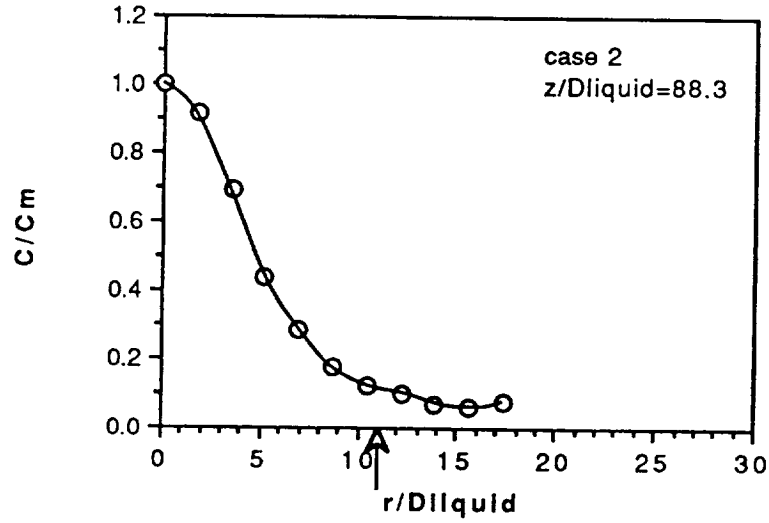
case 2
z/Dliquid=88.3
C/Cm
r/Dliquid
1.2
1.0
0.8
0.6
0.4
0.2
0.0
0
5
10
15
20
25
30

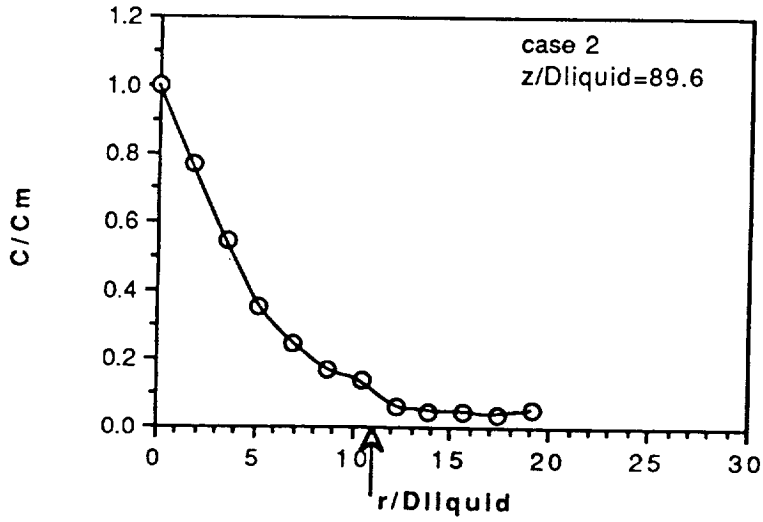
case 2
z/Dliquid=89.6
C/Cm
r/Dliquid
1.2
1.0
0.8
0.6
0.4
0.2
0.0
0
5
10
15
20
25
30

Figure 19b

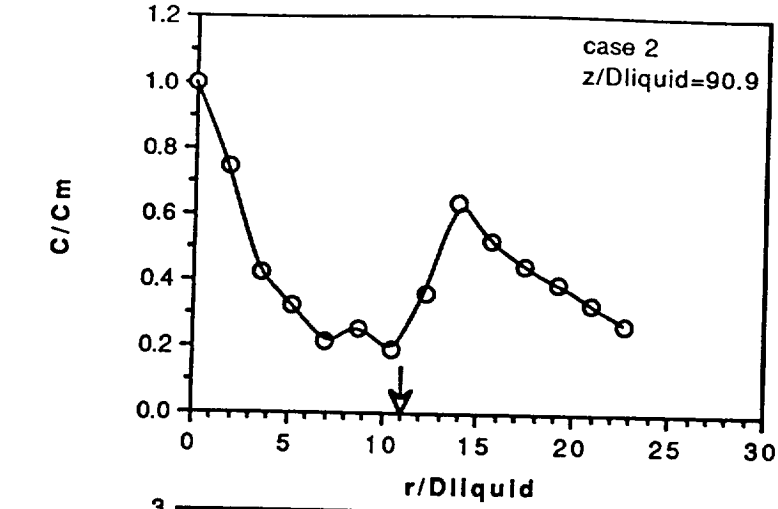
case 2
z/Dliquid=90.9
C/Cm
r/Dliquid

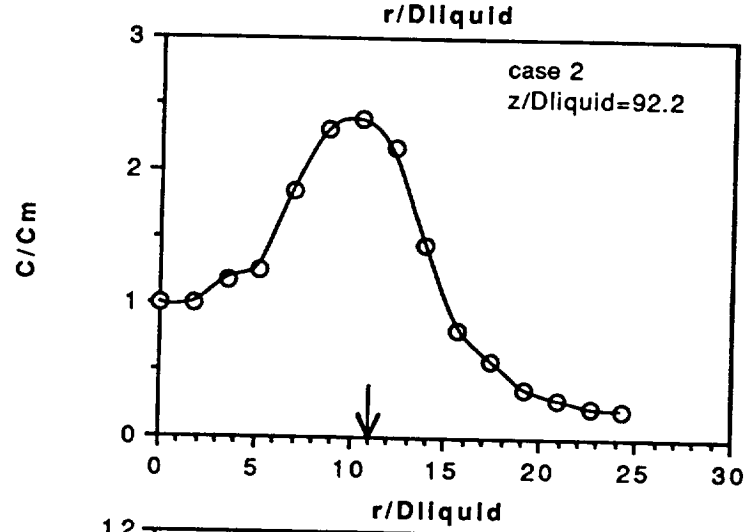
case 2
z/Dliquid=92.2
C/Cm
r/Dliquid

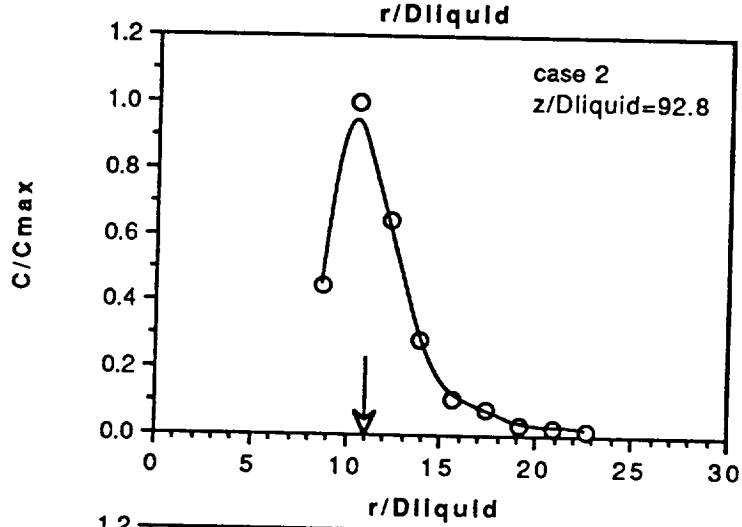
case 2
z/Dliquid=92.8
C/Cmax
r/Dliquid

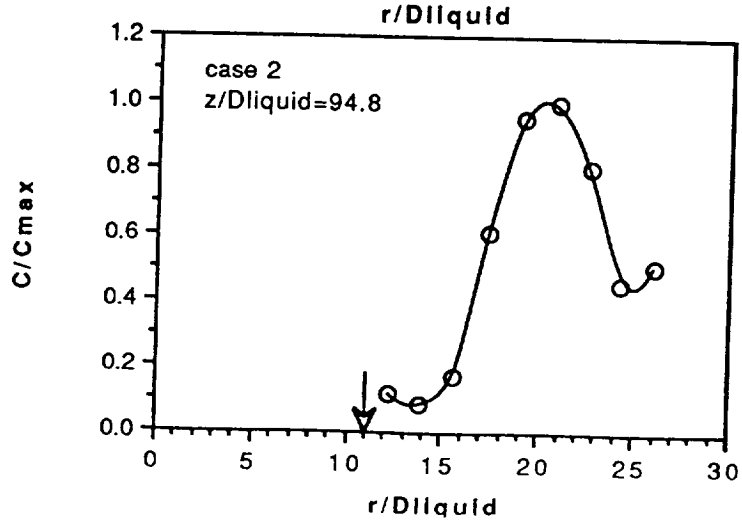
case 2
z/Dliquid=94.8
C/Cmax
r/Dliquid

Figure 19b

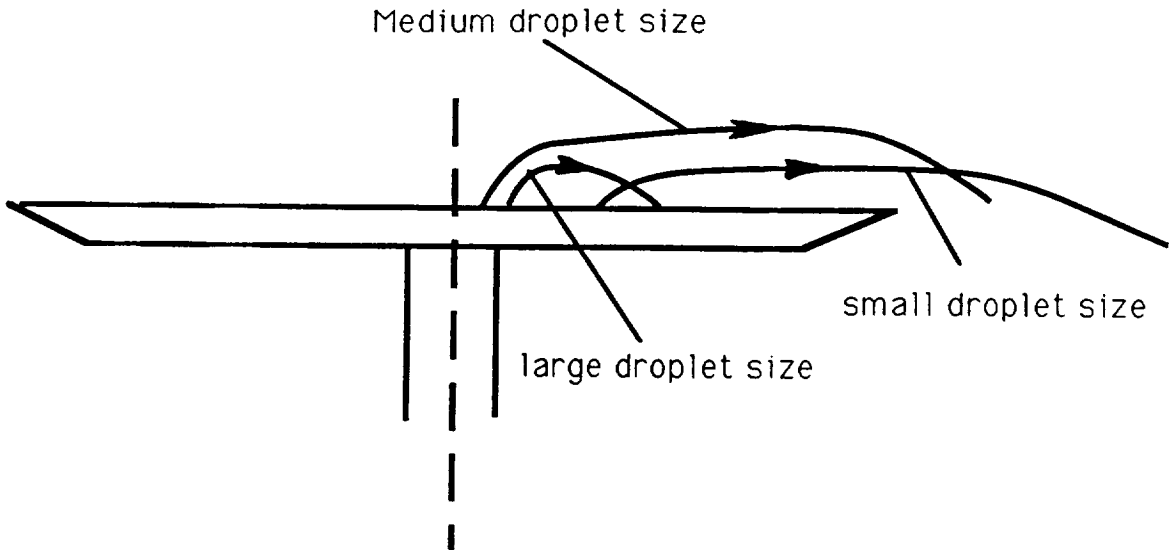

Figure 24. Drawing of reatomized droplet trajectories close to the surface of the disc.

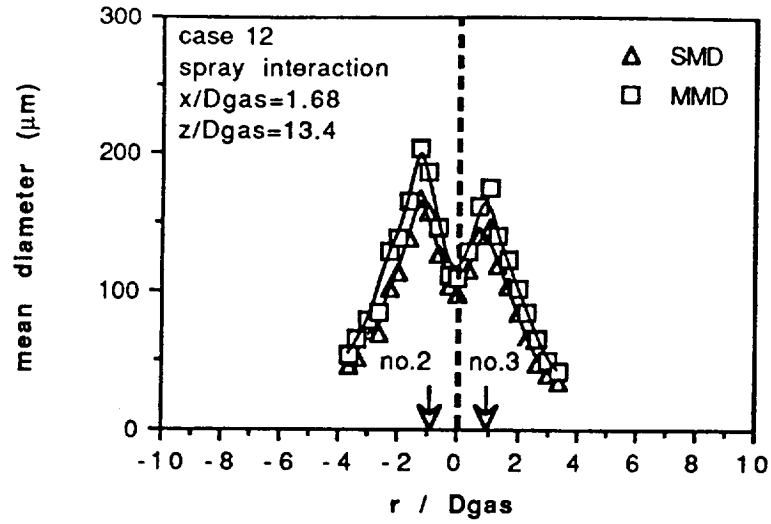

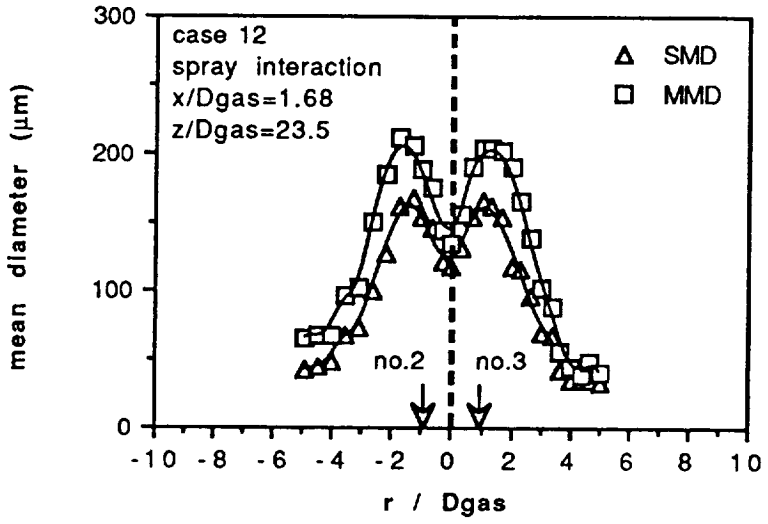

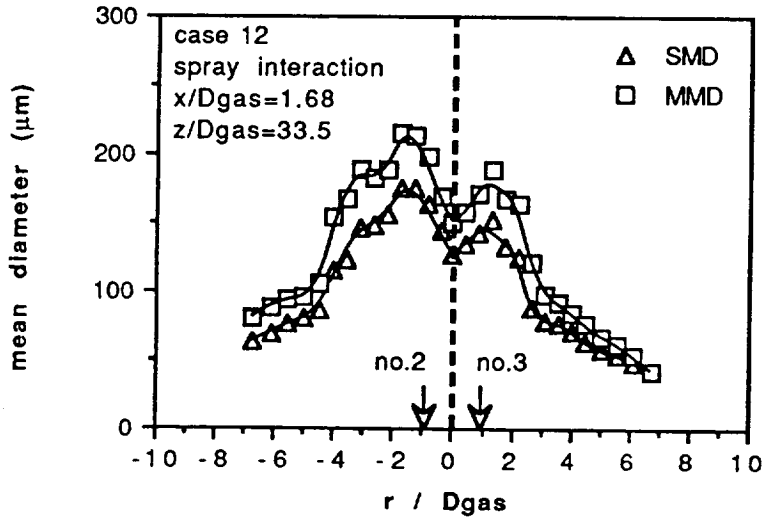

Figure 25a

Figure 25. Radial profiles of (a) mean diameters, (b) liquid flux and (c) mean axial velocity of 9, 50 and 105 μm droplets and single phase at axial distances z/D_{gas} = 13.4, 23.5 and 33.5 from the faceplate of three nozzles producing sprays according to case 12 of table 1a along the r direction at x/D_{gas} = 1.68.

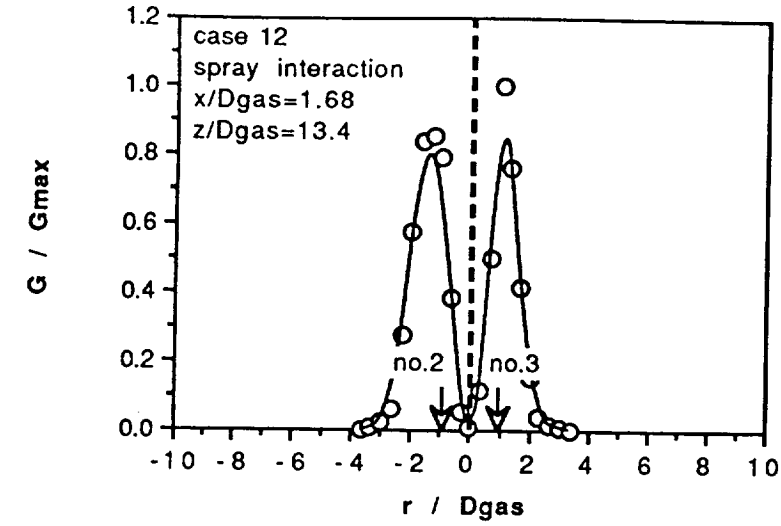
case 12
spray interaction
x/Dgas=1.68
z/Dgas=13.4
no.2
no.3
G / Gmax
r / Dgas

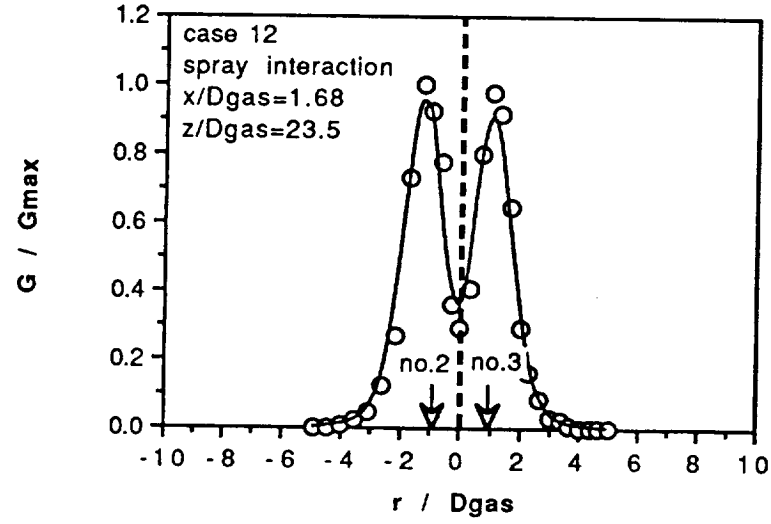
case 12
spray interaction
x/Dgas=1.68
z/Dgas=23.5
no.2
no.3
G / Gmax
r / Dgas

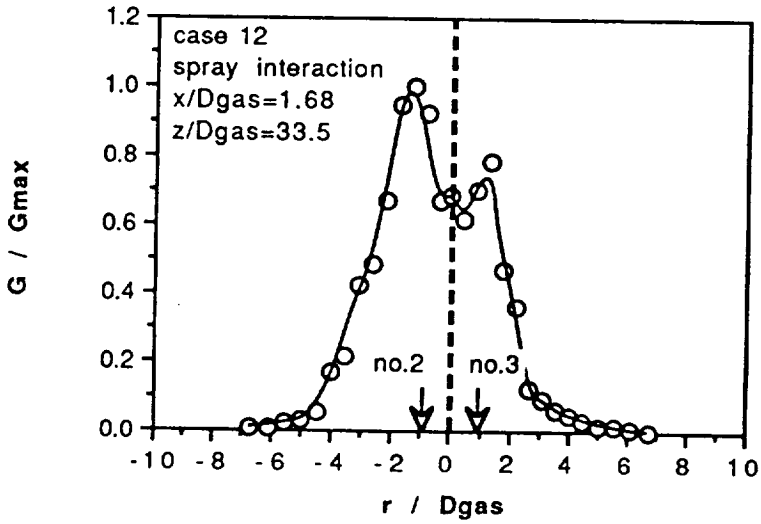
case 12
spray interaction
x/Dgas=1.68
z/Dgas=33.5
no.2
no.3
G / Gmax
r / Dgas

Figure 25b

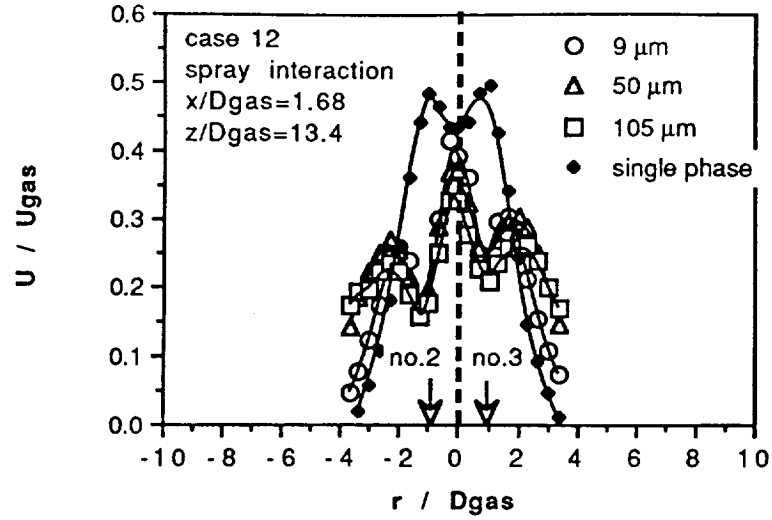
case 12
spray interaction
x/Dgas=1.68
z/Dgas=13.4
9 μm
50 μm
105 μm
single phase
no.2
no.3
U / Ugas
r / Dgas

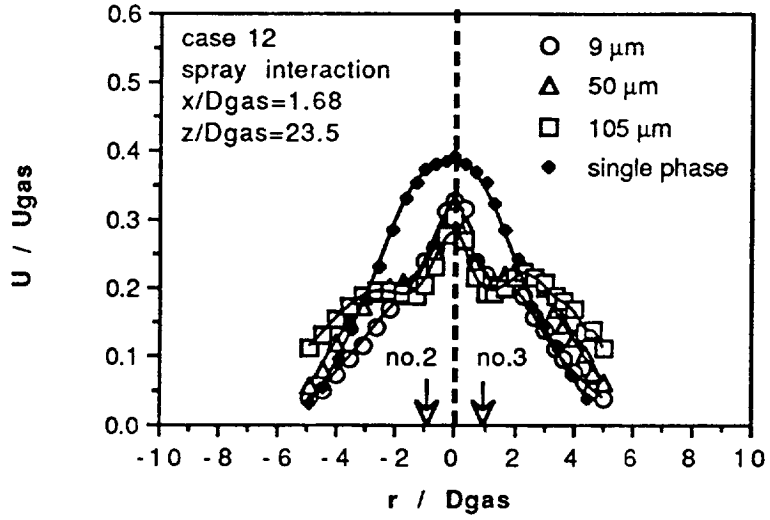
case 12
spray interaction
x/Dgas=1.68
z/Dgas=23.5
9 μm
50 μm
105 μm
single phase
no.2
no.3
U / Ugas
r / Dgas

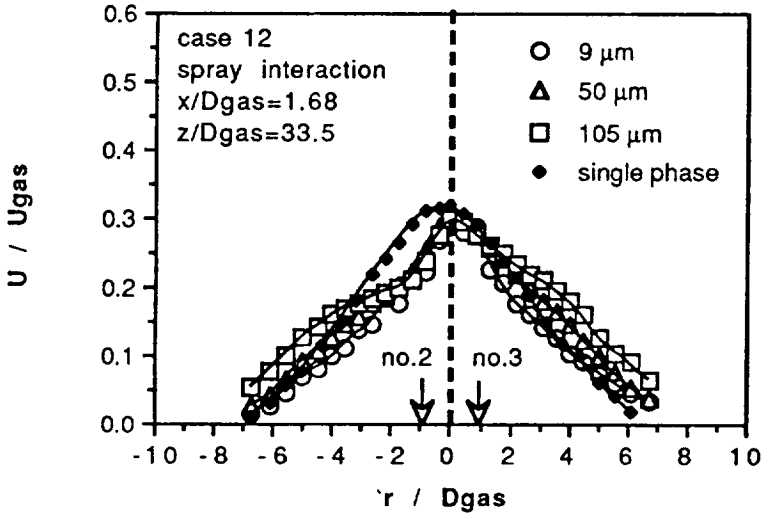
case 12
spray interaction
x/Dgas=1.68
z/Dgas=33.5
9 μm
50 μm
105 μm
single phase
no.2
no.3
U / Ugas
r / Dgas

Figure 25c

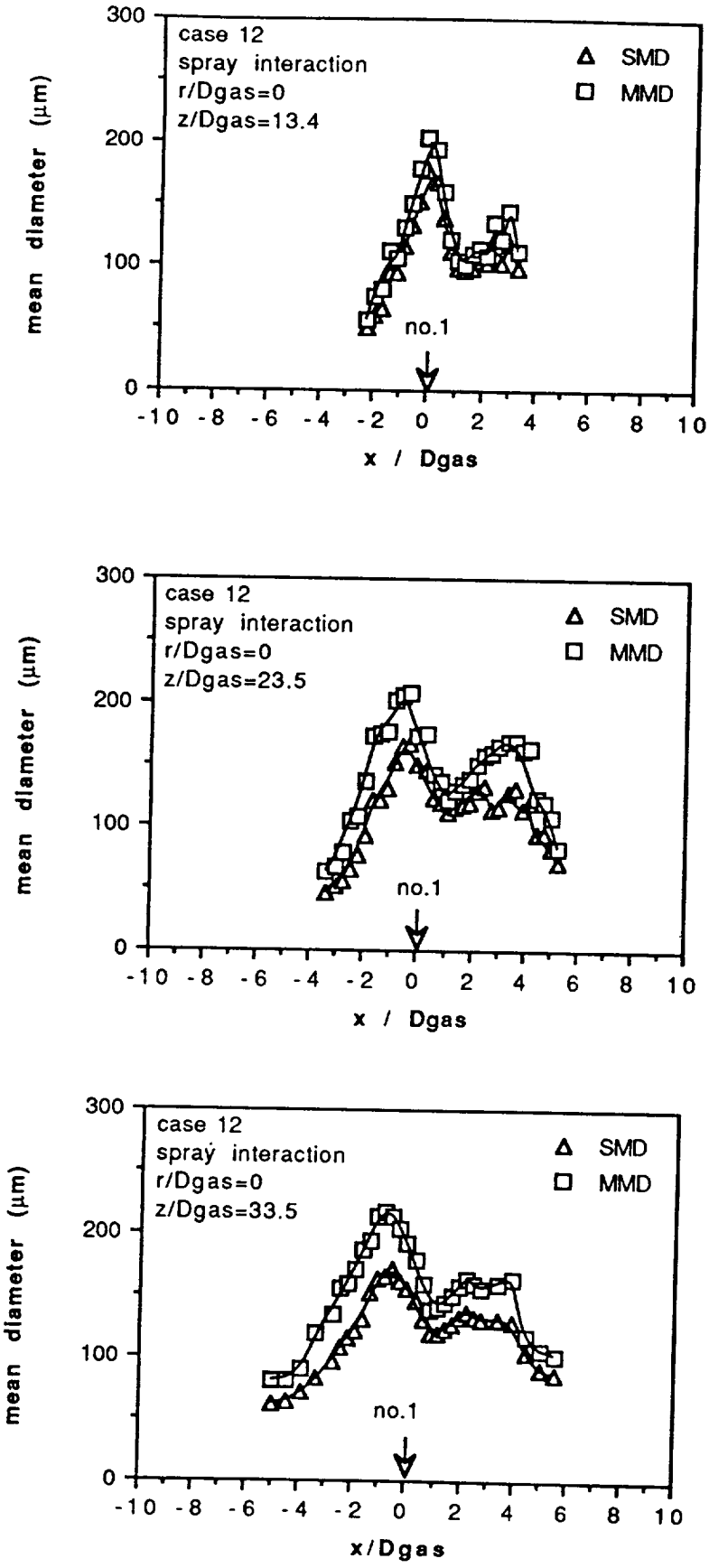

Figure 26a

Figure 26. Radial profiles of (a) mean diameters, (b) liquid flux and (c) mean axial velocity of 9, 50 and 105 µm droplets and single phase at axial distances z/D_{gas} = 13.4, 23.5 and 33.5 from the faceplate of three nozzles producing sprays according to case 12 of table 1a along the x direction at r/D_{gas} = 0.

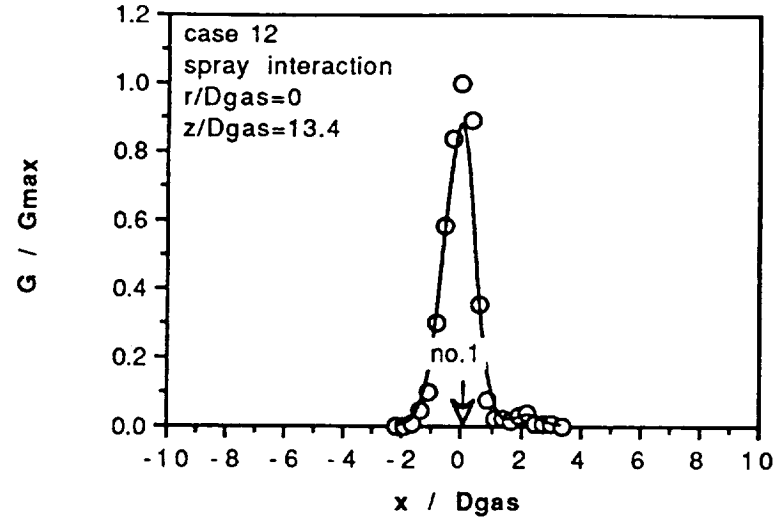
case 12
spray interaction
r/Dgas=0
z/Dgas=13.4
no.1
G / Gmax
x / Dgas

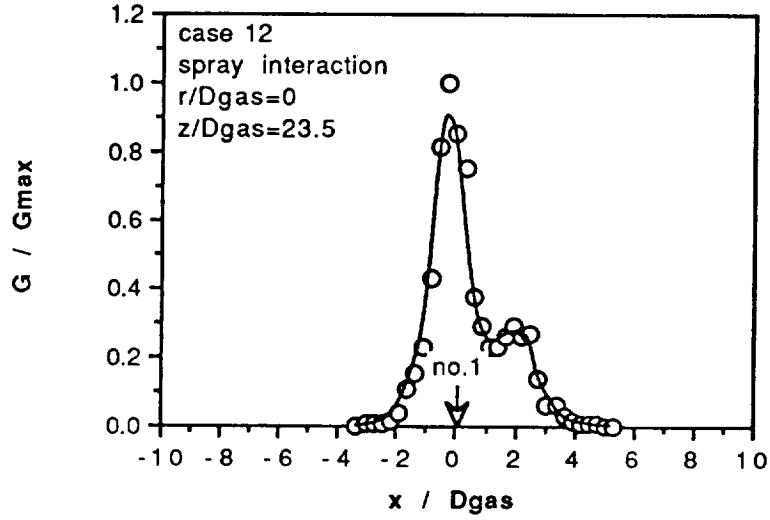
case 12
spray interaction
r/Dgas=0
z/Dgas=23.5
no.1
G / Gmax
x / Dgas

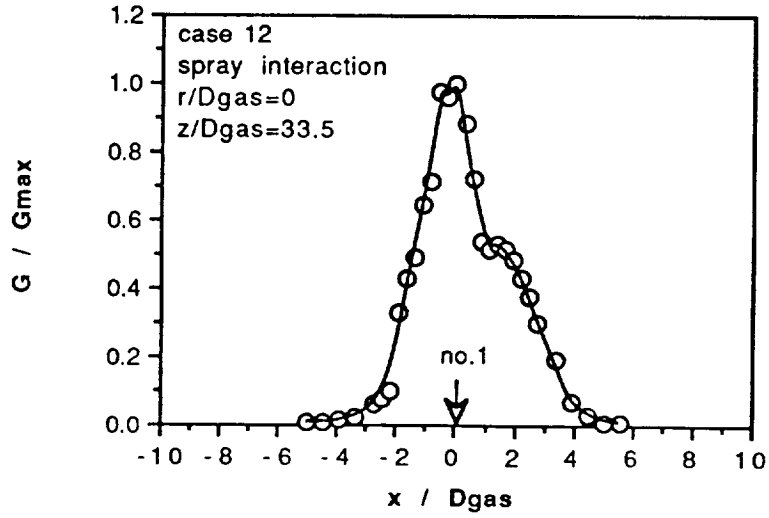
case 12
spray interaction
r/Dgas=0
z/Dgas=33.5
no.1
G / Gmax
x / Dgas

Figure 26b

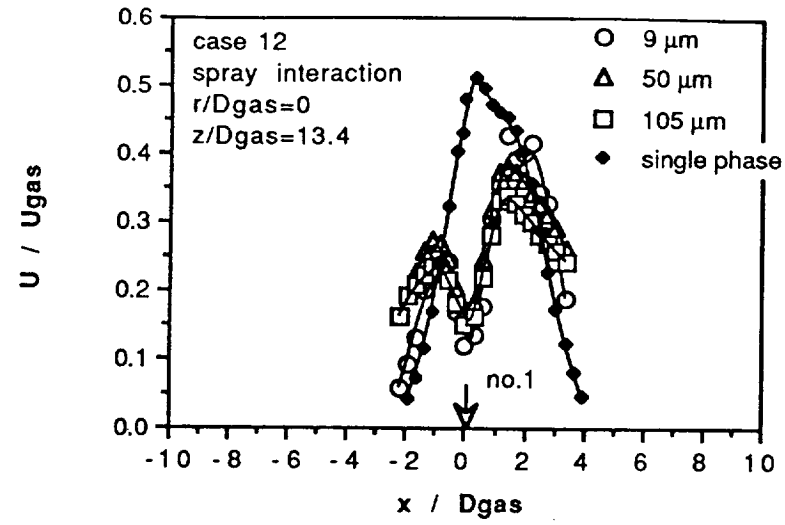
case 12
spray interaction
r/Dgas=0
z/Dgas=13.4
9 μm
50 μm
105 μm
single phase
no.1
U / Ugas
x / Dgas

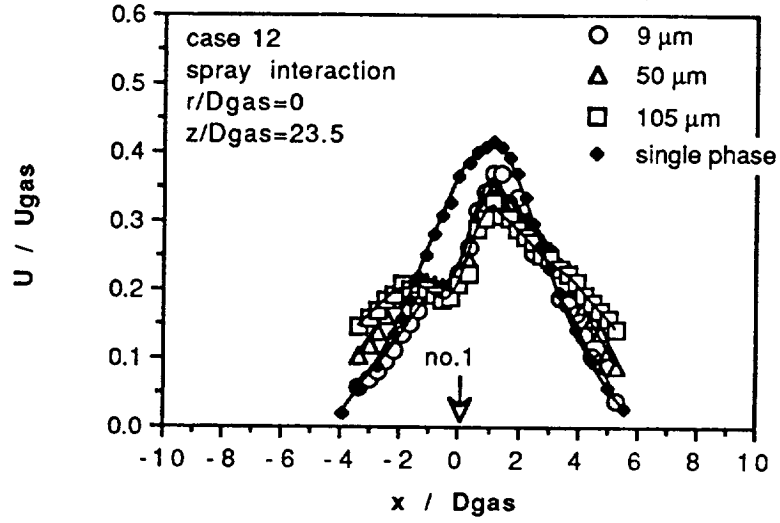
case 12
spray interaction
r/Dgas=0
z/Dgas=23.5
9 μm
50 μm
105 μm
single phase
no.1
U / Ugas
x / Dgas

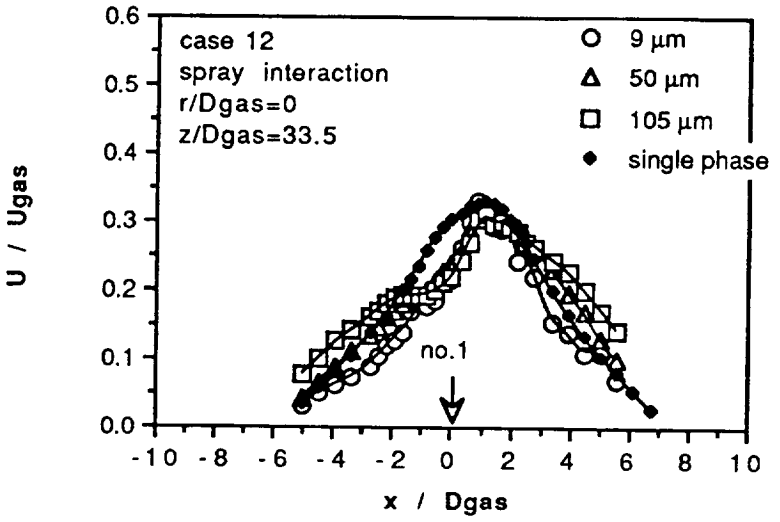
case 12
spray interaction
r/Dgas=0
z/Dgas=33.5
9 μm
50 μm
105 μm
single phase
no.1
U / Ugas
x / Dgas

Figure 26c

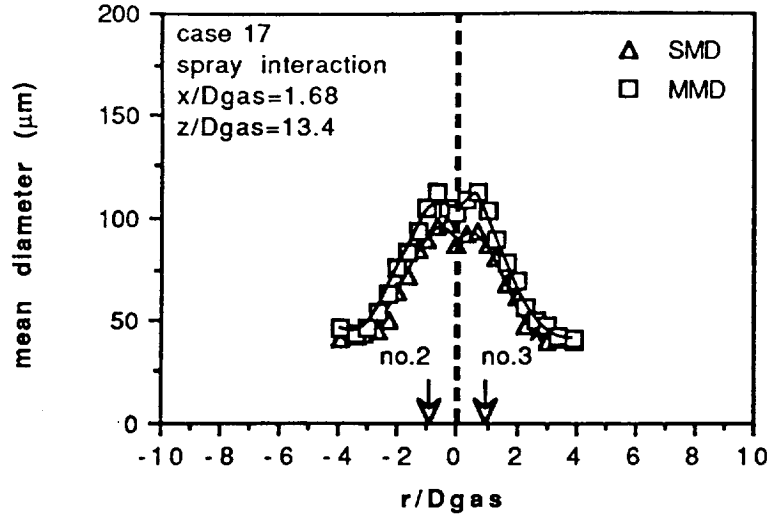

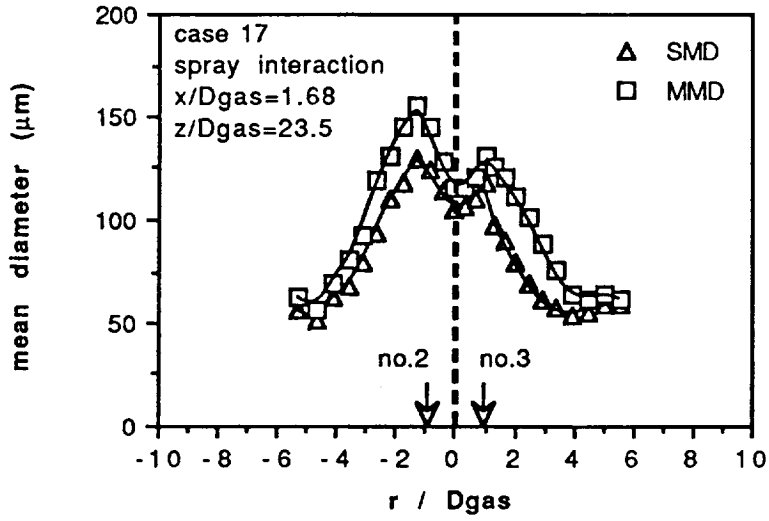

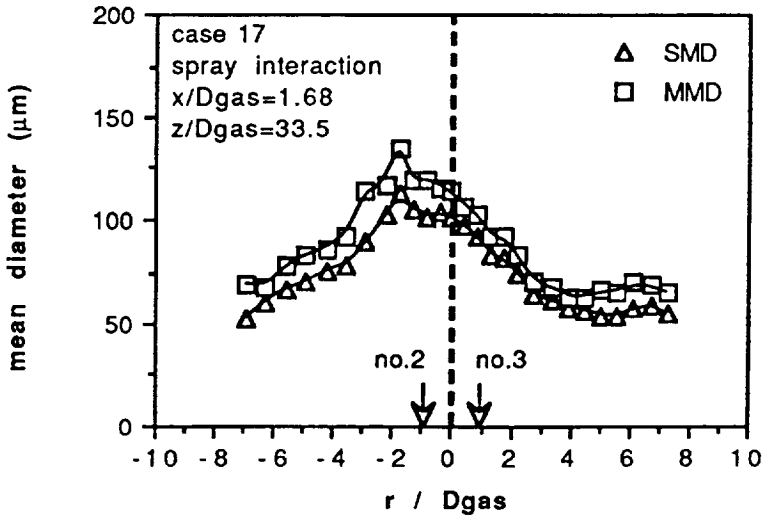

Figure 27a

Figure 27. Radial profiles of (a) mean diameters, (b) liquid flux and (c) mean axial velocity of 9, 50 and 105 μm droplets and single phase at axial distances z/D_{gas} = 13.4, 23.5 and 33.5 from the faceplate of three nozzles producing sprays according to case 17 of table 1a along the r direction at x/D_{gas} = 1.68.

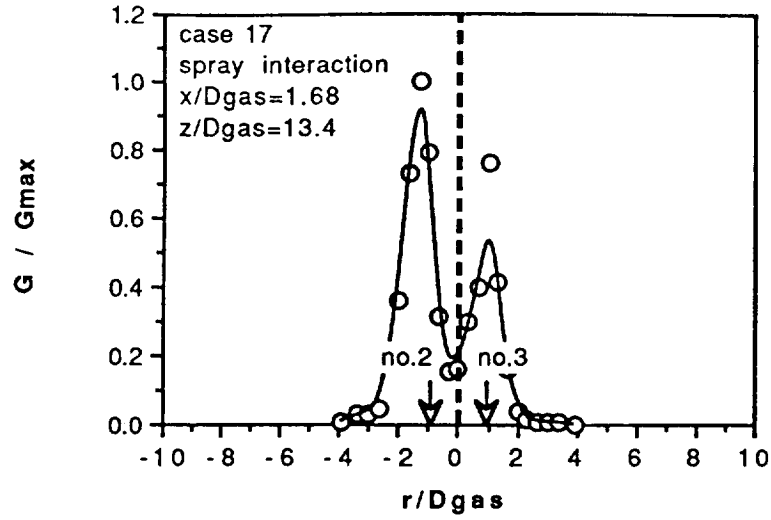
case 17
spray interaction
x/Dgas=1.68
z/Dgas=13.4
no.2
no.3
G / Gmax
r/Dgas

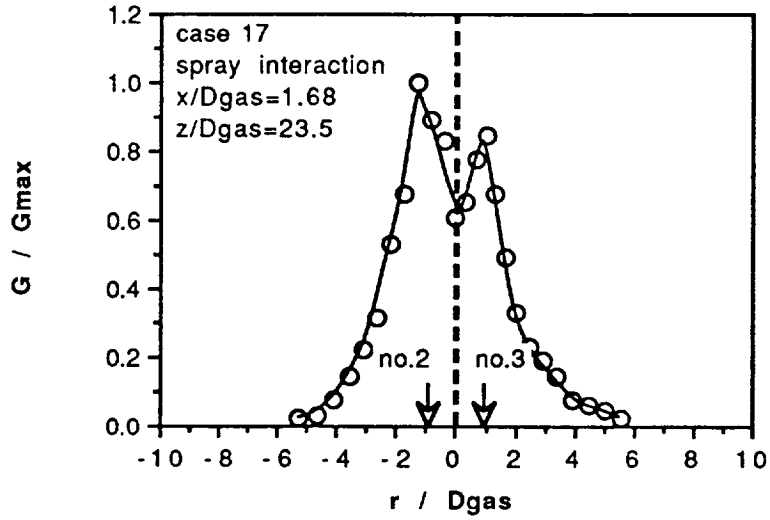
case 17
spray interaction
x/Dgas=1.68
z/Dgas=23.5
no.2
no.3
G / Gmax
r / Dgas

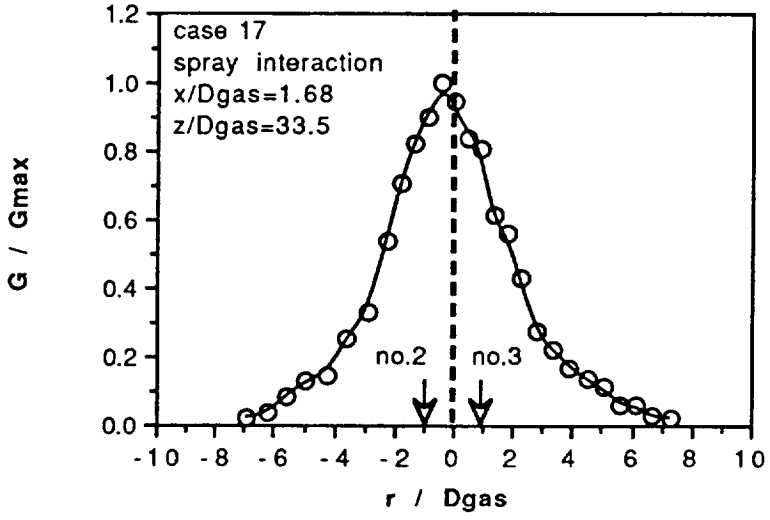
case 17
spray interaction
x/Dgas=1.68
z/Dgas=33.5
no.2
no.3
G / Gmax
r / Dgas

Figure 27b

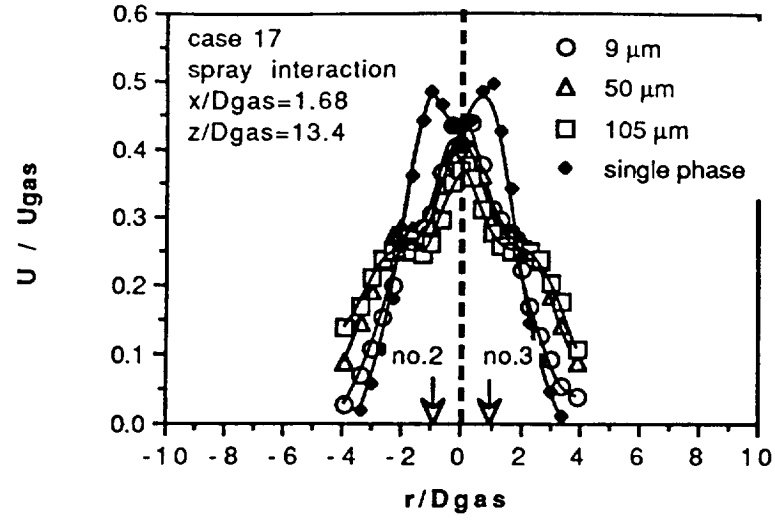
case 17
spray interaction
x/Dgas=1.68
z/Dgas=13.4
9 μm
50 μm
105 μm
single phase
no.2
no.3
U / Ugas
r/Dgas

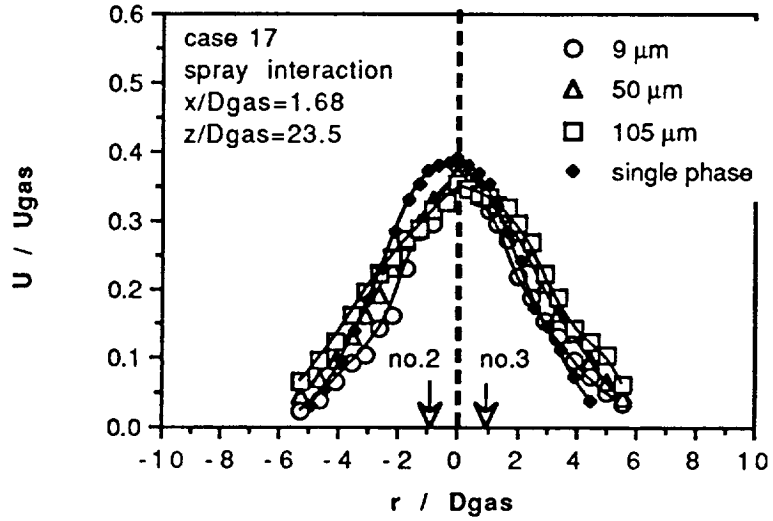
case 17
spray interaction
x/Dgas=1.68
z/Dgas=23.5
9 μm
50 μm
105 μm
single phase
no.2
no.3
U / Ugas
r / Dgas

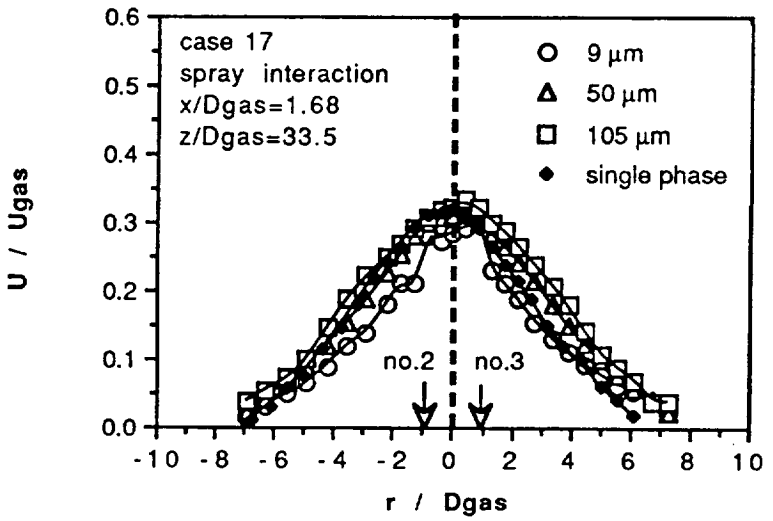
case 17
spray interaction
x/Dgas=1.68
z/Dgas=33.5
9 μm
50 μm
105 μm
single phase
no.2
no.3
U / Ugas
r / Dgas

Figure 27c

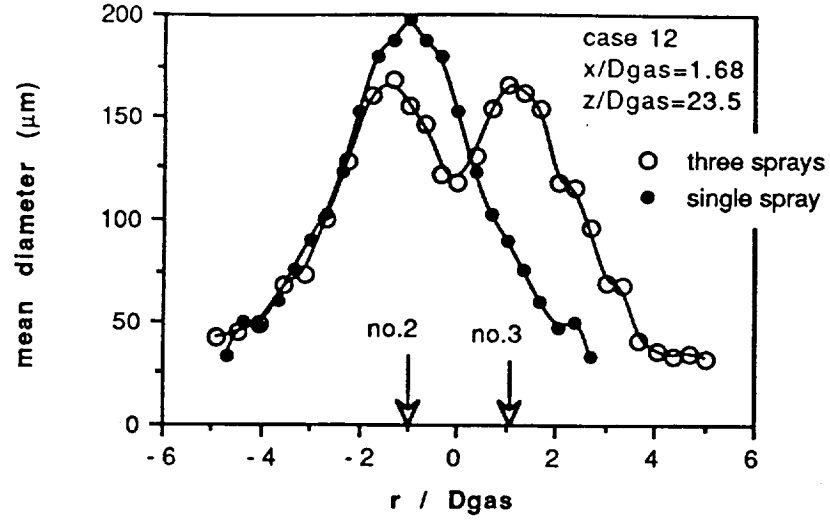

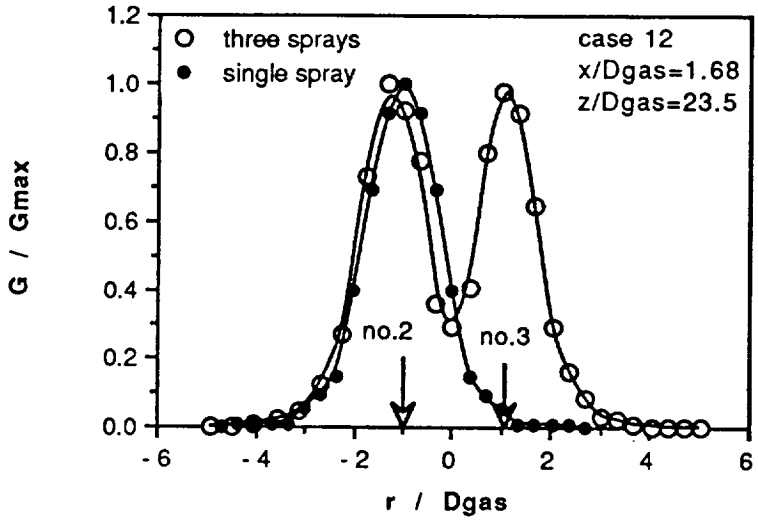

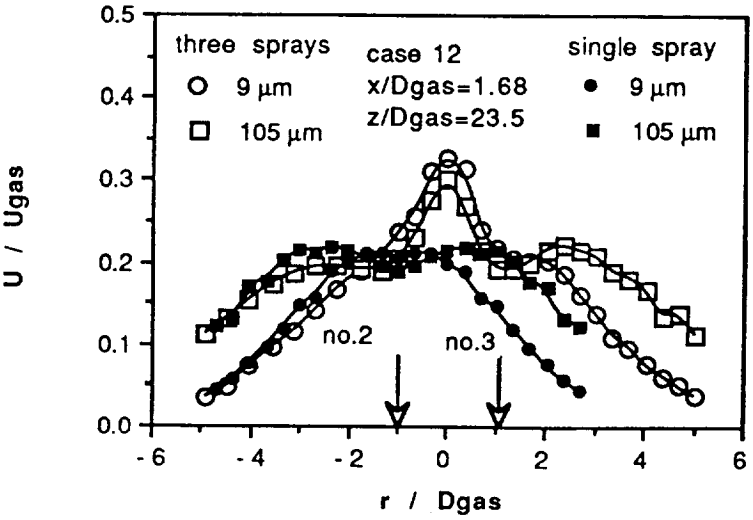

Figure 28a

Figure 28. Comparison between the Sauter mean diameter, the liquid flux and the axial velocity of the 9 and 105 μm droplets of the three interacting and the single sprays produced by nozzles according to case 12 of table 1a. (a) $z/D_{gas} = 23.5$, $x/D_{gas}=1.68$; (b) $z/D_{gas}=23.5$; $r/D_{gas}=0$.

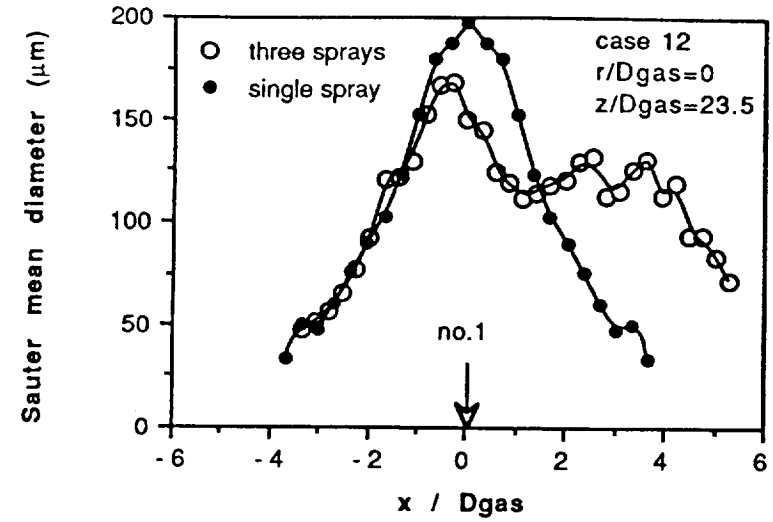
Sauter mean diameter (μm)
200
150
100
50
0
three sprays
single spray
case 12
r/Dgas=0
z/Dgas=23.5
no.1
-6
-4
-2
0
2
4
6
x / Dgas

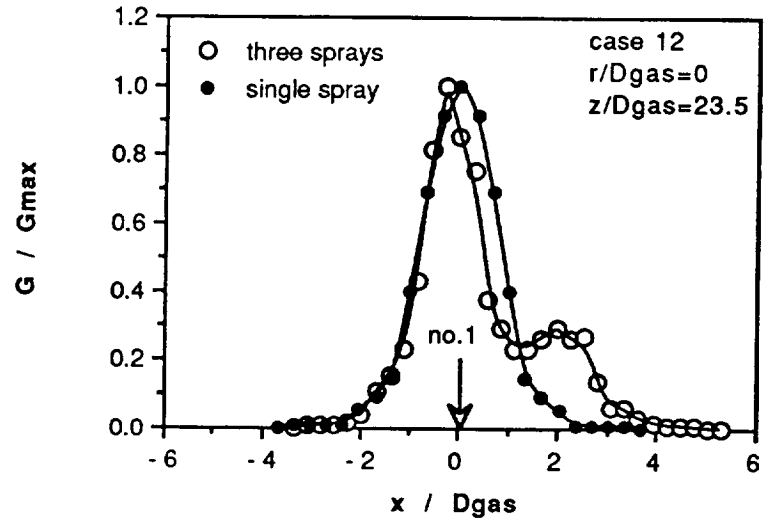
G / Gmax
1.2
1.0
0.8
0.6
0.4
0.2
0.0
three sprays
single spray
case 12
r/Dgas=0
z/Dgas=23.5
no.1
-6
-4
-2
0
2
4
6
x / Dgas

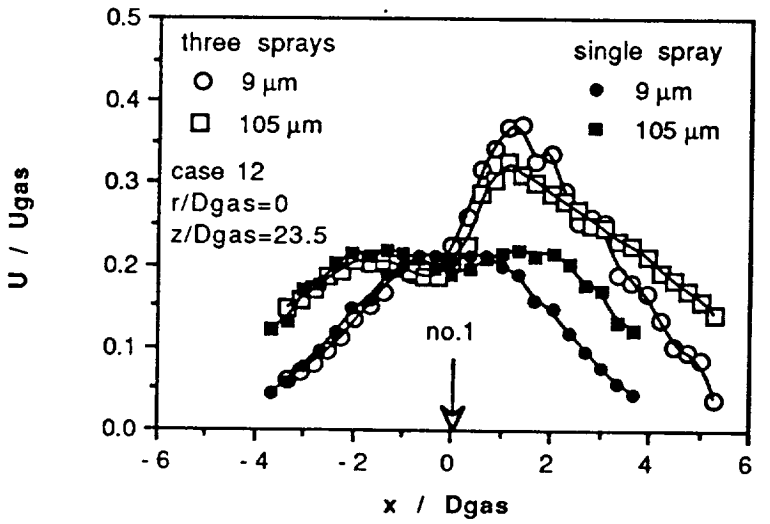
U / Ugas
0.5
0.4
0.3
0.2
0.1
0.0
three sprays
9 μm
105 μm
single spray
9 μm
105 μm
case 12
r/Dgas=0
z/Dgas=23.5
no.1
-6
-4
-2
0
2
4
6
x / Dgas

Figure 28b

Figure 29. Radial profiles along the directions $r/D_{gas} = 0$ and x/D_{gas}=0, 0.84 and 1.68 of (a) liquid flux, (b) mean diameter, (c) mean axial velocity and (d) mean tangential and radial velocity of the 15, 50 and 105 μm droplets and the single phase at axial distance $z/D_{gas} = 13.4$ from the faceplate of three nozzles producing sprays according to case S8 of table 3.

Figure 30. Radial profiles along the directions $r/D_{gas} = 0$ and x/D_{gas}=0 and 1.68 of (a) liquid flux, (b) mean diameter, (c) mean axial velocity and (d) mean tangential and radial velocity of the 15, 50 and 105 μm droplets and the single phase at axial distance $z/D_{gas} = 23.5$ from the faceplate of three nozzles producing sprays according to case S8 of table 3.

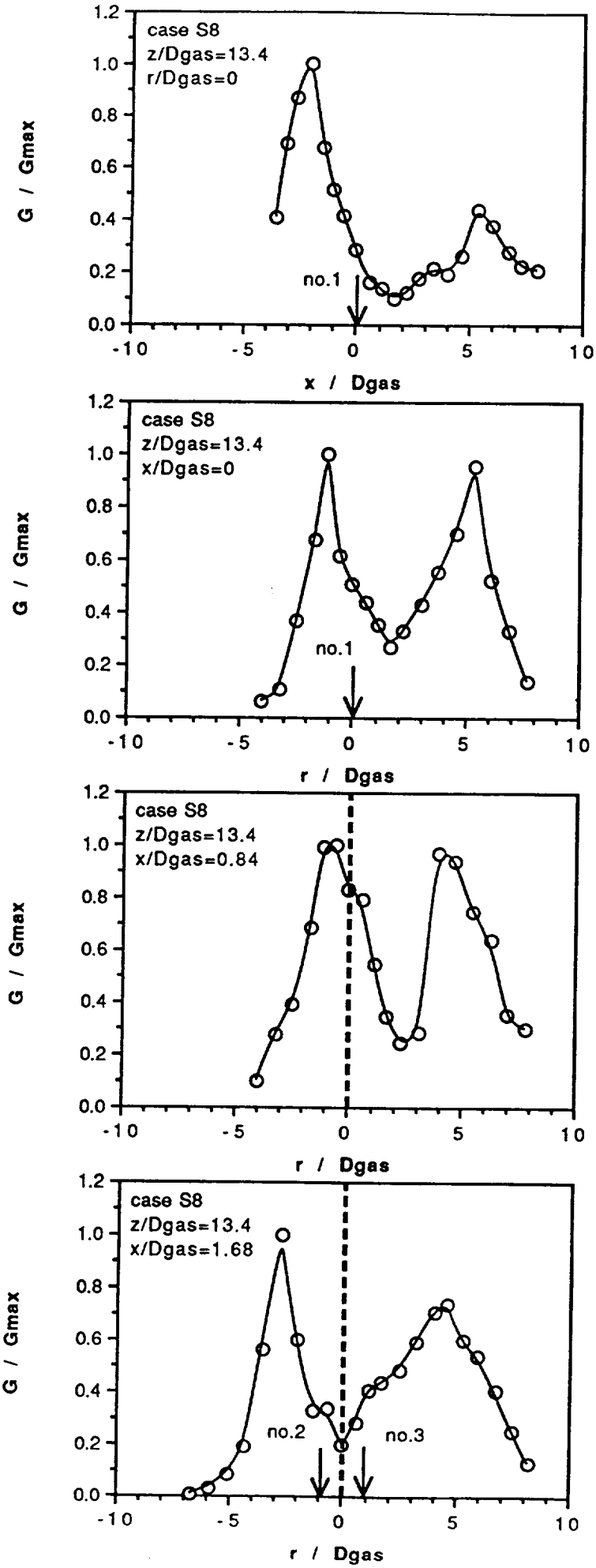
case S8
z/Dgas=13.4
r/Dgas=0
G / Gmax
x / Dgas
no.1
case S8
z/Dgas=13.4
x/Dgas=0
G / Gmax
r / Dgas
no.1
case S8
z/Dgas=13.4
x/Dgas=0.84
G / Gmax
r / Dgas
case S8
z/Dgas=13.4
x/Dgas=1.68
G / Gmax
r / Dgas
no.2
no.3

Figure 29a

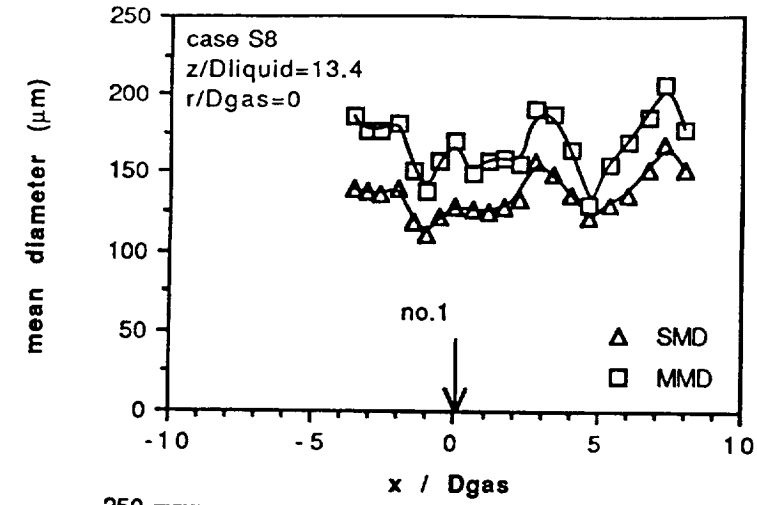
case S8
z/Dliquid=13.4
r/Dgas=0
mean diameter (μm)
250
200
150
100
50
0
-10
-5
0
5
10
x / Dgas
no.1
SMD
MMD

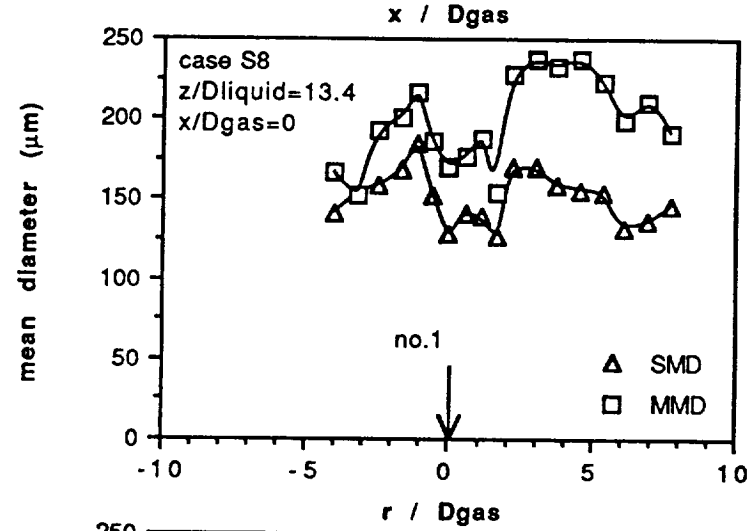
case S8
z/Dliquid=13.4
x/Dgas=0
mean diameter (μm)
250
200
150
100
50
0
-10
-5
0
5
10
r / Dgas
no.1
SMD
MMD

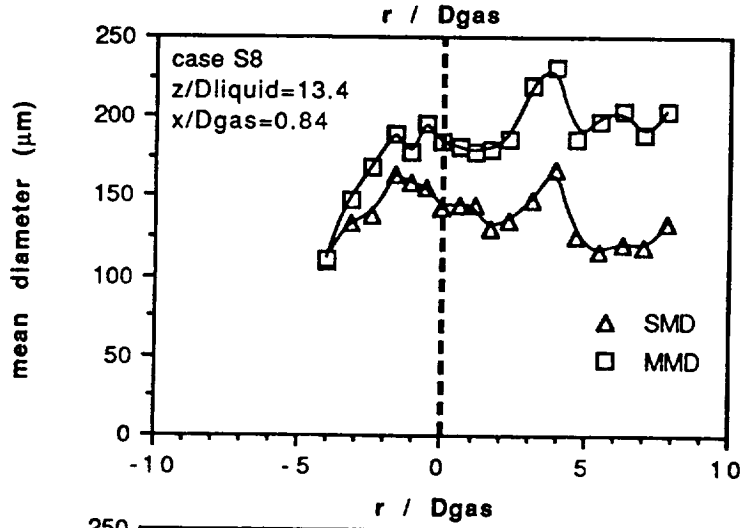
case S8
z/Dliquid=13.4
x/Dgas=0.84
mean diameter (μm)
250
200
150
100
50
0
-10
-5
0
5
10
r / Dgas
SMD
MMD

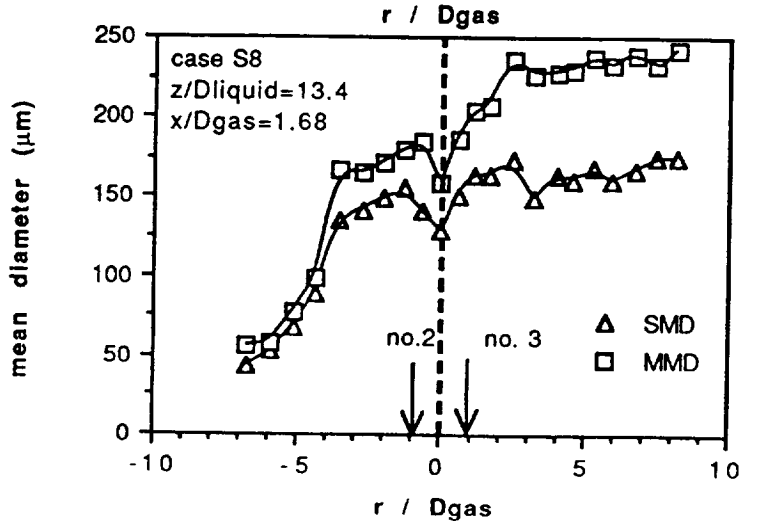
case S8
z/Dliquid=13.4
x/Dgas=1.68
mean diameter (μm)
250
200
150
100
50
0
-10
-5
0
5
10
r / Dgas
no.2
no. 3
SMD
MMD

Figure 29b

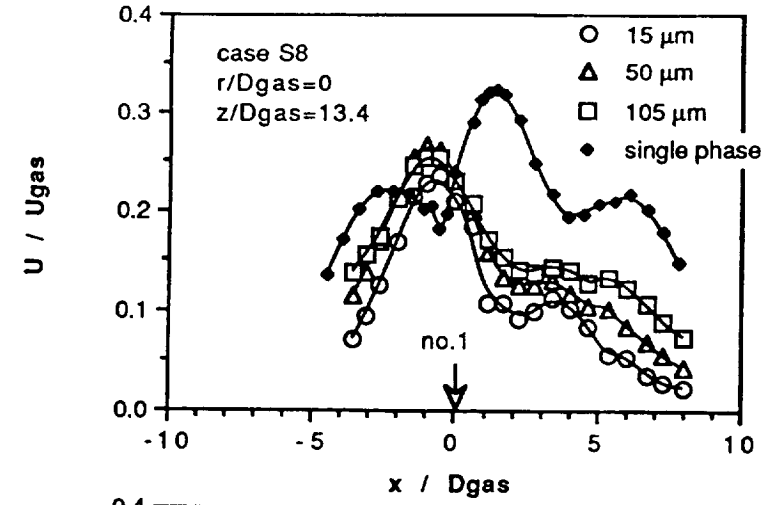
case S8
r/Dgas=0
z/Dgas=13.4
15 µm
50 µm
105 µm
single phase
no.1
U / Ugas
x / Dgas

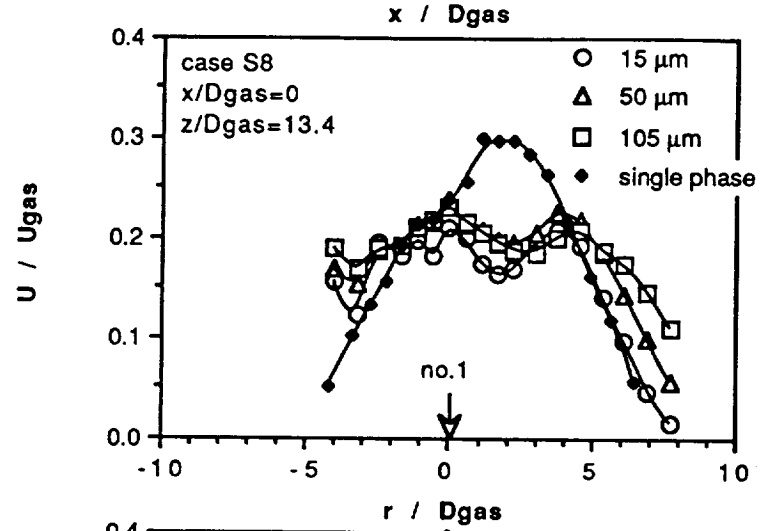
case S8
x/Dgas=0
z/Dgas=13.4
15 µm
50 µm
105 µm
single phase
no.1
U / Ugas
r / Dgas

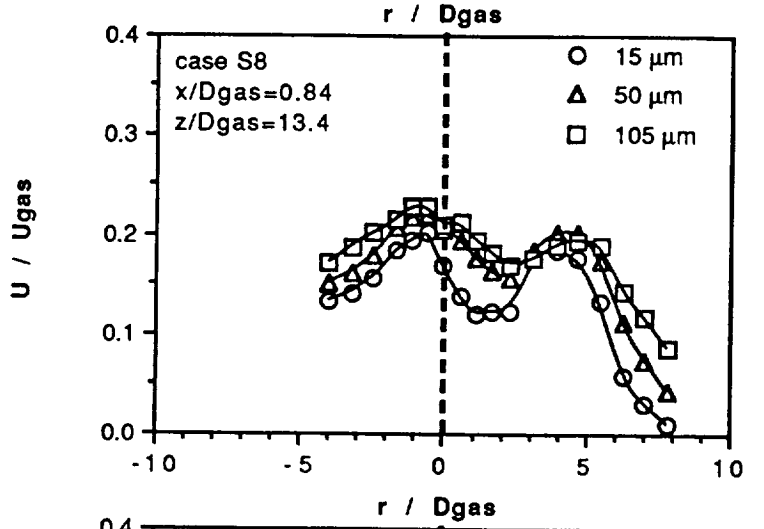
case S8
x/Dgas=0.84
z/Dgas=13.4
15 µm
50 µm
105 µm
U / Ugas
r / Dgas

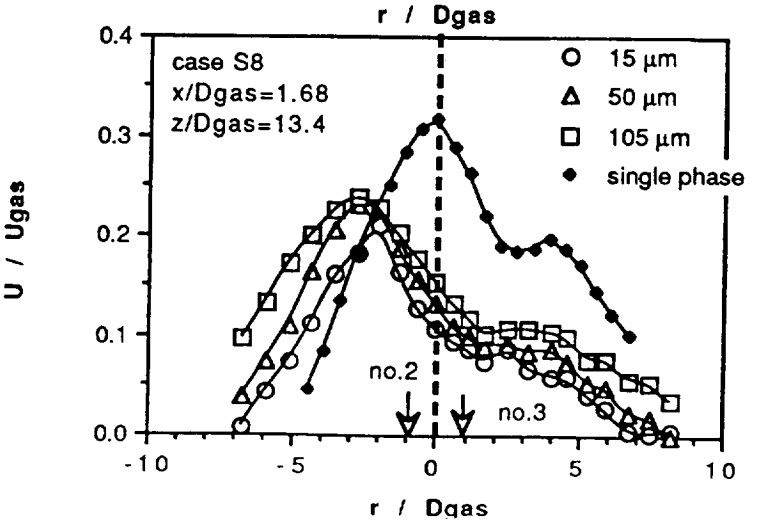
case S8
x/Dgas=1.68
z/Dgas=13.4
15 µm
50 µm
105 µm
single phase
no.2
no.3
U / Ugas
r / Dgas

Figure 29c

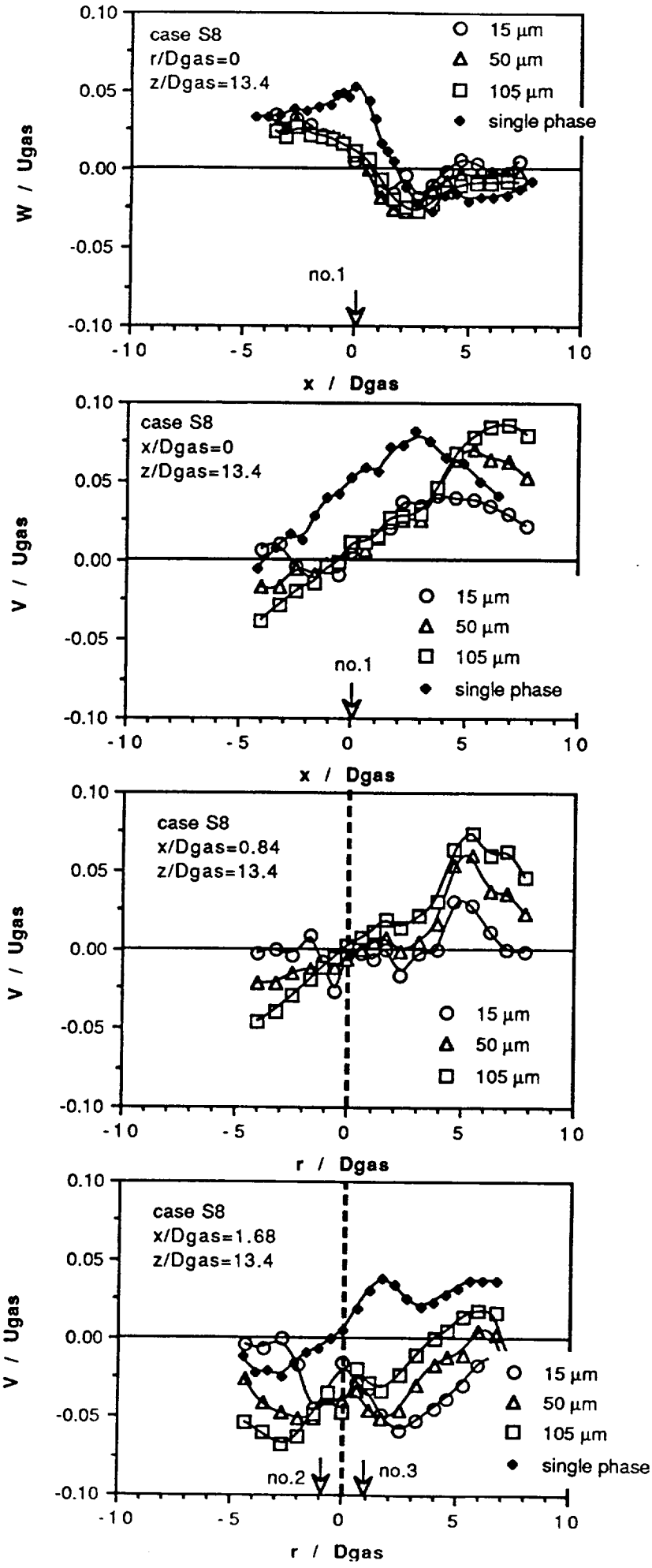
case S8
r/Dgas=0
z/Dgas=13.4
15 µm
50 µm
105 µm
single phase
no.1
W / Ugas
x / Dgas
case S8
x/Dgas=0
z/Dgas=13.4
V / Ugas
case S8
x/Dgas=0.84
z/Dgas=13.4
r / Dgas
case S8
x/Dgas=1.68
z/Dgas=13.4
no.2
no.3
0.10
0.05
0.00
-0.05
-0.10
-10
-5
0
5
10

Figure 29d

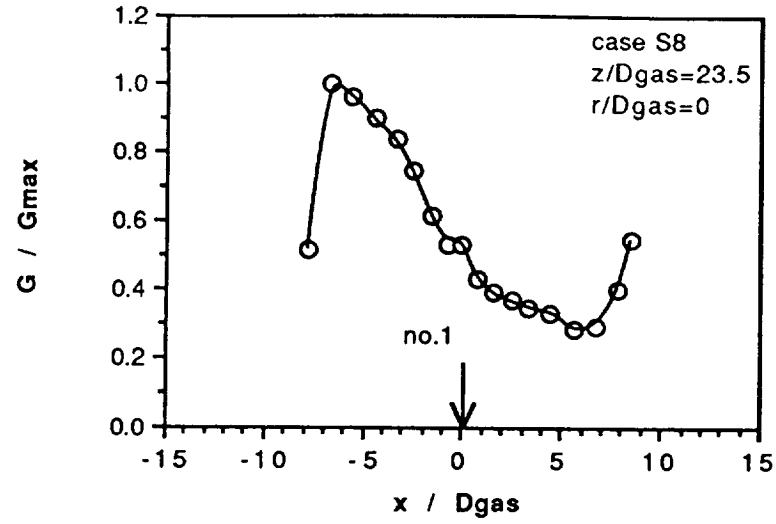
case S8
z/Dgas=23.5
r/Dgas=0
no.1
G / Gmax
x / Dgas

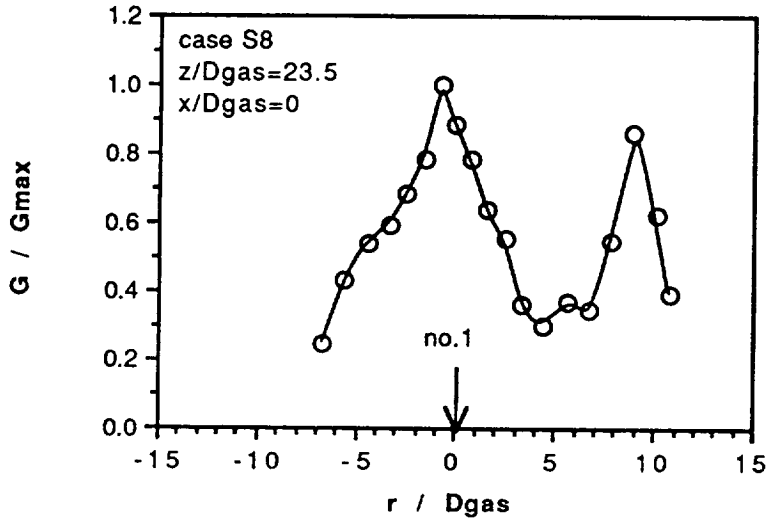
case S8
z/Dgas=23.5
x/Dgas=0
no.1
G / Gmax
r / Dgas

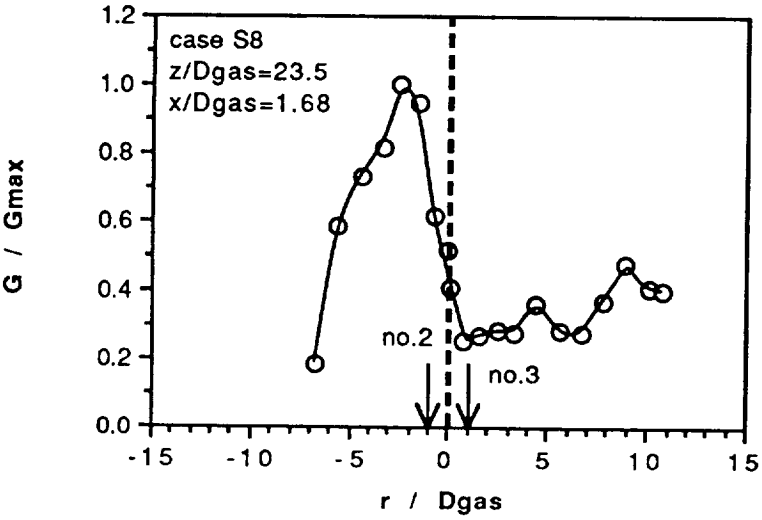
case S8
z/Dgas=23.5
x/Dgas=1.68
no.2
no.3
G / Gmax
r / Dgas

Figure 30a

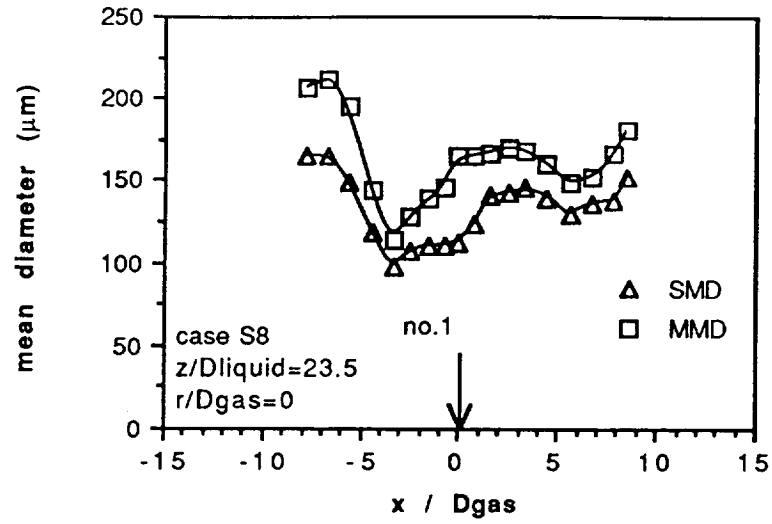
mean diameter (μm)
250
200
150
100
50
0
-15
-10
-5
0
5
10
15
x / Dgas
case S8
z/Dliquid=23.5
r/Dgas=0
no.1
SMD
MMD

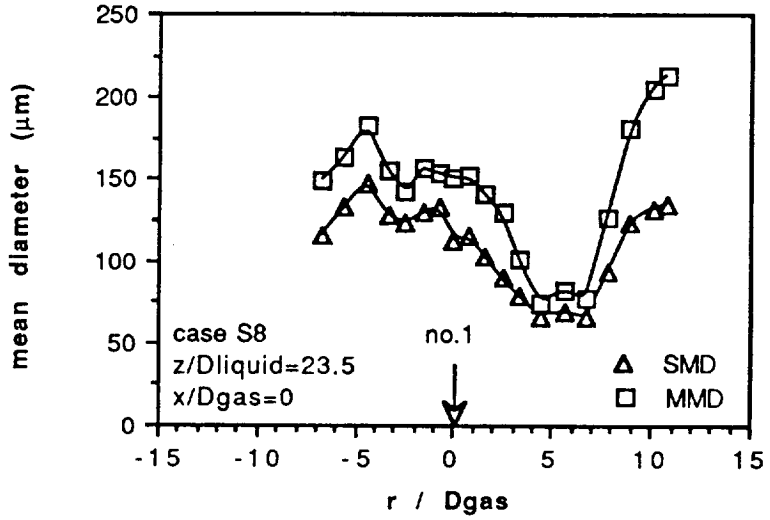
mean diameter (μm)
250
200
150
100
50
0
-15
-10
-5
0
5
10
15
r / Dgas
case S8
z/Dliquid=23.5
x/Dgas=0
no.1
SMD
MMD

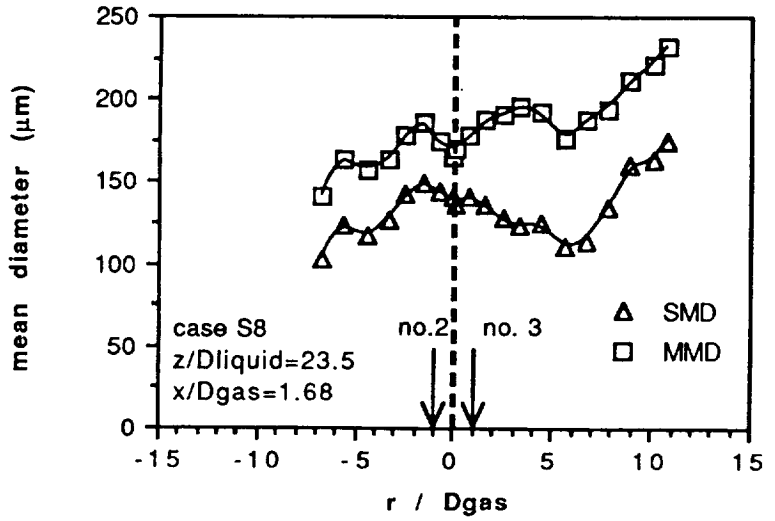
mean diameter (μm)
250
200
150
100
50
0
-15
-10
-5
0
5
10
15
r / Dgas
case S8
z/Dliquid=23.5
x/Dgas=1.68
no.2
no. 3
SMD
MMD

Figure 30b

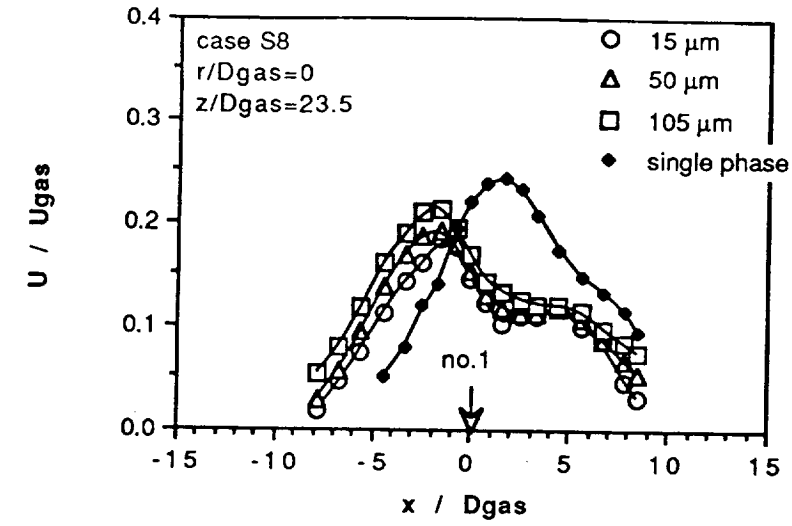
case S8
r/Dgas=0
z/Dgas=23.5
15 μm
50 μm
105 μm
single phase
no.1
U / Ugas
x / Dgas
0.4
0.3
0.2
0.1
0.0
-15
-10
-5
0
5
10
15

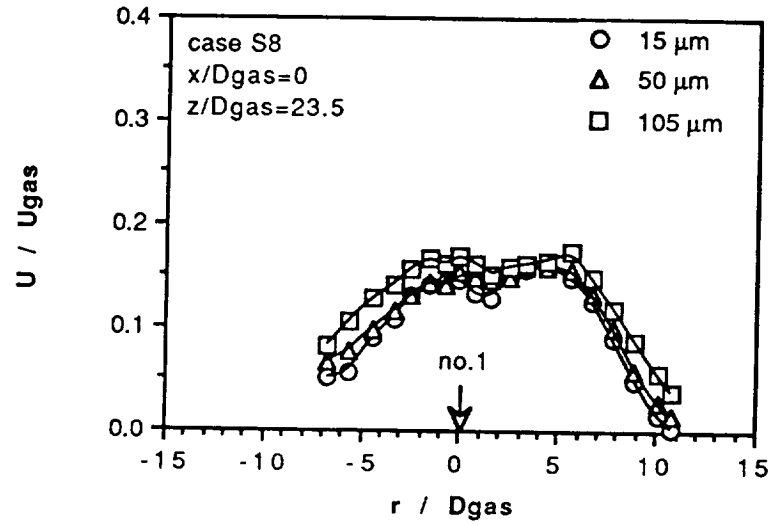
case S8
x/Dgas=0
z/Dgas=23.5
15 μm
50 μm
105 μm
no.1
U / Ugas
r / Dgas
0.4
0.3
0.2
0.1
0.0
-15
-10
-5
0
5
10
15

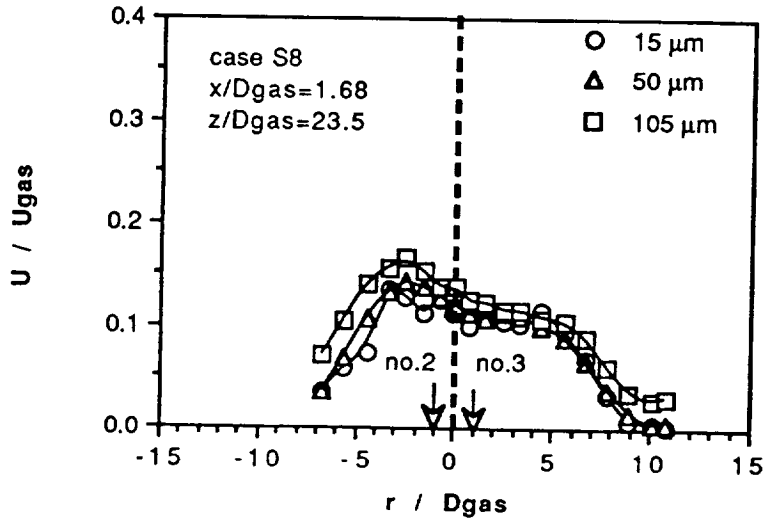
case S8
x/Dgas=1.68
z/Dgas=23.5
15 μm
50 μm
105 μm
no.2
no.3
U / Ugas
r / Dgas
0.4
0.3
0.2
0.1
0.0
-15
-10
-5
0
5
10
15

Figure 30c

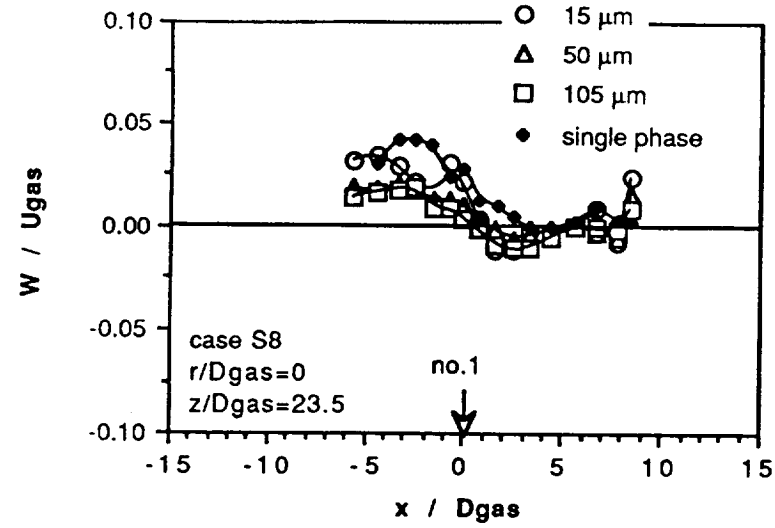
0.10
0.05
0.00
-0.05
-0.10
W / Ugas
15 μm
50 μm
105 μm
single phase
case S8
r/Dgas=0
z/Dgas=23.5
no.1
-15
-10
-5
0
5
10
15
x / Dgas

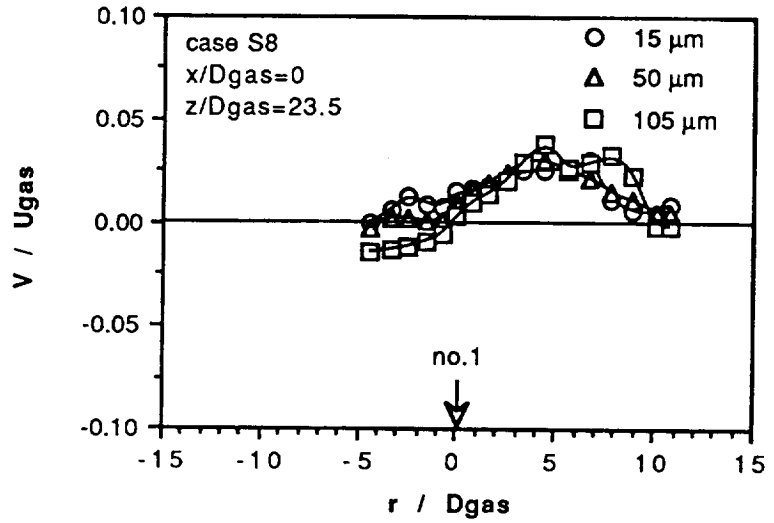
0.10
0.05
0.00
-0.05
-0.10
V / Ugas
case S8
x/Dgas=0
z/Dgas=23.5
15 μm
50 μm
105 μm
no.1
-15
-10
-5
0
5
10
15
r / Dgas

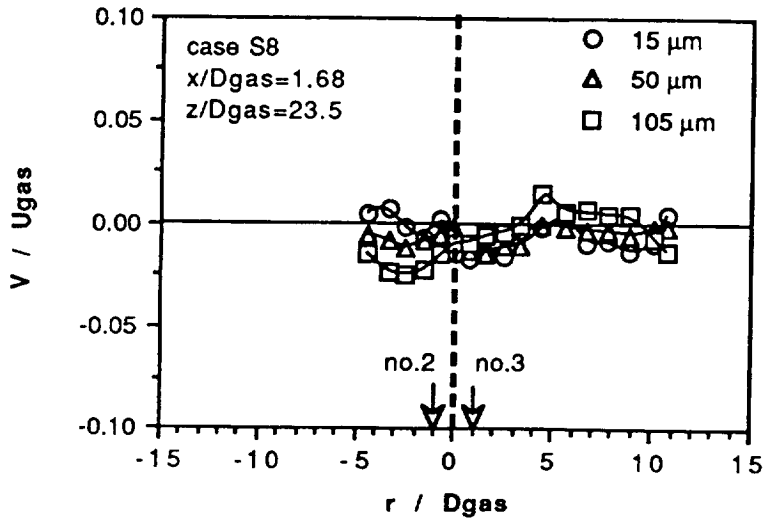
0.10
0.05
0.00
-0.05
-0.10
V / Ugas
case S8
x/Dgas=1.68
z/Dgas=23.5
15 μm
50 μm
105 μm
no.2
no.3
-15
-10
-5
0
5
10
15
r / Dgas

Figure 30d

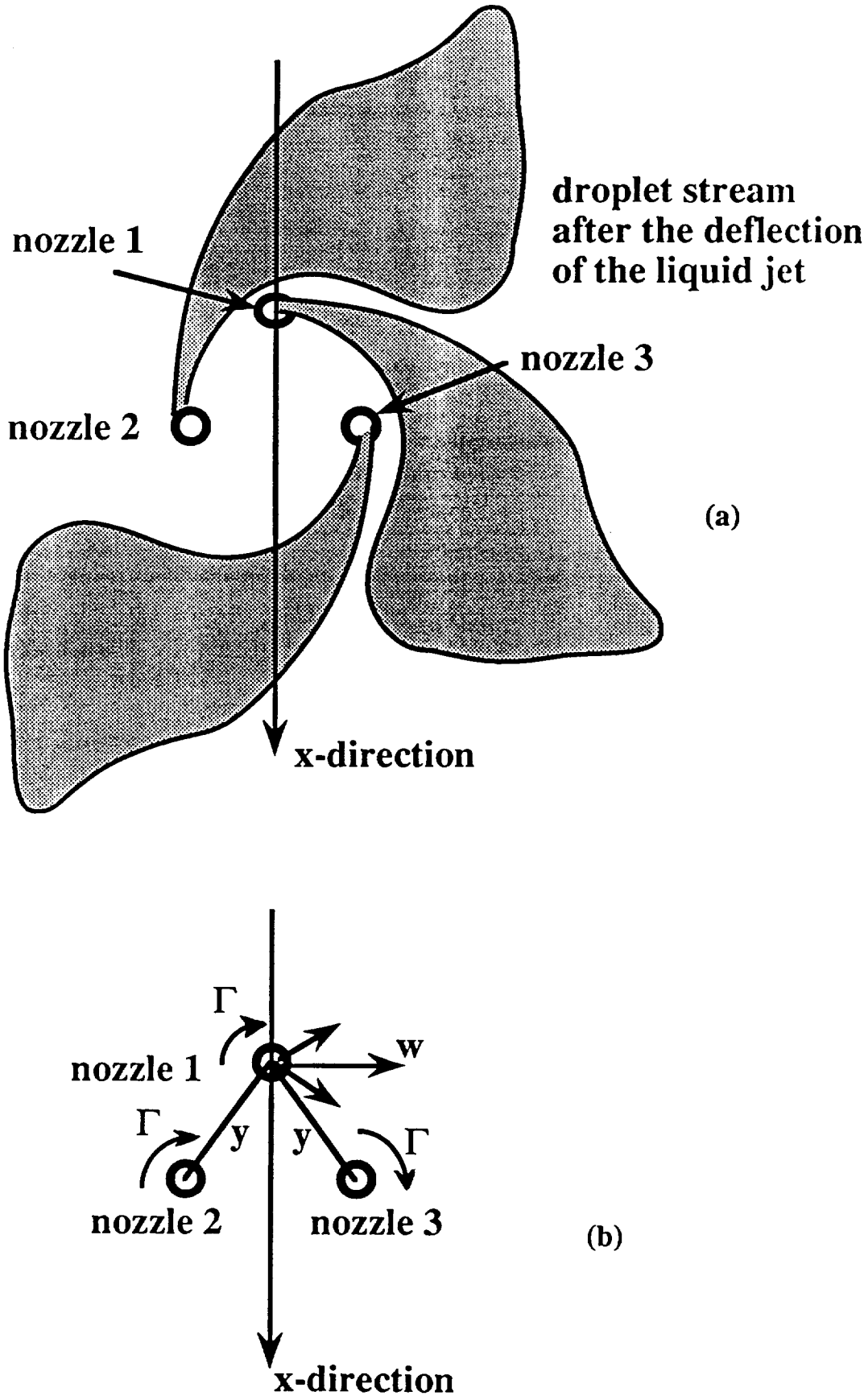

Figure 31. (a) Atomization mechanism in the three interacting sprays produced by nozzles with swirling gaseous stream. (b) The induced velocity by two irrotational vortices, nozzles 2 and 3, on the axis of the third, nozzle 1, explaining the deflection of the liquid jet.

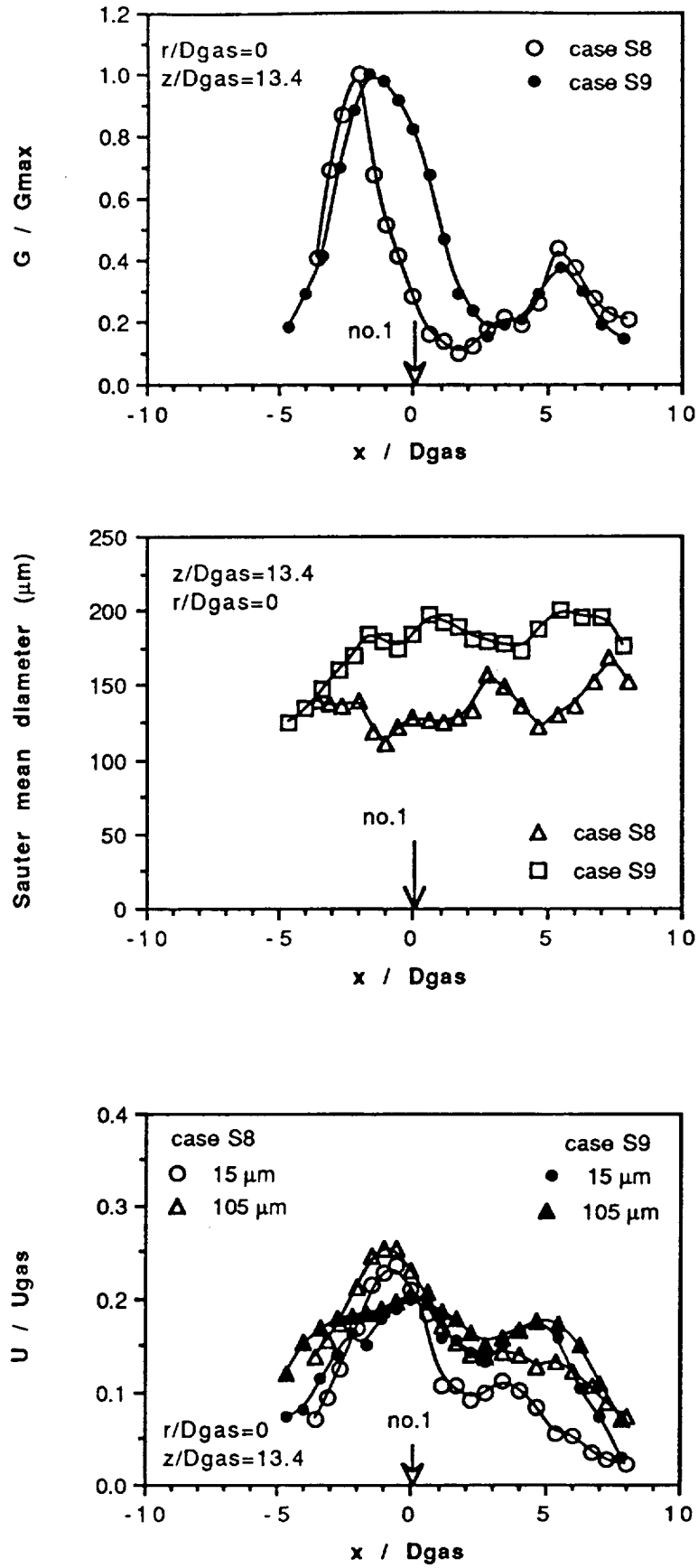

Figure 32a

Figure 32. Comparison between the liquid flux, the Sauter mean diameter and the axial velocity of the 15 and 105 μm droplets of the three interacting sprays produced by nozzles with 50% differences in the liquid flowrate according to cases S8 and S9 of table 3. (a) z/D_{gas} = 13.4, r/D_{gas}=0; (b) z/D_{gas}=23.5; x/D_{gas}=1.68.

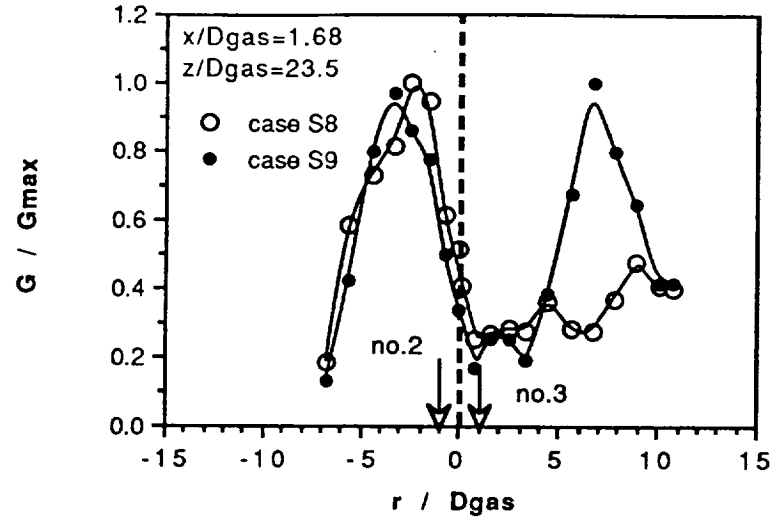
x/Dgas=1.68
z/Dgas=23.5
case S8
case S9
no.2
no.3
G / Gmax
r / Dgas

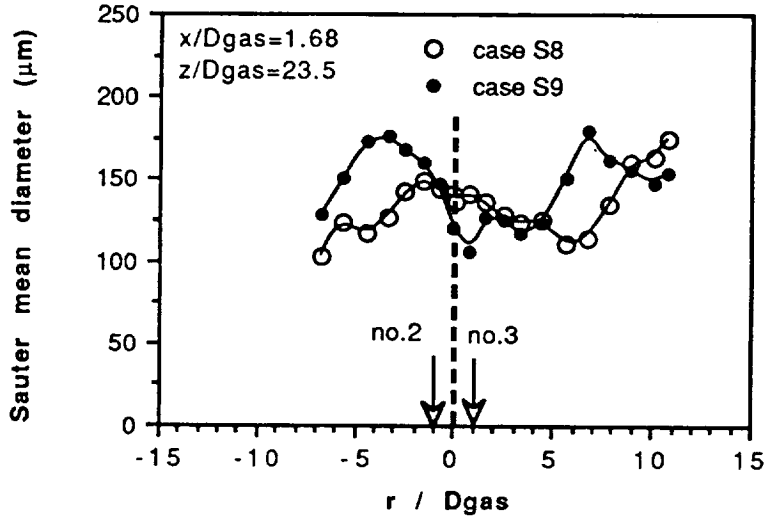
x/Dgas=1.68
z/Dgas=23.5
case S8
case S9
no.2
no.3
Sauter mean diameter (μm)
r / Dgas

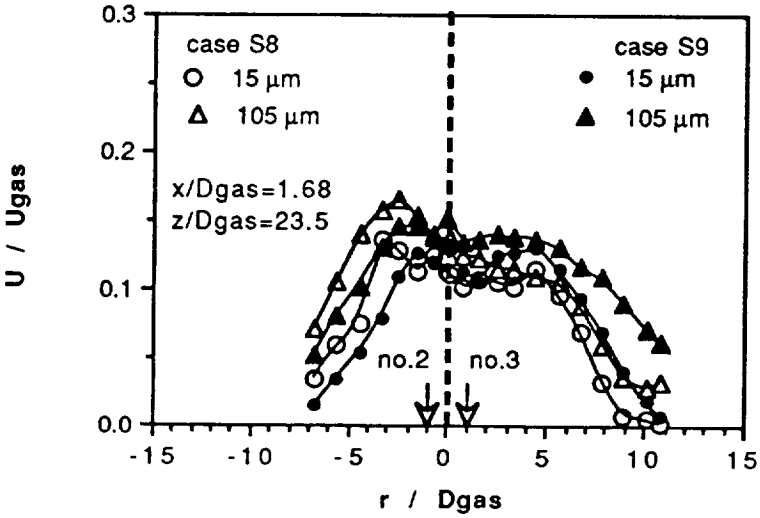
case S8
15 μm
105 μm
case S9
15 μm
105 μm
x/Dgas=1.68
z/Dgas=23.5
no.2
no.3
U / Ugas
r / Dgas

Figure 32b

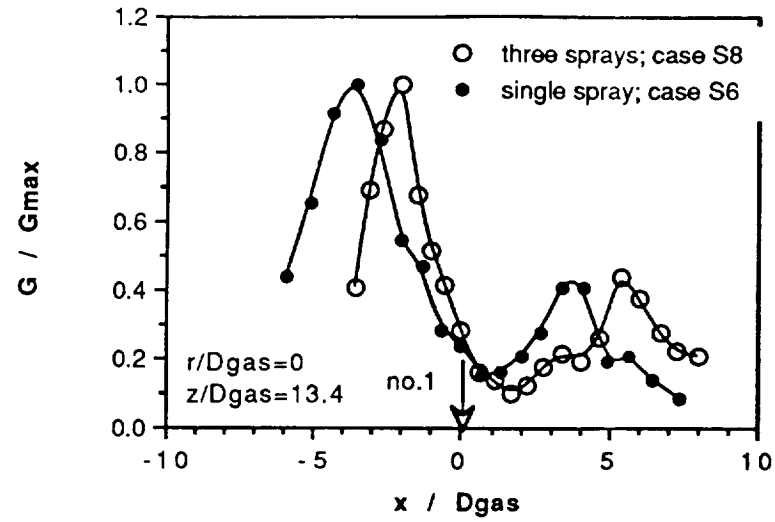

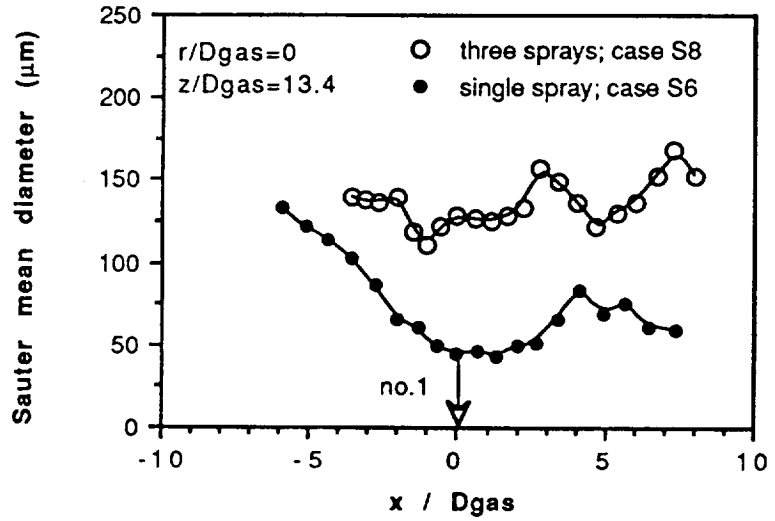

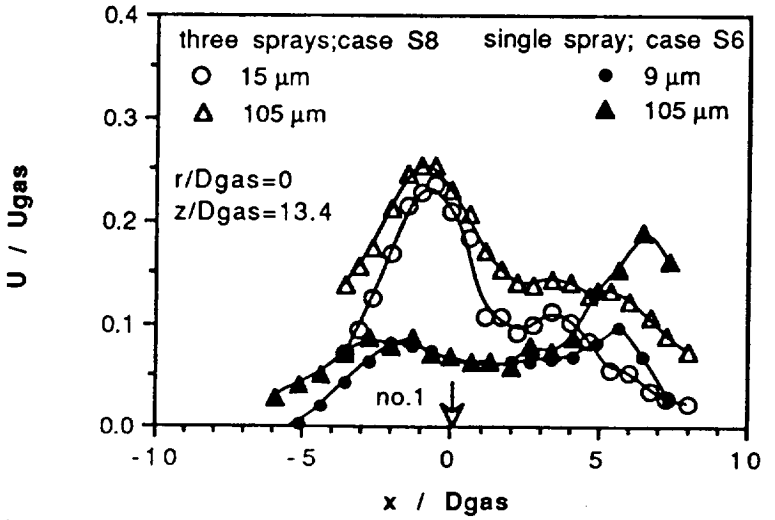

Figure 33a

Figure 33. Comparison between the Sauter mean diameter, the liquid flux and the axial velocity of the 9 and 105 μm droplets of the three interacting and the single sprays produced by nozzles according to case S8 and S6 of table 3 respectively. (a) z/D_{gas} = 13.4, r/D_{gas}=0; (b) z/D_{gas}=23.5; x/D_{gas}=1.68.

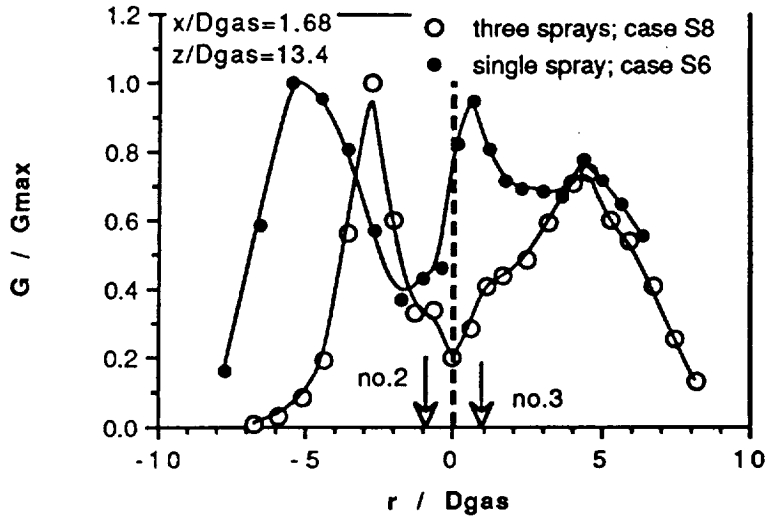
x/Dgas=1.68
z/Dgas=13.4
three sprays; case S8
single spray; case S6
G / Gmax
no.2
no.3
r / Dgas

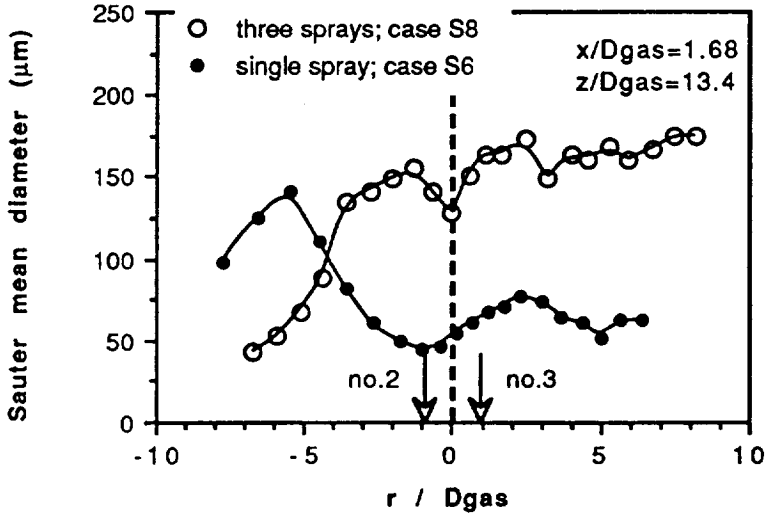
three sprays; case S8
single spray; case S6
x/Dgas=1.68
z/Dgas=13.4
Sauter mean diameter (μm)
no.2
no.3
r / Dgas

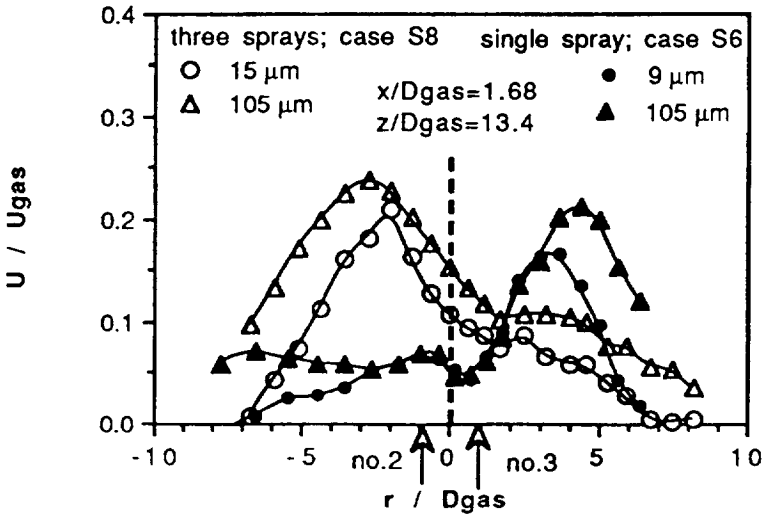
three sprays; case S8
15 μm
105 μm
single spray; case S6
9 μm
105 μm
x/Dgas=1.68
z/Dgas=13.4
U / Ugas
no.2
no.3
r / Dgas

Figure 33b

NASA
National Aeronautics and Space Administration

Report Documentation Page

1. Report No.	2. Government Accession No.	3. Recipient's Catalog No.

4. Title and Subtitle

Simulation of Preburner Sprays

5. Report Date

May 1993

6. Performing Organization Code

7. Author(s)

Volume I - Scientific Research Associates
Volume II - Imperial College - Y. Hardalupas & J.H. Whitelaw

8. Performing Organization Report No.

R93-9083-F

10. Work Unit No.

9. Performing Organization Name and Address

Scientific Research Associates, Inc.
50 Nye Rd., P.O. Box 1058
Glastonbury, CT 06033

11. Contract or Grant No.

NAS8-38872

13. Type of Report and Period Covered

Final 4/3/91 - 4/3/93

12. Sponsoring Agency Name and Address

NASA/George C. Marshall Space Flight Center
Marshall Space Flight Center, AL 35812

14. Sponsoring Agency Code

15. Supplementary Notes

16. Abstract

An experimental investigation was performed to quantify the characteristics of the sprays of coaxial injectors with particular emphasis on those aspects relevant to the performance of rocket engines. Measurements for coaxial air blast atomizers were obtained using air to represent the gaseous stream and water to represent the liquid stream. A wide range of flow conditions were examined for sprays with and without swirl for gaseous streams. The parameters varied include Weber number, gas flow rate, liquid flow rate, swirl and nozzle geometry. Measurements were made with a phase Doppler velocimeter. Major conclusions of the study focused upon droplet size as a function of Weber number, effect of gas flow rate on atomization and spray spread, effect of nozzle geometry on atomization and spread, effect of swirl on atomization, spread, jet recirculation and breakup and secondary atomization.

17. Key Words (Suggested by Author(s))	18. Distribution Statement
Coaxial jet spray, phase Doppler, secondary atomization	Unlimited

19. Security Classif. (of this report)	20. Security Classif. (of this page)	21. No. of pages	22. Price
Unclassified	Unclassified	205	

NASA FORM 1626 OCT 86